Small-scale cosmology with dwarf galaxies

Inauguraldissertation
zur
Erlangung der Würde eines Doktors der Philosophie
vorgelegt der
Philosophisch-Naturwissenschaftlichen Fakultät
der Universität Basel

von

Oliver Müller

aus Schlossrued, AG

2018

Genehmigt von der Philosophisch-Naturwissenschaftlichen Fakultät

auf Antrag von

Prof. Dr. Bruno Binggeli, Dr. Rodrigo Ibata

Basel, den 26.06.2018

Prof. Dr. M. Spiess, Dekan

Abstract

The universe has spawned millions of galaxies – from the largest elliptical galaxies containing billions of stars, to the smallest dwarf galaxies with only a few thousands of stars, just bright enough to not drown in the sea of atmospheric light. Dwarf galaxies are the most common galaxies in the universe and are the main focus of this PhD thesis. By studying the abundance and distribution of dwarf galaxies swarming larger galaxies, we can test our current model of structure formation.

In this PhD thesis a thorough search for hitherto undetected dwarf galaxies in the local neighbourhood, using advanced optical telescopes, i.e. the Dark Energy Camera and the Sloan Digital Sky Survey instrument, is presented. In total we have found 108 new dwarf galaxy candidates, corresponding to $\approx 10\%$ of the known galaxy population in the Local Volume – if confirmed. We have followed-up three newly detected objects with the Very Large Telescope to measure their distances by resolving the tip of the red giant branch stars and established the memberships of two. This pilot study will be extended in the future.

Of special interest is the Centaurus group – a galaxy group similar to our own with two massive galaxies (Cen A and M 83) – separated into two main aggregates. Around Cen A the dwarf galaxies tend to be arranged in two planar structures seen almost edge on, which allowed us to consider the positions of our newly detected dwarfs within these planes. Surprisingly, only one plane seems to be significant. We have furthermore determined that 14 out of 16 dwarf galaxy satellites follow a coherent movement within this plane – suggesting a co-rotating plane-of-satellite. Such structures are rare in cosmological simulations ($< 0.5\%$) but quite frequent in observations (making it the third case after our own Milky Way system and the Andromeda galaxy) – posing a major challenge to the standard model and with that, to our understanding of the structure formation on the scale of groups of galaxies.

Contents

Introduction

1

"Yet observation and theory are woven together, and it is futile to attempt their complete separation. Observations always involve theory. Pure theory may be found in mathematics but seldom in science. Mathematics, it has been said, deals with possible worlds – logically consistent systems. Science attempts to discover the actual world we inhabit. So in cosmology, theory presents an infinite array of possible universes, and observation is eliminating them, class by class, until now the different types among which our particular universe must be included have become increasingly comprehensible."

— Edwin Hubble
Pioneer of the distant stars.

"So much universe, and so little time."

— Sir Terry Pratchett
Beloved British author and amateur astronomer.

1.1 In a nutshell

For several decades, the question about the nature of dark matter has been one of the key topics of astrophysics and cosmology in general. The existence of dark matter was suggested by Swiss astronomer Fritz Zwicky in the early 1930ies. Dark matter today is thought to be the driving force of structure formation in the universe, i.e. the formation of galaxies and the environment they reside in. Special interest is given to dwarf galaxies, as these are the most abundant type of galaxies and the most dark matter dominated objects in the universe. Dwarf galaxies are key objects to test cosmological models of structure formation.

In the standard model of cosmology, the Λ + Cold Dark Matter (ΛCDM) model, the formation and evolution of the universe can be simulated using supercomputers: the initial condition and ingredients of the universe are known from the Big Bang and the laws of general relativity are assumed to be true. One key prediction of these

simulations is the abundance and distribution of dwarf galaxies around their host galaxies. However, there is a strong tension between observation and theory. While there are thousands of predicted dwarf galaxies swarming their hosts, only a handful of these anticipated satellites are actually found in our Local Group. And worse, while their distribution should be close-to isotropic and their motions random, they are aligned in thin planar structures which follow a common movement pattern – a co-rotation around their host – similar to the planets around the Sun. These findings are major challenges to the standard ΛCDM model.

This thesis aims at extending observations of the abundance and distribution of dwarf galaxies to other nearby galaxy groups. The goal is to increase the sample of known satellite systems and test their agreement with the concordance model. For this purpose we study several nearby galaxy groups, both in the northern and southern hemisphere with different telescopes, search for and characterize hitherto undetected dwarf galaxies, and analyse their group environment.

Let us now review the local galactic neighbourhood we reside in, the so-called Local Volume.

1.2 The Local Volume

Following an initial idea by Professor Gustav Tammann in Basel, Kraan-Korteweg & Tammann (1979) compiled a catalogue of 179 nearby galaxies (velocity $v < 500\,\mathrm{km/s}$, corresponding to a distance $D < 10\,\mathrm{Mpc}$) around the Local Group. It contained 7 groups of galaxies, i.e. the Local Group, the Maffei group, the M 81 group, the M 101 group, the CVn-I group, the Centaurus group, and the Sculptor group. Today, the successor of this catalogue – the Local Volume (LV) catalogue (Karachentsev et al. 2004, 2013) – contains over 1000 objects and is still growing. The LV includes all galaxies having radial velocities with respect to the Local Group smaller than 600 km/s or galaxies with distances smaller than 11 Mpc. It is one of Astronomy's never ending tasks to increase the census of galaxies inside the Local Volume and pursue the faintest galaxies possible to detect with today's technology. Multiple blind optical, radio, and spectroscopical surveys, together with dedicated surveys targeting individual galaxy groups, have enlarged the sample of known galaxies in the local neighborhood, shown in Fig. 1.1. The clustering of galaxies within groups and filaments is a common feature of cosmic structure, together with regions devoid of any visible objects (Boylan-Kolchin et al. 2009), e.g. the Tully Void.

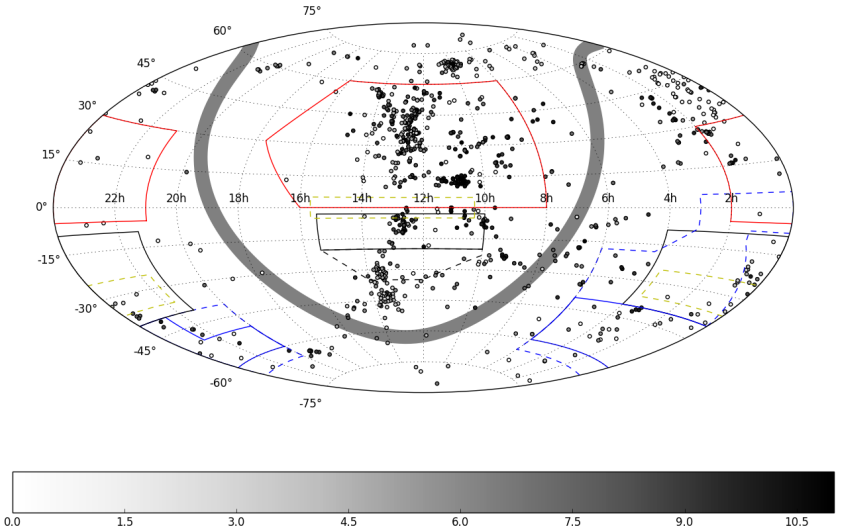

Fig. 1.1: The Local Volume in equatorial coordinates. Every point corresponds to a galaxy with its distance represented by a grayscale color between white (0 Mpc) and black (11 Mpc). The zone of avoidance defined by the Milky Way dust lane is indicated as gray band. Public survey footprints are marked as either straight (completed or mostly completed) or dashed (uncompleted) lines: SDSS (red), DES (blue), ATLAS (black), and KIDS (yellow). In green our dwarf galaxy surveys (Sections 5.1 - 5.4) are presented.

1.3 Surface photometry

In astronomy, the brightness of an object is typically given in units of magnitudes, formally defined as:

$$m = -2.5 \log_{10} \frac{I_1}{I_0},$$

where I_1 is the intensity of the object and I_0 is the reference intensity.

The apparent magnitude is the brightness of an object as observed on Earth. The absolute magnitude is the brightness an observer would measure, if being placed at a distance of 10 parsec to the object. The brighter the object is, the lower its magnitude value[1]. The Sun has an apparent magnitude of $m_{sun} = -26.7$, the Andromeda galaxy an apparent magnitude of $m_{M31} = 3.5$. In reality, the Andromeda galaxy – containing millions of stars – is much brighter than the Sun with an absolute magnitude of $M_{M31} = -21.5$ compared to an absolute magnitude of $M_{sun} = 4.8$. To compare the magnitudes in an intuitive way the brightness factor bf between two objects is given by:

$$bf = 10^{0.4 \Delta m}.$$

Therefore, the Sun appears $\sim 10^{12}$ brighter than Andromeda in the sky, but in reality the Andromeda Galaxy is $\sim 10^{10}$ brighter than the Sun. A difference of five magnitudes corresponds to a brightness factor of $bf = 100$.

[1] which can be quite confusing at times.

For extended sources it is convenient to describe the surface brightness μ of an object, given by the brightness per angular area A of its extent on the sky:

$$\mu = m + 2.5 \log_{10} A.$$

The surface brightness has a huge advantage over the brightness: it is independent of the distance of the object. The intensity of an object decreases with a square law of the distance, while the area also shrinks following a square law, cancelling each other out, hence the surface brightness remains constant over the distance. The surface brightness profile of an extended object can be fitted with a Sérsic profile (Sersic 1968):

$$\mu_{sersic}(r) = \mu_0 + 1.0857 \cdot \left(\frac{r}{r_0}\right)^n,$$

where μ_0 is the Sérsic central surface brightness, r_0 the Sérsic scale length, and n the Sérsic curvature index. In literature both n and $\frac{1}{n}$ are used to describe the exponential term. See Graham & Driver (2005) for an extensive discussion of the Sérsic profiles. A typical profile of a dwarf galaxy in the Centaurus Group is shown in Fig. 1.2.

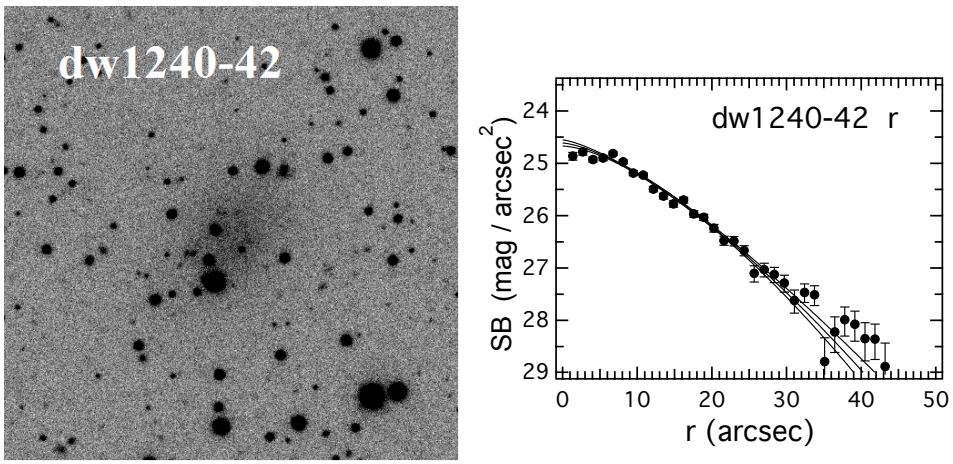

Fig. 1.2: A dwarf galaxy with its corresponding surface brightness profile. The lines correspond to the best fit Sérsic profile and the 1σ uncertainty. The galaxy is characterized by $\mu_0 = 24.6\,\mathrm{mag\,arcsec^{-2}}$, $r_0 = 15.4\,\mathrm{arcsec}$, and $n = 1.5$ (Müller et al. 2017a), see Section 5.2.

There are different properties to characterize an extragalactic object:

- Effective/half-light radius r_{eff}: The radius containing half the emitted light.
- Effective surface brightness μ_{eff}: The surface brightness at the effective radius.
- Mean effective surface brightness $\langle\mu\rangle_{eff}$: The mean surface brightness integrated inside the effective radius.
- Central surface brightness μ_0: The surface brightness at the centre.
- Scale length r_0: A shape-profile driven parameter, scaling the radius.

- Curvature index n: The strength of the exponential decrease.
- Position Angle $P.A.$: The alignment of the major axis of the object, measured from North counter-clock-wise.
- Ellipticity ϵ: The ratio between major and minor axis.

Calculating the mean effective surface brightness μ_{eff} from the effective radius and total magnitude m_{tot} can be done via:

$$\langle\mu\rangle_{eff} = m_{tot} + 2.5\log_{10}(\pi r_{eff}^2) + \Delta m,$$

where $\Delta m = 0.7526$ comes from a brightness factor $bf = 2$.

With an exponential profile $n = 1$, which is typical for dwarf galaxies (e.g. Crnojević et al. 2016), 99.1 % of the light resides within $< 4r_{eff}$ (Graham & Driver 2005), giving a good proxy for the visual extent of the object.

Photometry of dwarf galaxies is typically done with circular aperture steps (Binggeli et al. 1984; Binggeli & Cameron 1993; Jerjen et al. 2000a), even though it can also be done by fitting ellipses onto the galaxy (Lisker et al. 2008). While the former is model-independent, the latter already assumes a shape of the galaxy, which can be problematic if the object is very faint and errors become large.

Because the sky background adds to the measured light in the aperture, its contribution has to be subtracted. Several techniques exist to estimate the sky background. The simplest way is by measuring the sky in a reference aperture with equal size, i.e. an annulus around the object, and subtract the result from the intensity value of the object of interest. A more sophisticated approach is presented in Section 5.1 and consequently used in this thesis. It is based on varying the value of the sky background such that the radial growth curve becomes asymptotic flat in the outer region. When at a certain distance from the object only the sky contributes to the measured luminosity and exactly this contribution is subtracted, no remaining light should be measured and no further increase in the total measured luminosity should be found – the growth curve becomes asymptotic flat.

In literature the brightness of a galaxy is sometimes given in terms of Solar units. Again we can use our basic magnitude formula and the absolute magnitude of the Sun ($V_{Sun} = +4.83$ mag):

$$L_V = 10^{(V_{Sun} - M_V)/2.5}$$

where M_V is the brightness of the galaxy to transform. For the Milky Way dwarf Bootes II (Walsh et al. 2008) with an absolute magnitude of $M_V = -2.7$ (McConnachie 2012) a brightness of 1.03×10^3 in Solar units is estimated. The example was calculated in V-band, but of course is valid for all photometric filters.

1.4 Point Spread Function photometry

To accurately measure the brightnesses of stars in a field, especially when crowding becomes significant, satisfying results can no longer be obtained through surface photometry. The background estimate will become too uncertain, especially when the wings of the stellar profiles overlap. Therefore, another approach needs to be adopted. The standard procedure to measure star brightnesses in crowded fields, e.g. for resolved stars in a galaxy, amounts to the emplyoment of point spread function (PSF) photometry. A star, due its gargantuan distance from Earth, corresponds to a point source in the sky. However, through the atmosphere, the telescope, and the camera, the light emitted by this point source is distorted by a specific transfer function. The light will appear as an extended distribution rather than a point. Therefore we can estimate this transfer/point spread function by measuring the distortion of a point source in an image. The PSF is brightness independent but can vary within an image due to geometric effects in the optical path.

By constructing a PSF using isolated bona-fide stars, a model is created based on how a point source with given magnitude will appear in the image. This model star can be subtracted from an object in the image. If there is no apparent residual, the PSF is a good estimate for this kind of object. Instead of measuring the magnitude of the real object in the image, the analytic magnitude of the model is used. The advantage is that we now have an analytic model for the radial extent of the object. If two stars are close to one another, i.e. their wings overlap, we can fit two model stars onto this superposed profile and estimate the contribution by each individual star.

How exactly such a PSF can be constructed and used to perform photometry is discussed in Section 5.5. We use the software package DAOPHOT2, written by Peter Stetson (Stetson 1987)[2]. Other commonly used software packages for the purpose of PSF photometry are Source Extractor (Bertin & Arnouts 1996), DOPHOT (Schechter et al. 1993), and DOLPHOT (Dolphin 2016).

1.5 Astronomical magnitude systems

The total brightness emitted over all electromagnetic wavelengths is called the bolometric magnitude. It is of great use when measuring the total emitted energy of an object. However, the information of how much energy is emitted at which wavelength is lost. This is why it is interesting to use filters which only allow a certain range of wavelengths to pass through the optics and onto a detector.

[2]While this program is not available online, a quick mail to Peter Stetson is enough to get the newest version of DAOPHOT2. A manual for the use of this software can be found here: http://www.astro.wisc.edu/sirtf/daophot2.pdf.

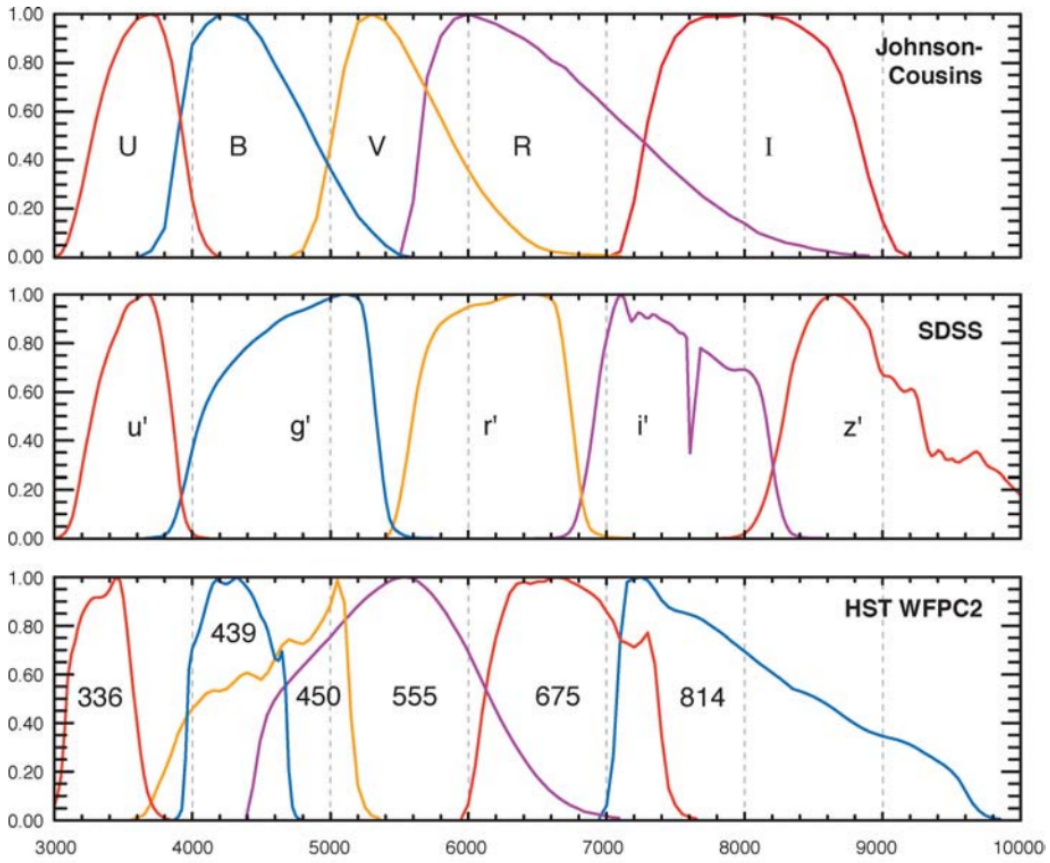

Fig. 1.3: Adopted from Bessell (2005). Transmission efficiency of the Johnson, SDSS, and HST magnitude systems as function of the wavelength.

Several different so-called passband filters were used in the past (see Bessell 2005 for a review). The Johnson-Cousin filter system is made up of $UBVRI$ bands, covering the full optical wavelength range. The Very Large Telescope with the FORS2 instrument employs this system. Historically, this was one of the most commonly used systems in the optical band, while recently the SDSS system gained in popularity. The SDSS system with its $ugriz$ bands has the advantage that there is almost no overlap in their different passbands, which makes it easier to estimate the colours of an object. It is used by the Sloan Digital Sky Survey (as the name suggests) and the Dark Energy Survey. The Hubble Space Telescope (WFPC2) uses its own specific system. See Figure 1.3 for the different bands and which wavelengths they allow to pass.

The different systems use several approaches on how to calibrate their zero magnitude. The Johnson system is defined such that the star Vega has a V band magnitude of 0.03 and all colours are equal to zero. The Gunn System is defined by several standard stars foremost of which is the star BD+17deg4708 to have colours equal to zero. The SDSS has employed this system. The AB system is defined such that a monochromatic flux is measured in erg sec^{-1} cm^{-2} Hz^{-1}. An object with a constant flux per unit frequency interval has zero colour. Sometimes the Johnson-Cousin

values are given in AB instead of Vega magnitudes. Transformations between these systems are given in Frei & Gunn (1994).

Dwarf galaxies

2

"Far, far below the deepest delvings of the dwarves, the world is gnawed by nameless things."

— J.R.R. Tolkien
Professor at Oxford, writer, poet and philologist.

Dwarf galaxies are the most abundant galaxies in the universe and the main objects of interest in this thesis. Surprisingly, exactly defining a dwarf galaxy is not an easy task, especially if going to the extreme limits of their properties. In the following I discuss the characteristics of a *typical* dwarf galaxy and how such dwarfs can be detected (and how they cannot).

2.1 Classifications of dwarf galaxies

The best studied populations of dwarf galaxies are found in the Local Group (McConnachie 2012) and in the nearby Virgo cluster (Binggeli et al. 1985). A possible classification scheme is provided by Sandage & Binggeli (1984), see Fig. 2.1 and 2.2. In this scheme dwarf galaxies are divided into several classes, which are differentiated according to the following criteria:

- **dwarf ellipctical (dE)**: the most abundant galaxy in the universe, dE galaxies are characterized by their smooth intensity distribution and featureless morphology. They come in two forms, with nucleus in the center (dE,N) and without. They typically follow a nearly flat radial profile ($n = 1$) in contrast to E-type galaxies ($n = 4$).
- **dwarf S0 (dS0)**: these dwarf galaxies resemble dE galaxies in their smooth and featureless intensity profile, but also show features of a galactic disk.
- **Magellanic spiral (Sm)**: late-type Sm galaxies can be thought as extension of the late-type Hubble sequence. They show traces of a single spiral arm and are named after their prototype: the Large Magellanic Cloud, which is visible by the naked eye in the southern hemisphere.
- **Irregular (Im)**: also late-type galaxies, Im dwarf galaxies show purely chaotic features, in contrast to the Sm, where the arm provides some kind of order.
- **Blue Compact Dwarf (BCD)**: the BCD has a high-surface brightness center sprinkled with knots, and a low-surface brightness halo with a similar profile as dE galaxies.

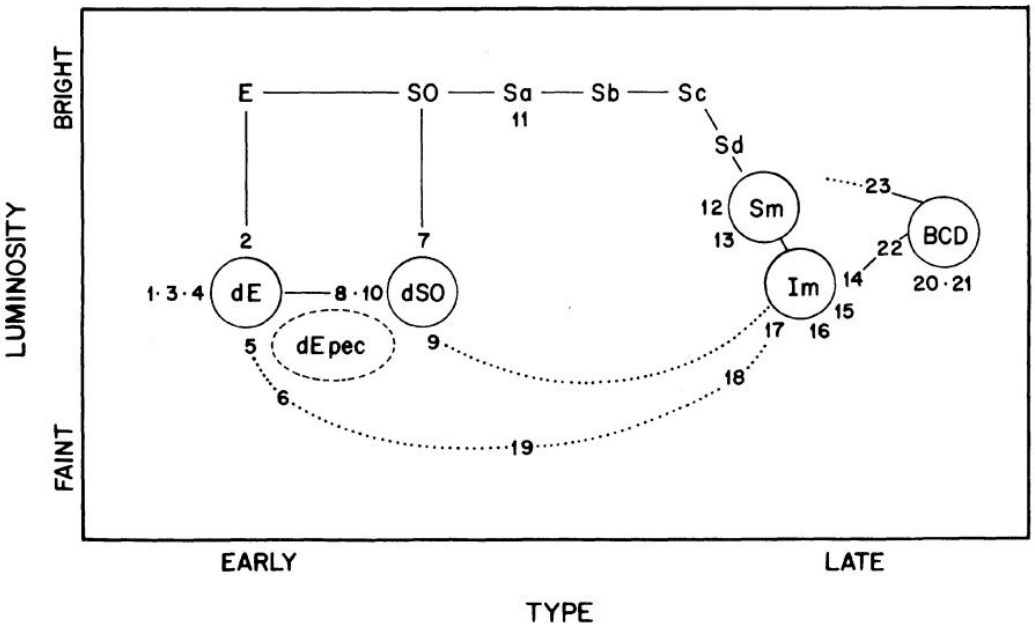

Fig. 2.1: Galaxy classification scheme taken from Sandage & Binggeli (1984). The lines indicate transitions between the types, the dotted line possible connections. In this scheme there are no real dwarf spirals.

There are other classification schemes used in literature, e.g. the extension of de Vaucouleurs et al. (1991) by Karachentsev et al. (2004, 2013), which uses the gas content/colour of the galaxy in addition to the morphological structure. Especially in the Local Group the terminology differs, i.e. the term dwarf spheroidal (dSph) is used instead of dE. This nomenclature made sense as the brightness of the detected objects in clusters (where we know most dE types) used to be several magnitudes larger than the dwarfs found in the Local Group. With new deep surveys the limit of known dwarfs in clusters is pushed into the dSph regime, blurring the border of the two classes. An arbitrary limit of $M_V < -10$ mag for dSph can be set to separate the two classes, meaning that this is a convenient rather than a physical argument.

In this thesis a simplified version of the classification scheme is used with only three classes (dE/dSph, dIrr, and BCD): early-type dE and dS0 galaxies are interchangeably called dE or dSph; late-type Sm and Im are called dwarf Irregulars (dIrr); and the classification of BCDs remains the same. Sometimes when the classification is not clear two types are provided, where the former is the more likely classification than the latter, e.g. as dSph/dIrr. It is most important to note and understand that classification of galaxies is a morphological rather than a physical process. We classify galaxies by eye on a specific set of data. Given better data, e.g. from longer exposure, better resolution or different bands, the classification of galaxies can and probably will change, see Figure 2.3 for an example.

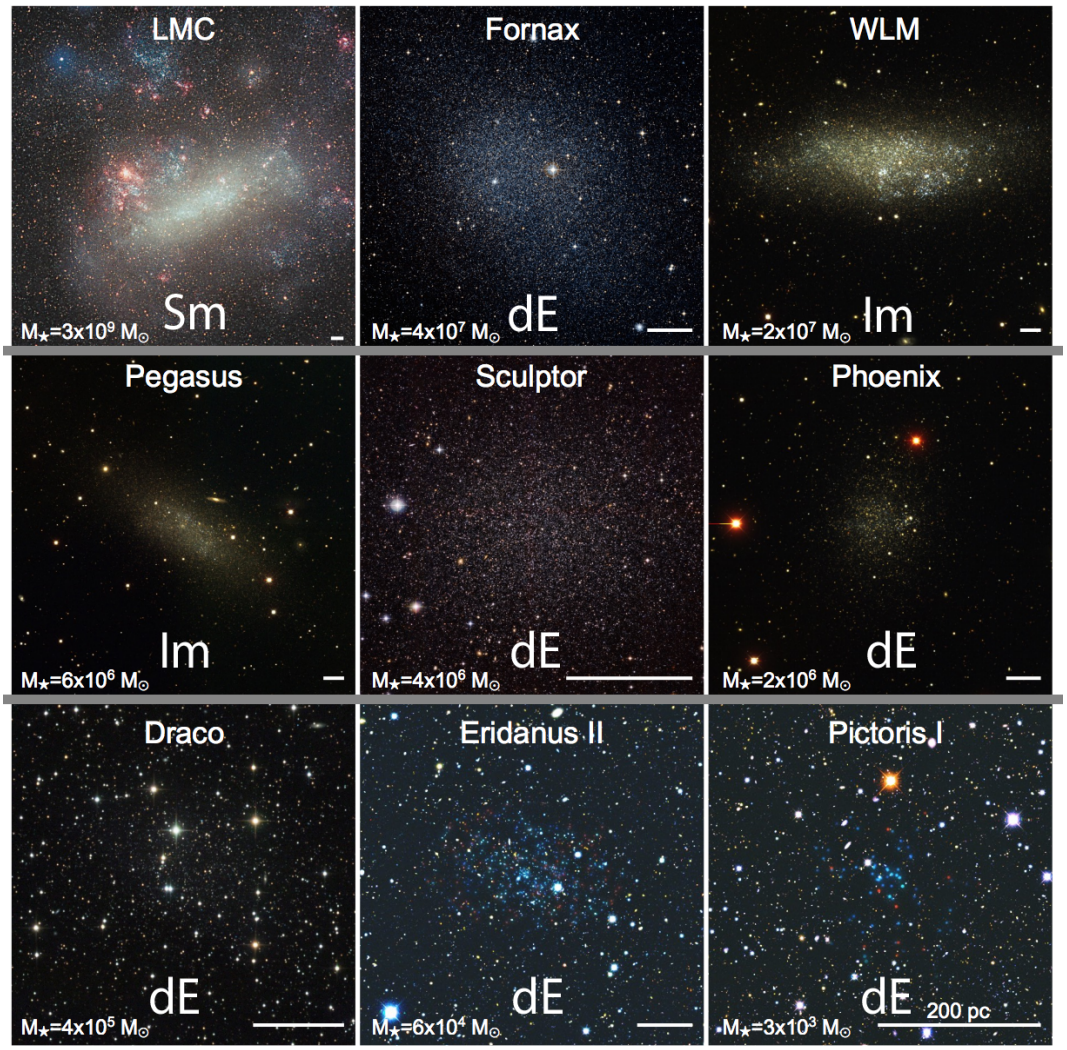

Fig. 2.2: Adopted from Bullock & Boylan-Kolchin (2017). Different Milky Way dwarf galaxies. Note the different scales for the galaxies (indicated by the white line corresponding to 200 pc). The galaxies were classified according to Sandage & Binggeli (1984). The rows correspond to different mass regimes, i.e. the bright dwarfs (top), the classical dwarfs (middle), and the ultra-faint dwarfs (bottom).

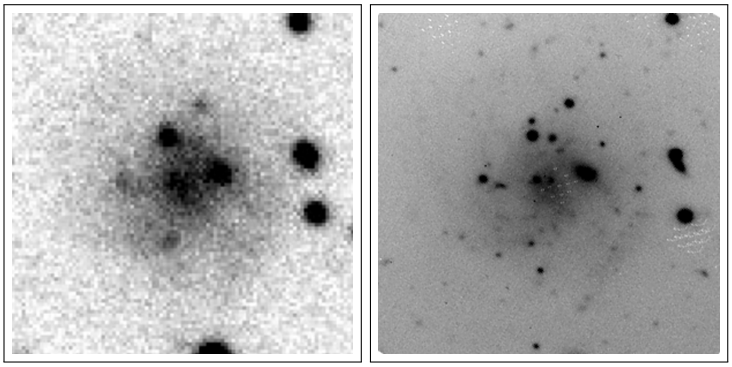

Fig. 2.3: The dwarf galaxy candidate Cen8/KK198 of the Centaurus group (Karachentsev et al. 2013). Left: The dwarf candidate visible as a faint object in a deep photometric plate (Jerjen et al. 2000a). Right: Our deeper VLT+FORS2 imaging reveals this candidate as a background low-surface brightness spiral galaxy. The fact that there are no resolved red giant branch stars puts this galaxy to a distance farther than 6 Mpc.

2.2 Properties of dwarf galaxies

The simplest way to define a dwarf galaxy is by its overall brightness (e.g. $M_B > -17.7$ mag). With such a definition the size of the galaxy does not matter, a point which will become relevant in the next section. From photometric studies of many dwarf galaxies in different environments we know that they tend to follow several relations (Sandage & Binggeli 1984; McConnachie 2012), e.g. their absolute magnitudes are correlated to their surface brightness, to their colour, and to their radial extent, see Figures 2.4. With decreasing luminosities dwarfs tend to become smaller and have fainter surface brightnesses. Theses relations will be extensively used in Sections 5.1 - 5.4 to characterize our newly discovered dwarf galaxies.

Comparing their structural parameters to those of other galactic objects shows that dwarf galaxies share a distinct region in these diagrams, see Figure 2.5, i.e. typical dwarfs are well separated from elliptical galaxies and globular clusters. However, one problem indicated in Figure 2.3 is their overlap with the disc component of spiral galaxies. If such a galaxy has no significant bulge (which occupies the same region as elliptical galaxies) or such a bulge is mistaken for a bright star, deep photometry is needed to resolve the underlying structure of the galaxy.

For cosmology the most relevant property of dwarf galaxies is the connection between their absolute magnitude and their dark matter content – the fainter the dwarf galaxy is, the more dark matter dominated it becomes (McConnachie 2012). Dwarf galaxies trace the fine-structure of the large scale structure of the Universe (Binggeli 1989).

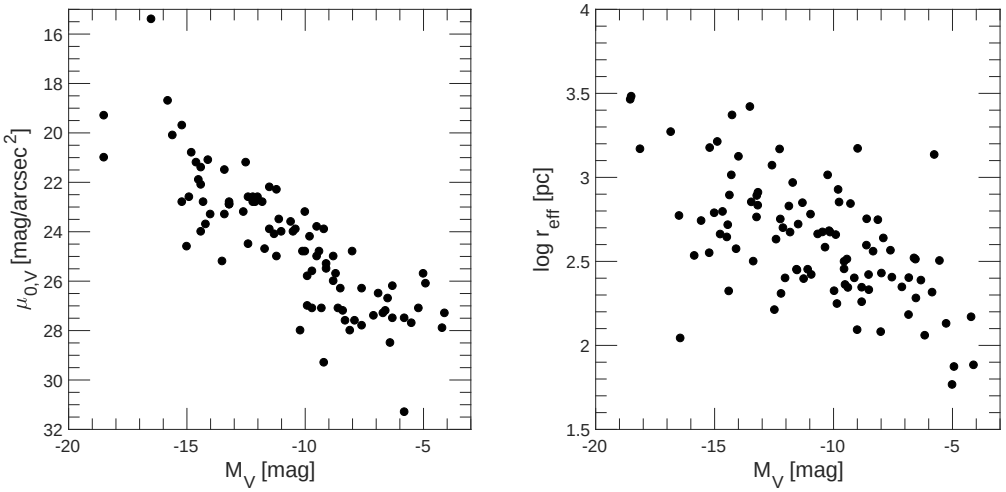

Fig. 2.4: The structural parameters of the Local Group dwarfs (McConnachie 2012) follow several relations; here shown are the central surface brightness to absolute magnitude (left) and effective radius to absolute magnitude (right) relations.

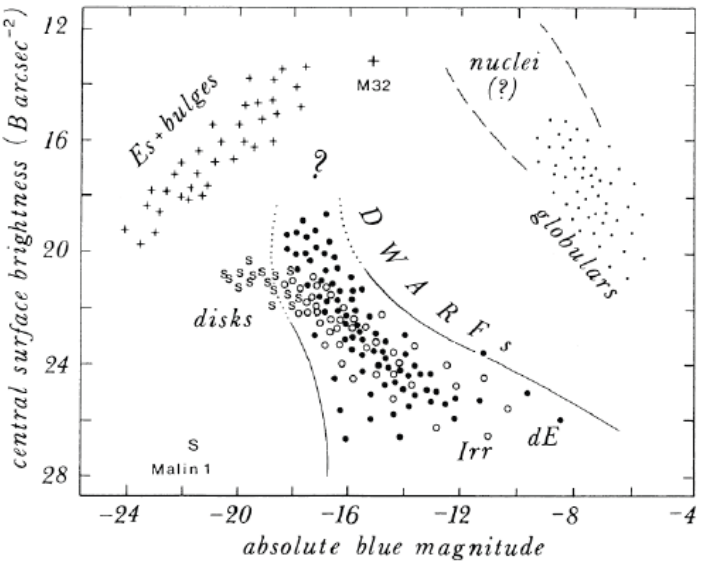

Fig. 2.5: Taken from Binggeli (1994). A Hertzsprung-Russell diagram for galaxies. As in Figure 2.4 the central surface brightness to absolute magnitude relation is shown, but this time with a larger magnitude range and different types of galactic objects, i.e. dwarf galaxies, the disk and the bulge components of spiral galaxies, elliptical galaxies, and globular clusters.

2.3 A new type of dwarf galaxies? The case of ultra diffuse galaxies

In 2015 van Dokkum et al. (2015b) announced their discovery of a new type of galaxy – ultra diffuse galaxies (UDGs). These low-surface brightness ($\mu_{0,g} > 24.0$ mag arcsec^{-2}) and extended ($r_{eff} > 1.5$ kpc) objects have now been found in many different environments (van der Burg et al. 2016), for example in clusters (van Dokkum et al. 2015a; Koda et al. 2015), and in groups (Merritt et al. 2016). However, it is widely overlooked in the community that this type of object was already noted in the Virgo Catalogue by Sandage & Binggeli (1984) and described as "a new type of very large diameter (10,000 pc), low central surface brightness (>25 B mag/arcsec^2) galaxy, that comes in both early (i.e., dE) and late (i.e., Im V) types". Several different formation scenarios have been proposed (e.g., Amorisco & Loeb 2016; Di Cintio et al. 2017) and are under intense debate.

The globular cluster population of UDGs are of special interest, because their kinematics allow the drawing of conclusions about the dark matter content of the galaxy by applying the virial theorem. van Dokkum et al. (2016) observed and studied the UDG Dragonfly 44 in the Coma Cluster hosting over 100 globular clusters and derive a dark matter fraction of 98% within one effective radius – this enclosed mass suggests a total of 10^{12} solar masses, which is similar to the mass of the Milky Way. The other extreme is NGC 1052-DF2 (van Dokkum et al. 2018) a UDG with a lack of dark matter. Using 10 bright globular clusters, a mass-to-light ratio of only 2 is derived – conforming with the mass of the galaxy only consisting of baryonic material – without any need for dark matter. This result was challenged since (Famaey et al. 2018; Laporte et al. 2018; Martin et al. 2018, Kroupa incl. Müller et al., submitted). The main disagreement is caused by the statistical approach chosen by van Dokkum

et al. (2018): By using a biweight estimator for the velocity dispersion they reject one outlying data point (of a total of ten data points). If this outlier is included in the analysis then the velocity dispersion would be in accordance with the galaxy containing dark matter. To make the problem more apparent: Within their 90% confidence range this galaxy possess no matter at all – a clearly unphysical prospect, but a conclusion which could be drawn from their proposed analysis.

2.4 Search for dwarf galaxies

The techniques of searching for and finding of dwarf galaxies are mainly divided into two categories: the classic approach of visual inspection and the identification via computer algorithms. These are presented in the following, with their advantages and caveats.

2.4.1 SDSS SkyServer queries

The SDSS survey has an in-built source detection algorithm, classifying objects and measuring their photometry. Those properties are made public for the community and are available via the SQL SkyServer[1], using simple SQL queries. This means that dwarf galaxies are potentially hidden inside the SDSS database, and can be crawled through SQL queries. Speller & Taylor (2014) did such a study for satellite systems of Local Group analogues in the nearby universe up to redshift $z < 0.01$, applying photometric constraints, e.g. a colour term between $-1 \leq (g - r) \leq 0.85$ and a magnitude dependent size cut, $24 < m_r - r_{exp} < 30$, to separate background galaxies from potential dwarfs. This cut removes 98% of the background, however, it also removes 50% to 70% of potential dwarf candidates. The results of their statistical study were published, however no list of dwarf galaxies is provided[2].

Are such queries suitable to search for nearby dwarf galaxies? The disadvantage of surveying nearby galaxy groups lies in the fact that the area in the sky occupied by the satellite systems is quite large, hence having a high contamination of possible false detections, still, it is worth a test. In Section 5.3 I describe how we detected multiple dwarf galaxies in the M 101/M 51/M 63 complex by performing a visual search in images taken from the SDSS. This survey is an excellent testbed to assess how reliably our results can be reproduced by queries. To this end I chose an area of $\approx$20 deg^2 around M 63, with six previously known dwarf galaxies and three newly discovered ones, to try to recover these dwarf galaxies using SQL queries.

Here are the constraints chosen for the test:

- An apparent magnitude between $16.5 \leq r \leq 19$.

[1] http://cas.sdss.org/dr7/en/tools/search/sql.asp

[2] The actual data is lost due to the undergraduate student who performed the analysis leaving the field (private communication with James Taylor).

- A colour term between $-1 \leq (g-r) \leq 1$ mag.
- A half-light radius between $9 \leq r_{eff} \leq 25$ arcsec.
- A mean effective surface brightness between $23.5 \leq \langle\mu\rangle_{eff} \leq 27.5$ mag arcsec^{-2}.

This is translated to an SQL query as follows:

```
SELECT
   p.objid,p.ra,p.dec,p.u,p.g,p.r,p.i,p.z,
   p.run, p.rerun, p.camcol, p.field
FROM PhotoObj AS p
WHERE
   p.r BETWEEN 16.5 AND 19
   AND (g-r) BETWEEN -1 and 1
        AND ra BETWEEN 195 AND 200
        AND dec BETWEEN 40 AND 45
        AND petroR50_r BETWEEN 9 AND 25
        AND (r+2.5*log10(3.14*petroR50_r*petroR50_r)+0.75)
                BETWEEN 23.5 AND 27.5
```

With these constraints a total number of 83 detections were found within the area. Each detection was visually inspected and classified according to its appearance, see Fig. 2.6. 81% out of the 83 detections were false positives, 11% corresponded to dwarf galaxies associated to background hosts, and only 8% were potential detections of M 63 dwarf galaxies. In total, however, only three of the previously known dwarfs (KK 191, KK 193, KK 194) were recovered, as there were multiple detections arising from the same dwarf, a problem well known in the SDSS pipeline – the so-called galactic shredding (Kniazev et al. 2004) – happening when an extended source is identified as a multiple of different objects.

In the end, none of the new dwarfs from Müller et al. (2017b) was recovered, even though they are present inside the SDSS database. Why is that? The problem arises from the inaccurate photometry of faint sources in the SDSS pipeline, i.e. dw1305+41 has apparent magnitudes of $g = 17.06$ and r= 16.70 (Müller et al. 2017b), compared to $g = 19.38$ and $r = 18.25$ coming from the SDSS pipeline. For this galaxy the colour and apparent magnitude constraints will fail. Loosening up the constraints to find these faint dwarfs however would introduce a huge amount of false positives (>1000), making it quite impossible to visually check and verify each and every detection.

This result is in agreement with the numbers provided by Speller & Taylor (2014) where the excess of satellites around their sample of 274 primaries is 4.6. With a stacked S/N ratio of 8.6 for the complete sample this results in a low S/N = $8.6/\sqrt{274} \approx 0.5$ per primary, meaning that roughly $(4.6/0.5)^2 \approx 85$ detections are expected to appear in my test area (private communication with James Taylor).

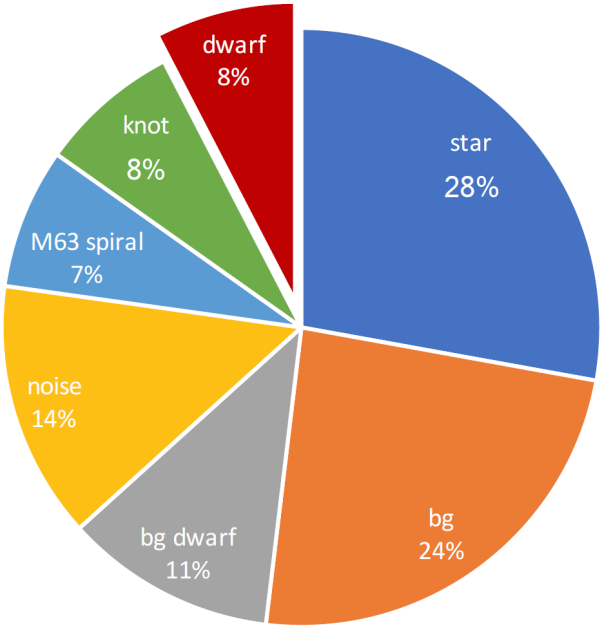

Fig. 2.6: Results for detections of dwarf galaxies around M 63 with SQL queries, classified by following scheme – star: star halo or part of a bright star; bg: very small galaxy or faint blended stars; bg dwarf: dwarf associated to a background galaxy; noise: reflection pattern from a bright star, mostly at the edge of a neighbouring CCD chip; M 63 spiral: a detection within the spiral arm of M 63; knot: region in a spiral arm of a background galaxy; dwarf: suitable dwarf candidate of the M 63 subgroup.

To summarize, for nearby groups of galaxies it is not feasible to use simple SQL queries to search for a complete census of new dwarfs. Too many false positives and especially the inadequate photometry coming from the automated SDSS pipeline would make it difficult to optimize the queries and collect all potential dwarf galaxies.

2.4.2 Source Extractor

The go-to software to automatically search for objects in astronomical images is called Source Extractor (Bertin & Arnouts 1996). Many teams have used it to search for dwarf galaxies in deep images (Merritt et al. 2014; Koda et al. 2015; van der Burg et al. 2016). Basically, the algorithm searches for a number of adjacent pixels greater than a certain threshold above the sky background. On these detections a set of photometric properties are derived from. While just asking for adjacent pixel is not a powerful approach by itself, the post-processing of these catalogues is the key to success. The problem is that the rate of detection of any kind of source is extremely high, with $>$ 10000 objects in a typical 1 deg^2 image.

There are several suggested workflows to reduce the catalogues to handleable sizes. van der Burg et al. (2016) used the following approach to identify UDGs in nearby galaxy clusters: (a) mask the stars by placing a circular mask at their locations; (b) use Source Extractor with a Gaussian filter with FWHM of 1 arcsec, and a detection threshold of 20 adjacent pixels with 0.8σ above the background. This yielded around 100000 sources per field (corresponding to 20 detections per arcmin^2); (c) reject detected stars by requiring $r_2 > 0.9 + r_7$ where r_2 and r_7 are the r-band magnitudes within a circular diameter of 2 and 7 arcsec, respectively. This reduces the detections to 6000 sources per field (a factor of 17); (d) perform surface photometry to extract

Sérsic profiles; and finally (e) select sources with $24.0 \leq \langle \mu_{r,reff} \rangle \leq 26.5$ mag arcsec^{-2}, a circularized effective radius of $1.5 \leq r_{eff} \leq 7.0$ kpc, that were fit within 7 pixels from the detected position, and have a Sérsic index $n \leq 4$. With this strategy van der Burg et al. (2016) extracted around 300 UDGs per cluster in the nearby universe with their MegaCam survey.

2.4.3 Visual inspection

While it is true that the computer is a powerful tool in the pursuit of science, the human body has developed some of the most advanced tools to find and process inputs: the eyes in cooperation with the brain. This framework allows humans to efficiently detect patterns, and more specifically, researchers to detect low-surface brightness objects in image data. However, we are not without aid. By using image-enhancing algorithms we can increase the Signal-to-Noise ratio (S/N) of an image – reducing the background noise as well as increasing the signal of astronomical objects. In this thesis, the search for dwarf galaxies is based mainly on visual inspection of astronomical data (see Sections 5.1 - 5.4). To increase the S/N ratio, I used following techniques:
Binning: Combining several pixels into one pixel, corresponding to an average filter.
Gaussian convolution: Rescaling the pixel values by a 2D Gaussian distribution on top of the pixel.
Ring Median convolution (Secker 1995): Rescaling the pixel values by the median of the pixel values in a annulus around the pixel.
Grayscale range: Setting the dynamic range of the image around the mean value of the sky background.

The workflow I used to search for dwarf galaxies is the following: (a) bin the large images to increase the S/N and reduce the size of the images; (b) apply a Gaussian filter with a small σ to further increase the S/N; (c) set the grey scale 2σ around the background; (d) perform a visual inspection of this processed image; and (e) apply more filters and re-inspect.

What is the advantage of using such an approach over automatic detections with Source Extractor? Source Extractor works well in constrained and dense fields where little background contamination is expected and some miss-identifications will not significantly change the result (in a cluster with thousands of dwarfs ± 20 false detections will not have a huge impact). In field galaxies with only few dwarfs and considerable background contaminations already some false positives will significantly change the result, that is, the shape of the faint-end of the luminosity function. On the other hand, using a classical approach to detect the dwarf galaxies by eye we can already reject background contaminations and suspicious detections, with the disadvantage that the results are not as straightforward to reproduce by other scientists.

ΛCDM cosmology

3

"***Frenk Principle**:*
If the Cold Dark Matter Model does not agree with observations, there must be physical processes, no matter how bizarre or unlikely, that can explain the discrepancy.
***Strong Frenk Principle**:*
1: The physical processes must be the most bizarre and unlikely.
2: If we are incapable of finding any physical processes to explain the discrepancy between CDM models and observations, then observations are wrong. "

— Professor George Efstathiou
Director of the Kavli Institute for Cosmology
and collaborator of Professor Carlos Frenk

"*Warm dark matter is okay, if it is cold enough.*"

— Professor Julio Navarro
University of Victoria

3.1 The standard model of cosmology

Originally proposed by Ostriker & Steinhardt (1995) the Λ + Cold Dark Matter (ΛCDM) cosmology has become *the* standard framework to answer the Ultimate Question of Life, the Universe, and Everything[1]. In more scientific terms, it combines the Friedmann-Lemaître-Robertson-Walker model of an expanding (or contracting) universe with the existence of an exotic dark matter sector (Spergel et al. 2007). These dark matter particles need to be cold, meaning that they are non-relativistic after decoupling from the photons during the Big Bang. The Λ describes the need for a non-zero cosmological constant.

[1] In Douglas Adams *Hitchhikers Guide to the Galaxy* the "Answer to the Ultimate Question of Life, the Universe, and Everything" is asked by a group of hyper-intelligent pan-dimensional beings, using the supercomputer Deep Thought. It took 8 million years to compute the answer. It turned out to be 42.

This standard model of cosmology (SMoC) is described by six parameters – the matter density, $\Omega_m h^2$; the baryon density, $\Omega_b h^2$; the Hubble constant, H_0; the amplitude of fluctuations, σ_8; the optical depth, τ; and the slope for the scalar perturbation spectrum, n_s (Spergel et al. 2007). Recent accurate measurements of the Cosmic Microwave Background (CMB, Spergel et al. 2007; Koda et al. 2009; Planck Collaboration et al. 2014, 2016) have constrained these parameters to a high precision and are in a 1% agreement with a flat geometry of the universe. Interestingly, after almost a century of debate there is still tension in the estimated value of the Hubble constant (Planck Collaboration et al. 2016; Riess et al. 2018)[2].

Fig. 3.1: Taken from Frenk & White (2012), showing the resulting dark matter distribution of high-resolution N-body simulations at $z = 0$. Left: A galactic halo with box size of 1 Mpc. Right: A rich cluster halo with a box size of 7 Mpc.

Using high-resolution N-body simulations with the initial conditions coming from the CMB, Navarro et al. (1997) suggest that dark matter haloes are formed through dissipationless hierarchical clustering: small structures are the first to decouple from the universal expansion, collapsing into bound objects and merging via minor and major mergers subsequently to larger and larger structures, through a statistical process with a wide range of masses deposited into the host haloes. The number density of dark matter haloes per mass interval (the so-called halo mass function) follows a universal form, shown in Fig. 3.1 for a galactic and a rich cluster halo. The two haloes look almost identical, even if their size differs by roughly an order of magnitude. An extensive review of the developement of the SMoC is given by Frenk & White (2012), the pioneers of the ΛCDM cosmology. Some important results of dark matter-only simulations are:

- Structure is formed hierarchically through mergers in a bottom-up scenario.
- The halo mass function has an approximately universal form.

[2]A controversy for the Hubble constant seems to be a law of nature by itself.

- The density profile of a halo is spherical and described by the NFW formula.
- The halo density is cuspy.
- The subhalo population is only recently accreted and tends to reside in the outer part of the host halo.

However, additionally implementing baryonic physics in simulations alters some of the results, e.g. the cuspiness of the haloes (de Blok 2010; Oñorbe et al. 2015). Baryonic physics are not well constrained which makes a direct comparison to observations increasingly demanding. In simulations a large parameter space needs to be covered to test the influence of baryonic physics, e.g. reionization, super nova feedback, and ram pressure stripping. From an observational point of view it is for example challenging to compare the extent of a galaxy to the simulated equivalent. Where does the galactic halo end? Another difficult task is to compare the star-formation history of a galaxy – only deducible by a snapshot of its momentary stellar population – to simulations where the history of galaxies can be directly observed. And more, not all theoretically possible effects and configurations will happen in nature.

3.2 Successes and failures

A number of observations on large (Gpc to Mpc) scale support the ΛCDM cosmology. Following is an incomplete list of the successes of the SMoC.

Successes:

- Imprint of baryonic acoustic oscillation in low-redshift universe (Eisenstein et al. 2005): Using a sample of 47000 luminous red galaxies from the Sloan Digital Sky Survey, the large-scale correlation function is measured, detecting a peak at $100\,h^{-1}$ Mpc, which matches the predictions from the imprint of the acoustic peak from the CMB on the low-redshift clustering of matter. Both the scale and the amplitude of the peak are in agreement with the predictions from the SMoC and support the idea of a linear structure formation history between $z = 1000$ to the present.
- Consistency of power spectra in CMB (Planck Collaboration et al. 2016): The base ΛCDM model, fitted by the temperature power spectrum alone, is in excellent agreement with the parameters derived from the polarization spectrum.
- Big Bang nucleosynthesis (Cooke et al. 2014; Planck Collaboration et al. 2016): The predicted abundance of primordial light elements (especially Deuterium) is in excellent agreement with observational data from *Planck*.

The SMoC is successful on the large scales of the universe. However, on small (Mpc to kpc) scales it has some serious failures and problems.

Failures:

- Missing satellite problem (Moore et al. 1999): The abundance of dwarf galaxies coming from high resolution simulations ($\sim$500) is in stark disagreement with the actual number of observed satellites around the Milky Way ($\sim$30).
- Too-big-too-fail problem (Boylan-Kolchin et al. 2011): The brightest observed dwarf galaxies around the Milky Way reside in only medium sized dark matter haloes. The predicted most massive dark matter subhaloes are not found in observations and are therefore empty of baryonic matter or do not exist.
- Cusp-core problem (de Blok 2010): The dark matter profiles in simulations are described by cuspy profiles, whereas the cores in measured profiles of dwarf galaxies are flat.
- Plane-of-satellite problem (Kroupa et al. 2005): The dwarf galaxies around the Milky Way are aligned in a thin plane and are co-orbiting inside this plane. On the other hand simulations of galactic haloes with their substructures predict isotropically distributed dwarfs with random motions.
- Radial Acceleration Relation (RAR, Lelli et al. 2017): The observed connection between the baryonic content of galaxies (for spirals, ellipticals, and dwarfs) and their internal kinematics is given by an extremely tight relation, where the spread is only driven by observational errors with almost no intrinsic scatter. ΛCDM – with its stochastical approach of galaxy formation – can reproduce the shape of the RAR, but not the scatter.
- Bulge mass to number of satellite relation (López-Corredoira & Kroupa 2016): There is a strong observational hint that the number of satellites correlates to the size of the host's bulge. In ΛCDM no such correlation is predicted as the number of satellites should only correlate to the dark matter halo mass of the host and not to the size of the bulge – which is thought to be formed in mergers.

Some of the problems can be explained by an incomplete understanding of the baryonic processes in the galaxies (e.g. super nova feedback), whereas other problems cannot be accommodated within today's ΛCDM cosmology.

3.3 Alternative cosmology

To solve the existing problems facing ΛCDM multiple alternatives were suggested, e.g. warm dark matter (WDM, Lovell et al. 2012), self-interacting dark matter (SIDM, Robles et al. 2017), or even modifications of the laws of gravity (MOND, Milgrom 1983), to name a few.

Warm Dark Matter: The WDM paradigm uses dark matter particles which are not relativistic, but also not cold. Structure is formed in later times than in CDM, producing less abundant and massive subhaloes, thus solving the missing satellite and too-big-too-fail problem (Lovell et al. 2012). In Fig. 3.2 the substructure of a galactic halo is shown. It is clearly visible that there are less subhaloes which are not as dense as their CDM equivalent. On large scales this model produces the same structure as the successful CDM model, making it a good alternative to CDM. The hypothetical sterile neutrino for example is a good WDM particle candidate (Boyarsky et al. 2009).

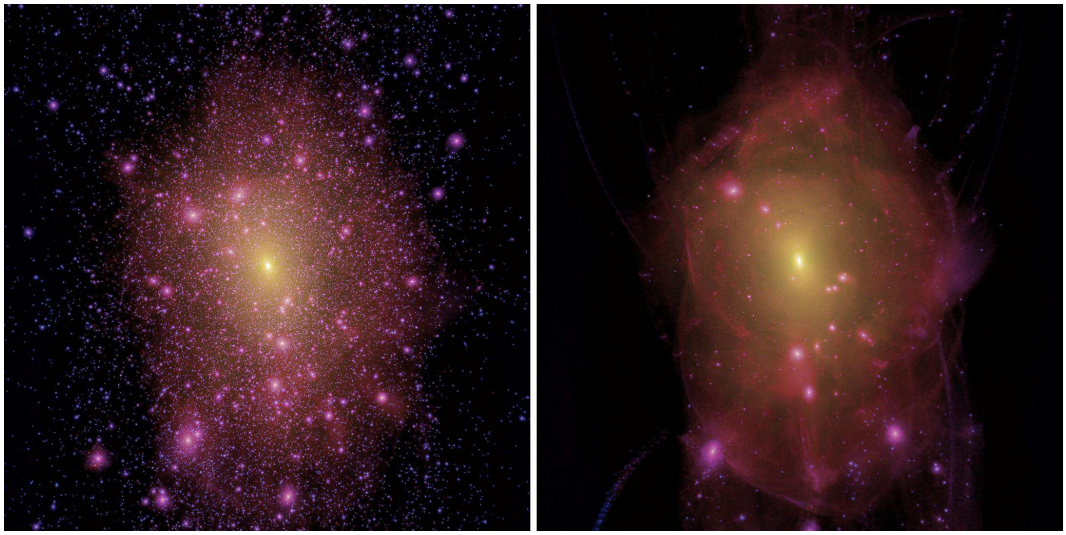

Fig. 3.2: Taken from Lovell et al. (2012), showing the cold dark matter (left) and warm dark matter (right) distributions of a galactic halo at redshift $z = 0$.

Self Interacting Dark Matter: The SIDM model, calling itself a "testable conspiracy" (Elbert et al. 2016), assumes a non-zero cross-section for the dark matter particles, hence introducing dark matter self-interaction. This interaction transforms the cuspy dark matter profiles into flat profiles, thus solving the cusp-core problem (Robles et al. 2017). The suppression of the formation of a galactic core is presented in Fig. 3.3, showing that the profile of the simulated dwarf galaxy is flatter than in the CDM analogue. SIDM models don't change the phase-space distribution of subhaloes.

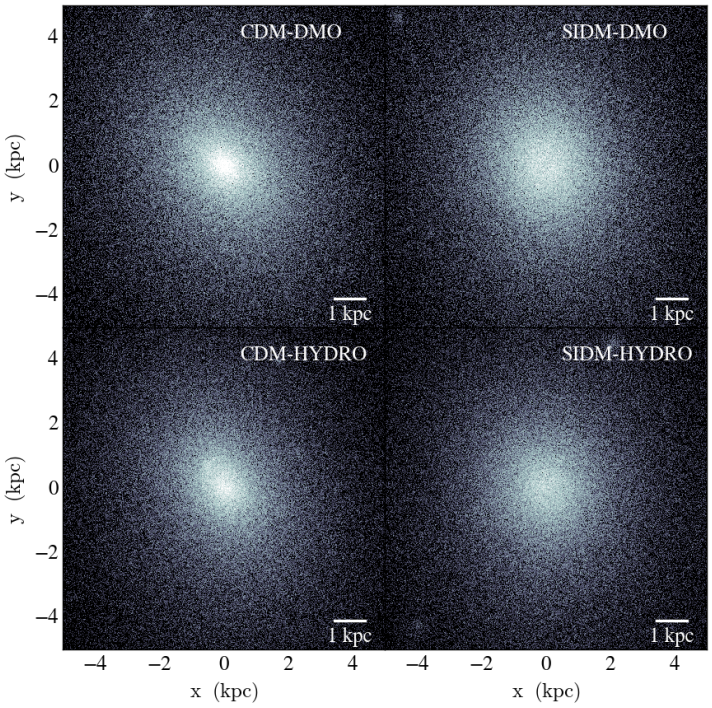

Fig. 3.3: Taken from Robles et al. (2017), showing the cold dark matter (left) and self-interacting dark matter (right) distributions of a simulated dwarf galaxy.

Modified Newton Dynamics (MOND): Proposed by Mordehei Milgrom in 1983 (Milgrom 1983) MOND removes the need for cold dark matter altogether, and instead changes the law of gravity in the regime of small accelerations. In the high acceleration regime gravity works as described by Newton's Law (Newton 1687). However, under a certain acceleration threshold a_0, the so called deep-MOND regime, the force F_N is given by:

$$F_N = m\frac{a^2}{a_0}.$$

Solving $F_N = F_G$ for a test mass m on a circular orbit with radius r around a host with mass M, the radial component r is cancelled out, and the resulting circular velocity is given by (Famaey & McGaugh 2012):

$$v_c^4(r) = v_c^4 = a_0 GM.$$

This formula explains the rotation curves of spiral galaxies (Babcock 1939, Bosma 1981; Rubin et al. 1985)[3], one of the original missing-mass problems. Note that the velocity is only driven by the mass of the host, not by the radius as opposed to Kepler's law of orbital motions. Even in the regime of the most dark matter-dominated objects of the universe, the dwarf galaxies, MOND works reasonably well. Angus (2008) studied the velocity dispersion of 8 classical Milky Way satellites and could match the line-of-sight velocity dispersion for 6 dwarfs (Draco and Sextans pose a problem

[3]It is noteworthy that Babcock already discovered the flat rotation curve for the Andromeda galaxy as early as 1939.

Fig. 3.4: Taken from Kroupa et al. (2010), showing the formation of cosmic structure in the form of a mangrove merger tree: purely baryonic galaxies merge (or interact) and thereby spawn new dwarf galaxies.

which could be due to the external field effect, see Famaey & McGaugh 2012 for a discussion of this effect).

The RAR, as discussed before, is a natural outcome of the MOND formula as it couples the baryonic mass with its dynamics. This is unlike in ΛCDM where the missing mass has to be modelled from the dynamics of the object. The WYSIWYG rule applies – What You See Is What You Get. From the distribution of the gas and the stars alone the resulting kinematics can be derived.

Up to this day, no consistent MONDian cosmological simulation exists, albeit codes are available (e.g. RAyMOND, Candlish et al. 2015). In comparison to ΛCDM simulations MONDian codes are non-linear, and therefore are much more difficult to code, and are computationally heavy to run (private comunication with Graeme Candlish), making it a tough challenge to create a MOND cosmology. Most of the MOND predictions on cosmological scales come from qualitative arguments (López-Corredoira & Kroupa 2016) or are performed on small-scales only (Pawlowski et al. 2011).

However, it is clear how structure formation on the scale of galaxy groups should happen in a MONDian framework: purely baryonic galaxies interact or merge, spawning new dwarf galaxies along their histories (Kroupa et al. 2010), see Fig. 3.4, which resembles a mangroven tree in a so-called top-down scenario.

One of the major issues for MOND is the power spectrum of the CMB. With only the baryonic matter to produce the oscillation, the shape of the power spectrum cannot be explained. However, the introduction of a single 11eV sterile neutrino can potentionally solve this problem (Angus 2009) but would introduce a kind of dark matter particle into the MONDian paradigm, which is per se not forbidden, but in tension with the original idea of solving the missing-mass problem without any new particle.

Planes-of-satellites

4

> *"My dear Kepler, what would you say of the learned here, who, replete with the pertinacity of the asp, have steadfastly refused to cast a glance through the telescope? What shall we make of this? Shall we laugh, or shall we cry?"*
>
> **— Galileo Galilei**
> Father of the scientific method

4.1 Historic overview

What began in the 70ies as small curiosity has become one of the most controversially discussed topics in cosmology. It was Kunkel & Demers (1976) and Lynden-Bell (1976) who noted that the then-known dwarf galaxies around the Milky Way are arranged in a thin, planar structure which is perpendicular to the spiral disc of the Milky Way. With only the Large and Small Magellanic Clouds, Draco, Ursa Minor and Sculptor, Lynden-Bell (1976) worked out that these satellites lie in a plane, aligned with streams of high velocity clouds. The only other known dwarf, Fornax, seemed to be off. Lynden-Bell suggested that the streams and even the dwarfs were pulled out of the Great Magellanic Galaxy – the theoretical progenitor of the LMC and SMC – by tidal forces on its orbit around the Milky Way. The similarities between the stellar populations of the dwarf spheroidal and the old population of the SMC (van den Bergh 1972) supported this idea.

At the time of the discovery of the plane we were still far away from a fully fledged cosmological structure formation scenario, hence the plane-of-satellites was not much of a worry to the cosmology community. This changed with the advance of supercomputers, making it possible to run computationally-heavy structure formation simulations within the ΛCDM cosmology (Navarro et al. 1997). The famous missing-satellite problem arose at the time of the millennium turn (Moore et al. 1999; Klypin et al. 1999). At the same time, the discovery of several more dwarf galaxies in the Local Group were made possible with new all-sky surveys like the Sloan Digital Sky Survey (SDSS, York et al. 2000). However, it took several more years until Kroupa et al. (2005) realised that the phase-space distribution of the then-known 16 Milky Way satellites are inconsistent with ΛCDM simulations (at a 99.5% confidence level). This was the kick-off for the plane-of-satellites problem. Following up this unexpected result and arguing that such planes should be common

if they have any physical meaning, Koch & Grebel (2006) found a plane-of-satellites around the Andromeda galaxy (= M 31).

These discoveries lead to a series of publications over the years (e.g. Metz et al. 2007, 2008; Angus et al. 2011; Pawlowski et al. 2011, 2012b; Shaya & Tully 2013; Pawlowski et al. 2014, 2015a; Libeskind et al. 2015; Cautun et al. 2015a; Sawala et al. 2016; Garaldi et al. 2018; Forero-Romero & Arias 2018 just to name a few), studying the phase-space correlation of the Local Group satellites with the advent of better and more accurate data, coming both from observations (Willman et al. 2005; Rekola et al. 2005; Belokurov et al. 2006; Koposov et al. 2015; Kim et al. 2015) and simulations (Genel et al. 2014; Sawala et al. 2016; Garaldi et al. 2018). One key finding was the discovery of coherently moving dwarf galaxies in the plane-of-satellites around M 31 (Ibata et al. 2013). This strongly suggests co-rotation around the Andromeda galaxy. The proper-motion measurements for the Milky Way satellites are highly uncertain (Koch & Grebel 2006) – due to our special observation position within the system – hence their true 3D motion is intensely debated. The discovery of phase-space correlated satellites around M31 underlines the reality of such structures.

Using kinematic information of pairs-of-satellites in SDSS, Ibata et al. (2014a) showed that co-rotation is quite common in the universe. This is an intriguing result, implying that we should discover more rotating structures if we just carefully search for them in the local universe. The discovery of a plane-of-satellites in the nearby Centaurus group (Tully et al. 2015; Müller et al. 2016) provide evidence that satellite planes are not just a special property of the Local Group, but are more common than anticipated.

4.2 In the Local Group

Co-rotating planes-of-satellites are found around the Milky Way – the so-called Vast Polar Structure (VPOS, Pawlowski & Kroupa 2013; Pawlowski et al. 2015b) – and around M 31 – the Great Plane of Andromeda (GPoA, Ibata et al. 2013). The calculated root-mean-square (rms) thickness for the VPOS is between 20 and 30 kpc, depending on which satellites are included as being part of the plane. Its extent corresponds to the virial radius of the Milky Way with $r_{virial} \approx 250$ kpc. A good estimate for the rms thickness is 21.3 kpc, using 34 satellite galaxies, including the recently discovered objects and excluding the outliers (Pawlowski et al. 2015b). Proper motion data is available for the 11 classical satellites[1], revealing that 7 to 9 out of the 11 satellites share a common orbital sense, which is aligned with the

[1] In the final weeks before the submission of this thesis the GAIA Data Release 2 updated and added new proper motions for several Milky Way satellites (Gaia Collaboration et al. 2018) which further enhanced the debate about the existence of the VPOS (Kallivayalil et al. 2018; Simon 2018; Fritz et al. 2018).

VPOS (Pawlowski & Kroupa 2013). It is encouraging that the picture of this planar structure is strengthened by the discovery of new Milky Way satellites (e.g. Kim et al. 2015). Furthermore, also a large population of young globular clusters and stellar and gaseous streams are part of the VPOS (Pawlowski et al. 2012b).

The other known planar structure is the GPoA around the Andromeda galaxy (Ibata et al. 2013). A survey of 400 deg^2 (McConnachie et al. 2009; Richardson et al. 2011; Martin et al. 2013) resulted in multiple detections of new satellites. From the 27 dwarf galaxies 15 lie in a remarkably thin plane, with a rms thickness of 14.1 kpc and extending to approximately ≈ 200 kpc. The plane is seen edge-on, opening the possibility to studying the kinematics using only the heliocentric velocities. Among the 15 satellites lying in the plane, 13 share a coherent movement, aligned with the plane (Ibata et al. 2013). As the satellites are bound objects, this motion can be explained by co-rotation of the dwarfs around the Andromeda galaxy, making it the second case of a co-rotating plane-of-satellites in the local universe.

4.3 Co-rotating planes in ΛCDM

The plane-of-satellites problem is best described by its three main characteristics (Pawlowski et al. 2015a):

1. Satellite galaxies are *aligned* in a highly flattened, planar structure.
2. Most of the satellites *share* the same orbital sense.
3. The satellites orbit *within* the plane.

The estimated probability of finding co-rotating satellite systems in ΛCDM simulations is very low. Depending on the constraints it is given as $< 0.1\%$ (e.g., Ibata et al. 2014b; Pawlowski et al. 2014) or 1% (Cautun et al. 2015a); both values are difficult to accommodate in the standard ΛCDM scenario. Therefore, the chance to observe two such systems in the local neighbourhood is diminishingly small, albeit not zero. Hence the key question for observational cosmology is the uniqueness of our Local Group. Do we find other similar systems in the local universe? If the Local Group is indeed only a statistical outlier we should detect no more of these structures, on the other hand, if satellite planes are more common than anticipated, we are missing a key element in our cosmological framework.

According to dark matter-only high-resolution simulations, the distribution of satellite galaxies are close-to isotropical with random orbital direction (Kroupa et al. 2005). The accretion of dark matter subhaloes in Milky Way-like hosts through infall from filaments will phase-mix and virialise the subhaloes, creating fairly isotropic distribution, with asymmetries up to only 15% (Aubert et al. 2004). Implementing baryonic physics should not change the resulting distribution of the satellites (Pawlowski et al. 2015a). As dwarf galaxies are dark matter dominated objects, the baryonic content only plays a minor role in their gravitational behaviour. However,

a recent publication by Ahmed et al. (2017) claims that baryonic physics will greatly alter the phase-space alignment of the satellites. Doing four Milky Way-mass dark matter simulations – each with baryonic physics turned on and off – the authors found that the detected planes in their simulations are different for the dark matter-only and the dark matter+baryons simulations, concluding that no dark matter-only simulation to date is comparable to observation. Be that as it may, this could very well be a selection effect – for the dark matter-only runs only the 30 most massive dark matter haloes at infall into the group were picked, assuming that those correspond to the 30 most luminous dwarf galaxies. Clearly this assumption can be challenged, as the too-big-to-fail problem revealed that the most luminous dwarf galaxies observed around the Milky Way reside only in medium sized dark matter haloes (Boylan-Kolchin et al. 2011).

There are several proposed solutions to save the current concordance model, all of which are unsatisfactory (see Pawlowski 2018 and references therein)[2]. Within the ΛCDM model, there are three main explanations given, i.e. accretion of subhaloes through filaments, infall of a single dwarf group, and tidal interactions. The first two options are already self-consistently implemented in the cosmological simulations and produce a small number of co-rotating structures. The filaments feeding the groups are too thick to produce the observed narrow planar structures. While infall as a single group naturally produces the coherent movement, the required rms extent of such groups would need to have a similar thickness as the observed planes-of-satellites. However, observed dwarf associations have a rms extent of 200 kpc and typically only 3-4 members.

There are several solutions tailored to the Local Group. Libeskind et al. (2015) proposed the expansion of the Tully Void as a possible mechanism to induce planar structures. The Local Group resides in a filament bordering the Tully Void and is compressed by its expansion and at the same time stretched by the nearby Virgo Cluster. However, *co-rotation* of the planes is not considered in this scenario. Another easier solution is given by Lipnicky & Chakrabarti (2017), who claim that the VPOS is not a dynamically stable structure. From the proper motion measurements Lipnicky & Chakrabarti (2017) calculated the orbits of the classical satellites backwards in time and found that the plane will disperse within a dynamical time. There are several concerns regarding their analysis. First and foremost, the mass of the Milky way is poorly constrained and mass estimates can differ by a factor of 5 (Watkins et al. 2010) – which is not considered by Lipnicky & Chakrabarti (2017). Another problem is the huge uncertainty of the proper motion measurements of the satellites, making a clear prediction of the evolution of the plane rather difficult. On a more philosophical level we could ask ourselves why we would live exactly in this special time where we observe such a planar structures around the Milky Way and the Andromeda galaxy, if they are just transient objects. The work by Lipnicky & Chakrabarti (2017)

[2] A recent review on the plane-of-satellites problem including all relevant literature.

reveals a fundamental difficulty in the small-scale community. How do we compare simulations to observations? With their simulations the authors only showed that their chosen set of parameters does not result in a stable mock-VPOS. But this set was only one of many configurations most of which weren't tested. Only if the *complete* parameter space was tested and every single configuration dissipated, the claim that the observed VPOS cannot be a stable structure would be valid.

In summary, even though there are claims that the plane-of-satellite problem is no problem at all (e.g. Maji et al. 2017a,b, but see Pawlowski et al. 2017 for an immediate rebuttal from the community), the existence of such co-rotating structures is evident by observations. As Hubble (1936) has stated, for a theory to persist it must survive the process of elimination through observations – certainly not vice versa.

4.4 Tidal remnants – a solution to the plane-of-satellites problem?

While accretion of subhaloes by infall through filaments cannot satisfactorily produce the observed planes, there is another proposed scenario, namely, creating Tidal Dwarf Galaxies (TDG) in a tidal interaction. Interestingly, these second generation objects were first invoked to explain the VPOS by Lynden-Bell (1976). In an interaction between two massive galaxies, tidal arms will form along the plane of interaction. These tidal arms – consisting of gas and stars – will collapse under their own gravity and form TDGs. These TDGs will inherit the angular momentum and start to co-rotate around the host capturing the dwarf (e.g. Hammer et al. 2013).

However, there are also several caveats to this scenario. First and foremost, TDGs will contain no dark matter – the spherical dark matter halo is dynamically too hot to be disturbed by such an interaction. Observations from Local Group dwarfs suggest the existence of a large amount of dark matter in these objects. Some of those have over 1000 times more inferred mass than what is seen by the light of stars (see McConnachie 2012, and references therein). One way to alleviate this tension is by questioning the assumption that these objects have to be relaxed (Hammer et al. 2018a). Only if the observed dwarfs are indeed relaxed their masses can be estimated by the virial theorem. Another more severe approach would be modifying the underlying gravity model, i.e. with Modified Newton Dynamics (Milgrom 1983). Second, the Star Formation History (SFH) for each of these TDGs should roughly be the same. Again, observations of the Local Group dwarfs show a variety of different SFHs (Tolstoy et al. 2009). And third, the metallicities of these TDGs also should be (roughly) the same, because they were formed from the same material from the progenitor galaxy. Again, observations show a plethora of metallicities for the dwarf galaxies in the Local Group (McConnachie 2012).

Nevertheless, the suggestion that the planes-of-satellite members are TDG is an intriguing option. High-resolution simulations within the ΛCDM paradigm (Hammer et al. 2013, 2018b), as well as MONDian simulations (Bílek et al. 2017; Banik et al. 2018), have shown the creation of planes-of-satellites in tidal interactions, explaining the abundance of nearby observed planes-of-satellites, but on the other hand bringing the previously discussed problems with them.

4.5 Outside the Local Group

The appearance of two co-rotating planes-of-satellites in the Local Group naturally raises the question about the frequency of these structures in the nearby universe. Is the Local Group unique in this respect, or is this a common phenomenon? This is one of the key questions aimed to answer in this thesis.

A first indication that there is indeed more phase-space correlation than expected is given by an over-abundance of spectroscopically confirmed co-rotating pairs-of-satellites in SDSS (Ibata et al. 2014a), a result which was followed by a series of papers debating the results' significance (Cautun et al. 2015b; Ibata et al. 2015; Phillips et al. 2015). The main disagreement was about the extent of the satellite system: Cautun et al. (2015b) claim that the signal weakens when considering satellites at radii $> 150\,\mathrm{kpc}$. Ibata et al. (2015) addressed the raised concerns, extended the analysis and confirmed their previous findings. Further Ibata et al. (2015) studied the appearance of such correlated structures in ΛCDM simulations where such an over-abundance is indeed not expected.

The discovery of co-rotating *planes-of-satellites* outside the Local Group would be a strong indication that this phenomenon is more frequent than expected. A perfect testbed for such studies is the nearby Centaurus group in the southern hemisphere. Tully et al. (2015) found two parallel planes of satellites around Cen A, the major galaxy in the Centaurus group. However, with subsequent discoveries of new dwarf galaxies in this group by Crnojević et al. (2016) and us (see Section 5.1 and 5.2) we showed that there is likely only one thicker plane, which is discussed in Section 5.6. Additionally we propose the possibility of another plane of satellites around M 83 – the second major galaxy in the Centaurus group – based on newly measured distances, see Section 5.5. The question about co-rotation within the plane around Cen A is finally discussed in Section 5.7. A thin planar arrangement of galaxies in the M 101 galaxy group is presented in Section 5.3.

5 Results published in peer-reviewed journals

> *"You can lead a theorist to data, but you can't make him think."*
>
> **— Professor Stacy McGaugh**
> @DudeDarkMatter, hero to some; nightmare to others.

The next seven Sections correspond to the first-author papers I have published during my PhD studies (Müller et al. 2015, 2016, 2017a,b, 2018a,b,c).

In Sections 5.1 - 5.4 we present newly discovered dwarf galaxy candidates in the Local Volume for the Centaurus group, the M 101 group, and the Leo-I group based on deep photometric images taken with the Dark Energy Camera and the Sloan Digital Sky Survey. Surface photometry is performed for all new dwarf candidates and their structural parameters are compared to other known dwarfs to estimate memberships of the groups.

In Section 5.5 a first follow-up of three of the dwarf galaxy candidates of the Centaurus group (presented in Section 5.1) is conducted to measure the distances by resolving the tip of the red giant branch stars using the Very Large Telescope under excellent seeing conditions. PSF photometry is applied to create a Colour-Magnitude diagram and obtain the distance with a Sobel Edge detection.

In Sections 5.6 and 5.7 we will focus on the plane-of-satellites in the Centaurus group, where we apply statistical methods to test the bimodality of the structure suggested by Tully et al. (2015) by using our newly discovered dwarf galaxies, study the geometrical alignment of the apparent plane, and the kinematics of the satellite distribution using archival line-of-sight velocities.

5.1 New dwarf galaxy candidates in the Centaurus group

— Oliver Müller, Helmut Jerjen, Bruno Binggeli —

Astronomy & Astrophysics, 2015, 583, A79

Abstract

Recent studies of the distribution and kinematics of the Milky Way and Andromeda satellite galaxy systems have confirmed the existence of coplanar, corotating structures of galaxies. In addition to the 'missing satellite problem', these structures pose a major challenge to the standard ΛCDM scenario of structure formation. We complement the efforts made by the dwarf galaxy community to extend these studies to other nearby galaxy groups by systematically searching for faint unresolved dwarf members with a low surface brightness in the Southern Centaurus group of galaxies. The aim is to determine whether these coplanar, corotating structures are a universal phenomenon. We imaged an area of 60 square degrees (0.3 Mpc^2) around the M 83 subgroup with the wide-field Dark Energy Camera (DECam) at the CTIO 4 m Blanco telescope in g and r down to a limiting surface brightness of $\mu_r \approx 30$ mag arcsec^{-2}. Various image-filtering techniques were applied to the DECam data to enhance the visibility of extremely low-surface brightness objects. We report the discovery of 16 new dwarf galaxy candidates in the direction of the M 83 subgroup, roughly doubling the number of known dwarfs in that region. The photometric properties of the candidates, when compared to those of the Local Group, suggest membership in the M 83 subgroup. The faintest objects have a central star density of $\approx 1.3\,L_\odot$ pc^{-2} and a total magnitude of $g = 20.25$, corresponding to $M_g = -9.55$ at the nominal distance of 4.9 Mpc. The sky distribution of the new objects is significantly prolonged toward Cen A, suggesting that many of them belong to the Cen A subgroup or a common halo. We also provide updated surface photometry for the brighter, known dwarf members in the surveyed area. Modern survey CCD cameras and sophisticated detection algorithms can be used to systematically probe the faint end of the galaxy luminosity function around the M 83 subgroup of galaxies. We aim at finding more and fainter members over a larger area to obtain a complete picture of the satellite galaxy substructure in the Centaurus group down to a total magnitude limit of $M_V \approx -10$.

1. Introduction

Dwarf galaxies are key objects for the study of structure formation on galaxy scales. In particular, dwarf spheroidals are traditionally known to host large amounts of dark matter (DM) as inferred by their internal dynamics (e.g., Simon & Geha 2007;

Walker 2013). The mere abundance and large-scale distribution of these systems are an important testbed for DM and structure formation. There is the heavily discussed so-called missing satellite problem, which describes the observed deficiency of dwarf satellites around the Milky Way galaxy when compared to the CDM prediction of DM subhalo numbers (Moore et al. 1999; Klypin et al. 1999; Diemand et al. 2006, 2008). This discrepancy has not been substantially diminished by the discovery of numerous ultra-faint Milky Way satellite galaxies in the Sloan Digital Sky Survey (SDSS) and other surveys (e.g., Willman et al. 2005; Koposov et al. 2015, and references therein). An even stronger challenge to structure formation with DM is posed by the highly asymmetric features in the distribution of dwarf satellites around the best-studied Milky Way and Andromeda galaxies. The Vast Polar Structure (VPOS) of the Milky Way (Pawlowski et al. 2012b, 2015b) and the Great Plane of Andromeda (GPoA, Ibata et al. 2013) are planar structures that are difficult to accommodate in a standard ΛCDM scenario (e.g., Pawlowski et al. 2014, and references therein).

In the context of the existing disagreement between near-field cosmology observations and the predictions of the best cosmological models on galaxy scales, it is imperative to extend such studies on the abundance and distribution of dwarf galaxies to other nearby galaxy aggregates beyond the Local Group (LG), to see whether or not the relative sparseness and asymmetric distribution of faint dwarf satellite galaxies is a common phenomenon in the nearby Universe. Given the extreme surface brightness regime of the target galaxies and the large angular extents of nearby galaxy groups, this poses an observational challenge. There is of course no hope, for many years to come, that we will be able to map the analogs of the ultra-faint ($M_V \geq -8$) dwarfs swarming around the Milky Way at larger distances. But present-day technology allows us to aim at a dwarf galaxy census of other nearby groups down to $M_V \approx -10$, cleary surpassing the achievements of the photographic Schmidt surveys and the SDSS. Very recently, Tully et al. (2015) have reported hints of a double-planar structure in the Centarus group of galaxies, based on previously known (i.e., still fairly bright) dwarf members of the group. This is encouraging because it means that a study of the distribution of faint, but not necessarily ultra-faint, dwarfs in the nearby groups will provide important constraints for structure formation models.

Several teams have taken up the effort to conduct dedicated deep, wide-field imaging surveys of nearby galaxy groups in the local volume closer than 10 Mpc (Karachentsev 2005; Karachentsev et al. 2013) to detect ever fainter dwarf galaxy members. In the northern hemisphere this was successfully done by Chiboucas et al. (2009, 2013) for the M 81 group and by Merritt et al. (2014) for the M 101 group. In the same spirit, we have started a survey of the Centaurus and Sculptor groups in the southern hemisphere, based on images taken with the Dark Energy Camera (DECam) at the 4m Blanco telescope at Cerro Tololo Inter-American Observatory

(CTIO) and the SkyMapper telescope of the Australian National University. A similar imaging survey of the two groups, albeit much more restricted in sky area but to greater depths, is underway (Sand et al. 2014).

In this paper we report on our first harvest of candidate dwarf members in a region of 60 square degrees of the Centaurus group around M 83. The Centaurus group is the richest and most massive group of galaxies in the local volume at a distance of $\approx$ 4 Mpc (Kraan-Korteweg & Tammann 1979; Jerjen et al. 2000a, Fig. 2 therein, and following references), covering a huge area of $\approx$ 500 square degrees of southern sky. It can be considered the southern analog to the similarly rich and nearby M 81 group in the northern hemisphere. As a result of various studies of the region conducted in the late 1990s that aimed to find new group members in the optical (Cote et al. 1997; Karachentseva & Karachentsev 1998; Jerjen et al. 2000a) and at 21 cm (Banks et al. 1999), and the subsequent membership confirmation by distance measurements (Jerjen et al. 2000b; Karachentsev et al. 2002), there are around 60 Centaurus group members known to date (see Karachentsev et al. 2002, 2014). We note that the optical surveys mentioned above were all based on the same Schmidt photographic plates; an SDSS analog for the southern hemisphere with the SkyMapper telescope (Keller et al. 2007) has only just started. The Centaurus group has a pronounced bimodal structure, consisting of a larger aggregate centered on the massive peculiar galaxy NGC 5128 = Centaurus A at a mean distance of 3.8 Mpc, and a smaller galaxy concentration around the giant spiral NGC 5236 = M 83 at a mean distance of 4.9 Mpc (Karachentsev et al. 2002, 2014; Tully et al. 2015; Tully 2015b). In the following, we refer to the main concentrations as the Cen A and M 83 subgroup, respectively, the whole complex as the Centaurus group, or also Centaurus A group, as it is known in the literature up to the present.

The paper is organized as follows. In Sect. 2 we give the details of the imaging with DECam. Section 3 describes the techniques and the results of our search for faint diffuse dwarfs on the observed fields. In Sect. 4 we report on the photometry done for the new candidates as well as the known Cen members in the search area. Finally, a critical discussion of our findings is given in Sect. 5, followed by our concluding remarks in Sect. 6.

2. Imaging

Observations were conducted on 2014 July 17-19 using the Dark Energy Camera (DECam) at the CTIO 4m Blanco telescope as part of observing proposal 2014A-0624 (PI: H. Jerjen). DECam has an array of sixty-two 2k $\times$ 4k CCD detectors with a 3 sqr deg field of view and a pixel scale of 0.27 arcsec per pixel (unbinned). We obtained a series of 3$\times$40 s dithered exposures in g and r bands under photometric conditions for 22 pointings with slight overlap. The mean seeing was 1.0 arcsec in both filters. The fully reduced and stacked images were produced by the DECam community

pipeline (Valdes et al. 2014). Figure 1 shows the surveyed area around M 83 with the known galaxies highlighted with filled circles. The new dwarf galaxy candidates are shown as stars.

For the photometric calibration, we regularly observed Stripe 82 of the SDSS throughout the three nights with 50 s single exposures in each band. To determine the photometric zero points and color terms, we matched the instrumental magnitudes of stars with the Stripe 82 stellar catalog to a depth of 23 mag and fit the following equations:

$$m_g = m_{g,instr} + Z_g + c_g \cdot (m_{g,instr} - m_{r,instr}) - k_g X$$

$$m_r = m_{r,instr} + Z_p + c_r \cdot (m_{g,instr} - m_{r,instr}) - k_r X,$$

where Z_g and Z_r are the photometric zero points, c_g and c_r are the respective color terms, k_g and k_r are the first-order extinctions, and X is the mean airmass. The best-fitting parameters are $Z_g = 29.41$, $Z_r = 29.45$, $c_r = 0.126$, and $c_g = 0.092$. The most recent extinction values $k_r = 0.10$ and $k_g = 0.20$ for CTIO were obtained from the Dark Energy Survey team, and the airmass X was given for the respective exposure. To allow for a direct comparison with Local Group dwarfs, we converted the gr photometry into the V band (Lupton 2005) using the transformation equation

$$V = g - 0.5784 \cdot (g - r) - 0.0038 \ .$$

This formula applies to m and μ. For the comparison of the Sérsic parameters with Virgo and LG dwarfs we had to convert them from B into r band (Lupton 2005) assuming a color index of 0.6 (Lisker et al. 2008)

$$r = B - 0.6 - 0.3130 \cdot 0.6 - 0.2271 \ .$$

3. Search and detection of new dwarf candidates

With the chosen equipment and exposure time we do not expect any new dwarf spheroidal candidate at the distance of M 83 to be resolved into stars. Taking the stellar population of the Sculptor dSph as a reference, we can assume $M_I = -4.1$ and $V - I = 1.5$ for the TRGB of an old stellar population (Rizzi et al. 2007a). With $V - r \approx 0.2$ this translates into $M_r \approx -2.8$, or at a distance of 4.9 Mpc and with $A_r = 0.15$ (see Table 2) into an expected r-band magnitude of 25.8 for the RGB tip. In comparison, the faintest stars on our DECam fields turned out to have m_r between 25.0 and 25.5. Hence we clearly miss the tip, that is, we lack the stellar resolution of the suspected dwarf members of the M 83 subgroup. The search for new dwarf candidates is therefore a search for extended unresolved objects with a very low surface brightness in the fields.

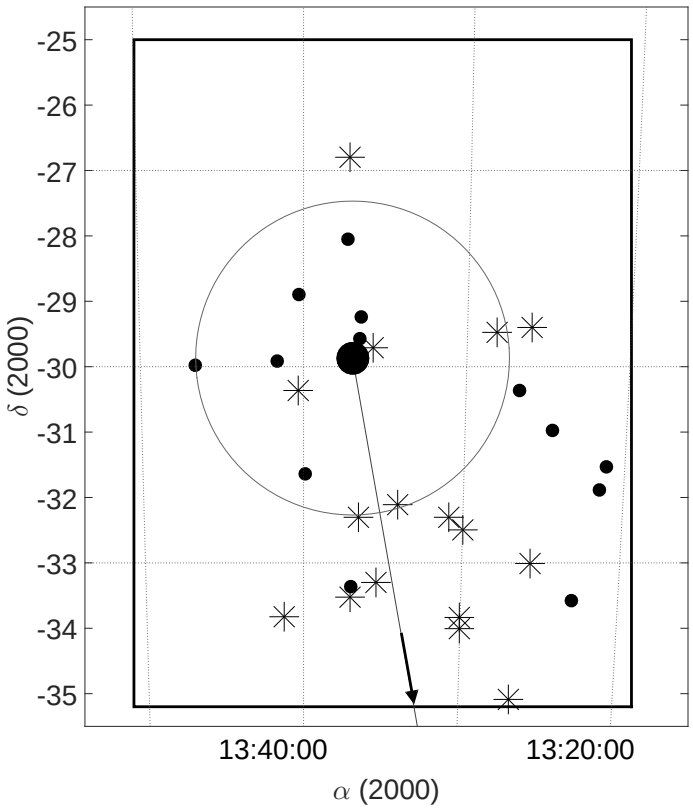

Fig. 1: Survey area of 60 sqr degrees (rectangle) around the galaxy M 83 (large filled circle). The newly detected dwarf galaxy candidates are indicated with stars. Small filled circles are known M 83 group members. The large circle indicates the virial radius of the M 83 subgroup (see text). The vector points toward the Cen A galaxy. We note an overdensity of new dwarfs in that direction.

Different filtering techniques and gray-level manipulations were applied to enhance the contrast and low surface brightness features on the images. Each of the reduced g and r frames were individually visually inspected and then stacked and inspected again. The dynamical range of the screen display was set so that the lowest and highest level was 2 sigma above and below the sky background. This provides the optimal resolution in the intensity regime where we expect the low surface brightness features of faint dwarf galaxies. The most important advantage of observing the g and r frames separately is that we can rule out artifacts such as noise fluctuations or scattered light. Finally, we used two different filtering techniques, a Gaussian convolution and the ring median filter (Secker 1995), to enhance the images even further. The ring median filter replaces each pixel value with the median of a narrow annulus around the pixel at a characteristic radius r_c. This filter has the effect of removing objects smaller than r_c but leaving objects larger than r_c mostly unaffected. Using these two filters in combination with different values for kernel width and radius revealed the same number of low surface brightness dwarf candidates. We note that the discovery rate by naked eye is surprisingly high in comparison with computer-based detections. Chiboucas et al. (2009) and Merritt et al. (2014) drew similar conclusions. The list with the coordinates of the 16 new dwarf galaxy candidates is presented in Table 1. A gallery of the r-band images of the candidates is given in Fig. 2.

Tab. 1: Names and coordinates (epoch 2000.0) of the new dwarf candidates.

Name	α	δ	Notes
dw1325-33	13:25:41	−33:00:25	
dw1326-29	13:26:04	−29:24:16	Irr?
dw1326-35	13:26:44	−35:05:00	
dw1328-29	13:28:12	−29:28:45	
dw1329-32	13:29:58	−32:29:46	BCD?
dw1330-32	13:30:54	−32:18:21	
dw1330-33	13:30:04	−33:50:06	Background?
dw1330-34	13:30:02	−34:00:14	
dw1334-32	13:34:05	−32:06:28	Cirrus?
dw1335-29	13:35:46	−29:42:24	
dw1335-33	13:35:25	−33:18:00	Cirrus?
dw1336-32	13:36:33	−32:18:05	
dw1337-26	13:37:13	−26:48:10	
dw1337-33	13:37:02	−33:31:25	
dw1340-30	13:40:19	−30:21:35	
dw1341-33	13:41:13	−33:49:30	

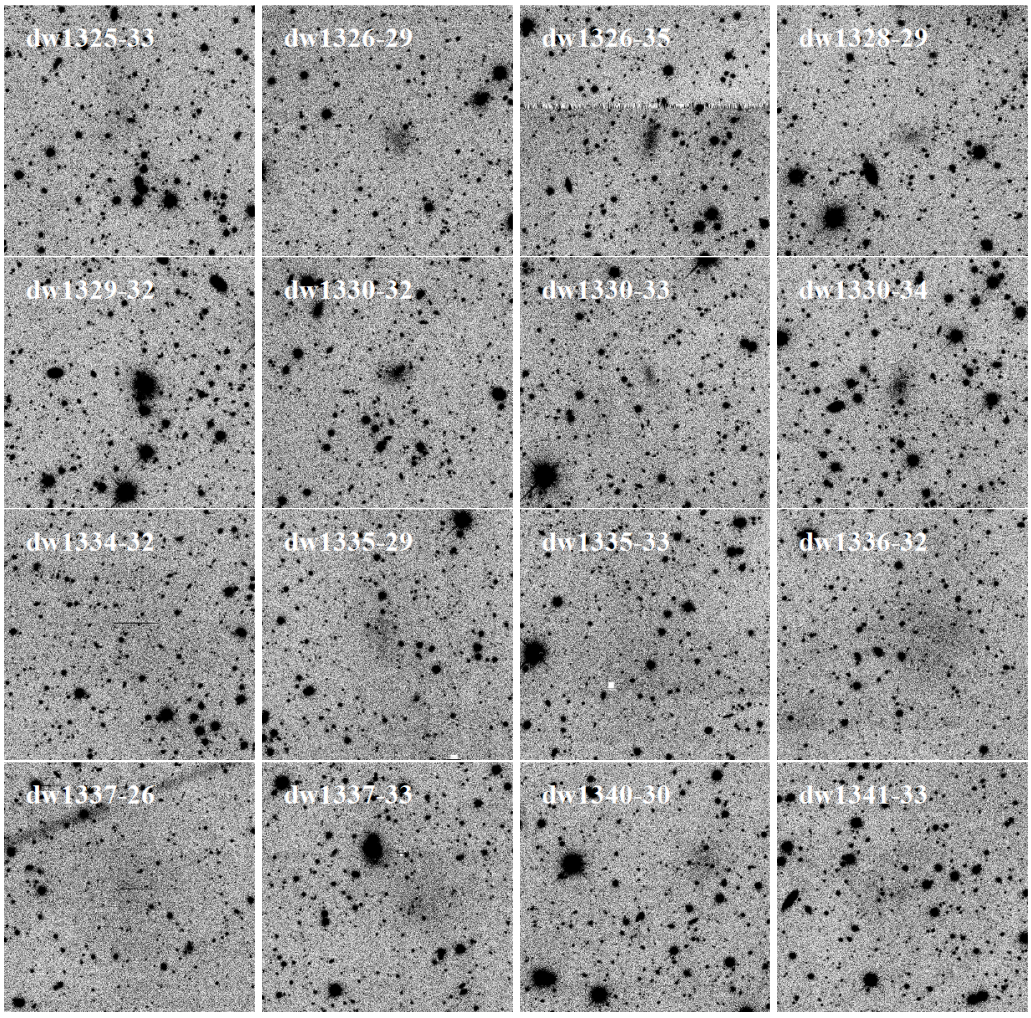

Fig. 2: Gallery of r-band images of all new M 83 subgroup dwarf galaxy candidates. One side of an image is 4.5 arcmin or 6.6 kpc at 4.9 Mpc.

We note that the relatively high Galactic foreground in the direction of the M 83 subgroup could be a major obstacle when searching for new dwarf candidates. Therefore we reanalyzed the DECam images after removing foreground stars with the Otsu threshholding method (Otsu 1979) and with SourceExtractor (Bertin & Arnouts 1996). No more dwarf galaxy candidates have been detected with these methods. Another difficulty of high Galactic foreground is the presence of very faint, low surface brightness cirrus clouds (reflection nebulae), which can closely mimick faint dwarf galaxies. This is a known problem also in the region of the M 81 group (Chiboucas et al. 2009). Most cirrus is, however, morphologically distinct due to its large angular size, flat SB profile, or the presence of sharp edges. Still, in two cases (candidates dw1334-32 and dw1335-33, see Table 1) we cannot entirely exclude the possibility that we were misled in this way. The two objects are huge (Fig. 2), very flat (Fig. 5), and one of them (dw1334-32) is also unusually blue (Table 2).

To assess the efficiency and brightness limitations of our detection methods, we blindly added a number of artificial galaxies to several fields at random positions. Assuming exponential profiles (i.e., Sérsic $n = 1$, which is roughly fulfilled by our candidates, see below), the r-band total magnitude and central surface brightness of the fake galaxies were varied from $m_r = 17$ to 20 mag and from $\mu_{0,r} = 25$ to 18 mag arcsec^{-2}, respectively. In this way, judged a posteriori, the brightest galaxies would certainly be visible or detectable, the faintest galaxies certainly not. Varying the two parameters independently in half-magnitude steps led to a set of $7\times7 = 49$ artificial galaxies that were ingested in one field (corresponding to one of the 22 pointings). As the whole region is densely covered with stars and occasionally also cirrus patches, which will render the detectablity of a faint dwarf difficult, the same set of artificial galaxies was randomly placed five times in a given field. If a test galaxy with a given magnitude and surface brightness was discovered by the same methods used for the real galaxies in one or more cases, it was judged as detectable in principle. The number of its detection at different random positions is then a measure of the detection efficiency. This whole procedure was applied for five fields (pointings) distributed over the whole search area (one central field and four fields toward the corners) to test for positional variations.

Figure 3 gives an impression of an artificial galaxy as compared to a real one with the same photometric parameters. Figure 4 gives the results of the whole test procedure. Shown are the 49 parameter combinations of the artificial galaxies in the $\mu - m$ plane with their efficiency values averaged over all five fields (0 = no detection, 10 = 100% detection). As expected, the detection limit is primarily given by the surface brightness. Below a central μ of 27, our artificial galaxies could rarely be recovered (if so, then it was more likely due to a mismatch with sky background noise). $\mu_{0,r} = 27$ mag arcsec^{-2} is indeed also the surface brightness limit of our dwarf candidates (see Fig. 6 and Table 2). The recovery efficiency is 80 to 90% for bright galaxies (at the upper left in the $\mu - m$ plane), significantly dropping near

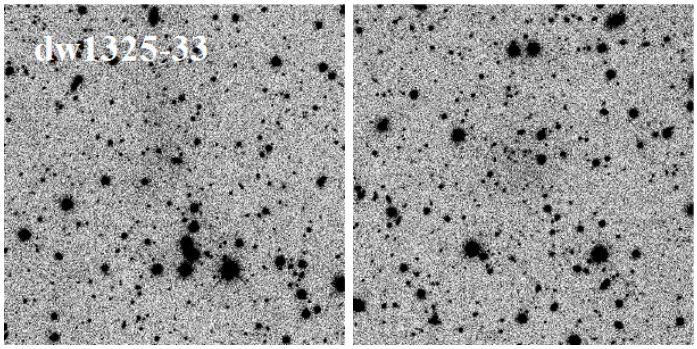

Fig. 3: Dwarf candidate dw1325-33 (left) and its artificial twin at a random position (right), easily detectable at a $\mu_{0,r} \approx 26$ mag arcsec^{-2} .

the surface brightness limit (downward), but also, albeit to a lesser degree, with increasing compactness (steeper profile, toward the right in the $\mu - m$ plane). As the typical dwarf galaxy is discovered by its characteristic low surface brightness *and* flat profile, this is no surprise. Classically, a completeness boundary for a galaxy survey is drawn on the assumption that all galaxies that are larger than a given diameter (= 2 r_{lim}) within a given isophotal level of μ_{lim} are detected. For exponential profiles this two-parametric completeness limit turns into the form (see Ferguson 1990; Ferguson & Sandage 1988)

$$m_{tot} = \mu_0 - 5\log(r_{lim}) - 2.18 + 5\log(\mu_{lim} - \mu_0)$$

With r_{lim} = 20 arcsecs and μ_{lim} = 28 mag arcsec^{-2} (in the r or V band, there is only a $\approx$ 0.2 mag difference), this curve gives a fair description of the completeness boundary for our real dwarf candidates, as shown in Fig. 6 below. The same curve is plotted here in Fig. 4 for the artificial galaxies. Clearly, some of the more compact (steep profile) artificials recovered as possible dwarfs fall outside (to the right) of this completeness boundary. With one exception, no dwarf candidates in the corresponding parameter range were found, which is of course due to the $\mu - m$ relation for dwarf galaxies (see Fig. 6).

We finally note that no positional variation of the detection efficiency was found. Differences among the five fields are within Poisson noise. This is indeed expected because there is no strong stellar density gradient over the face of the survey area.

We did not attempt to morphologically classify our dwarf candidates at this stage of first imaging. Most of them will, once confirmed, be dwarf spheroidals. Two candidates show signs of irregularity, as noted in Table 1. One of them is a possible blue compact dwarf (BCD, dw1329-32) according to a clear hint of resolution into (presumably) knots of active star formation. We note that our search for new dwarf members is clearly biased toward low surface brightness objects through the adopted search method. There might be more dwarf members of a compact nature.

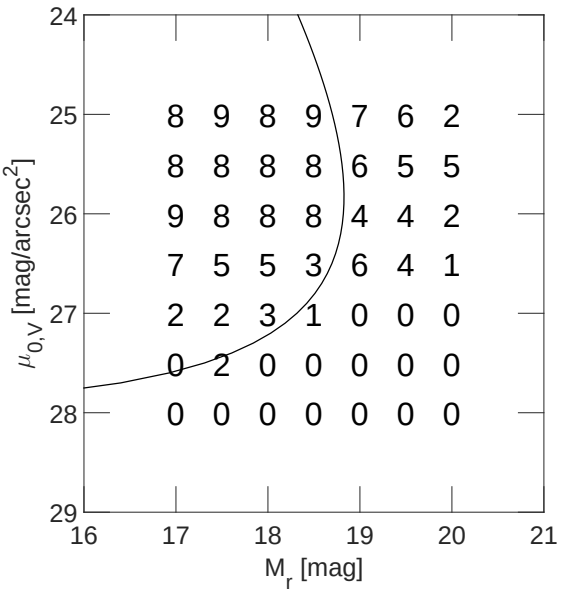

Fig. 4: Set of 49 artificial galaxies in the $\mu - m$ plane. The numbers indicate the detection efficiency (0 = no detection, 1...10 = 10%...100% detection). The curve gives a completeness boundary for the real dwarf candidates (see text and Fig. 6).

4. Photometry

Surface photometry was measured for all new dwarf galaxy candidates and for twelve of the thirteen known dwarfs in the survey area (KK208 (Karachentseva & Karachentsev 1998) was dismissed because it lacks a well-defined center). Great care was taken when removing foreground stars and background galaxies in the vicinity of the dwarf galaxy candidate by replacing the affected pixels with patches of sky from the surrounding area. The IRAF command $radprofil$ written by one of us was used to compute the total instrumental apparent magnitude m_{instr}, the effective radius r_{eff}, mean effective surface brightness $\langle\mu\rangle_{eff}$, and the best-fitting Sérsic (Sersic 1968) parameters r_0, μ_0 , and n in both g and r bands. The center of each object was estimated from the faint outer isophotes, which does not necessarily coincide with the peak surface brightness. The sky brightness was determined from the asymptotic behavior of the galaxy growth curve (cumulative intensity profile). We measured the radial surface brightness profile with a radial step size of 1.35 arcsec, except for dw1330-33, where a smaller step size of 0.54 arcsec was required given the small angular size of the galaxy. All profiles are shown in Fig. 5. Sérsic profiles were fitted at the surface brightness profiles using the equation

$$\mu_{sersic} = \mu_0 + 1.0857 \cdot \left(\frac{r}{r_0}\right)^n$$

where μ_0 is the Sérsic central surface brightness, r_0 the Sérsic scale length, and n the Sérsic curvature index. We note that some authors use $1/n$ instead of n.

We give a general error estimate for magnitudes on the order of 0.3. Errors arise from the star subtraction ($\approx$ 0.2 mag, difference in magnitude between the galaxy with star removal and without), zero-point calibration (less than 0.04 mag) and

the determination of the sky from the variation of the asymptotic growth curve ($\approx$ 0.2 mag, given by the highest and lowest value of the sky level where the end of the growth curve is still asymptotically flat). For absolute magnitudes there are the additional errors based on the assumed distance (0.5 mag for an uncertainty in distance of ± 0.5 Mpc) and Galactic extinction (typically 0.015 mag). We assumed a mean distance for the M 83 subgroup of 4.9 Mpc (Karachentsev et al. 2002, 2014). If some of the candidates are found to belong to the closer Cen A subgroup (see below), they would be intrinsically brighter by up to 0.7 mag. Uncertainties for the half-light radius $\Delta r_{eff} = 1.3$ arcsec and the mean effective surface brightness $\Delta\langle\mu\rangle_{eff} = 0.01$ mag, not accounting for the magnitude uncertainty, were again determined by the variation of the growth curve. The errors for the Sérsic parameters are based on numerics and are given in Table 2. We note that the galaxy NGC 5264 was located at the edge of the DECam image and thus has a higher level of uncertainty.

Three of the already known dwarfs (CenA-dE2, Cen8, and CenA-dE4) are part of the sample of Jerjen et al. (2000a). A comparison of the photometric parameters shows good agreement; differences in magnitudes and surface brightness are within 0.3 mag. A systematic comparison of our photometry with other mostly much older literature sources is beyond the scope of this paper. To check the internal consistency of our photometry, we also applied our surface photometry machinery to a number of our artificial galaxies (Sect. 3). The central surface brightness could always be reproduced to within 0.1 mag, the exponential scale to within a factor of 1.1. To reproduce the total magnitude to within less than 0.3 mag, we had to choose an extra-large aperture; real galaxies obviously have a cutoff and do not extend to infinity as the exponential model does. These artificial galaxy tests have confirmed the error estimates we reported above. The photometry we present, of the candidates and the known dwarfs alike, has the main purpose of assessing the plausibility of our candidates as dwarf members of the Centaurus group.

In Table 2 we present the photometric data of all dwarf candidates and known dwarfs in the survey area. For KK208 we were unable to do photometry because it lacks a well-defined center. The items listed are as follows: (1) Name of candidate or previously known dwarf. (2) Total apparent magnitude in the r band. (3) Total apparent magnitude in the g band. (4) Galactic extinction in r according to Schlafly & Finkbeiner (2011). (5) Galactic extinction in g according to Schlafly & Finkbeiner (2011). (6) Absolute magnitude in the r band. The assumed distance for the candidates is 4.92 Mpc. For the known dwarfs TRGB distances were adopted according to Karachentsev et al. (2013). CenA-dE2, CenA-dE4, and CEN8 have no TRGB distance, therefore the nominal distance of 4.92 Mpc is applied. (7) Extinction-corrected color index $g - r$. (8) Sérsic central surface brightness in the r band. (9) Sérsic scale length in the r band. (10) Sérsic curvature index in the r band. (11) Mean effective surface brightness in the r band. (12) Effective radius in the r band.

Tab. 2: Photometric parameters of the candidates and the known dwarf galaxies in the M 83 subgroup.

Name	m_r	m_g	A_r	A_g	M_r	$(g-r)_0$	$\mu_{0,r}$	$r_{0,r}$	n_r	$\langle\mu\rangle_{eff,r}$	$r_{eff,r}$
	mag	mag	mag	mag	mag	mag	mag arcsec^{-2}	arcsec		mag arcsec^{-2}	arcsec
(1)	(2)	(3)	(4)	(5)	(6)	(7)	(8)	(9)	(10)	(11)	(12)
dw1325-33	18.45	18.87	0.177	0.227	-10.19	0.37	26.06 ± 0.17	19.65 ± 3.24	0.89 ± 0.11	26.88	18.64
dw1326-29	17.85	18.67	0.142	0.205	-10.75	0.75	25.09 ± 0.08	15.32 ± 0.99	0.72 ± 0.05	25.63	13.67
dw1326-35	18.13	18.80	0.142	0.205	-10.47	0.61	24.31 ± 0.12	7.56 ± 0.99	1.02 ± 0.09	25.27	10.29
dw1328-29	18.45	19.01	0.126	0.182	-10.14	0.51	24.76 ± 0.22	6.07 ± 1.73	1.37 ± 0.17	26.12	12.88
dw1329-32	16.65	17.29	0.124	0.179	-11.94	0.59	22.84 ± 0.02	8.83 ± 0.15	0.71 ± 0.02	23.43	8.83
dw1330-32	18.17	18.96	0.115	0.166	-10.40	0.74	24.71 ± 0.07	11.28 ± 0.63	0.63 ± 0.05	25.09	9.42
dw1330-33	19.05	20.43	0.139	0.2	-9.55	1.32	24.54 ± 0.09	7.40 ± 0.58	0.76 ± 0.08	25.05	6.30
dw1330-34	18.05	18.91	0.135	0.195	-10.55	0.80	24.38 ± 0.10	8.10 ± 0.89	1.05 ± 0.08	25.25	10.72
dw1334-32	18.13	18.27	0.134	0.194	-10.47	0.08	26.97 ± 0.48	52.49 ± 27.27	1.14 ± 0.50	28.14	38.32
dw1335-29	17.82	18.87	0.104	0.151	-10.74	1.00	25.85 ± 0.09	27.31 ± 1.66	0.56 ± 0.05	26.36	20.22
dw1335-33	17.25	18.56	0.126	0.182	-11.33	1.25	26.87 ± 0.09	57.74 ± 2.97	0.44 ± 0.07	27.24	39.37
dw1336-32	16.81	17.89	0.13	0.188	-11.78	1.03	25.88 ± 0.07	37.19 ± 2.41	0.83 ± 0.07	26.53	34.62
dw1337-26	17.34	18.23	0.141	0.204	-11.26	0.82	25.34 ± 0.35	11.78 ± 6.49	1.69 ± 0.32	27.07	34.61
dw1337-33	17.20	17.82	0.114	0.165	-11.37	0.56	25.30 ± 0.16	17.99 ± 3.44	1.19 ± 0.13	26.30	25.51
dw1340-30	17.86	18.70	0.132	0.191	-10.73	0.78	25.50 ± 0.10	18.96 ± 1.81	0.81 ± 0.10	26.03	16.86
dw1341-33	17.20	18.22	0.11	0.159	-11.37	0.97	25.05 ± 0.49	4.88 ± 5.64	2.70 ± 0.62	27.00	35.43
KK195	16.63	16.82	0.14	0.20	-12.10	0.12	24.01 ± 0.07	13.33 ± 0.84	0.88 ± 0.05	24.79	16.36
CenA-dE2	16.93	17.74	0.15	0.22	-11.68	0.74	24.51 ± 0.06	17.78 ± 0.83	0.69 ± 0.04	25.05	16.34
Cen8	16.40	17.16	0.16	0.23	-12.22	0.70	23.22 ± 0.03	11.56 ± 0.35	0.74 ± 0.03	23.85	12.04
KK200	14.66	15.44	0.16	0.23	-13.82	0.70	22.00 ± 0.03	10.21 ± 0.29	1.15 ± 0.01	23.32	21.05
IC4247	13.46	14.05	0.15	0.21	-15.17	0.52	20.14 ± 0.02	7.62 ± 0.14	$1,12 \pm 0.01$	21.44	15.32
ESO444-78	14.47	15.09	0.12	0.17	-14.25	0.56	22.11 ± 0.01	15.70 ± 0.24	0.83 ± 0.02	22.92	19.10
HI J1337-33	16.81	17.28	.11	0.16	-11.50	0.42	21.76 ± 0.03	4.36 ± 0.09	0.85 ± 0.01	22.70	5.77
ESO444-84	14.25	14.71	0.16	0.23	-14.23	0.39	22.47 ± 0.02	22.59 ± 0.24	0.65 ± 0.01	22.98	21.39
NGC5253	9.85	10.36	0.13	0.18	-18.03	0.45	16.88 ± 0.02	6.11 ± 0.13	1.79 ± 0.04	19.24	29.15
IC4316	12.90	13.64	0.13	0.18	-15.44	0.69	20.99 ± 0.02	12.64 ± 0.29	1.30 ± 0.02	22.54	33.24
NGC5264	11.56	12.27	0.12	0.17	-16.96	0.66	20.54 ± 0.01	27.34 ± 0.24	0.92 ± 0.01	21.40	36.44
CenA-dE4	16.25	17.01	0.14	0.20	-12.35	0.69	23.79 ± 0.04	14.67 ± 0.54	0.91 ± 0.03	24.71	19.27

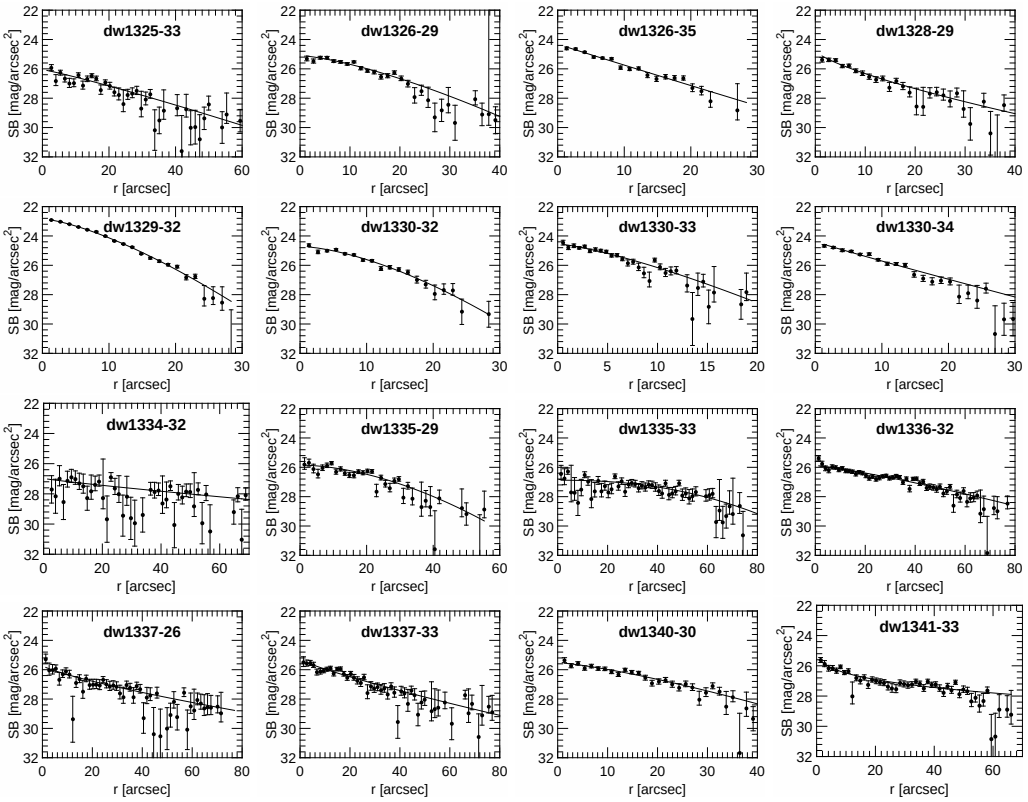

Fig. 5: Radial surface brightness profiles and best-fitting Sérsic profiles for all dwarf candidates in the r band.

5. Discussion

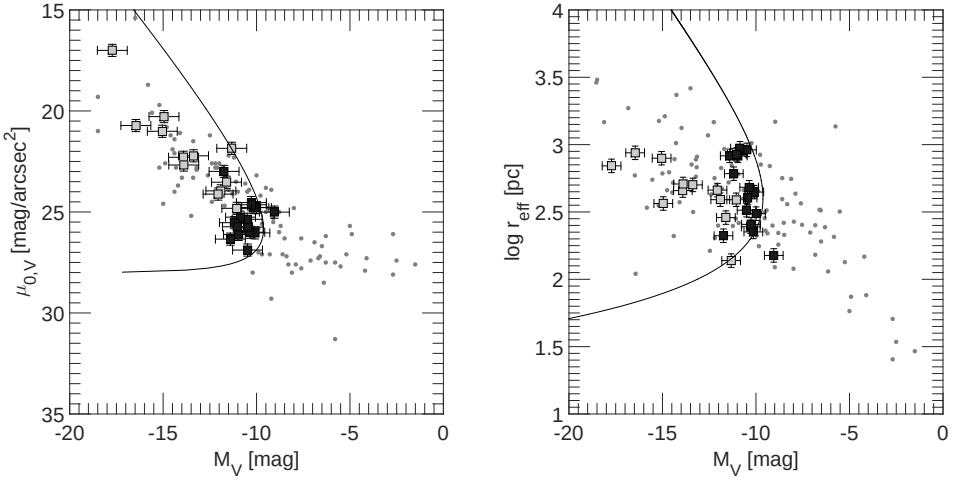

Fig. 6: Left: The $\mu_0 - M$ relation in the V band (see text for conversion formula) for our candidates (black squares), the known dwarfs of the M 83 subgroup (gray filled squares) and LG dwarfs (dots, McConnachie 2012). Right: The same for the effective radius, $\log r_{eff}$, instead of central surface brightness. Conservative global error bars of 0.5 mag for M, 0.3 mag for μ, and 0.05 for $\log r$ are plotted. Absolute magnitudes assume a distance of 4.9 Mpc (M 83). The curves indicate the completeness limit of the present survey on the assumption that every candidate larger than 40 arcsecs in diameter within an isophotal level of 28 mag arcsec^{-2} is included (see text).

To test the credibility of our new dwarf candidates, we compared them with the photometric properties of the known dwarfs in the survey region and with the dwarfs in the Local Group. The classical tool for such a comparison is the $\mu - M$ (surface brightness – absolute magnitude), or equivalently the $\log r - M$ (radius – absolute magnitude) relation. In Fig. 6 we have plotted the central μ (left panel) and the effective radius, $\log r_{eff}$, (right panel) versus M in the V band, which is the photometric band provided for LG dwarfs by McConnachie (2012). The transformation of our gr photometry into V for the purpose of comparison is given above in Sect. 2. Figure 6 clearly suggests that our candidates, when placed at a nominal distance of 4.9 Mpc, appear as a natural extension of the known members of the M 83 subgroup toward fainter luminosities. Moreover, most candidates are in good accord with the photometric relations traced out by the local dwarfs – as expected if they are indeed members of the Centaurus group.

We also plot here the completeness boundary curve we have introduced in Sect. 3, in the context of artificial galaxies. The boundary assumes that we detected all dwarf candidates that are larger than 40 arcsecs in diameter (= 2 r_{lim}) within an isophotal level of μ_{lim} = 28 V mag arcsec^{-2}. Assuming exponential profiles (Sérsic n = 1), the curve in the $\mu - M$ plane (Fig. 6 left) is given in Sect. 3. In the $\log r_{eff} - m$ representation the curve has the following form:

$$m_{tot} = \mu_{lim} - \frac{r_{lim}}{0.5487 r_{eff}} - 2.5 \log[2\pi \cdot (0.5958 \cdot r_{eff})^2]$$

(see Ferguson 1990; Ferguson & Sandage 1988). To obtain the $\log r_{eff}$[pc]$-M$ relation as shown in the right panel of Fig. 6, the distance of 4.92 Mpc (M 83) has to be taken into account.

Our candidates lie on the left side of theses boundaries, as expected, with the exception of dw1330-33, the faintest candidate in terms of total brightness, which is fairly small for its surface brightness; it is accordingly noted as a possible background object in Table 1. The one high surface brightness candidate in Fig. 6 is the BCD candidate dw1329-32. The two cirrus candidates, dw1334-32 and dw1335-33, are at the lower surface brightness end of the completeness boundaries. Given the large cosmic scatter of the $\mu - M$ and $\log r - M$ relations, their dwarf membership cannot be excluded at this point, however.

In Fig. 7 we compare our candidates with known dwarfs in the Sérsic $n - M$ relation. The comparison sample consists of the known M 83 subgroup dwarfs, LG dwarfs (Jerjen et al. 2000a), Virgo dwarfs (Binggeli & Jerjen 1998), and M 81 group dwarfs (Chiboucas et al. 2009). While at the bright end the relation is quite narrow, it spreads with decreasing luminosity. The large scatter is clearly not explained by photometric errors alone. Our candidates fit well into this spread defined by the LG and confirmed M 81 group dwarfs. The one outlier at the top is dw1341-33.

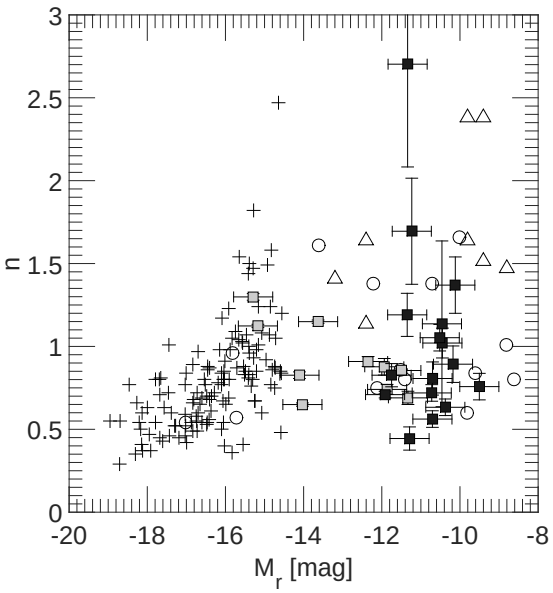

Fig. 7: Sérsic $n - M$ relation in the r band for our new dwarf candidates (black squares), the known dwarfs in the survey region (gray filled squares), Virgo dEs (plus signs, Binggeli & Jerjen 1998), LG dwarfs (open circles, Jerjen et al. 2000a), and M81 dwarfs (open triangles, Chiboucas et al. 2009). The vertical error bars shown for our dwarf candidates and previously known M 83 subgroup members are taken from Table 2. Horizontal error bars are a global ± 0.5 mag for their absolute magnitudes.

With $n = 2.70$ this candidate is rather cuspy (see also Fig. 5). This object has many foreground stars and a very diffuse shape. Improper star removal and a poor choice of the center for the radial profile could lead to an error in the best fit and therefore in the Sérsic n. But in summary, both the $\mu - M$ and $n - M$ relations clearly render most of our candidates quite plausible as dwarf members of the Centaurus complex.

Is the number of new candidates consistent with what we expect based on the suspected faint-end luminosity function of the group? Figure 6 shows that our survey has pushed down the completeness limit by roughly 2 magnitudes, from $M_V \approx -12$ to $M_V \approx -10$. If we take the luminosity functions of other nearby groups (Cen A, M81, and And) given in Fig. 35 of Chiboucas et al. (2009) as a measure, we expect an increase of the number of group members by a factor of between 1.48 and 1.74, depending on the steepness of the faint end of the LF. For the surveyed region with 14 known members (Fig. 1) we therefore predict (in retrospect) a discovery of between 7 and 10 new members in the given luminosity interval, not accounting for a detection efficiency of less than 100%. With actually 16 new candidates we thus have discovered even more than expected! This excess can be interpreted in different ways. The most obvious interpretation is that some of our candidates are no dwarf galaxies, after all. We have indeed singled out four doubtful cases. Another, or additional, possibility is that many of these new objects actually belong to the richer Cen A subgroup with which the M 83 subgroup heavily overlaps in the sky. It is indeed very intriguing that most of the new candidates and many of the known dwarf members lie in the SW corner of the search region – precisely in the direction to Cen A. Our artificial galaxy tests exclude the possibility that this is due to an inhomogeneous detection efficiency. In Fig. 1 we have drawn the direction to Cen A and also an estimate of the virial radius of the M 83 subgroup to indicate its

gravitational size. The virial radius is conventionally defined as the radius within which the mean mass density of a group is 200 times the critical density of the Universe, encompassing the sphere of matter that has collapsed to a halo at the present epoch (e.g., Tully 2015a). For the M 83 subgroup this amounts to 0.21 Mpc, corresponding to 2.4 degrees in the sky. The virial radius of the more massive Cen A subgroup is larger with 4 degrees, but does not reach M 83 (see also Tully et al. 2015). Many, if not most of the new dwarf candidates clearly lie outside the virial radius of the M 83 subgroup and thus might belong to the Cen A outskirts or a common envelope of the two subgroups.

6. Conclusions

We have carried out a search for new dwarf galaxies in deep images taken with the Dark Energy Camera at CTIO in an area of 60 square degrees covering the M 83 subgroup of the Centaurus complex. We found 16 new dwarf candidates in the magnitude range $17 < m_r < 19$, all of which, with the exception of one BCD candidate, being of very low surface brightness, in the range $25 < \langle\mu\rangle_{eff,r} < 28$. A comparison with the photometric properties of the known brighter M 83 subgroup members and all Local Group dwarfs in the $\mu - M$, $\log r - M$ and Sérsic $n - M$ planes suggests that most of the new candidates are very likely dwarf members of the M 83 subgroup, extending the LF of its known population down to $M_r \approx -10$. The distribution of the candidates is significantly prolonged toward the richer and somewhat closer Cen A subgroup. Some of the new candidates might belong to the Cen A subgroup or be part of a wider envelope of the Centaurus complex; these would intrinsically be somewhat brighter. Very recently, Tully et al. (2015) reported evidence that the Cen A subgroup itself has a double-planar structure. Most Cen A members seem to lie in either of two parallel thick sheets that are separated by about 300 kpc. The M 83 subgroup is roughly lying in the extension of the sheet going through Cen A. It will therefore be highly rewarding to widen and deepen the present survey and to conduct follow-up observations of the candidates, not only to confirm their Centaurus membership, but to derive TRGB distances to allow a more detailed study of the 3D structure of the Centaurus complex.

Acknowledgements

OM and BB are grateful to the Swiss National Science Foundation for financial support. HJ acknowledges the support of the Australian Research Council through Discovery project DP150100862. The authors also thank the referee Nicholas Martin for helpful comments and suggestions, which contributed to improving the quality of the publication. This project used data obtained with the Dark Energy Camera (DECam), which was constructed by the Dark Energy Survey (DES) collaborating

institutions: Argonne National Lab, University of California Santa Cruz, University of Cambridge, Centro de Investigaciones Energeticas, Medioambientales y Tecnologicas-Madrid, University of Chicago, University College London, DES-Brazil consortium, University of Edinburgh, ETH-Zurich, Fermi National Accelerator Laboratory, University of Illinois at Urbana-Champaign, Institut de Ciencies de l'Espai, Institut de Fisica d'Altes Energies, Lawrence Berkeley National Lab, Ludwig-Maximilians Universitat, University of Michigan, National Optical Astronomy Observatory, University of Nottingham, Ohio State University, University of Pennsylvania, University of Portsmouth, SLAC National Lab, Stanford University, University of Sussex, and Texas A&M University. Funding for DES, including DECam, has been provided by the U.S. Department of Energy, National Science Foundation, Ministry of Education and Science (Spain), Science and Technology Facilities Council (UK), Higher Education Funding Council (England), National Center for Supercomputing Applications, Kavli Institute for Cosmological Physics, Financiadora de Estudos e Projetos, Fundao Carlos Chagas Filho de Amparo a Pesquisa, Conselho Nacional de Desenvolvimento Cientfico e Tecnolgico and the Ministrio da Cincia e Tecnologia (Brazil), the German Research Foundation-sponsored cluster of excellence "Origin and Structure of the Universe" and the DES collaborating institutions.

5.2 New low surface brightness dwarf galaxies in the Centaurus group

— Oliver Müller, Helmut Jerjen, Bruno Binggeli —

Astronomy & Astrophysics, 2017, 597, A7

Abstract

The distribution of satellite galaxies around the Milky Way and Andromeda and their correlation in phase space pose a major challenge to the standard ΛCDM model of structure formation. Other nearby groups of galaxies are now being scrutinized to test for the ubiquity of the phenomenon. We conducted an extensive CCD imaging survey for faint, unresolved dwarf galaxies of very low surface brightness in the whole Centaurus group region, encompassing the Cen A and M 83 subgroups lying at a distance of roughly 4 and 5 Mpc, respectively. The aim is to significantly increase the sample of known Centaurus group members down to a fainter level of completeness, serving as a basis for future studies of the 3D structure of the group. Following our previous survey of 60 square degrees covering the M 83 subgroup, we extended and completed our survey of the Centaurus group region by imaging another 500 square degrees area in the g and r bands with the wide-field Dark Energy Survey camera at the 4 m Blanco telescope at CTIO. The surface brightness limit reached for unresolved dwarf galaxies is $\mu_r \approx 29$ mag arcsec^{-2}. The faintest suspected Centaurus members found have $m_r \approx 19.5$ mag or $M_r \approx -8.8$ mag at the mean distance of the group. The images were enhanced using different filtering techniques. We found 41 new dwarf galaxy candidates, which together with the previously discovered 16 dwarf candidates in the M 83 subgroup amounts to almost a doubling of the number of known galaxies in the Centaurus complex, if the candidates are confirmed. We carried out surface photometry in g and r, and report the photometric parameters derived therefrom, for all new candidates as well as previously known members in the surveyed area. The photometric properties of the candidates, when compared to those of Local Group dwarfs and previously known Centaurus dwarfs, suggest membership in the Centaurus group. The sky distribution of the new objects is generally following a common envelope around the Cen A and M 83 subgroups. How the new dwarfs are connected to the intriguing double-planar feature recently reported must await distance information for the candidates.

1. Introduction

In addition to their traditional role as dark matter (DM) tracers by their internal dynamics (Walker 2013), faint dwarf galaxies are a very powerful testbed for DM and structure formation models by their mere abundance and spatial distribution.

There is the long-standing missing satellite problem (e.g., Kauffmann et al. 1993; Klypin et al. 1999; Moore et al. 1999) and the too big to fail problem (Boylan-Kolchin et al. 2011), both of which might be attributable to an incomplete understanding of baryonic physics (e.g., Simon & Geha 2007; Wetzel et al. 2016). However, a major challenge for the standard picture of structure formation with DM is now posed by the highly asymmetric features found in the distributions of dwarf galaxies in the Local Group (Kroupa et al. 2005). There is the vast polar structure (VPOS; Pawlowski et al. 2015b, 2012b), which is a thin (rms height $\approx$ 30 kpc) highly inclined, corotating substructure of faint satellite galaxies, young globular clusters, and streams, spreading in Galactocentric distance between 10 and 250 kpc. Following an earlier suggestion by Koch & Grebel (2006), a similar feature was found in the Andromeda galaxy surroundings (Metz et al. 2007; Ibata et al. 2013), called the Great Plane of Andromeda (GPoA). Moreover, there are two galaxy planes (diameters of 1-2 Mpc) that contain all but one of the 15 nonsatellite galaxies in the Local Group (Pawlowski et al. 2013). Such planar structures on galactic and intergalactic scales are difficult to accommodate in a standard ΛCDM scenario, where extreme satellite planes are found in $< 0.1\%$ of simulated systems (e.g., Pawlowski et al. 2014). Still, the most conservative estimate from cosmological simulations including the look-elsewhere effect, but ignoring observational uncertainties, finds the frequency of two prominent satellite structures in the Local Group to be ~ 1 per cent (Cautun et al. 2015a). These controversial results demonstrate the need for more observational data to scrutinize ΛCDM predictions and assess the degree of conflict with that model.

If the relative sparseness and asymmetric distributions of low-mass dwarf galaxies are a common phenomenon in the local universe, a major revision of our view of structure formation would be necessary. Recently, Tully et al. (2015) reported evidence of a double-planar structure in the nearby Centaurus group of galaxies, based on hitherto known (i.e., still fairly massive) galaxy members of the group. This result is encouraging, as it means that systematic studies of the spatial distribution of fainter dwarf galaxies in nearby groups can provide important observational constraints for further testing structure formation models. In a first step, deep and wide-field imaging is required to detect dwarf galaxy members of nearby galaxy groups with faint luminosity and surface brightness levels. Present-day technologies allow a dwarf galaxy census of other nearby groups down to $M_V \approx -10$, equivalent to Local Group dwarfs like Sculptor, Sextans, and Tucana, clearly surpassing the achievements of the Sloan Digital Sky Survey (SDSS; Ahn et al. 2014; York et al. 2000) with respect to the detection of unresolved dwarf candidates.

Several international teams have taken up the effort to conduct dedicated imaging surveys of other nearby galaxy groups in the search for faint and ultra-faint dwarf galaxies in the northern hemisphere; see, for example, Chiboucas et al. (2009, 2013) for the M 81 group (14 confirmed new members over 65 deg^2), and Merritt et al.

(2014) and Javanmardi et al. (2016) for the M 101 group (8 dwarf candidates over 7 deg^2). In the southern hemisphere, the deep but spatially limited Panoramic Imaging Survey of Centaurus and Sculptor (PISCeS) of NGC 253 in the Sculptor group and NGC 5128 (Cen A) in the Centaurus group (Sand et al. 2014; Crnojević et al. 2014, 2016) revealed 9 extremely faint dwarf galaxies ($25.0 < \mu_{r,0} < 27.3$, $-13 < M_V < -7.2$) in the vicinity ($\sim 11\,\mathrm{deg}^2$) of Cen A. Group memberships of these dwarfs have been confirmed with the tip of the red giant branch (TRGB) method.

In the same spirit we conducted a large-scale survey of the Centaurus Group using the Dark Energy Camera (DECam) at the 4 m Blanco telescope at CTIO. Our survey has a photometric surface brightness limit that is slightly less sensitive than PISCeS, but a 50 times larger footprint. The survey covers a region of ≈ 550 deg^2, thus providing complete CCD coverage of this southern galaxy group, for the first time, going significantly deeper than with the SDSS in the north outside the Local Group. Owing to its greater depth, PISCeS is a search for resolved dwarf objects, while our survey is able to detect only unresolved dwarf members of the Centaurus group. This paper is the second report on our DECam survey of the Centaurus group region. We refer to the Centaurus group as the whole complex and the two main concentrations as Cen A and M 83 subgroup, respectively. The Cen A subgroup is dominated by the massive peculiar galaxy Cen A (=NGC5128) at a mean distance of 3.8 Mpc and the M 83 subgroup by the giant spiral M 83 (=NGC 5236) at a mean distance of 4.9 Mpc (Karachentsev et al. 2004, 2013; Tully et al. 2015; Tully 2015b). In our first paper (Müller et al. 2015, hereafter MJB15) we reported the discovery of 16 new dwarf galaxy candidates from our survey of the M 83 subgroup, covering an area of 60 deg^2 based on the images taken with DECam. One of the new dwarfs, dw1335-29, has already been confirmed as group member based on HST archival data (Carrillo et al. 2016).

In this paper we present our extended DECam survey of the entire Centaurus group and report on the discovery of another 41 new dwarf candidates in addition to the 16 dwarf galaxy candidates reported in MJB15. Even if we assume that a few objects will turn out to be background galaxies, this sample essentially doubles the number of known galaxies in the Centaurus group.

The paper is organized as follows. In Sect. 2 we give the details of the DECam observations. Sect. 3 describes our search strategy for, and detection of, faint diffuse dwarf galaxy candidates in the survey footprint. In Sect. 4 we present the results from the surface photometry analysis conducted for the new candidates and the known Centaurus group members. Finally, a first assessment of the dwarf galaxy distribution and a critical discussion of our findings are given in Sect. 5, followed by our conclusions in Sect. 6.

2. Observations and photometric calibration

We obtained images in the g and r bands over two observing runs on 2014 July 17–19 and 2015 June 4–9 using the Dark Energy Camera at the 4 m Blanco telescope at Cerro Tololo Inter-American Observatory (CTIO) as part of the observing proposals 2014A-0624 and 2015A-0616 (both PI: H. Jerjen). With an array of 62 2k×4k CCD detectors the DECam has a 3 square degree field of view and a pixel scale of 0.27 arcsec. In 2014 we obtained a complete data set for 24 fields under dark time conditions (blue circles in Fig.1). Exposure times were 3×40 sec in both bands. During the 2015 observing run two exposures were taken in each band for a total of 163 fields (red circles in Fig.1). To fill the inter-chip gaps, we dithered diagonally by half of a CCD chip. The measured median seeing was 1.0 arcsec. As we were observing under waning moon conditions, we strategically collected the r-band images in the first four nights with exposure times between 2×120 and 2×210 sec and the g-band images in the last four nights with exposure times between 2×100 and 2×170 sec, depending on the sky brightness and the angular distance of the target field from the moon.

The images were fully reduced and stacked using the DECam community pipeline (Valdes et al. 2014). Fig. 1 shows the survey footprint superimposed on the distribution of the known galaxies in the Centaurus group. The circles correspond to the individual DECam fields while the colors indicate the different data sets. Black circles indicate the 22 DECam fields of MJB15.

To determine the photometric zero points and color terms for each DECam field, we matched the instrumental magnitudes of typically 100-200 stars in each field with their corresponding photometric data from the AAVSO Photometric All-Sky Survey (APASS) catalog (Henden & Munari 2014) using the DAOPHOT package (Stetson 1987) in IRAF and fitted the following two equations:

$$m_g = m_{g,instr} + Z_g + c_g \cdot (m_{g,instr} - m_{r,instr}) - k_g X$$

$$m_r = m_{r,instr} + Z_p + c_r \cdot (m_{g,instr} - m_{r,instr}) - k_r X,$$

where Z_g and Z_r are the photometric zero points, c_g and c_r are the color terms, k_g and k_r are the atmospheric extinction coefficients, and X is the mean airmass. The most recent extinction values $k_r = 0.10$ and $k_g = 0.20$ for CTIO were kindly provided by the Dark Energy Survey team. The airmass X was given in the header of each exposure.

To allow a direct comparison with available photometry for Local Group dwarf galaxies in the literature, we converted our gr photometry (see section 4) into the V band using the transformation equation by Lupton (2005) as follows:

$$V = g - 0.5784 \cdot (g - r) - 0.0038. \tag{5.1}$$

This formula can be used for the total magnitudes and surface brightness parameters of the galaxy. To further compare our results from the Sérsic profile fitting with the B-band results for Local Group and Virgo cluster dwarf galaxies, we also converted the literature values from the B to r band using the equation (Lupton 2005),

$$r = B - 1.3130 \cdot (g - r) - 0.2271, \tag{5.2}$$

where we adopted a color index of $(g-r) = 0.6$ suitable for early-type dwarf galaxies (Lisker et al. 2008). The entire survey area (this paper and MJB15) is subdivided into three different data sets (see Fig. 1). As we mentioned before, the exposure times for the fields obtained in the 2015 run (red circles in Fig. 1) were adjusted to compensate for the sky brightness variation due to lunar illumination to achieve approximately equal photometric depth across the survey area. To test photometric uniformity we sampled the faintest stars in different regions and measured their apparent magnitudes. The variance is in the range of 0.3 mag. Overlapping DECam fields from different data sets were also compared for their detection quality. We find no significant difference.

3. Search and detection of new dwarf candidates

Finding new dwarf galaxy candidates in the Centaurus group required the search for unresolved, low surface brightness objects in the DECam images. With the relative short exposure times we cannot resolve galaxies at the distance of the Centaurus group into RGB stars. A quick estimate of the TRBG magnitude shows that we miss the RGB tip by a few tenths of a magnitude. For this estimate we took the stellar population of the Sculptor dwarf galaxy as a reference with $M_I = -4.1$ and $V - I = 1.5$ for its TRGB (Rizzi et al. 2007a). This translates into $M_r \approx -2.8$ with an assumed color index of $V - r \approx 0.2$. We assume a mean Galactic extinction of $A_r = 0.15$ for our survey field; see Table 2 for the exact extinction values for all the galaxies in the survey. At the distance of 4.9 Mpc (M 83) this gives an expected apparent magnitude of $m_r = 25.8$ for the RGB tip. At the distance of 3.8 Mpc (Cen A) the expected apparent magnitude is $m_r = 25.3$. The faintest stars detectable in the survey data have a magnitude ≈ 25, and thus we can expect to see the brightest stars in galaxies only if they have a shorter distance than Cen A. Faint individual stars are indeed visible in some of the galaxy candidates, but in most of the cases we

Tab. 1: Names and coordinates of the 41 new dwarf galaxy candidates.

Name	α (J2000)	δ (J2000)	Type	Notes
dw1240-42	12:40:02	− 42:24:44	dSph	
dw1241-32	12:41:27	− 42:53:45	dSph	
dw1243-42	12:43:13	− 42:27:48	dSph	pair: dw1243-42b
dw1243-42b	12:43:11	− 42:26:37	dIrr	
dw1251-40	12:51:56	− 40:19:53	dSph	pair: dw1252-40
dw1252-40	12:52:01	− 40:21:55	dSph	bg?
dw1252-43	12:52:25	− 43:05:58	dSph	
dw1257-41	12:57:45	− 41:22:52	dSph	
dw1258-37	12:58:29	− 37:07:21	dSph	
dw1301-30	13:01:28	− 30:06:43	dSph	
dw1302-40	13:02:49	− 40:08:35	dSph	
dw1306-29	13:06:48	− 29:53:30	dSph	bg?
dw1314-28	13:14:02	− 28:12:12	dIrr/dSph	bg?
dw1315-45	13:15:56	− 45:45:02	dIrr	
dw1318-21	13:18:04	− 21:53:06	dSph	bg?
dw1318-44	13:18:58	− 44:53:41	dSph	
dw1321-27	13:21:08	− 27:44:56	dSph	
dw1322-27	13:22:06	− 27:34:45	dIrr/dSph,N	bg?
dw1322-39	13:22:32	− 39:54:20	dIrr	
dw1323-40	13:24:53	− 40:45:41	dSph	
dw1323-40b	13:23:55	− 40:50:09	dSph	
dw1323-40c	13:23:37	− 40:43:17	dSph	
dw1326-37	13:26:22	− 37:23:08	dIrr?	bg?
dw1329-45	13:29:10	− 45:10:31	dSph	
dw1330-38	13:30:41	− 38:10:03	cirrus?	
dw1331-37	13:31:32	− 37:03:29	dSph	
dw1331-40	13:31:26	− 40:15:47	cirrus?	
dw1336-44	13:36:44	− 44:26:50	dIrr	
dw1337-41	13:37:55	− 41:54:11	cirrus?	
dw1337-44	13:37:34	− 44:13:07	dIrr?	
dw1341-43	13:41:37	− 43:51:17	dSph	
dw1342-43	13:42:44	− 43:15:19	dIrr?	
dw1343-34	13:43:49	− 34:56:07	cirrus?	
dw1357-28	13:57:00	− 28:55:15	dSph	
dw1401-32	14:01:25	− 32:37:46	dSph	
dw1403-33	14:03:18	− 33:24:14	dSph	
dw1406-29	14:06:41	− 29:08:10	dSph	
dw1409-33	14:09:03	− 33:49:40	dSph	
dw1410-34	14:10:47	− 34:52:07	dIrr	
dw1413-34	14:13:08	− 34:23:33	dSph	
dw1415-32	14:15:41	− 32:34:21	dIrr?	

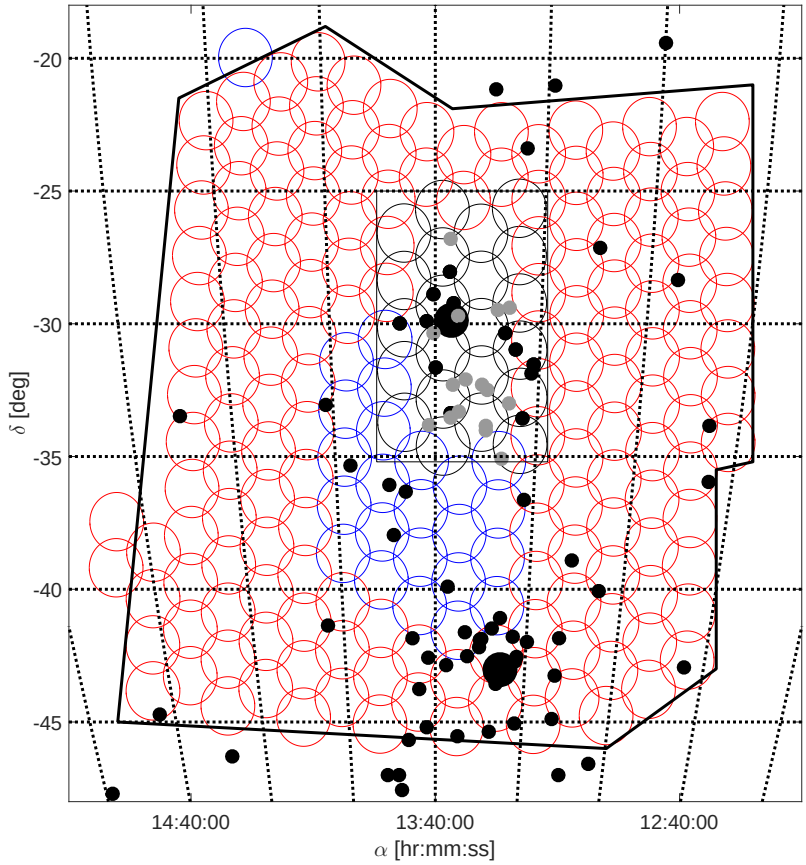

Fig. 1: Surveyed area of ≈550 square degrees in the Centaurus group. The individual DECam fields are represented by circles. The colors indicate the three different sets of data; the fields around M83 were discussed in the MJB15 study and are shown as black circles. The blue and red fields were observed in 2014 and 2015, respectively, and analyzed for the present paper. The small black dots are the known dwarfs in the Centaurus group listed in the Local Volume Catalog (Karachentsev et al. 2004, 2013) complemented by the recently discovered nine dwarfs of Crnojević et al. (2014, 2016). The larger black dots are the two dominant group galaxies M 83 (13h37m00.9s, −29d51m56s) and Cen A (13h25m27.6s, −43d01m09s).

miss the tip. Therefore this is a search for unresolved stellar systems.

All gr band images available for an individual DECam field were co-added using the SWarp program (Bertin et al. 2002). The SWarp program subtracts the background of every frame, resamples them onto a common coordinate system, stacks them, and puts the combined image into a single file (hereafter deep image). The frames were combined using the weighted co-addition algorithm.

Gray-level manipulation was applied on the deep images to enhance the contrast. We carefully estimated the local background RMS noise and chose a range of $2 \times RMS$ below and above the estimated sky background level. This is the regime where we expect the low surface brightness dwarfs to be most prominent. In a first step,

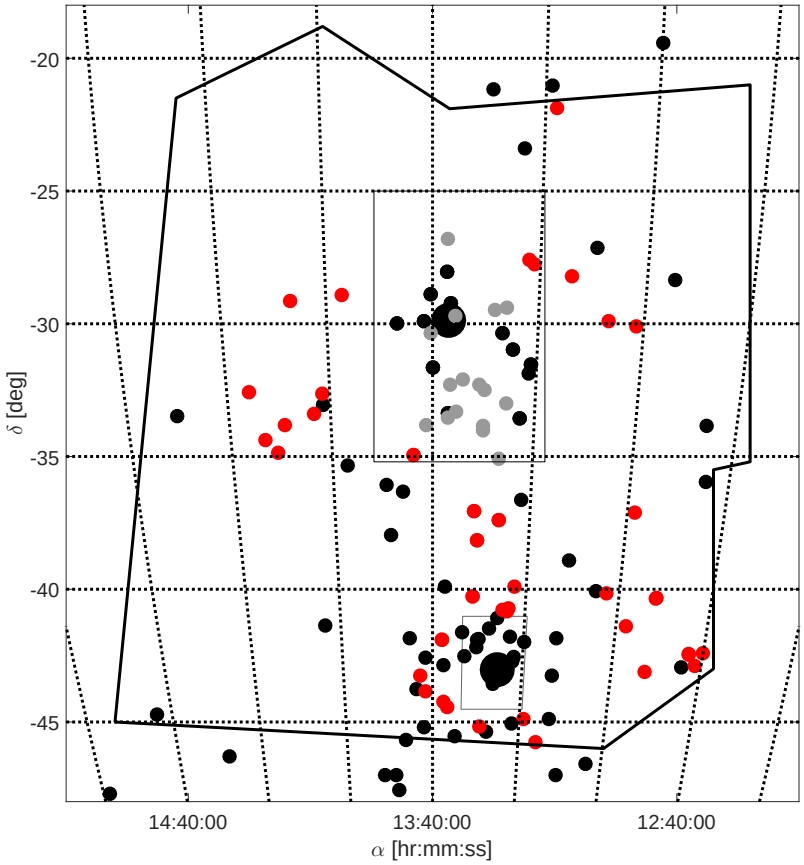

Fig. 2: Same as Fig. 1 but without the DECam pointings, showing the 41 newly detected dwarf galaxy candidates as red dots. The 16 dwarf candidates we previously reported in the vicinity of M 83 (MJB15; survey footprint shown as large rectangle) are indicated as small gray circles. The survey area of the Crnojević et al. (2014, 2016) study around Cen A is approximated with the small rectangle.

the deep images were visually inspected. Then different filtering techniques like the Gaussian convolution and the ring median filter (Secker 1995) were applied to enhance the presence of any low-surface brightness features. This strategy can potentially lead to losing high surface brightness objects, such as bright background galaxies or Blue Compact Dwarfs (BCD) in the Centaurus group. We refer to Section 3 in MJB15 for more details about the search strategy.

The region of the Centaurus group is at low Galactic latitudes and thus has a relatively high level of contamination from foreground stars and Galactic cirrus. Although cirrus can sometimes resemble low surface brightness dwarf galaxies in shape and size, it is often possible to distinguish them morphologically. When a low surface brightness object was detected in or near a structure of Galactic nebula (cirrus) it was dismissed as a dwarf galaxy candidate (see Fig. 3 for an example). As part of this decision process real dwarf galaxies could have been accidentally rejected.

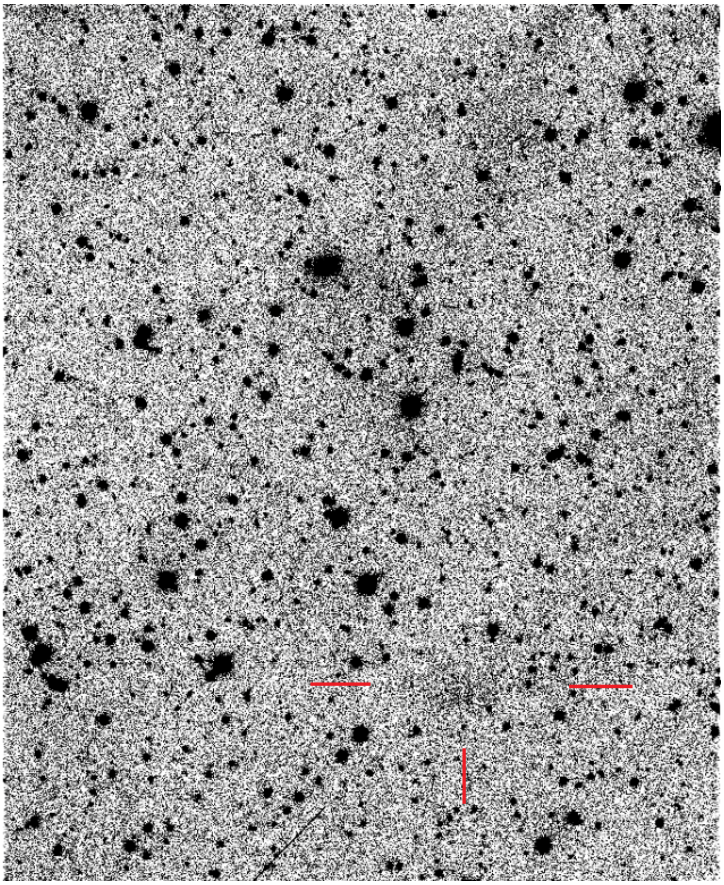

Fig. 3: Example of a low surface brightness feature (indicated with red lines) close to Galactic cirrus. The object was dismissed as dwarf galaxy candidate for reasons explained in the text.

We found 41 new Centaurus group dwarf galaxy candidates. Their distribution among the known group members is shown in Fig. 2 (red dots). A gallery of the r-band images of the candidates is presented in Fig. 4 and Fig. 5. The coordinates and morphological type are compiled in Table 1. The morphological type is based on the assumption that the object is a member of the Centaurus group. The photometric and structural parameters of the dwarf candidates are listed in Table 2.

Three new candidates are in the MJB15 footprint. Just outside of the MJB15 footprint, dw1343-34 is visible when comparing Fig. 1 and Fig. 2; albeit fully visible in MJB15, dw1321-27 and dw1322-27 were then rejected and assumed to be satellites of NGC 5101 in the background. With the background relation test carried out in this paper (see Fig. 10), we estimate that at least one of these candidates is too big in size relative to its surface brightness to be associated with the background galaxy, while the other candidate can be argued as background or foreground dwarf. Still, we list both of them here as new candidates of the Centaurus group. Distance measurements will give a final answer to their membership.

We also checked for 21 cm emission within 8 arcmin of the direction of the candidates using the spectra from the HI Parkes All Sky Survey (HIPASS) survey (Barnes et al. 2001). None of the galaxies were detected in HI. Using the faint HI signal of the

Centaurus group member HIPASSJ1348-37 as a reference ($S_{int} = 2.5\,\mathrm{Jy\,km\,s^{-1}}$), we derive an upper limit for the HI content of the new dwarfs at $M_{HI} < 8.5 \times 10^6 M_\odot$.

4. Galaxy photometry

We measured gr surface photometry for the new dwarf candidates and for the known Centaurus group dwarfs in the surveyed region, where possible. Pixels affected by foreground stars, background galaxies, and cosmic rays were replaced with patches of sky from the surrounding area to match the statistical properties of the local sky background. To find the center of the galaxy, we fitted a circle at the outer isophotes and took its center as the galaxy center. For each photometric band, we computed the total apparent magnitude, the mean effective surface brightness $\langle\mu\rangle_{eff}$, and the effective radius r_{eff}. To determine the sky brightness we varied the growth curve (cumulative intensity profile) of the galaxy until it became asymptotically flat at large radii. Radial surface brightness profiles were measured using a radial step size of 1.35 arcsec for galaxies visually larger than 13 arcsec (radius) and 0.54 arcsec for smaller galaxies. A circular aperture was used for the photometry. Sérsic profiles (Sersic 1968) were fitted at the radial surface brightness profiles using the equation

$$\mu_{sersic}(r) = \mu_0 + 1.0857 \cdot \left(\frac{r}{r_0}\right)^n,$$

where μ_0 is the Sérsic central surface brightness, r_0 the Sérsic scale length, and n the Sérsic curvature index. We note that some authors use $1/n$ instead of n. Although we clearly stated that we use n, even we were confused and used $1/n$ in Table 2 of MJB2015. In Figure 7 of the same paper Sérsic indices were plotted with $1/n$ instead of n for our photometry. Our group membership argument does not change because most of the values are in the range between 0.8 and 1.2, still falling into the relation. We plot the correct values in Fig. 11 here.

The combined uncertainty for the total magnitudes was estimated to be on the order of 0.3 mag. Contributions to the error budget come from the star subtraction ($\approx$ 0.2 mag), zero-point calibration (less than 0.04 mag) and the estimated sky background ($\approx$ 0.2 mag); the star subtraction is estimated by the average difference in magnitudes between the galaxy with star removal and without, assuming no bright star is in the vicinity. An additional error for the absolute magnitudes (column 6 in Table 2) comes from the assumed distance ($\approx$ 0.25 mag for an uncertainty of ± 0.5 Mpc). Uncertainties for the structural parameters arise from the determination of the growth curve ($\Delta r_{eff} = 1$ arcsec, $\Delta\langle\mu\rangle_{eff} = 0.3$ mag) and for the Sérsic fit from numerics (see Table 2 for the corresponding errors).

One of our candidates (dw1326-35 from MJB15) is at the border of two different observation runs and is visible in both of them (see Fig. 2). We performed photometry

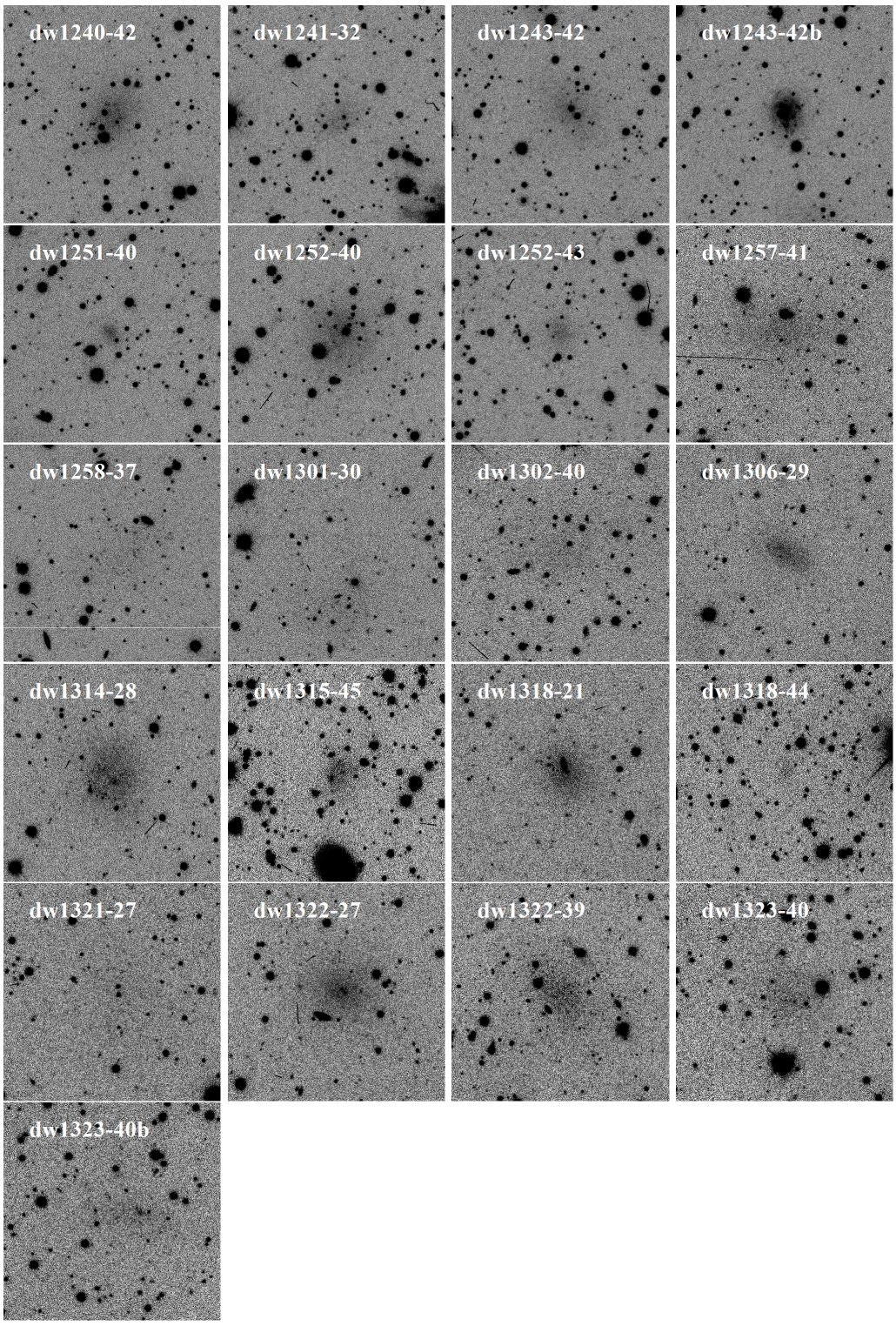

Fig. 4: Gallery showing DECam r-band images of the new Centaurus group dwarf galaxy candidates. One side of an image is 2.25 arcmin or 3.0 kpc at 4.5 Mpc. North is to the top, east to the left.

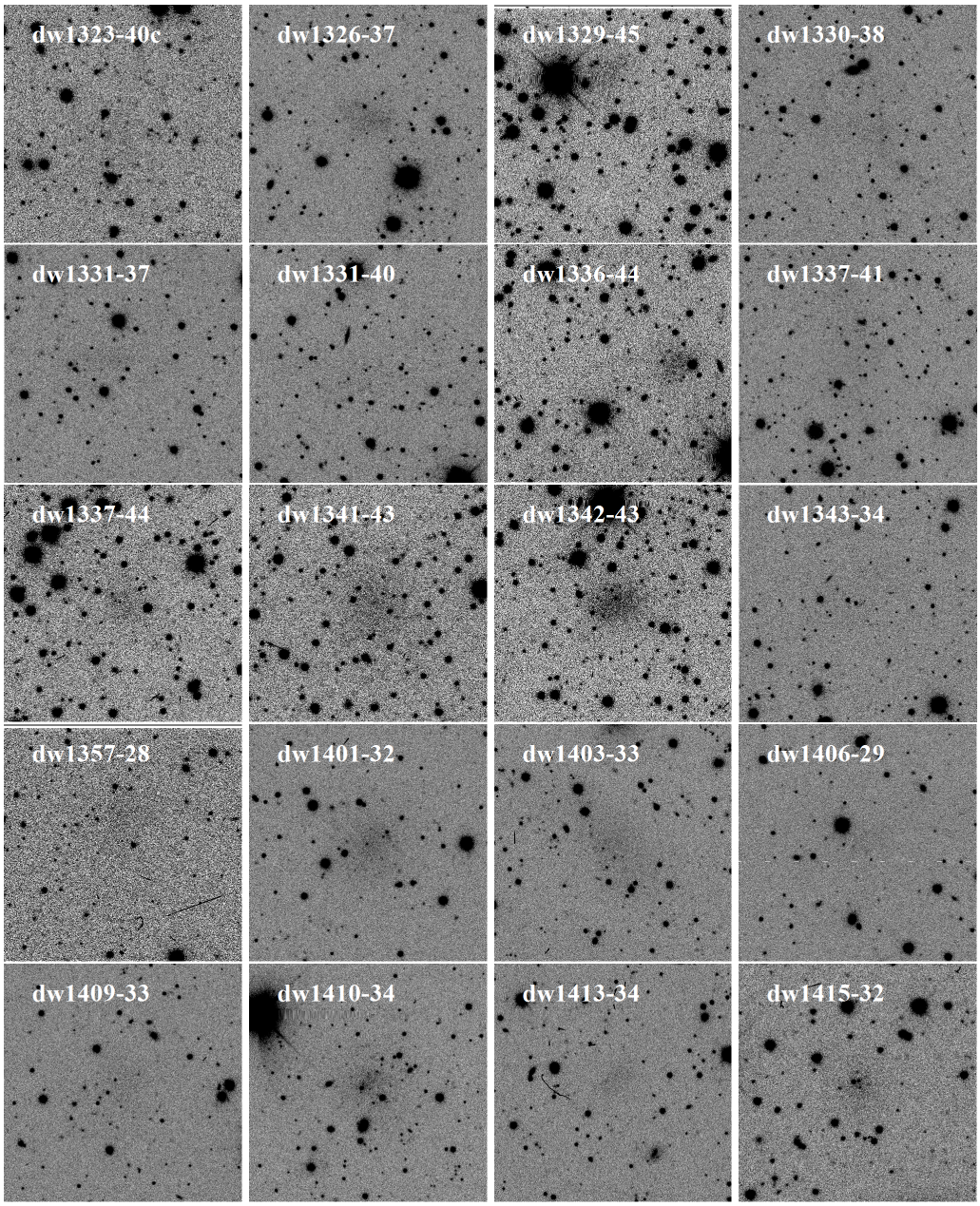

Fig. 5: Same as Fig. 4, continuing the image gallery.

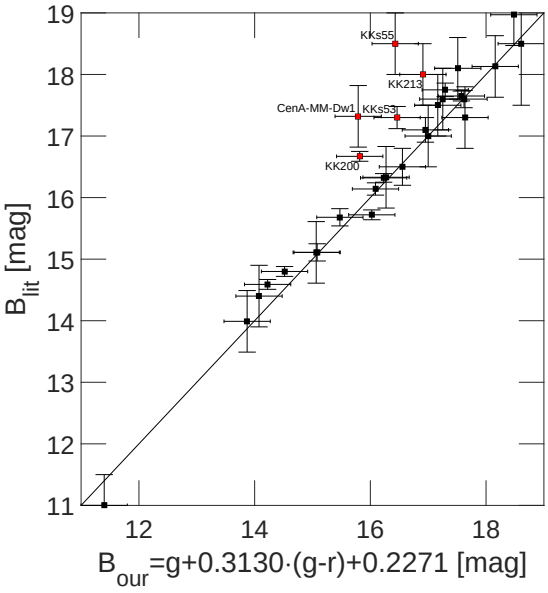

Fig. 6: Comparison of B-band photometry for known Centaurus group galaxies in our survey area. Values from the literature (for references see Table 3) versus the B-band magnitude we derived from our gr photometry. We adopt a conservative error of 0.4 mag for our data, which includes the uncertainties for both filters. Photometric uncertainties for the literature values were taken from the publications. The unity line is shown as a solid line. For five galaxies the magnitude difference is larger than the error tolerance (indicated in red). These discrepant cases are discussed in the text.

on the images of both runs to test the internal consistency of our photometry pipeline. We calculated the differences in apparent magnitude, which were $\Delta_r = 0.21$ mag and $\Delta_g = 0.06$ mag. These values are well within the estimated total uncertainty of 0.3 mag. There exists an overlap of two known galaxies with the MJB15 region (KK200 and CenA-dE4). The photometric differences are $\Delta_B = 0.095$ mag and $\Delta_B = -0.144$ mag, respectively, which is well within the estimated error.

Another test of performance is to compare our photometry with literature values. For that purpose we transformed our gr photometry into a B-band magnitude using the formula given in Section 2. We plot the total B magnitude from the literature for 30 known dwarfs in our survey data versus the B magnitude from our photometry in Figure 6. The references for the literature values are given in Table 3, and no adjustments were made for different methods to derive the photometry. We note that 24 of the known dwarfs are missing in the lists provided in this paper and in MJB15 as they happen to lie either outside of our survey footprint (10), or are close to or even on the edge of a CCD field (7), are stretched over multiple CCD tiles (4), or in the case of the ultra-faint dwarfs are too faint to measure (3).

All but five galaxies (KK200, KKs53, KKs55, KK213, and CenA-MM-Dw1) agree within our estimated errors. If we exclude these five discrepant cases the mean difference and standard deviation are $\langle \Delta\mu \rangle = 0.10$ mag and $\sigma = 0.37$ mag, respectively. The discrepancy for the five objects can be explained as follows: (a) KK200 (Metcalfe et al. 1994) was only integrated to the $\mu_b = 26.75$ mag arcsec^{-2} isophote, cutting the outskirts of the galaxy. The listed value is fainter than the real value (b) for KKs53, KKs55, and KK213 (Huchtmeier et al. 2001), and the magnitudes were

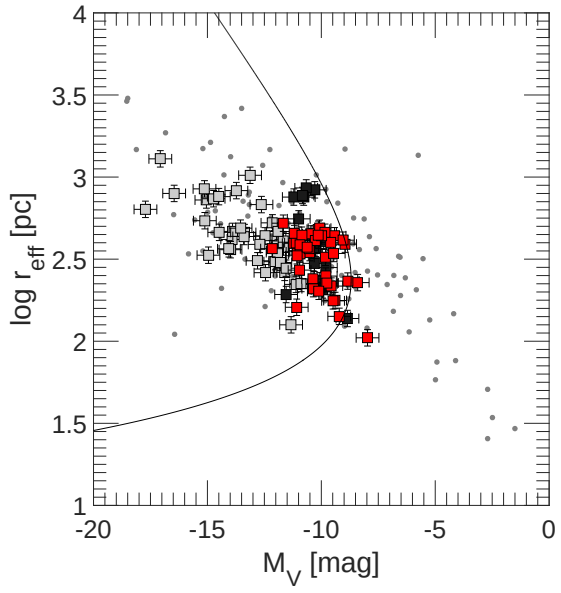

Fig. 7: For our candidates, $\log(r_{eff}) - M$ relation in the V band (red squares), all known dwarfs of the Centaurus group in the surveyed area for which photometry was possible (gray filled squares), Local Group dwarf galaxies (gray dots; McConnachie 2012) and the candidates from MJB15 (black squares). Also plotted are conservative error bars of 0.5 mag for M_V and 0.05 for $\log(r_{eff})$. Absolute magnitudes are based on a mean distance of 4.5 Mpc to all Centaurus galaxy candidates. The solid curve represents the completeness limit of the survey. It suggests that most low surface brightness galaxies larger than 26 arcsec in diameter at the isophotal magnitude of 28 mag arcsec^{-2} were detected (for more details see text).

estimated by visual inspection only; no quantitative photometry was performed; and (c) for CenA-MM-Dw1, the case is described in detail in the following.

Among the nine ultra-faint dwarfs found by Crnojević et al. (2014, 2016) photometry was possible for CenA-MM-Dw1, Dw4 and Dw9. We point out the good agreement for the photometric quantities of Dw4 and Dw9. For CenA-MM-Dw4, $\mu_{0,r} = 25.1$ and $r_{eff,r} = 20.3$ arcsec versus $\mu_{0,r} = 25.0$ and $r_{eff,r} = 18.6$ arcsec (Crnojević et al. 2016); for CenA-MM-Dw9, $\mu_{0,r} = 25.9$ and $r_{eff,r} = 24.4$ arcsec versus $\mu_{0,r} = 26.1$ and $r_{eff,r} = 23.4$ arcsec (Crnojević et al. 2016); whereas for CenA-MM-Dw1, $\mu_{0,r} = 25.1$ and $r_{eff,r} = 65.3$ arcsec versus $\mu_{0,r} = 27.0$ and $r_{eff,r} = 78.6$ arcsec (Crnojević et al. 2014) clearly differs from our results. Private communication with D.C. confirmed that our values are correct. CenA-MM-Dw2 is also visible on our DECam images but its small angular size and the presence of a number of bright foreground stars (see Figure 2 of Crnojević et al. (2016)) prevented us from conducting accurate photometry. Moreover, Dw3 is a tidal dwarf galaxy that is extended over 1.5 degrees making it impossible to perform aperture photometry, while Dw5 and Dw7, with central surface brightnesses $\mu_{0,r} \approx 26.5$, were too faint. Dw6 is just visible when knowing the position, but too faint to be detected as dwarf galaxy. Dw8 is on the edge of an image.

In Table 2 we present the photometric data for the 41 newly detected dwarf galaxy candidates. Where possible we also performed photometry for known Centaurus group dwarfs in the survey area (Table 3). The quantities listed are as follows: (1) name of candidate, or name, morphological type, and coordinates of the known galaxy; (2+3) total apparent magnitude in the g and r bands; (4+5) Galactic extinction values in g and r according to Schlafly & Finkbeiner (2011); (6) extinction-

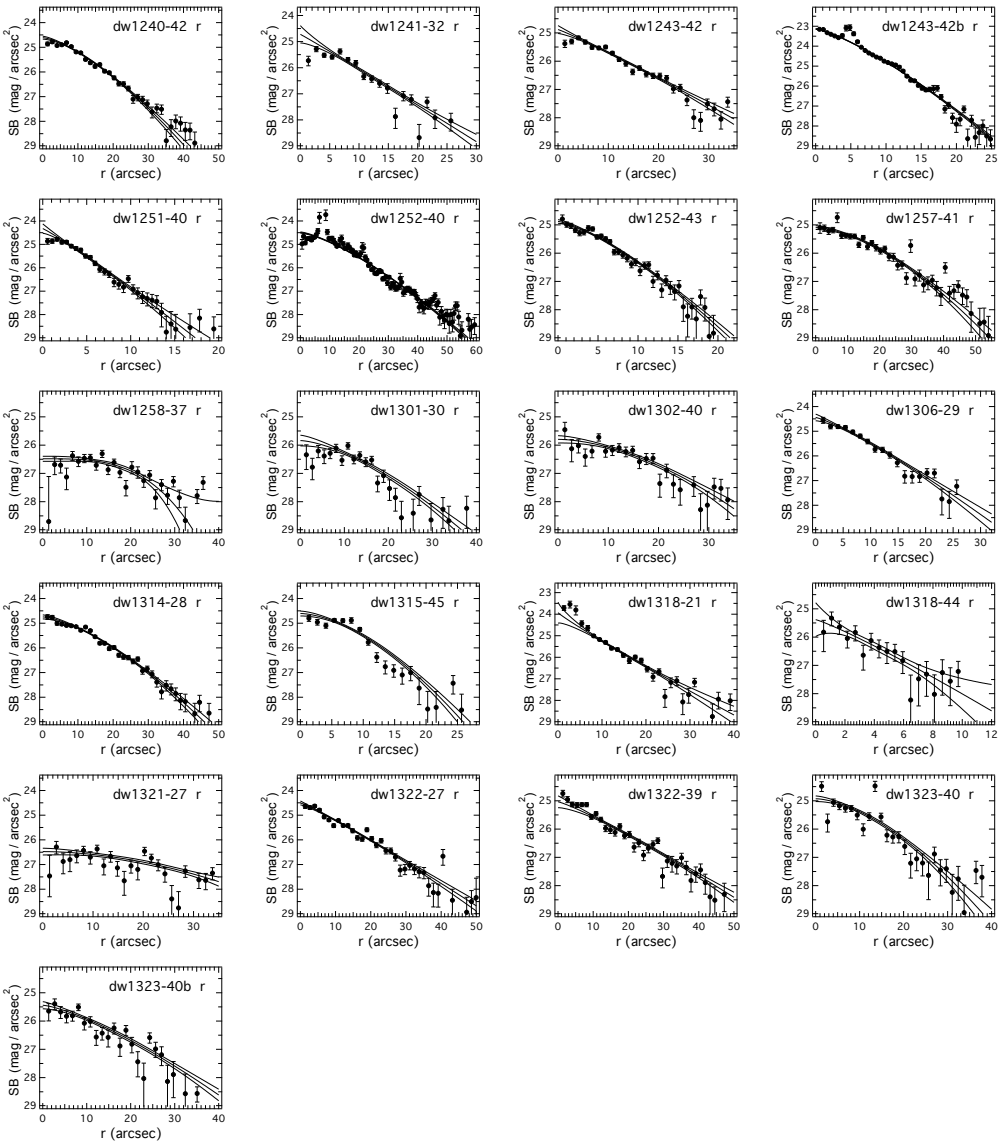

Fig. 8: Radial surface brightness profiles and best-fitting Sérsic profiles with 1σ confidence intervals for all dwarf candidates in the r band.

corrected absolute r-band magnitude. The assumed distance for the candidates is the mean distance of the Centaurus group (4.5 Mpc). For the known galaxies we used the individual distances listed in the Updated Nearby Galaxy Catalog (Karachentsev et al. 2013); (7) extinction-corrected integrated $g-r$ color; (8) Sérsic central surface brightness in the r band; (9) Sérsic scale length in the r band; (10) Sérsic curvature index in the r band; (11) mean effective surface brightness in the r band; and (12) effective radius in the r band.

5. Discussion

Prior to our study there were about 60 group members known in the whole Centaurus group (Karachentseva & Karachentsev 1998; Karachentsev et al. 2002, 2013; Jerjen

Tab. 2: Photometric and structural parameters of the new Centaurus group dwarf candidates in the surveyed region.

Name	g_{tot}	r_{tot}	A_g	A_r	M_r	$(g-r)_{0,tot}$	$\mu_{0,r}$	$r_{0,r}$	n_r	$\langle\mu\rangle_{eff,r}$	$r_{eff,r}$
	mag	mag	mag	mag	mag	mag	mag arcsec^{-2}	arcsec		mag arcsec^{-2}	arcsec
(1)	(2)	(3)	(4)	(5)	(6)	(7)	(8)	(9)	(10)	(11)	(12)
dw1240-42	17.94	17.21	0.366	0.253	-11.29	0.613	24.61 ± 0.06	15.35 ± 0.70	1.45 ± 0.10	25.24	16.0
dw1241-32	19.08	18.46	0.322	0.223	-10.02	0.519	24.72 ± 0.33	8.21 ± 2.51	1.03 ± 0.22	25.76	11.4
dw1243-42	18.40	17.76	0.329	0.227	-10.72	0.542	24.88 ± 0.14	13.04 ± 1.77	1.08 ± 0.16	25.78	15.8
dw1243-42b	17.64	17.19	0.230	0.171	-11.24	0.387	23.14 ± 0.02	7.24 ± 0.12	1.30 ± 0.02	23.57	7.4
dw1251-40	19.54	19.21	0.358	0.248	-9.30	0.220	24.33 ± 0.20	4.56 ± 0.84	1.09 ± 0.17	25.32	6.5
dw1252-40	16.70	16.17	0.353	0.244	-12.33	0.427	24.49 ± 0.03	20.19 ± 0.42	1.38 ± 0.03	24.32	16.7
dw1252-43	19.39	18.94	0.321	0.222	-9.54	0.353	24.88 ± 0.06	8.13 ± 0.44	1.37 ± 0.10	25.53	8.11
dw1257-41	17.33	16.66	0.424	0.293	-11.89	0.536	25.10 ± 0.07	24.75 ± 1.21	1.63 ± 0.16	25.63	24.0
dw1258-37	18.63	18.04	0.182	0.126	-10.34	0.532	26.48 ± 0.09	26.50 ± 1.44	3.30 ± 1.28	26.78	22.0
dw1301-30	18.94	18.47	0.265	0.183	-9.97	0.382	25.84 ± 0.19	18.17 ± 2.62	1.52 ± 0.28	26.38	14.8
dw1302-40	18.58	17.78	0.372	0.258	-10.74	0.684	25.79 ± 0.13	21.87 ± 2.00	1.73 ± 0.35	26.40	20.6
dw1306-29	18.58	17.90	0.347	0.240	-10.60	0.576	24.44 ± 0.14	10.31 ± 1.27	1.20 ± 0.16	25.15	10.9
dw1314-28	17.58	17.04	0.260	0.180	-11.39	0.453	24.74 ± 0.08	18.34 ± 1.09	1.49 ± 0.13	25.35	18.1
dw1315-45	18.39	18.06	0.348	0.241	-10.44	0.227	24.61 ± 0.10	11.24 ± 0.82	1.67 ± 0.17	25.02	9.5
dw1318-21	18.06	17.26	0.353	0.245	-11.24	0.691	23.93 ± 0.49	8.14 ± 3.68	0.93 ± 0.25	24.72	12.4
dw1318-44	20.51	20.61	0.332	0.230	-7.88	-0.190	25.38 ± 0.60	4.59 ± 2.54	1.13 ± 0.72	26.13	4.8
dw1321-27	18.67	18.13	0.210	0.145	-10.27	0.473	26.47 ± 0.14	32.94 ± 2.72	1.87 ± 0.71	26.89	22.3
dw1322-27	17.71	17.05	0.218	0.151	-11.35	0.593	24.50 ± 0.08	14.76 ± 1.12	1.10 ± 0.09	25.36	18.2
dw1322-39	17.60	17.12	0.293	0.203	-11.34	0.387	25.03 ± 0.21	18.70 ± 3.42	1.15 ± 0.19	25.74	20.7
dw1323-40	17.74	17.33	0.373	0.258	-11.19	0.301	24.93 ± 0.10	16.99 ± 1.31	1.64 ± 0.23	25.27	15.2
dw1323-40b	18.16	17.84	0.401	0.277	-10.69	0.193	25.44 ± 0.13	18.09 ± 2.03	1.35 ± 0.19	26.06	17.1
dw1323-40c	18.62	18.32	0.380	0.263	-10.20	0.181	26.40 ± 0.16	27.12 ± 2.48	2.48 ± 1.21	26.90	20.2
dw1326-37	18.90	18.47	0.226	0.156	-9.95	0.358	25.49 ± 0.11	14.28 ± 1.17	1.72 ± 0.27	25.57	10.2
dw1329-45	19.15	18.81	0.305	0.211	-9.66	0.243	25.48 ± 0.09	12.70 ± 0.81	1.84 ± 0.27	25.86	9.9
dw1330-38	19.44	18.63	0.154	0.107	-9.74	0.758	25.91 ± 0.42	11.81 ± 5.42	0.99 ± 0.47	27.14	20.1
dw1331-37	20.15	19.06	0.256	0.177	-9.38	1.005	26.40 ± 0.18	16.71 ± 1.83	1.90 ± 0.72	27.28	17.8
dw1331-40	20.53	19.80	0.297	0.206	-8.67	0.637	26.38 ± 0.35	13.11 ± 3.69	1.41 ± 0.60	26.89	10.4
dw1336-44	19.54	18.80	0.400	0.277	-9.74	0.618	25.09 ± 0.05	11.26 ± 0.36	2.45 ± 0.20	25.34	8.07
dw1337-41	18.98	18.88	0.301	0.208	-9.59	0.006	26.81 ± 0.14	28.19 ± 2.43	2.04 ± 0.51	27.29	18.3
dw1337-44	18.72	18.86	0.353	0.244	-9.65	-0.240	25.05 ± 0.40	7.78 ± 2.98	1.02 ± 0.27	26.06	10.3
dw1341-43	17.92	17.47	0.309	0.214	-11.00	0.348	25.58 ± 0.10	21.37 ± 1.10	2.14 ± 0.49	26.06	20.2
dw1342-43	17.98	17.23	0.263	0.182	-11.21	0.676	24.36 ± 0.09	12.69 ± 0.88	1.38 ± 0.11	25.19	15.5
dw1343-34	19.81	19.07	0.205	0.142	-9.34	0.681	26.82 ± 0.20	25.42 ± 3.52	1.82 ± 0.52	27.45	18.9
dw1357-28	19.36	18.70	0.204	0.141	-9.70	0.598	26.40 ± 0.16	21.29 ± 1.77	2.90 ± 1.36	26.72	15.6
dw1401-32	18.37	17.59	0.217	0.150	-10.82	0.715	25.16 ± 0.08	17.15 ± 1.24	1.37 ± 0.15	25.69	16.8
dw1403-33	18.69	17.82	0.232	0.160	-10.60	0.803	25.84 ± 0.10	23.87 ± 1.28	2.06 ± 0.37	26.16	18.8
dw1406-29	18.62	18.56	0.197	0.137	-9.83	0.000	26.12 ± 0.22	16.42 ± 2.51	1.69 ± 0.63	27.27	21.1
dw1409-33	18.59	18.39	0.229	0.158	-10.02	0.124	26.18 ± 0.25	18.15 ± 3.32	1.46 ± 0.58	26.96	20.0
dw1410-34	17.68	17.41	0.239	0.165	-11.01	0.204	23.42 ± 0.58	2.90 ± 2.37	0.55 ± 0.14	25.70	17.7
dw1413-34	19.98	19.34	0.231	0.160	-9.08	0.569	25.80 ± 0.13	10.29 ± 1.00	1.59 ± 0.34	26.48	10.6
dw1415-32	18.69	18.09	0.227	0.157	-10.32	0.525	23.89 ± 0.18	4.91 ± 1.01	0.85 ± 0.11	24.94	9.2

Absolute magnitudes in column 6 assume a mean distance of 4.5 Mpc. Total magnitudes have a mean uncertainty of 0.3 mag (see text). The last digit of the listed parameters (hundredth of magnitude) is therefore not significant. However, we leave this digit here so as not to introduce rounding errors, should these quantities be used in further arithmetic operations.

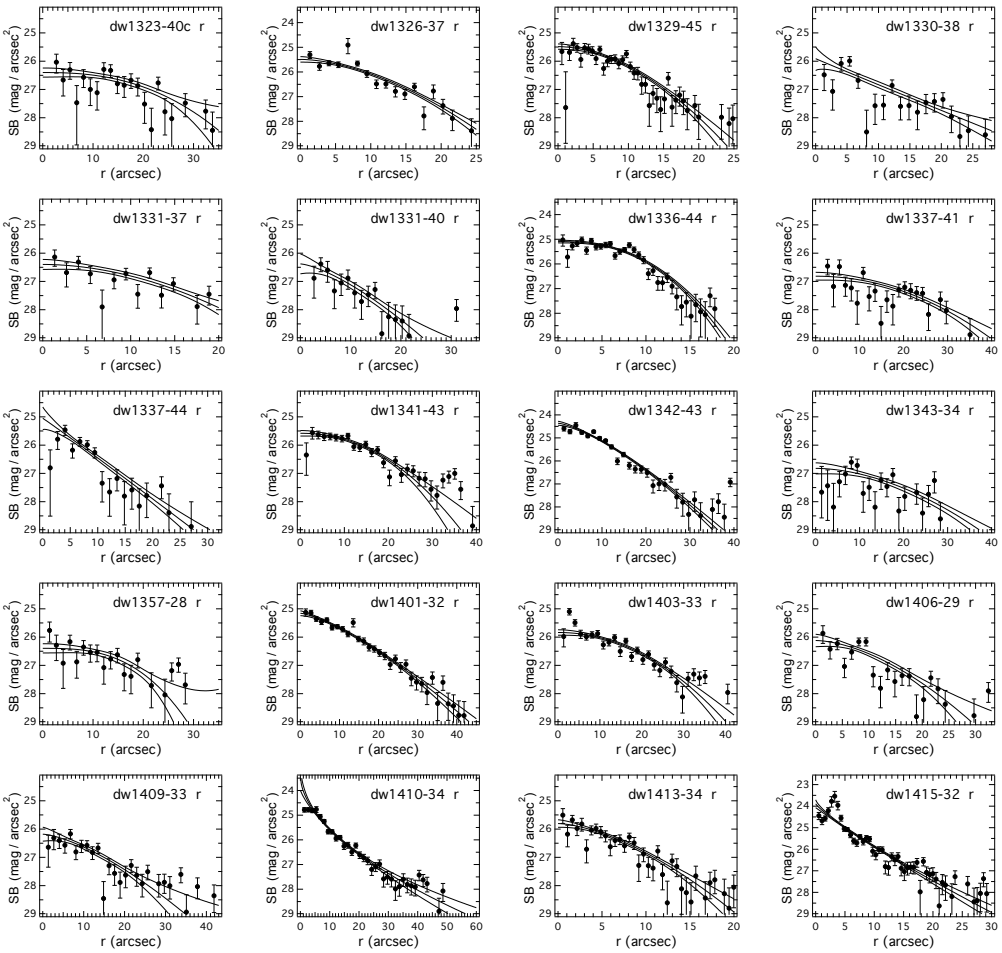

Fig. 9: Fig. 8 continued.

et al. 2000a,b; Crnojević et al. 2014, 2016), half of these have accurate distances while the others got preliminary membership based on morphology or velocity measurements. This galaxy population has the potential to almost double in size if the majority of the 41 + 16 (MJB15) new dwarf galaxies are confirmed as group members. In this context a number of interesting questions arise: What are our detection limits? How plausible are the new candidates? Are their photometric and structural properties comparable to the Local Group and known Centaurus group dwarfs, or are they perhaps associated with background galaxies? Due to the lack of distance information these questions shall be addressed with the help of the available photometric results.

Detection limits

As mentioned at the end of Sect. 2, the photometric depth for the various DECam observing campaigns, including the one our previous study (MJB15) was based on, is uniform within a range of 0.3 mag. In MJB15 we conducted extensive artificial galaxy tests to determine the detection limits and efficiency of our search for low

surface brightness objects. The results of this testing, also valid for the present study, are shown in Fig. 4 of MJB15. The figure shows the fraction of detected artificial galaxies as a function of total magnitude and central surface brightness. The detection efficiency is generally above 80% for galaxies brighter than m=19 r mag and with a central surface brightness $\mu < 26.5$ V mag. An alternative way to represent detection efficiency is the completeness boundary curve of Ferguson (1990) and Ferguson & Sandage (1988), assuming exponential surface brightness profiles (Sérsic Index $n = 1$) for the objects. The corresponding equation for this completeness curve is

$$m_{tot} = \mu_{lim} - \frac{r_{lim}}{0.5487 r_{eff}} - 2.5 \log[2\pi \cdot (0.5958 \cdot r_{eff})^2],$$

meaning that (nearly) all, or most objects with a diameter larger than $2r_{lim}$ at the surface brightness level of μ_{lim} should have been detected. Our best estimates for the two free limiting parameters in MJB15 (see Figs. 4 and 6 there) was $r_{lim} \approx 20$ arcsec and $\mu_{lim} \approx 28$ V mag arcsec^{-2}. For the present study we found a slightly smaller radius of $r_{lim} \approx 13$ arcsec gives a boundary curve that better fits the data.

To allow for a comparison of our results with the Local Group dwarfs (data from McConnachie 2012) we used Eq. (1) to transform our gr photometry to the V band. Having all the galaxies on the same photometric system, in Fig.7 we plot the effective radius versus total V-band luminosity relation for our candidates, all known Centaurus dwarfs in the survey area for which we have photometry in Table 3, Local Group dwarf galaxies, and the candidates from MJB15. Absolute magnitudes for the Centaurus galaxy candidates are based on a mean distance of 4.5 Mpc. The solid curve represents the completeness boundary curve given above with best estimates $r_{lim} \approx 13$ arcsec and $\mu_{lim} \approx 28$ V mag arcsec^{-2}, suggesting that we detected most dwarf galaxy candidates in our survey footprint with diameters larger than 26 arcsec (≈ 600 pc) at a surface brightness of 28 V mag arcsec^{-2}. These quantities translate roughly into a luminosity limit of $M_V \approx -10$ or $M_r \approx -9.5$. The completeness boundary curve, properly transformed to the $\mu - M$ plane, is also shown in Fig. 9.

Centaurus group membership

As we discussed in section 3, the photometric depth of our survey data reached the brightest stars in some of the dwarf candidates, but photometry of red giant branch stars at least 1 mag fainter would be necessary to establish TRGB distances for the dwarf candidates. Another means to measure distances of galaxies is the surface brightness fluctuation method (SBF; Tonry & Schneider 1988). This method was successfully tested for early-type dwarfs by Jerjen et al. (2000b) and used to measure distances to five dE galaxies in the Centaurus group and many more in the Local Volume (Jerjen et al. 2001; Rekola et al. 2005). The minimum exposure time required for the SBF method to work can be calculate using equation (1) in Dunn

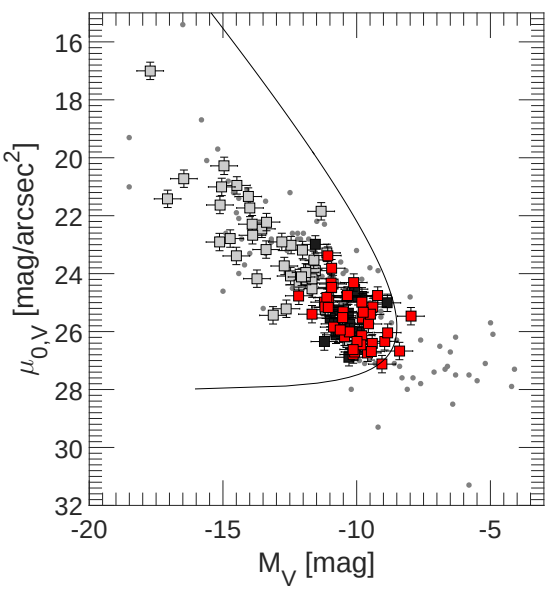

Fig. 10: For our dwarf candidates, $\mu_0 - M$ relation in the V band (red squares), all known dwarfs of the Centaurus group in the survey area (gray filled squares), Local Group dwarf galaxies (dots; McConnachie 2012) and the candidates from MJB15 (black squares). The newly discovered Centaurus dwarf candidates have similar properties to those of known Centaurus dwarfs and Local Group dwarfs.

& Jerjen (2006). Using $\mu_{gal} = 25$ mag arcsec^{-2} for the mean surface brightness of a typical dwarf candidate in this survey, the sky surface brightness $\mu_{sky} = 21$ mag arcsec^{-2}, a distance modulus of 28.0 for the Cen A subgroup, the fluctuation luminosity of the underlying stellar population $\overline{M_r} = -1.3$ mag, and the photometric zero point $m_1 = 24$ mag gives an integration time of 2400 sec (S/N=5), which is six times longer than the exposure times of our DECam images.

As the new dwarf candidates are not resolved into stars and the SBF method requires longer integration times, the only way to test (or rather suggest) group membership at the moment is to compare the photometric and structural properties of the galaxy candidates with the known dwarfs in the Centaurus group and Local Group. This can be achieved with the surface brightness – luminosity relation. To calculate the luminosities of the candidates we placed them at the mean distance of the Centaurus group (4.5 Mpc). Because the surface brightness is a distance independent quantity, the only parameter that decides how well a candidate fits into the $\mu - M$ relation is the luminosity and thus the assumed distance. We plot the central surface brightness μ_0 for all galaxies versus their estimated absolute magnitude M_V for Local Group dwarfs, the known Centaurus dwarfs, candidates from MJB15, and candidates from this work in Fig. 10. The Local Group dwarf μ_0 values come from King or exponential profiles, while our photometric parameter comes from Sérsic fits. Our candidates are in good accord with the photometric values of known dwarfs. They all fit into the relation outlined by the Local Group dwarfs and naturally bridge the gap to the more luminous dwarfs in the Centaurus group. This agreement provides qualitative evidence that the majority of the new dwarf candidates are indeed Centaurus group members.

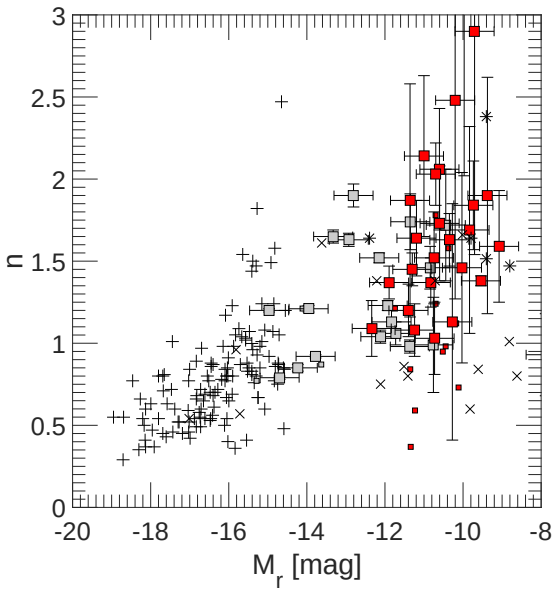

Fig. 11: Shape parameter - luminosity (Sérsic $n - M_r$) relation for early-type dwarf galaxies. The known Centaurus dSph dwarfs in the survey region (gray squares), Virgo dEs (plus signs; Binggeli & Jerjen 1998), M 81 dSph dwarfs (stars; Chiboucas et al. 2009), Local Group dSph (crosses; Jerjen et al. 2000a), MJB15 known and candidates dSph (small gray and red squares) and the new dSph known dwarfs and candidates of this study (gray and red squares), respectively. Error bars for our candidates and previously known dwarfs in the survey area come from numerics and are listed in Table 2. The error bars for the absolute magnitudes is globally chosen to be $\pm$0.5 mag. We compare n_B (Virgo) with n_r (M 81, Local Group, MJB15, and this work).

Complementary to this we can compare the shape parameter n from the best-fitting Sérsic profiles of our dwarfs with the Sérsic indices of Local Group, Virgo, M 81, and the known Cen A dwarfs (Fig. 11). The faint end of the shape parameter - luminosity relation is notably widespread. Still, the Sérsic indices of the candidates are in good agreement with the known dwarfs and fit into the relation.

We can also look into the membership question by studying the 3D distribution of galaxies in the direction of the survey region. No massive galaxies are known in the immediate vicinity behind the Centaurus group. This is illustrated in Fig. 12, where we plot the wedge diagram in right ascension for the galaxies with measured distances. Data were taken from the Cosmicflows-2 catalog (Tully et al. 2013). The Centaurus group is the prominent overdensity covering the distance range $3.0 < D < 6.5$ Mpc. Behind the group is the Local Void (Tully et al. 2008, 2015) followed by a low density environment made up of a population of field galaxies and small groups. There is no larger concentration of galaxies within 30 Mpc. The conclusion is that galaxies found in our survey area either belong to the Centaurus group or must be background galaxies at least $2 - 3$ times further away.

We further tested the hypothesis that some of our candidates are satellites of luminous background galaxies. For example, dw1321-27 and dw1322-27 are approximately 20 arcmin away from the barred spiral galaxy NGC 5101, which has a velocity of 1868 km s^{-1} (Koribalski et al. 2004) and a luminosity-line width distance of 27.4 Mpc (Tully & Fisher 1988). At that distance the linear separation between these galaxies would be around 164 kpc. This is comparable with the distance between Fornax and the Milky Way (McConnachie 2012). Nine of our candidates have a background galaxy within a radius of 60 arcmin. We plotted these candidates

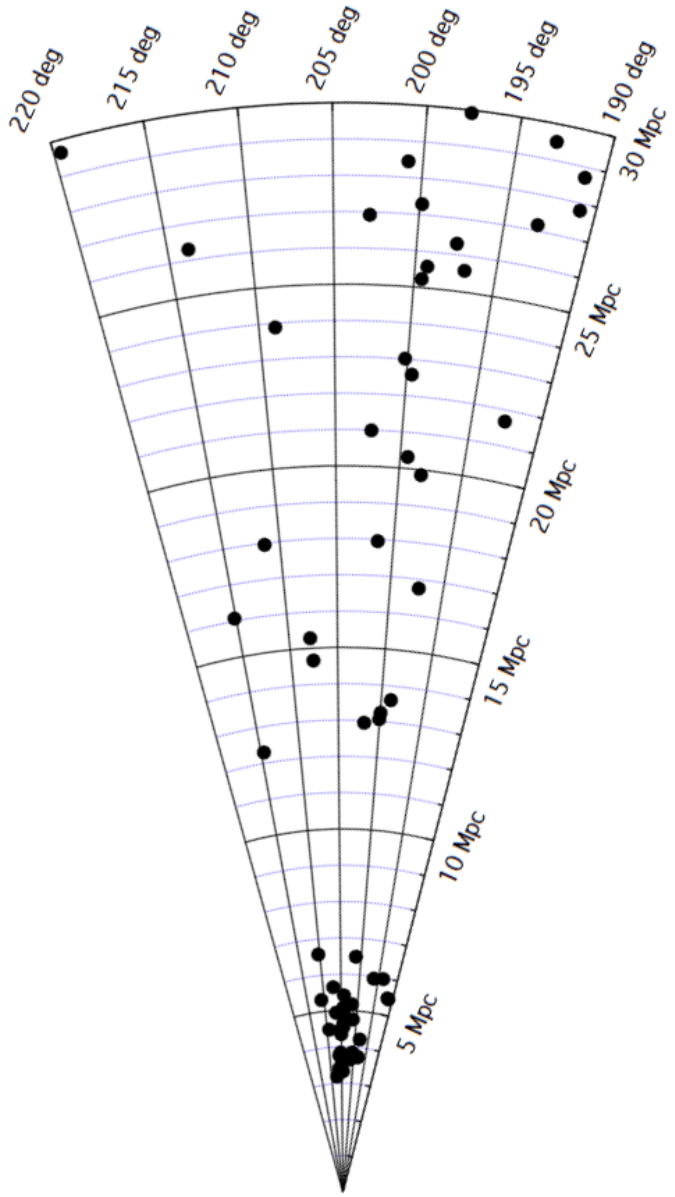

Fig. 12: Wedge diagram in right ascension for all galaxies with measured distances in the direction of the survey region ($190^\circ < \alpha < 220^\circ$ and $-45^\circ < \delta < -20^\circ$). Data taken from the Cosmicflows-2 catalog (Tully et al. 2013). The Centaurus group is the prominent overdensity covering the distance interval $3 < D < 6.5$ Mpc. The region behind the Centaurus group is the Local Void followed by a low density environment made up of a small number of field galaxies with distances $D > 12$ Mpc.

again in the $\mu - M$ diagram (Fig. 13) this time with an absolute magnitude that corresponds to the velocity distance of the background galaxy. The three candidates, dw1301-30, dw1321-27, and dw1403-33, now fall outside of the relation defined by the known dwarfs, making their association to a background galaxy unlikely. The situation for the other six candidates remains ambiguous in this test, and thus they got a *bg?* label in Table 1. However, given that these candidates are located at the edge of the general trend makes them more likely to be Centaurus group members than background galaxies.

Crnojević et al. (2014) found the first close pair of faint dwarf galaxies outside the Local Group in the halo of Cen A, namely the pair CenA-MM-Dw1 and CenA-MM-Dw2, with a projected distance of 3 kpc. Our galaxy sample contains two other potential pairs of dwarf galaxies in the same group, (dw1243-42, dw1243-42b) and

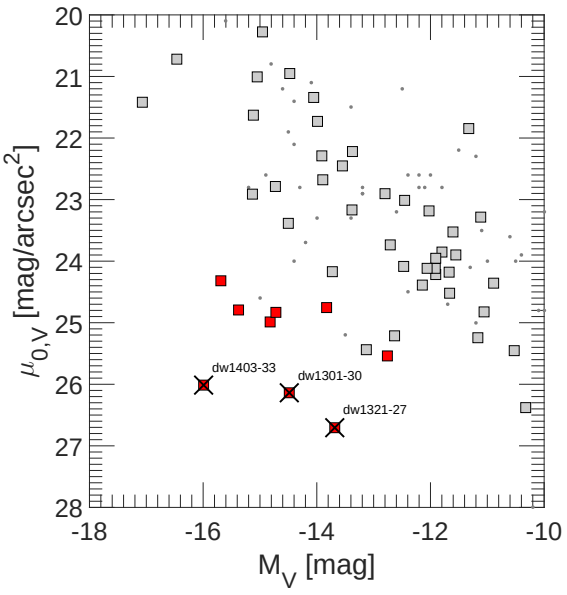

Fig. 13: $\mu_0 - M$ relation for the Local Group and Centaurus group galaxies. We added nine dwarf candidates (red squares) adopting the distances of background galaxies that were close to the dwarf in the sky. If a candidate is a satellite of the background galaxy, it should follow the same relation as defined by the Centaurus and Local Group dwarfs. We crossed out the candidates that we dismissed as possible background galaxies, meaning that they are more probably Centaurus group members. The candidates that are closer than 1 mag (radial distance) from any known dwarf in the relation could be background dwarf galaxies and are indicated as *bg?* in Table 1. All such *bg?* candidates are still outside of the relation, making them unlikely to be background dwarfs; this is why we still present them as possible Centaurus group members.

(dw1251-40, dw1252-40). They are separated by 75 arcsec (1.6 kpc at 4.5 Mpc) and 135 arcsec (2.9 kpc at 4.5 Mpc), respectively.

Galaxy distribution

Tully et al. (2015) reported that almost all members of the Cen A subgroup with known distances are distributed in two thin parallel planes. The authors further noted that one of these planes points in the direction of M 83. Interestingly, all but one of the nine dwarfs detected in the PISCeS survey also belong to the two planes (Crnojević et al. 2016). Looking at the 2D distribution of our new dwarf candidates, we find that a significant number of those candidates in the vicinity of Cen A are aligned in the Cen A-M 83 direction (see Fig. 2). This confirms the result of the PISCeS survey that most of their galaxies were found in the northward direction. The opposite situation is observed in the M 83 subgroup where the MJB15 candidates are preferentially found southward of M 83 in the direction of Cen A. Intriguingly, even when looking on the galactic scale there is evidence of asymmetry, such as the lopsided distribution of star-forming regions in the outer disk of M83 with a large number detected on the southern side and only a few on the northern side as evident in deep GALEX images (Thilker et al. 2005). Is this a hint of some kind of dwarf galaxy substructure between the two main galaxies, possibly a filament of dwarf galaxy infall, or an extension of the Cen A plane? Another interesting feature revealed by the new candidates is an elongated, filamentary structure that runs diagonally through the group, from $(\alpha/\delta) \approx$ (14:20,−33) to ≈ (12:40,−43), seemingly separating the two subgroups (see Fig. 2). At the distance of 4.5 Mpc this structure extends over 1.8 Mpc. Accurate distances to the new dwarf galaxy

candidates will be needed for a more quantitative assessment of the substructural properties of the Centaurus group.

6. Conclusions

We have conducted the first CCD-based, large-scale survey of the nearby Centaurus group covering an area of over 500 square degrees or 3.3 Mpc^2. We found a total of 41 new dwarf galaxy candidates (in addition to 16 new candidates reported on previously in MJB15) in the magnitude range $17 < r < 20.5$ mag and surface brightness range of $24 < \langle\mu\rangle_{eff,r} < 27$ mag asec^{-2} pushing the absolute magnitude limit of the galaxy population down to $M_r \approx -9.5$. Although no distance information is currently available, except for dw1335-29 (Carrillo et al. 2016), the comparison of the photometric and structural parameters of the candidates with the known dwarf galaxies strongly suggests that the majority of the galaxies belong to the Centaurus group. Follow-up measurements of the distances are crucial to confirm their membership. There are a number of research areas that will greatly benefit from further analysis of the new galaxies. The mere abundance and spatial distribution of the Centaurus galaxies will be a new empirical benchmark to test structure formation processes and the cosmological models behind them. Is the Local Group a statistical outlier or does the conflict with ΛCDM also apply to the Centaurus group? In this context, understanding the two galaxy planes will play a central role. How were they formed and why are they almost parallel? Is there a dwarf galaxy bridge from Cen A to the M 83 subgroup? The expected small distance uncertainties in the range of 0.2-0.5 Mpc from the TRGB method will be instrumental to trace the 3D galaxy distribution along the 2 Mpc line-of-sight depth of the Centaurus group. It will be intriguing to see how the new dwarf galaxies are distributed in the double planar structure. One possibility is that they will increase the statistical significance of the bimodality, proving the double structure to be real beyond any doubt. The exact significance level will depend on the intrinsic thickness of the planes, the plane orientations relative to the line-of-sight, and the number of galaxies in each component. Another possible outcome is that the new galaxies fill the ≈0.1 Mpc gap between the two planes (see histogram on the right side of Fig. 1 of Tully et al. (2015)) and thus reveal that the double planar structure was in fact an artifact of small number statistics. How do the stellar populations in the new Centaurus dwarfs compare to Local Group look-alikes? Crnojević et al. (2010, 2011a,b, 2012) conducted an extensive study of the resolved stellar content of dwarf galaxies in the Centaurus group. They investigated their star formation histories and metallicity content, and what effect the denser environment has on shaping these properties. With the large number of new dwarf galaxies available from our study, this work can be extended and pushed toward lower limits, allowing statistically more robust comparisons with the Local Group dwarf galaxy population.

Acknowledgements

OM and BB are grateful to the Swiss National Science Foundation for financial support. HJ acknowledges the support of the Australian Research Council through Discovery projects DP120100475 and DP150100862. The authors would like to thank Dmitry Makarov and the anonymous referee for helpful comments that improved the paper. This project used data obtained with the Dark Energy Camera (DECam), which was constructed by the Dark Energy Survey (DES) collaborating institutions: Argonne National Lab, University of California Santa Cruz, University of Cambridge, Centro de Investigaciones Energeticas, Medioambientales y Tecnologicas-Madrid, University of Chicago, University College London, DES-Brazil consortium, University of Edinburgh, ETH-Zurich, Fermi National Accelerator Laboratory, University of Illinois at Urbana-Champaign, Institut de Ciencies de l'Espai, Institut de Fisica d'Altes Energies, Lawrence Berkeley National Lab, Ludwig-Maximilians Universitat, University of Michigan, National Optical Astronomy Observatory, University of Nottingham, Ohio State University, University of Pennsylvania, University of Portsmouth, SLAC National Lab, Stanford University, University of Sussex, and Texas A&M University. Funding for DES, including DECam, has been provided by the U.S. Department of Energy, National Science Foundation, Ministry of Education and Science (Spain), Science and Technology Facilities Council (UK), Higher Education Funding Council (England), National Center for Supercomputing Applications, Kavli Institute for Cosmological Physics, Financiadora de Estudos e Projetos, Fundao Carlos Chagas Filho de Amparo a Pesquisa, Conselho Nacional de Desenvolvimento Cientfico e Tecnolgico and the Ministrio da Cincia e Tecnologia (Brazil), the German Research Foundation-sponsored cluster of excellence "Origin and Structure of the Universe" and the DES collaborating institutions. This research was made possible through the use of the AAVSO Photometric All-Sky Survey (APASS), funded by the Robert Martin Ayers Sciences Fund.

Tab. 3: Photometric parameters of known dwarf galaxies in the surveyed region.

Names (alt. names) (1)	type	α (J2000.0)	δ (J2000.0)	g_{tot} mag (2)	r_{tot} mag (3)	A_g mag (4)	A_r mag (5)	M_r mag (6)	$(g-r)_{0,tot}$ mag (7)	$\mu_{0,r}$ mag arcsec^{-2} (8)	$r_{0,r}$ arcsec (9)	n_r (10)	$\langle\mu\rangle_{eff,r}$ mag arcsec^{-2} (11)	$r_{eff,r}$ arcsec (12)
KKs51	dE	12:44:21	-42:56:23	17.22	16.61	0.288	0.199	-11.36	0.513	22.98 ± 0.07	7.37 ± 0.47	0.98 ± 0.04	24.16	12.7
ESO381-018	dIrr	12:44:42	-35:57:59	15.47	14.42	0.208	0.144	-14.39	0.978	21.29 ± 0.02	11.60 ± 0.19	1.27 ± 0.02	22.06	13.6
ESO381-020	dIrr	12:46:00	-33:50:13	13.81	13.69	0.217	0.150	-15.14	0.051	22.77 ± 0.02	31.36 ± 0.38	1.38 ± 0.02	23.29	31.9
ESO443-009	dIrr	12:54:54	-28:20:27	16.70	16.50	0.212	0.147	-12.52	0.142	24.23 ± 0.03	18.93 ± 0.33	2.12 ± 0.08	24.45	15.1
Cen6 (KK182)	dIrr	13:05:02	-40:04:58	15.94	15.63	0.339	0.234	-13.46	0.206	23.00 ± 0.04	13.98 ± 0.44	1.36 ± 0.04	23.64	15.0
MCG-04-31-038	dIrr	13:09:36	-27:08:26	14.73	14.42	0.252	0.174	-15.20	0.235	21.60 ± 0.02	12.98 ± 0.17	1.40 ± 0.02	22.29	14.3
Cen7 (KKs53)	dE,N	13:11:14	-38:54:22	16.03	15.38	0.300	0.208	-12.14	0.552	23.84 ± 0.02	25.26 ± 0.38	1.52 ± 0.03	24.33	24.5
CenA-dE1 (KK189)	dE	13:12:45	-41:49:55	16.93	16.49	0.366	0.253	-11.93	0.319	23.54 ± 0.03	12.35 ± 0.28	1.23 ± 0.03	24.32	14.4
ESO269-066	dE,N	13:13:08	-44:53:21	13.78	13.12	0.314	0.217	-14.96	0.570	22.46 ± 0.01	34.37 ± 0.25	1.20 ± 0.01	23.17	40.6
NGC5011C	dE,N	13:13:11	-43:15:55	14.08	13.43	0.398	0.276	-14.69	0.528	20.92 ± 0.05	9.51 ± 0.41	0.79 ± 0.01	22.48	25.4
KK195	dIrr?	13:21:08	-31:31:45	16.77	16.91	0.203	0.140	-11.81	-0.200	24.19 ± 0.09	11.26 ± 1.13	0.91 ± 0.06	25.34	18.4
CenA-dE2 (KKs54)	dSph	13:21:32	-31:53:11	17.76	17.24	0.215	0.148	-11.35	0.453	24.98 ± 0.08	20.29 ± 1.06	1.74 ± 0.17	25.38	16.6
KK196	dIrr?	13:21:47	-45:03:47	15.70	15.20	0.276	0.191	-12.97	0.412	22.69 ± 0.03	13.03 ± 0.37	1.11 ± 0.03	23.27	16.0
KK197 (SGC1319.1-4216)	dE,N	13:22:01	-42:32:08	15.02	14.31	0.511	0.353	-13.95	0.548	23.87 ± 0.02	39.46 ± 0.63	1.21 ± 0.02	24.56	44.4
KKs55	dSph	13:22:12	-42:43:44	16.02	15.44	0.472	0.327	-12.80	0.428	24.92 ± 0.02	45.55 ± 0.74	1.90 ± 0.07	25.28	36.4
Cen8 (KK198)	dIrr	13:22:56	-33:34:22	17.20	16.74	0.043	0.030	-11.73	0.445	23.64 ± 0.04	12.48 ± 0.36	1.52 ± 0.06	24.12	11.7
CenA-MM-Dw4	dSph	13:23:02	-41:47:10	18.16	17.48	0.415	0.287	-10.75	0.551	25.10 ± 0.37	14.40 ± 5.32	0.99 ± 0.29	26.03	20.3
AM1320-230	dE	13:23:29	-23:23:35	16.83	16.51	0.267	0.184	-12.11	0.237	23.02 ± 0.05	8.28 ± 0.41	1.04 ± 0.04	24.10	12.8
AM1321-304 (KK200)	dE/dIrr	13:24:36	-30:58:18	15.39	14.76	0.228	0.158	-13.77	0.554	22.23 ± 0.02	11.57 ± 0.28	0.92 ± 0.01	23.40	21.1
CenA-MM-Dw1	dSph	13:30:14	-41:53:25	15.37	14.76	0.419	0.290	-13.33	0.605	25.11 ± 0.02	65.29 ± 1.03	1.65 ± 0.04	25.61	58.3
CenA-MM-Dw9	dSph	13:33:01	-42:31:48	18.12	17.72	0.382	0.265	-10.44	0.288	25.89 ± 0.14	23.41 ± 2.41	1.72 ± 0.34	26.71	24.4
HIPASSJ1337-39	dIrr	13:37:25	-37:53:48	16.31	16.26	0.247	0.171	-12.43	-0.020	23.01 ± 0.05	11.04 ± 0.35	1.48 ± 0.05	23.48	10.6
KKs57	dSph	13:41:38	-42:34:55	17.28	17.28	0.297	0.206	-10.84	-0.090	24.18 ± 0.10	12.23 ± 0.91	1.46 ± 0.13	24.80	12.0
KK211 (AM1339-445)	dE,N	13:42:05	-45:12:20	15.80	15.15	0.368	0.254	-12.92	0.530	23.42 ± 0.02	24.68 ± 0.33	1.63 ± 0.04	23.86	21.8
KK213	dE	13:43:35	-43:46:09	16.60	16.37	0.322	0.223	-11.72	0.131	23.89 ± 0.07	12.63 ± 0.91	1.06 ± 0.07	25.01	20.5
ESO325-011	S/Irr	13:45:00	-41:51:37	13.55	13.28	0.291	0.201	-14.57	0.181	23.22 ± 0.01	50.28 ± 0.46	1.56 ± 0.02	23.67	46.1
CenA-dE4 (KK218)	dE	13:46:40	-29:58:41	17.24	16.77	0.198	0.137	-11.83	0.409	24.16 ± 0.10	13.95 ± 1.28	1.13 ± 0.10	25.01	17.0
HIPASSJ1348-37	dIrr	13:48:47	-37:58:29	16.95	16.73	0.257	0.178	-12.20	0.140	24.25 ± 0.13	13.54 ± 1.81	0.97 ± 0.09	25.23	19.2
ESO383-087	S/Irr	13:49:17	-36:03:48	10.98	10.40	0.237	0.164	-17.28	0.513	21.03 ± 0.01	48.84 ± 0.59	1.06 ± 0.01	22.04	83.4
ESO384-016	dE/dIrr	13:45:04	-35:05:21	14.69	14.19	0.245	0.169	-14.23	0.427	21.01 ± 0.04	7.72 ± 0.29	0.85 ± 0.02	22.37	16.7

References for the B-band photometry: ESO443-009 and ESO383-087 (Lauberts & Valentijn 1989); AM1321-304/KK200 (Metcalfe et al. 1994); HIPASSJ1337-39 and HIPASSJ1348-37 (Banks et al. 1999); CenA-dE1/KK189, KK197/SGC1319.1-4216, Cen8/KK198, KK211/AM1339-445, CenA-dE2/KKs54, ESO381-018, CenA-dE4/KK218, ESO384-016, ESO269-066 and KK196 (Jerjen et al. 2000a); Cen7/KKs53 and KKs55 (Huchtmeier et al. 2001); AM1320-230, ESO325-011, ESO381-020, Cen6/KK182, KK195, KK213, KKs51 and KKs57 (Karachentsev et al. 2002, 2004, 2013); NGC5101C (Saviane & Jerjen 2007); MCG-04-31-038 (Makarova et al. 2009); CenA-MM-Dw1, CenA-MM-Dw4 and CenA-MM-Dw9 (Crnojević et al. 2014, 2016). No adaption for different photometry techniques were made.

5.3 The M 101 group complex: new dwarf galaxy candidates and spatial structure

— Oliver Müller, Roberto Scalera, Bruno Binggeli, Helmut Jerjen —

Astronomy & Astrophysics, 2017, 602, A119

Abstract

The fine details of the large-scale structure in the local universe provide important empirical benchmarks for testing cosmological models of structure formation. Dwarf galaxies are key object for such studies. Our aim was to enlarge the sample of known dwarf galaxies in the local universe. We performed a search for faint unresolved low-surface-brightness dwarf galaxies in the M 101 group complex, including the region around the major spiral galaxies M 101, M 51, and M 63 lying at a distance of 7.0, 8.6, and 9.0 Mpc, respectively. The new dwarf galaxy sample can be used in a first step to test for significant substructure in the 2D distribution and in a second step to study the spatial distribution of the galaxy complex. Using filtering algorithms we surveyed 330 square degrees of imaging data obtained from the Sloan Digital Sky Survey. The images were visually inspected. The spatial distribution of known galaxies and candidates was analyzed and the system transformed into a M 101 eigenframe using the geometrical alignment of the group. We discovered 15 new dwarf galaxies and carried out surface photometry in the g and r bands. The similarity of the photometric properties of these dwarfs to those of Local Group dwarfs suggest membership to the M 101 group complex. The sky distribution of the candidates follows the thin planar structure outlined by the known members of the three subgroups. The ~ 3 Mpc long filamentary structure has a rms thickness of 67 kpc. The planar structure of the embedded M 101 subgroup is even thinner, with $rms = 46$ kpc. The formation of this structure might be due to the expansion of the bordering Local Void. Other implications are discussed as well. We show the viability of SDSS data to extend the sample of dwarfs in the local universe and test cosmological models on small scales.

1. Introduction

Searching the night sky for new stellar systems of ever lower luminosity and surface brightness, with the aim of enlarging the census of known galaxies in the Local Volume (LV, $D \leq 10$ Mpc, Karachentsev et al. 2013), is a permanent and important task of extragalactic astronomy. Aside from an assessment of the faint-end slope of the galaxy luminosity function (e.g., Trentham & Tully 2002), which is a key observation for models of galaxy formation and evolution, it is above all the study of the "fine structure of large-scale structure" (Binggeli 1989), i.e., the 3D distribution

of low-mass galaxies on large scales, that is fed and fostered by the detection of new nearby dwarf galaxies. Low-mass galaxies are expected to trace the distribution of non-baryonic dark matter (DM) on scales from kpc to Mpc, thus serving as a major test bed for models of structure formation. This is highlighted by the recent discovery of surprisingly thin planes of dwarf satellites in the Local Group (LG), around the Milky Way and the Andromeda galaxy (Pawlowski et al. 2012b, 2013; Ibata et al. 2013). The significance of these structures in the context of ΛCDM or alternative cosmological models is hotly debated (cf. Kroupa 2012, Pawlowski et al. 2015a and Libeskind et al. 2014, Cautun et al. 2015a). But what is not debated is the urgent need to test other nearby groups of galaxies for the existence of similar features as the ubiquity of the phenomenon would be a challenge to the standard ΛCDM scenario of structure formation.

The well-known groups of galaxies in the LV (e.g., the Local Group, M81 Group, Cen A/M83 Group, IC 342/Maffei Group, Sculptor filament, and Canes Venatici cloud) have been, and are being, searched for new dwarfs to various surface brightness depths. Three surveys were recently conducted in the southern hemisphere in the directions of the loose Sculptor filament and the rich Centaurus group. There is the very deep but spatially limited (15 deg^2) PISCeS survey (Sand et al. 2014; Crnojević et al. 2014, 2016); the Dark Energy Survey Camera (DECam) based SCABS survey (21 deg^2) in five photometric bands $ugriz$ (Taylor et al. 2016, 2017); and our own 550 deg^2 DECam large-field survey (Müller et al. 2015, 2017a), resulting in the discovery of dozens of new dwarf galaxies. One of our candidates, dw1335-29, has already been confirmed using the TRGB method (Carrillo et al. 2017), and more data is to follow (Müller et al. in preparation). Tully et al. (2015) reported two almost parallel satellite planes in the Centaurus A group. However, with the detection of multiple new dwarf galaxies around Cen A, this bimodal structure is now called into question (Müller et al. 2016). In the northern hemisphere, dedicated deep searches, resulting in the detection of numerous new dwarfs down to a completeness limit of $M_R \approx -10$, were carried out in the rich M 81 group by Chiboucas et al. (2009, 2013). The authors noted that the satellites lie in a flattened (though not planar) distribution. In the M 101 group, which is the focus of the present study, the Dragonfly telescope (Merritt et al. 2014) and an amateur collective (Javanmardi et al. 2016) detected eight new dwarf candidates. Both surveys were confined to the immediate vicinity of M 101 (9 deg^2), leaving out a large portion of the M 101 group complex that includes M 51 and M 63 (see below). A recent HST follow-up of the seven Dragonfly dwarf candidates has revealed that four candidates (M101-DF4-7) are in fact ultra-diffuse galaxies most likely associated with a background group containing the ellipticals NGC5485 and NGC5473 at a distance of ∼27 Mpc (Merritt et al. 2016).

Surprisingly, two of the three new faint Dragonfly dwarf members of the M101 group (Danieli et al. 2017) are also visible on images of the shallower Sloan Digital Sky

Survey (SDSS)[1]. Equally surprising, with few exceptions (Kniazev et al. 2004), the SDSS has not been employed for systematic searches for unresolved low-surface-brightness (LSB) dwarf galaxies over a large sky area. We therefore decided to hunt for new dwarfs in a large SDSS region of 330 square degrees covering not only the M 101 group, but the smaller neighboring groups around M 51 and M 63 as well, which seem to be connected to the former in a filamentary structure (see Fig. 3 in Courtois et al. 2013, also Fig. 1 below), a structure that we tentatively call here the M 101 group complex.

The M 101 group is more distant at 6.95 Mpc (Nataf 2015; Karachentsev et al. 2013) when compared to the rich M 81 and Centaurus A groups (at 4-5 Mpc), and it is completely dominated by the bulgeless spiral galaxy M 101. The group is known for its lack of low-mass galaxies and is possibly the poorest group in the LV (Bremnes et al. 1999). Eleven of the 14 confirmed members of the M 101 group complex are late-type spirals and dwarf irregular (dIrr) galaxies: KK 191, NGC 5023, DDO 182, Holm IV, NGC 5474, NGC 5477, KKH 87, DDO 194 (Karachentsev et al. 2013); NGC 5195 (Tonry et al. 2001); DF1 (Danieli et al. 2017); and NGC 5585 (Karachentsev et al. 1994). Only one is an early-type dwarf elliptical (dE) (UGC 08882; Rekola et al. 2005), and two are dwarf spheoridal (dSph) galaxies (DF2, DF3; Danieli et al. 2017). This stands in direct contrast to rich groups and clusters where early-type dwarf galaxies are the most abundant type of galaxies (Binggeli et al. 1987). The neighboring and environmentally related spiral galaxies M51 (8.6 Mpc; McQuinn et al. 2016) and M 63 (9 Mpc; Jacobs et al. 2009) with their entourage are slightly farther away. It has been debated whether M 51 and M 63 plus satellites should be counted as members of the M 101 group. Tikhonov et al. (2015) argue against this view. In the present work, based on our analysis of the galaxy distribution in the region, we use the term "M 101 group complex" for all three galaxies and their satellites and the term "subgroup" for an individual host and its satellite population (M 101 subgroup, M 51 subgroup, and M 63 subgroup).

In the first part of the paper (Sections 2-4) we present our search for new low-surface-brightness dwarfs in the region of the M 101 group complex with publicly available SDSS data. We report the discovery of 15 dwarf candidates and perform standard r and g surface photometry for them. As shown in Sect. 6.1, the photometric parameters of most candidates do suggest galaxy membership in the complex. In the second part of the paper (Sections 5, 6.2) we study the structure of the M 101 group complex by introducing a suitable reference frame (Sect. 5). By a cosmic coincidence, it happens that the best-fitting plane through the M 101 subgroup members with known distances is seen almost edge-on with respect to our line of sight (LoS, similar to the Centaurus group, Müller et al. 2016). This allows a first assessment of where the new candidates lie in the complex without distance information. The filamentary

[1] www.sdss.org

or planar structure of the M 101 group complex is critically discussed in Sect. 6.2, followed by a general conclusion in Sect. 7.

2. SDSS Data

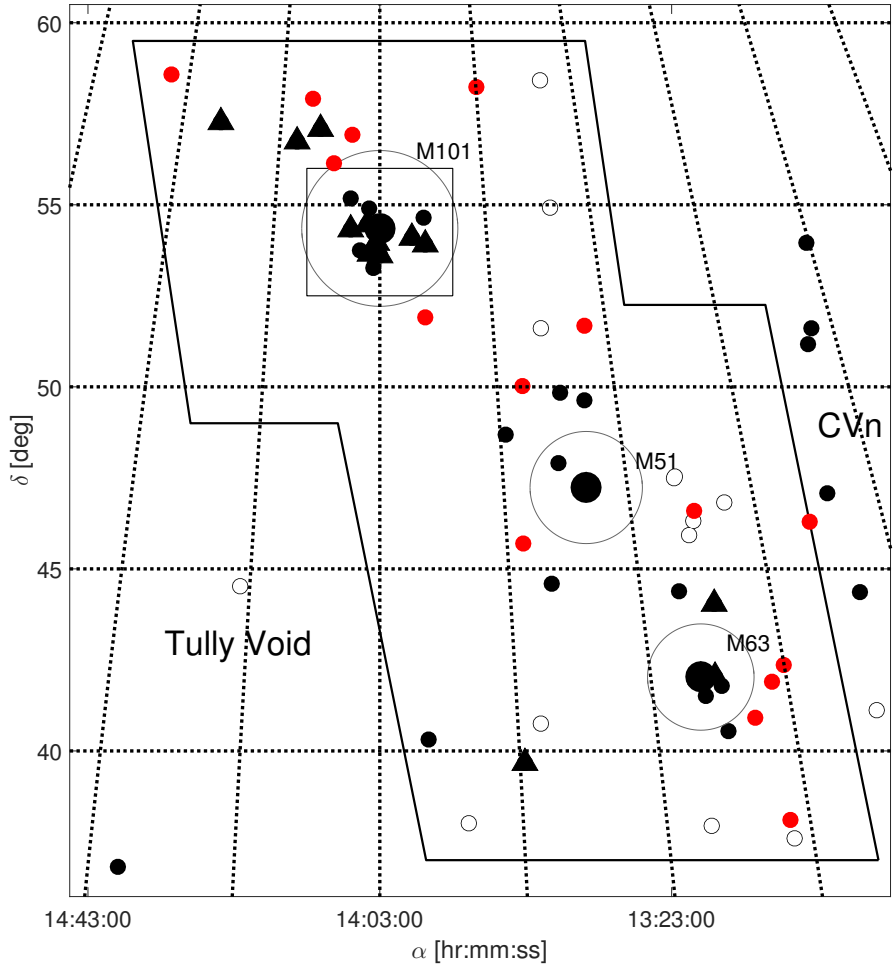

Fig. 1: Survey area of ≈ 330 square degrees in the M101 group region. The black triangles are confirmed dwarf galaxies with distances in the M101 group complex. The small black dots are members based on their photometric properties, compiled from the Local Volume Catalog (Karachentsev et al. 2004, 2013). The large black dots are the major galaxies that define the three subgroup centers in the region: M 101 (14h03m12.5s +54d20m56s), M 51 (13h29m52.7s +47d11m43s), and M 63 (13h15m49.3s +42d01m45s). The red dots indicate the positions of our 15 new dwarf candidates. Open circles are confirmed foreground (<5 Mpc) galaxies taken from the LV Catalog. The footprint of the Dragonfly survey around M101 is outlined by the rectangle. The circles indicate the virial radii of ≈ 260 kpc (for M 101; Merritt et al. 2014) for the three major galaxies (assuming the same virial radius for M 51 and M 63 as for M 101).

The Sloan Digital Sky Survey (Gunn et al. 2006) contributed a tremendous amount to the knowledge of the dwarf galaxy population in the Local Group. Numerous

resolved dwarfs were discovered by several teams (e.g., Belokurov et al. 2010; Kim et al. 2015), pushing the limits of the known dwarfs into the regime of ultra-faint dwarf galaxies ($M_V > -4$ mag). There is currently no instrument that would enable us to discover such extremely faint galaxies outside of the LG. The typical limiting total luminosity reached beyond the LG is $M_V \sim -9.5$ mag, several magnitudes brighter than the LG ultra-faints. At the distance of M 101, with SDSS data we can reach an absolute magnitude of $M_V \sim -10$.

Taking the LG Sculptor dwarf galaxy as a typical dwarf spheroidal galaxy (at the faint end of the dE luminosity function), we can assume $M_I = -4.1$ mag and $V - I = 1.5$ mag for the tip magnitude and color of the red giant branch (TRGB) (Rizzi et al. 2007a). This translates into $M_r \approx -2.8$ mag with $V - r \approx 0.2$ mag. Assuming a distance of 7 Mpc for the dwarfs in the M 101 group we calculate an apparent TRGB magnitude of $m_r = 26.3$ mag. The limiting magnitudes for point sources are provided by the SDSS Collaboration and are $g = 23.3$ mag and $r = 23.1$ mag, respectively (York et al. 2000). Thus, it becomes clear that in the SDSS data the TRGB is not resolved for dwarf galaxies in the M 101 group and group complex.

For our search of unresolved dwarf galaxies we used 323 tiles in g and r from the SDSS Data Release 12 (Alam et al. 2015). Each tile covers a 1 square degree area put together in an online pipeline provided by the SDSS team, where the tiles overlap by 0.05° on each side, giving a gap-free survey area of ≈330 square degrees and covering the whole M 101 group complex including the vicinities of M 101, M 51, and M 63. Figure 1 shows the footprint of the survey. Also indicated is the much smaller footprint of the Dragonfly survey (van Dokkum et al. 2014; Merritt et al. 2014, 2016; Danieli et al. 2017).

3. Search and detection of new dwarf candidates

Lacking the power to resolve new faint dwarf galaxies into stars at that distance, we searched for extended, low-surface-brightness features. The surveyed region contains 29 known dwarf galaxies, with 14 confirmed members via distance measurements, including the most recent Dragonfly dwarfs (Danieli et al. 2017), and 15 candidates where membership was estimated from their photometric and morphological properties. There are also 11 known foreground dwarf galaxies, with distance estimations smaller than 5 Mpc.

Each tile was first binned (mapping 9×9 pixels onto 1 pixel using the mean value) and convolved with a 3×3 pixel Gauss kernel. This dramatically increased the signal-to-noise ratio by a factor of ~ 30 and thus the visibility of low-surface-brightness features against the background sky. The tiles were visually inspected by two people from our team (OM and RS), where the grayscale was varied such that different

Tab. 1: Names, coordinates, and morphological types of the 15 new dwarf galaxy candidates of the M 101 group complex.

Name	α (J2000)	δ (J2000)	Type	Notes
M 101 subgroup				
dw1343+58	13:43:07	+ 58:13:40	BCD	
dw1355+51	13:55:11	+ 51:54:29	dSph	
dw1408+56	14:08:41	+ 56:55:38	dSph	
dw1412+56	14:12:11	+ 56:08:31	dSph	
dw1416+57	14:16:59	+ 57:54:39	dIrr/dSph	bg dwarf?
dw1446+58	14:46:60	+ 58:34:04	dSph	
M 51 subgroup				
dw1313+46	13:13:02	+ 46:36:08	dIrr/BCD	bg spiral?
dw1327+51	13:27:01	+ 51:41:08	dSph	
dw1338+50	13:38:49	+ 50:01:10	dSph	bg dwarf?
dw1340+45	13:40:37	+ 45:41:54	dIrr	
M 63 subgroup				
dw1255+40	12:55:02	+ 40:35:24	dSph	CVn I mem?
dw1303+42	13:03:14	+ 42:22:17	dIrr	
dw1305+38	13:05:58	+ 38:05:43	dSph	bg dwarf?
dw1305+41	13:05:29	+ 41:53:24	dIrr/dSph	
dw1308+40	13:08:46	+ 40:54:04	dSph	

dynamical ranges could be examined. This procedure led to the discovery of 15 new dwarf galaxy candidates in the M 101 group complex (red dots in Fig. 1). Their coordinates and morphological classifications are compiled in Table 1 and the candidate images presented in Fig. 2. We classified the candidates according to their morphological appearance: objects that appear symmetric, diffuse, and elliptical as dSph (dwarf spheroidal); objects with an uneven brightness distribution, e.g., due to HII regions, as dIrr (dwarf irregular); and objects with a clumpy high-surface-brightness (HSB) central component and a diffuse halo as BCD (blue compact dwarfs). There are three cases where the morphology is ambiguous. We present the two possible classes separated with a slash, e.g., dIrr/dSph, where the first is the more likely morphological type.

We have assigned each dwarf galaxy candidate to one of the three subgroups (see Table 1). The assignment is based on the shortest angular distance to either M 101, M 51, or M 63. We use the individual parent galaxy's distance to calculate absolute magnitudes for the new candidates as the distances of the three major galaxies systematically differ.

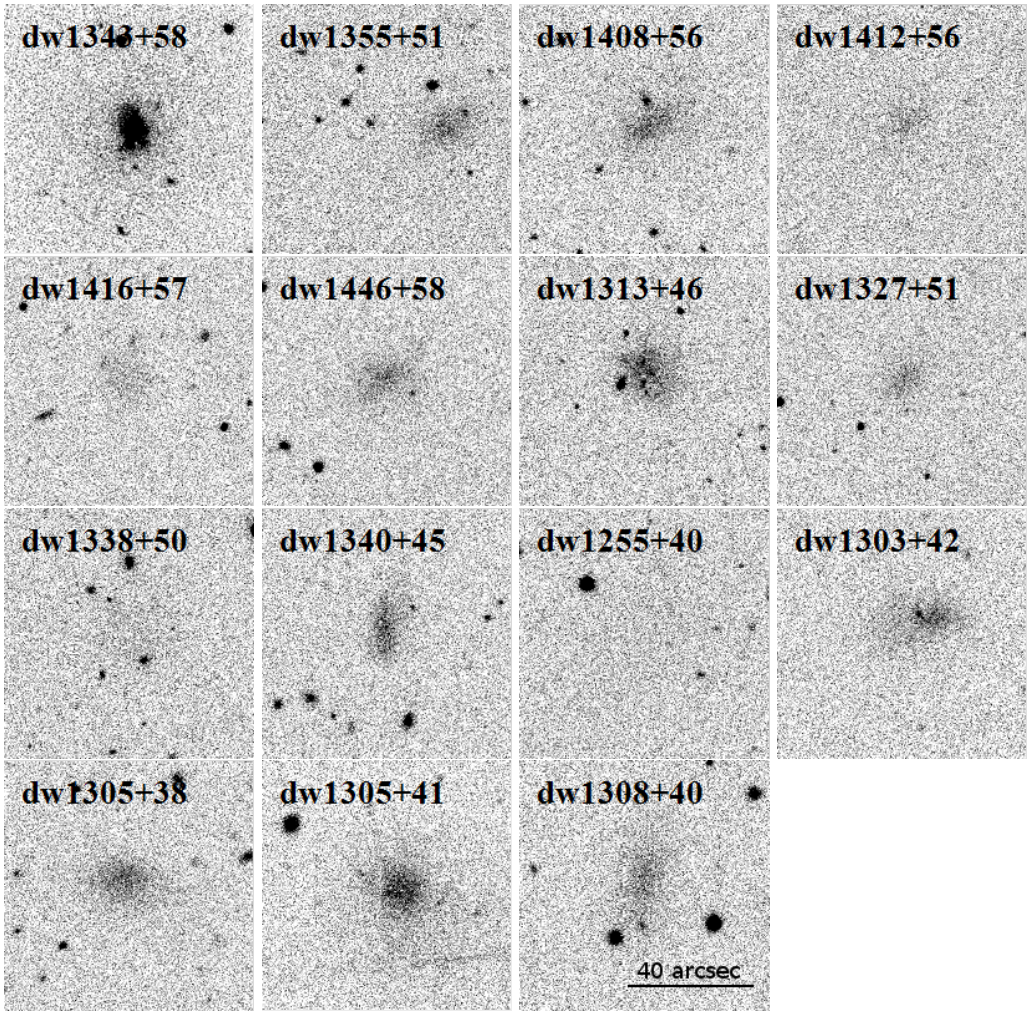

Fig. 2: Gallery showing SDSS r-band images of the 15 new M 101 group dwarf galaxy candidates. We note that dw1355+51 is at the edge of the CCD and is not centered in the stamp but offset to the right, and dw1255+40 is barely visible without a strong Gauss convolution. One side of an image corresponds to 80 arcsec or 2.7 kpc at the distance of 7 Mpc. North is to the right, east to the top.

The biggest challenge of our Cen A survey (Müller et al. 2015, 2017a) was the contamination of foreground stars and Galactic nebulae (cirrus). Cirrus can appear in every shape and size and thus can mimic the morphology of a dwarf galaxy. Fortunately, our survey area around M 101 is at high Galactic latitudes ($b \approx 60°$), i.e., far away from the Galactic plane where the density of Galactic cirrus and foreground stars is supposedly very small. Hence the problem of false positive detections is minimal.

Nevertheless, we performed artificial galaxy tests to estimate our detection efficiency and the depth (surface brightness limit) of the survey. For this we superimposed artificial galaxies on real images in two different tiles. The profiles for the artificial galaxies were created using a Sérsic profile with $n = 1$ (exponential profile; see below for the formula). The central surface brightness range was between 23 and 27 mag arcsec^2 and the apparent magnitude range between 16 and 20 mag, with a

step size of 0.5 mag and 0.5 mag arcsec^{-2}, respectively. At a distance of 6.95 Mpc this corresponds to absolute magnitudes between -13.2 and -9.2. This gives a total of 49 galaxies in an array of the surface brightness–absolute magnitude plane to detect per mosaic and iteration. We did five iterations; in each iteration we randomly placed all artificial galaxies into an r band tile. This was repeated for two different tiles such that we had ten iterations in total. In Fig. 3 the results are presented in a $\mu_{0,r} - M_r$ diagram. The number of times an artificial galaxy was detected is plotted: zero means no detection and ten corresponds to a 100 % detection rate. We do not expect a detection rate of 100 % even for clearly detectable galaxies because artificial galaxies can be randomly placed behind bright and extended stars or galaxies. It is important to note that not all parameter combinations lead to reasonable LSB dwarf galaxies, e.g., a high $\mu_{0,r}$ value (low SB) together with a small M_r value (relatively high luminosity) will lead to very extended and faint objects, which are not found in the Local Group (see Fig. 6). There is no significant difference in the detection rate between the two different tiles.

It can be seen that essentially all artificial objects with $\mu_{0,r} \leq 25.5$ r arcsec^{-2} and $M_r \leq -11$ are detected. A more appropriate completeness boundary of the survey is provided by the following analytic forms (see Ferguson 1990; Ferguson & Sandage 1988):

$$m_{tot} = \mu_0 - 5\log(r_{lim}) - 2.18 + 5\log(\mu_{lim} - \mu_0)$$

$$m_{tot} = \mu_{lim} - \frac{r_{lim}}{0.5487 r_{eff}} - 2.5\log(2\pi(0.5958 r_{eff})^2),$$

where all galaxies larger than $2r_{lim}$ within a given isophotal level of μ_{lim} should be detected. The first equation is for the $\mu_{0,r} - M_r$ relation; the second equation is for the $r_{eff} - M_r$ relation, where r_{eff} corresponds to the half-light radius of the object. To calculate the absolute magnitude M_r we assumed a distance of 7 Mpc. We estimated the two parameters such that the completeness boundary would contain all bins of the $\mu - M$ array where the detection rate is higher than 70 %, resulting in $r_{lim} = 13$ arcsec and $\mu_{lim,r} = 26.4$ r mag arcsec^{-2}. This completeness curve is shown in Fig. 3.

The identification of high-surface-brightness dwarf members (against a background of apparently small spiral galaxies) is more difficult and our detection efficiency for these objects cannot easily be assessed by an artificial galaxy test. In general we have to expect that potential high SB dwarf members of the M 101 group complex essentially go unnoticed in our survey. However, one rather convincing case of a blue compact dwarf (BCD, dw1343+58) has been found. On the other hand, a good low SB candidate could of course be in the near background (hence the remark "bg dwarf?" in Table 1, where this seemed equally possible) or the near foreground. In fact, towards the western boundary, the M 101 group region overlaps in the sky with the closer Canes Venatici (CVn) cloud (see also Fig. 1). One candidate in the M 63

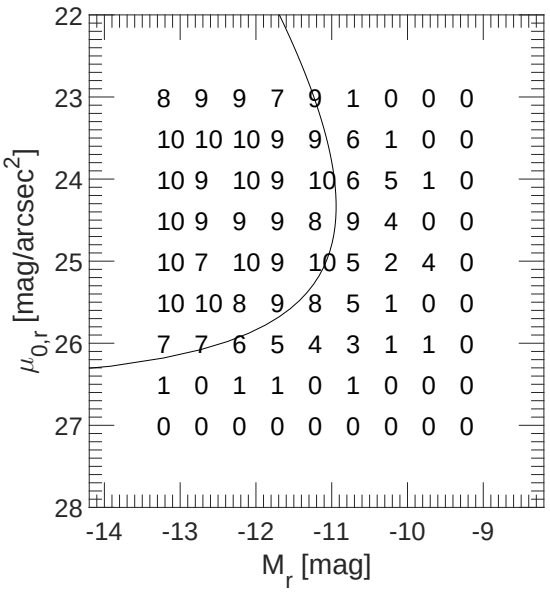

Fig. 3: Results of our artificial galaxy detection test shown as an array of numbers indicating the detection efficiency in the surface brightness–absolute magnitude plane. A 10 means 100 % detection and a 0 means no detection. The test array is divided into half-magnitude bins. The thin line corresponds to the estimated 70% completeness boundary; see text for the formula.

subgroup, dw1255+40, is indeed a possible member of that cloud. The problem of confusion is more generally addressed in Sect. 6.1.

We rejected candidates that were close to ultraviolet sources (UvS, e.g., brilliant young foreground stars) listed in the Nasa Extragalactic Database. Such sources can illuminate surrounding dust clouds and make them appear as faint low-surface-brightness objects. While closely resembling the morphology of a dwarf spheroidal galaxy the unusually blue color ($g - r < 0.1$ mag) of such objects raises doubts that these objects are dwarf candidates. A good example was found at the coordinates 14h09m12s, +51d13m27s, which is only separated from a UvS by 0.136 arcmin. It mimics the morphology and has structural parameters of a diffuse dwarf galaxy, but was suspiciously blue.

The reader may wonder why we did not use the SDSS data reduction pipeline directly for the detection of dwarf-like low-surface-brightness objects. There is indeed a tool implemented in the data reduction pipeline for the detection of extended sources. However, Kniazev et al. (2004) pointed out that galaxies are shredded by this tool, as different luminosity knots from the same source are detected and defined as separate, individual SDSS objects. Tests have shown (Kniazev et al. 2004) that the SDSS pipeline tool is unsuited for the detection of LSB objects: it gives a low detection rate of test galaxies and too many false detections. Nevertheless, we checked the SDSS database for the presence of any kind of detection counterpart for our new candidates. Indeed, all our candidates have matches in the SDSS database, but the link between these SDSS objects and a possible group membership of M 101 was not made before the present work. In addition, the SDSS photometry for these low-surface-brightness objects is unreliable, as stated by the SDSS photometry pipeline for those objects. The SDSS database also provides redshifts when available, but

none of our candidate galaxies, not even the high-surface-brightness dw1343+58, has a measured redshift.

As alluded to in the introduction, it is interesting to note that six of the seven candidate members from the Dragonfly survey are clearly visible in the SDSS images, thus were redetected in our survey, which strongly suggests that the SDSS data still contains many hidden treasures waiting to be discovered. This is insofar not surprising as the central surface brightness range of these candidates is between 25.1 and 26.8 r mag arcsec^{-2}, which is still detectable according to our artificial galaxy tests.

4. Surface photometry

We performed gr surface photometry for the new candidates in the surveyed area. Cosmic rays, foreground stars, and background galaxies were replaced with patches of sky from the surrounding area using IRAF to maintain the statistical properties of the local sky background. The nominal galaxy center was determined using a circle that best represents the shape of the outer isophotes of the galaxy. We emphasize that this center is a proxy for the underlying mass distribution, but does not necessarily coincide with the location of maximum surface brightness. The sky background was estimated by varying the galaxy growth curve until it became asymptotically flat. For each galaxy we computed the total apparent magnitude, the mean effective surface brightness $\langle\mu\rangle_{eff}$, and the effective radius r_{eff} in both bands. We used a circular aperture to measure the surface brightness profiles with a step size of $0,396$ arcsec (corresponding to 1 pixel). Sérsic profiles (Sersic 1968) were fitted at the radial surface brightness profiles using the equation

$$\mu_{sersic}(r) = \mu_0 + 1.0857 \cdot \left(\frac{r}{r_0}\right)^n,$$

where μ_0 is the Sérsic central surface brightness, r_0 the Sérsic scale length, and n the Sérsic curvature index. See Fig. 4 for all surface brightness profiles in the r band and the associated Sérsic fits.

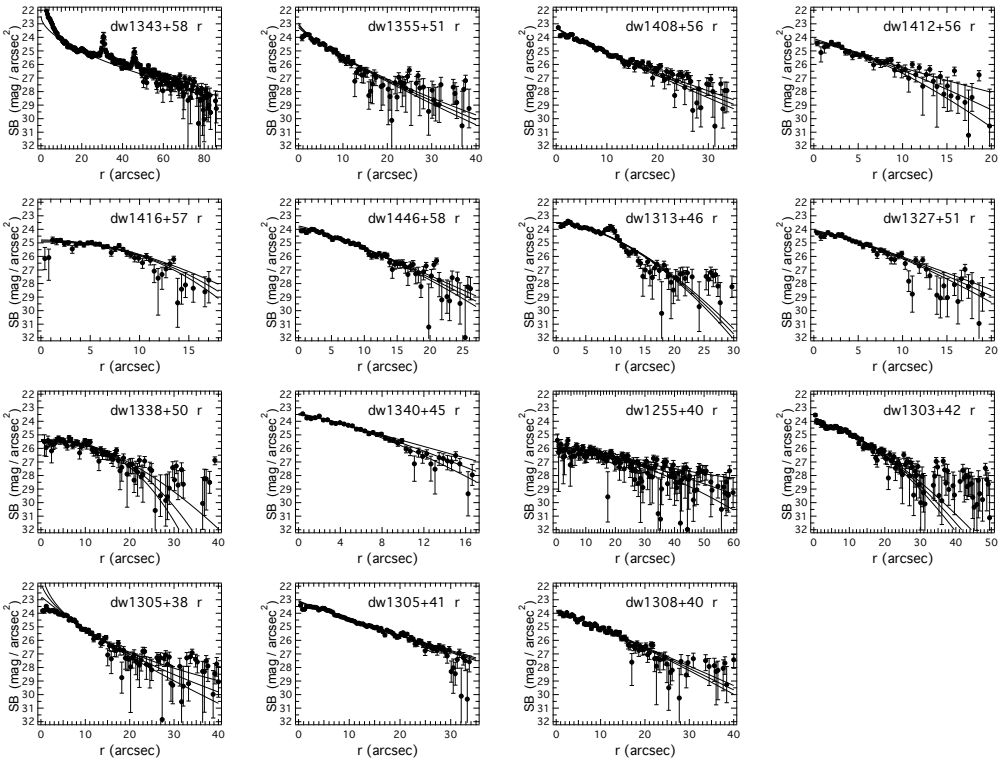

Fig. 4: Surface brightness profiles of all dwarf galaxy candidates in r and the best-fitting Sérsic profiles with 1σ confidence intervals.

The total magnitude uncertainty is estimated to be around ≈ 0.3 mag. It is made up of uncertainties related to foreground star removal (≈ 0.2 mag) and sky background estimation (≈ 0.2 mag). The uncertainty for the mean effective surface brightness is driven by the uncertainty in the measured total apparent magnitude. The error for the half-light radius (≈ 1.3 arcsec) is given by the determination of the growth curve. See Müller et al. (2015) for a more detailed explanation of the uncertainty estimates. Numerical uncertainties for the Sérsic parameters are shown in Table 2.

To compare our gr photometry and the structural parameters with dwarf galaxies in the literature, we used the following transformation equations (Lupton 2005):

$$V = g - 0.5784 \cdot (g - r) - 0.0038$$

$$B = r + 1.3130 \cdot (g - r) + 0.2271$$

In Müller et al. (2017a) we tested the quality of our photometry against literature values. The agreement was well within the uncertainties. In the same spirit, we conducted a comparison of the photometric values for 19 known dwarfs in the field of M 101 taken from Bremnes et al. (1999) with our own SDSS photometry. The values are in excellent agreement within our error estimates (see Fig. 5). We measured a standard deviation of $\sigma_{\Delta B} = 0.18$ mag and a mean of $\mu_{\Delta B} = 0.00$ mag was calculated.

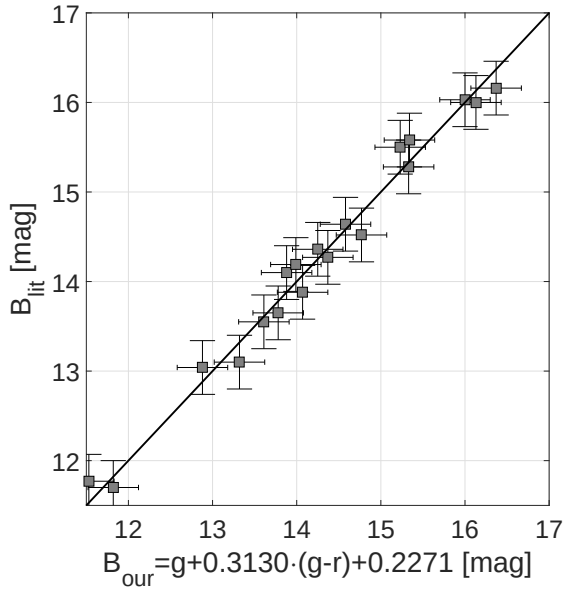

Fig. 5: Our photometry for 19 known M 101 dwarf galaxies converted to B band versus the literature values taken from Bremnes et al. (1999). The line corresponds to unity.

As stated earlier, the M 101 survey area is at high Galactic latitudes; therefore, the Galactic extinction values for the g and r band are less than 0.05 mag, much smaller than the photometric uncertainties. Hence, no corrections for Galactic extinction were applied when calculating absolute magnitudes.

In Table 2 we present the photometric data for the 15 newly detected dwarf galaxy candidates in the M 101 group complex.

5. Geometrical alignment

In preparation for an analysis of the spatial structure of the M 101 group complex (Sect. 6.2) we first define a natural spatial reference frame for the complex by fitting a plane through the galaxy positions in the close environment of M 101 itself. In a similar manner, Tully et al. (2015) introduced a reference frame for the Cen A subgroup as the system where two planes of satellites almost lie in the xy-plane, with the normal of the planes corresponding to the z-axis (see also Müller et al. 2016). To find a reference system for the M 101 group we fitted a plane with the help of a singular value decomposition (svd; Golub & Kahan 1965) at all galaxies lying closer than 1.5 Mpc from M 101. The svd method is a technique generally used in linear algebra. It is an eigendecomposition, where the data will be represented by eigenvectors and eigenvalues corresponding to a least-square fit to the data. The resulting sample of eleven galaxies is listed in Table 3. The normal vector of the best fit is given in supergalactic coordinates by $\mathbf{n_{ref}} = (0.6285, -0.0228, -0.7775)$. The plane has a rms thickness of 46 kpc. To see how much the distance uncertainties contribute to the fit, we ran Monte Carlo simulations where we draw the distance of the galaxy from a normal distribution with a 5% distance uncertainty as σ and

Tab. 2: Photometric and structural parameters of the new dwarf candidates in the surveyed region of the M 101 group complex.

Name	g_{tot}	r_{tot}	M_r	$(g-r)_{0,tot}$	$\mu_{0,r}$	$r_{0,r}$	n_r	$\langle\mu\rangle_{eff,r}$	$r_{eff,r}$	$\log r_{eff,r}$
	mag	mag	mag	mag	mag arcsec^{-2}	arcsec		mag arcsec^{-2}	arcsec	log pc
(1)	(2)	(3)	(4)	(5)	(6)	(7)	(8)	(9)	(10)	(11)
M 101 subgroup										
dw1343+58	15.54	15.17	-14.0	0.370	18.93 ± 2.26	0.04 ± 0.77	0.27 ± 0.12	24.45	28.6	2.98
dw1355+51	18.76	18.09	-11.1	0.666	23.09 ± 0.17	3.67 ± 0.69	0.78 ± 0.07	24.44	7.44	2.39
dw1408+56	18.01	17.50	-11.7	0.507	23.28 ± 0.06	5.48 ± 0.38	0.89 ± 0.06	24.71	11.0	2.57
dw1412+56	19.46	18.75	-10.5	0.702	24.26 ± 0.16	5.64 ± 0.80	1.22 ± 0.29	25.29	8.08	2.43
dw1416+57	19.06	18.83	-10.4	0.227	24.86 ± 0.08	10.19 ± 0.47	2.16 ± 0.31	25.16	7.35	2.39
dw1446+58	18.46	17.90	-11.3	0.559	23.87 ± 0.12	7.62 ± 0.74	1.27 ± 0.13	24.66	8.97	2.48
M 51 subgroup										
dw1313+46	17.63	17.36	-12.3	0.274	23.53 ± 0.04	9.33 ± 0.26	1.73 ± 0.07	23.78	7.69	2.50
dw1327+51	19.34	18.79	-10.9	0.550	24.16 ± 0.09	6.36 ± 0.51	1.29 ± 0.15	24.74	6.19	2.41
dw1338+50	19.15	18.35	-11.3	0.809	25.41 ± 0.07	16.16 ± 0.66	2.43 ± 0.42	25.62	11.3	2.67
dw1340+45	18.28	18.14	-11.5	0.136	23.48 ± 0.06	5.76 ± 0.29	1.25 ± 0.18	24.24	6.61	2.44
M 63 subgroup										
dw1255+40	18.41	17.82	-11.9	0.594	25.88 ± 0.14	25.14 ± 2.48	1.34 ± 0.42	26.49	21.6	2.97
dw1303+42	18.06	17.29	-12.5	0.770	24.13 ± 0.06	12.19 ± 0.54	1.61 ± 0.12	24.56	11.3	2.69
dw1305+38	17.69	17.51	-12.3	0.178	21.57 ± 1.37	1.31 ± 1.87	0.59 ± 0.23	24.41	9.57	2.62
dw1305+41	17.06	16.70	-13.1	0.354	23.12 ± 0.06	8.21 ± 0.53	0.94 ± 0.05	24.14	12.2	2.72
dw1308+40	18.19	17.54	-12.2	0.650	23.84 ± 0.07	8.81 ± 0.60	1.11 ± 0.07	24.74	11.0	2.68

The quantities listed are as follows: (1) name of candidate; (2+3) total apparent magnitude in the g and r bands; (4) absolute r band magnitude. For candidates of the M 101 subgroup, the mean distance of the M 101 group (6.95 Mpc) is assumed; for candidates of the M 51 and M 63 subgroups, the distances of these major galaxies is 8.6 and 9.0 Mpc, respectively; (5) integrated $g-r$ color; (6) Sérsic central surface brightness in the r band; (7) Sérsic scale length in the r band; (8) Sérsic curvature index in the r band; (9) mean effective surface brightness in the r band; (10) effective radius in the r band. These photometric data are used in the section 6.1 to assess the M 101 group complex membership of the candidates; (11) the logarithm of the effective radius in the r band, converted to pc with a distance assumption according to the subgroup.

the literature distance itself as μ. In every run we compared the angle between the normal of our best fit $\mathbf{n_{ref}}$ with the normal of the run. To determine the contribution of the individual galaxies a second test was conducted. In every run eleven galaxies were randomly drawn from the sample shown in Table 3; each selection was put back into the sample before the next was chosen such that some galaxies might not be chosen, while others might be chosen twice or more (known as a bootstrap test with reshuffle). The angle difference in both tests has a maximum of 1.5 degrees, which clearly indicates that the best-fitting plane is well defined and can be used as statistically robust reference frame.

Tab. 3: Galaxies within a $r = 1.5$ Mpc sphere around M 101 used for the plane fitting.

Galaxy Name	α_{2000} (deg)	δ_{2000} (deg)	D (Mpc)	Ref
NGC 5195	202.4916	47.2681	7.66	(1)
Holm IV	208.6875	53.9047	7.24	(2)
UGC 08882	209.3083	54.1008	8.32	(3)
M 101	210.8000	54.3505	6.95	(2)
M101-DF3	210.7708	53.6156	6.52	(4)
M101-DF1	210.9375	53.9444	6.38	(4)
NGC 5474	211.2583	53.6630	6.98	(2)
NGC 5477	211.3875	54.4608	6.76	(2)
M101-DF2	212.1542	54.3253	6.87	(4)
NGC 5585	214.9500	56.7303	5.70	(5)
DDO 194	218.8500	57.2567	5.81	(2)

We choose the x-axis such that it corresponds to the projection of the line of sight onto the plane. The angle between the LoS to M 101 and this new x-axis is only 3.6°, meaning that this plane is lying almost along the LoS. The flat structure extends over 3 Mpc, showing that the plane is not an artifact of distance uncertainties. The x-axis together with the normal vector $\mathbf{n_{ref}}$ define the reference frame. In order to center M 101 at its origin the supergalactic coordinates need to be shifted by

$$v_{SG,M101} = v_{SG} + \begin{pmatrix} -2.8547 \\ -5.7457 \\ -2.6721 \end{pmatrix} \text{ [Mpc]}$$

The transformation from the shifted supergalactic coordinates to the reference system is then given by the following rotation matrix

$$\boldsymbol{R} = \begin{bmatrix} -0.4498 & -0.8283 & -0.3393 \\ -0.6362 & 0.5630 & -0.5308 \\ 0.6285 & -0.0228 & -0.7775 \end{bmatrix}.$$

The final transformation is

$$v_{M101} = \boldsymbol{R} \cdot v_{SG,M101}$$

The best-fitting (reference) plane is shown and discussed below (Sect. 6.2, Fig. 7).

We note that the geometrical analysis was initially performed before the distance of three additional Dragonfly galaxies were published (Danieli et al. 2017). Including these new galaxies (DF1, DF2, DF3) the normal of the best-fitting plane changes only by an angle of 0.4 degrees, showing that the plane is statistically robust. With the additional three galaxies the rms thickness of the plane decreased from 49 kpc to 46 kpc.

6. Analysis and discussion

In this section we assess the possible membership of the candidates based on their photometric properties, and we analyze the structure of the M 101 group and the whole complex in the light of the enlarged sample.

New dwarf galaxy candidates

The usual way to test group membership of dwarf galaxies without direct distance measurements is by comparing their photometric parameters with those of confirmed dwarf galaxies with known distances (e.g., Jerjen et al. 2000a; Chiboucas et al. 2009; Merritt et al. 2014; Müller et al. 2017a). Dwarf galaxies tend to follow a fairly narrow relation in the central surface brightness–absolute magnitude diagram and the effective radius–absolute magnitude diagram (see Fig. 6). We note that the central surface brightness is a distance-independent quantity. If a candidate is a background galaxy not associated with the group or complex, the assumed distance for calculating M_V will place the galaxy outside of the relation. In other words, if the parameter values of a candidate fit into the relation with the assumed distance, they are comparable to those of known dwarf galaxies and the candidate can be associated with the group. This convenient test gives us a preliminary, rough handle on the membership status before embarking on a time consuming confirmation by direct distance measurements.

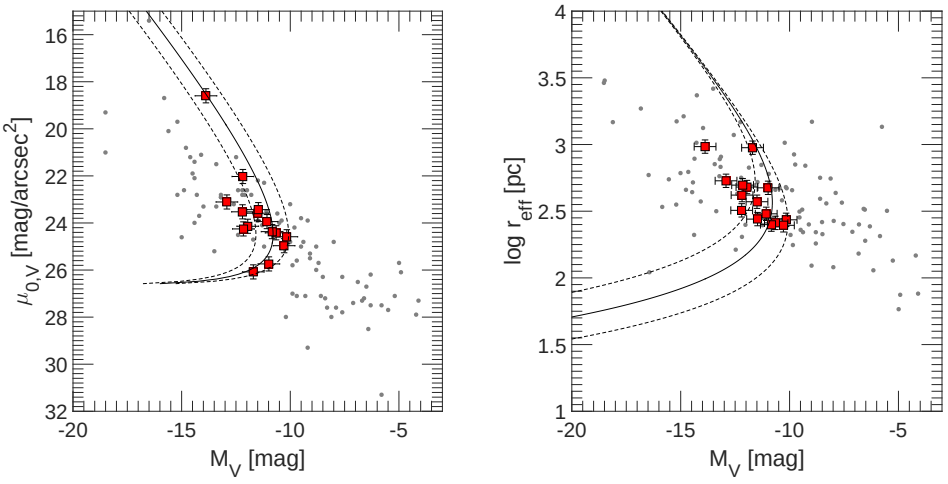

Fig. 6: Left: μ_0–M_V relation for the photometric parameters of the known Local Group dwarfs (gray dots, McConnachie 2012) and the new candidates (red squares). Indicated by the thin line is the assumed completeness boundary (Sect. 3) at 7 Mpc, which is bracketed by lines corresponding to assumed distances of 5 Mpc and 10 Mpc to take care of the expected distance spread. Right: Same data and color-coding, but for the $\log r_{eff}$–M_V relation.

The performance of the present dwarf candidates in this photometric test is shown in Fig. 6. We note that we have assumed different distances for our candidates depending on their position relative to the major galaxy they are assigned to (Table 1), roughly 7 Mpc around M 101 and 9 Mpc around M 51/M 63. Moreover, given that the dwarfs, even as members of the complex, will be distributed in a large halo around the subgroups, we have to allow for – or expect – a total distance spread of the candidates from $\sim$ 5 to 10 Mpc, giving rise to an additional spread in the photometric relations. The distance spread is also taken care of by overlaying in the relations shown in Fig. 6 a set of completeness boundaries (cf. Sect. 3) for distances of 5, 7, and 10 Mpc.

Figure 6 shows that all but one of the new dwarf candidates fit into both of the relations, thus suggesting, or at least being in agreement with, their membership in the M 101 group complex. We note that the outlier is a BCD which does not have to fit into the relations.

The membership status of dw1343+58 which we classified as a blue compact dwarf (BCD) has to be assessed in a different way. Morphologically, the galaxy consists of a high-surface-brightness irregular central region and an elliptical low-surface-brightness component around it, which is characteristic for BCDs (e.g., Kunth et al. 1988). Papaderos et al. (1996a,b) studied the optical structure of BCDs by decomposing their surface brightness profiles into three parts: (i) an underlying extended low-surface-brightness component, (ii) an exponential plateau which is mostly seen in iE BCDs, and (iii) an inner HSB region exhibiting a luminosity excess over the plateau which can be fitted with a Gaussian profile. Papaderos et al. (1996a) give the 25 mag isophote radius in the R-band of the HSB Gaussian component

(P_{25}) for a sample of BCDs (see their Table 5). If we exclude the outliers Haro 2, Mkn 297, and I Zw 89, we end up with a mean size of $P_{25} = 0.55$ kpc for BCDs. Now, the estimated P_{25} size of our candidate dw1343+58 is ~ 15 arcsec. Assuming $P_{25} = 0.55$ kpc would then put it at a distance of 7.8 Mpc, which is indeed in accord with M 101 group membership. We note that this candidate is listed as a galaxy in the HYPERLEDA catalog (Paturel et al. 2003), but not as a BCD or a M 101 dwarf.

As mentioned, the Canes Venatici (CVn) cloud of galaxies is partially overlapping with the M 101 group complex in sky projection. It is conventionally split at a line-of-sight velocity division line of 400 km s^{-1} (~ 5.7 Mpc) into the CVn I and CVn II clouds. CVn I cloud members peak at ∼300 km s^{-1} (~ 4.2 Mpc) and CVn II cloud members at ∼560 km s^{-1} (~ 8.0 Mpc) (Makarov et al. 2013). The whole CVn complex is an extended structure consisting mostly of late-type galaxies of low luminosity and is part of the Coma-Sculptor Cloud, a huge (∼10 Mpc long) prolate filament, which also includes the Sculptor Cloud, the Local Group, the M 81 group, and the Cen A group (Tully 1988a; Karachentsev et al. 2003). In our search area, 11 known galaxies have distances smaller than 5.0 Mpc, identifying them as part of the CVn I cloud. So, it is conceivable that some of our candidates could in fact be foreground dwarf galaxies. In particular, spiral galaxy M 94 at a distance of 4.5 Mpc (Karachentsev et al. 2003), one of the major members of CVn I (Makarov et al. 2013), is less than 0.5 degrees off our search border (at 12h50m53.5s +41d07m10s). The dwarf candidate dw1255+40 is at a projected distance of only 0.95 degrees from M 94, corresponding to a separation of 75 kpc at the distance of M 94. Placing this candidate in the vicinity of M 94 (at 4.5 Mpc) rather than in the M 101 group complex (at 7 or 9 Mpc) would still be fine for the photometric test, i.e., the adjusted structural parameters of the candidate would still fit into the relations. Here, a direct distance measurement is needed to confirm its membership in either structure.

Structure of the M101 group complex

How do these new dwarf galaxy candidates fit into the group complex? We now focus on the structure and geometry of the complex and discuss its impact on the formation history. The 15 galaxies with known distances in the survey region are plotted in supergalactic coordinates and centered at M101 in Fig. 7. Also shown is the best-fitting plane through eight members of the M 101 subgroup, as calculated in Sect. 5. The galaxies are cast orthogonally onto the SGXSGZ– and SGYSGZ–planes, where they appear as shadows. The highly flattened filamentary distribution of the galaxies, especially in the SGXSGZ–plane, is quite striking. The M 101 plane is a good representation of the whole complex, i.e., the planar structure of the M 101 subgroup is embedded in a larger flattened structure that encompasses what we call the M 101 group complex.

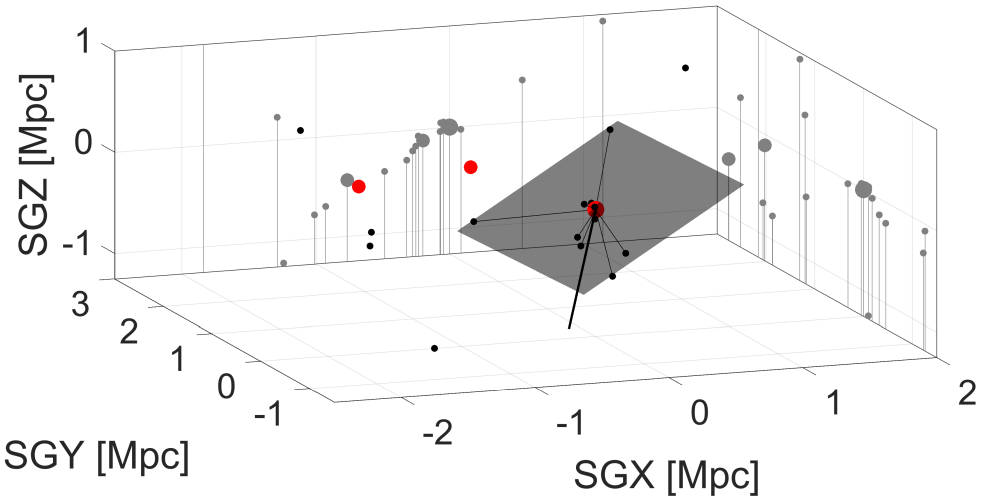

Fig. 7: 3D distribution, in supergalactic coordinates, of all galaxies with distance measurements in the surveyed M 101 group complex, centered at M 101. The red dots correspond to the major galaxies M 101, M 51, and M 63; the black dots indicate dwarf galaxies. The gray dots (shadows) appearing on the SGXSGZ– and SGYSGZ–walls are orthogonal projections. The best-fitting plane through the M 101 subgroup is shown as the gray plane and has a rms of only 46 kpc. The line of sight between the Milky Way and M 101 is indicated by the thick black line pointing downwards.

To further study this flat structure and locate our dwarf candidates in it we now switch to the M 101 reference frame introduced in Sect. 5. In this system the best fit corresponds to the $M101_X M101_Y$–plane, which has its origin at (0,0,0). As previously mentioned, the normal of the best-fitting plane is almost perpendicular to the LoS. When this normal is perpendicular to the LoS, then the LoS for the dwarf galaxy candidates will be (almost) parallel to the best-fitting plane. As the plane is not perfectly parallel to our view, the LoS of the candidates will be systematically shifted along the negative direction of the $M101_Z$–axis. The $M101_X M101_Z$– and $M101_X M101_Y$–projections in this reference system are shown in Fig 8. In the top left panel the galaxies with known distances and their 5% uncertainties are shown. In the top right panel the possible positions of the candidates (dwarfs presented here and the candidates taken from the LV Catalog) are indicated by lines. All lines have a relatively shallow slope and cover between 0.06 Mpc and 0.35 Mpc in the $M101_Z$ direction over an interval of 3.25 Mpc along the $M101_X$–axis (or LoS depth of the M 101 group complex). This narrow spread in $M101_Z$ enables us to study the possible distribution of the candidates without exact knowledge of their distances. All we need are the sky positions and the fact that the M 101 group complex is flattened almost along the LoS. In the edge-on view it is easy to determine whether or not a candidate is part of the filamentary structure. The bottom panels show the structure in the $M101_X M101_Y$–plane, giving a face-on view onto the best-fitting plane.

Looking at the $M101_X M101_Z$–projection (the edge-on view, top right of Fig. 8) we first verify that almost all known galaxies in the region, notably M 51 and M 63, are

close to the best-fitting plane through the M 101 subgroup (the thick red dotted line). That plane through eight members of the subgroup had a rms thickness of 46 kpc. If instead a fit is performed at all 16 galaxies lying along the planar structure (KH 87, M 63, M 51, NGC 5195, UGC 08882, KK 191, Holm IV, M 101, NGC 5474, DF2, NGC 5477, DF3, DF1, NGC 5023, NGC 5585, and DDO 194), we calculate a $rms = 67$ kpc, which is still remarkably thin. Only DDO 182 falls outside of the structure. Moreover, it is clearly visible that most of the candidate dwarfs lie within (or near) the flattened structure outlined by the know members of the M 101 group complex.

Looking at the $M101_XM101_Y$–projection (face-on view, bottom right) we note that only three candidates lie in the space between M 101 and M 51 (ignoring the lines close to M 101). This is further evidence that the M 101 and M 51/M 63 subgroups form separate groups as suggested by Tikhonov et al. (2015). Most new dwarf candidates are in the direction of M 101.

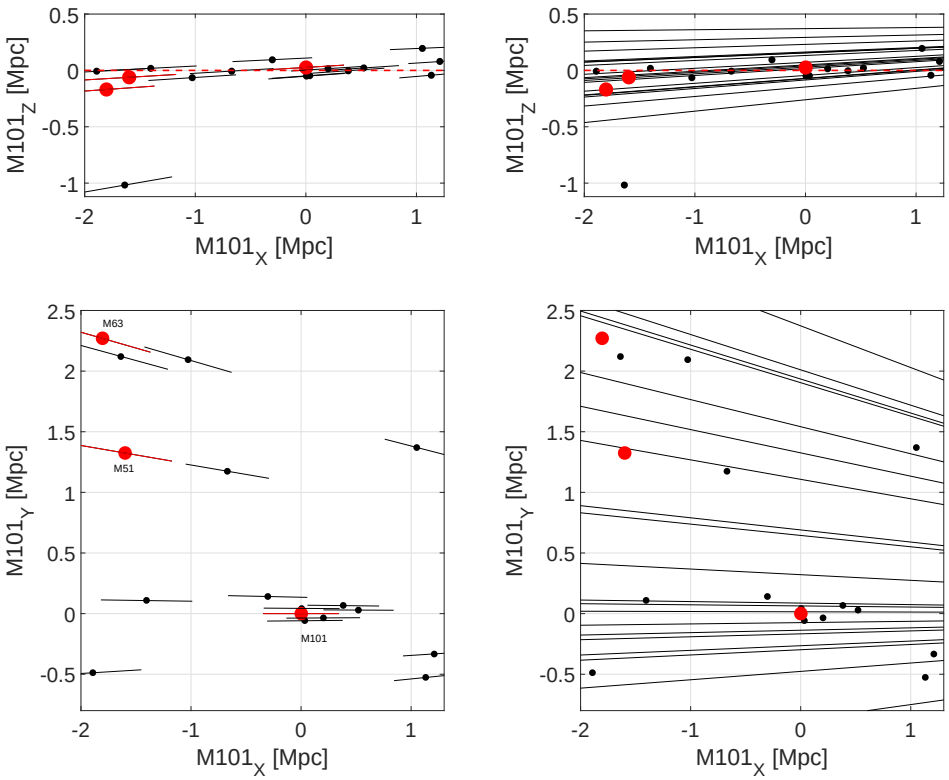

Fig. 8: $M101_XM101_Z$–projection (top) and $M101_XM101_Y$–projection (bottom) of known members and candidate members of the M 101 group complex in the M 101 reference system. The top panels essentially give an edge-on view of the complex, the bottom panels a face-on view. Red dots correspond to the three major galaxies M 101, M 51, and M 63; black dots indicate dwarf galaxies with distances. The thick red dotted line is the best-fitting (reference) plane lying in the $M101_XM101_Y$–plane. The left panels show the known members with 5% distance errors indicated by the short lines along the LoS. The right panels additionally give the possible positions of our new dwarf candidates and the candidates from the LV Catalog, in absence of distance measurements shown as long thin black lines again running along their LoS.

With a length of over 3 Mpc this flattened structure could be attributed to the cosmic web where the galaxies are known to be aligned along dark matter filaments. The question, then, is how this structure compares to other filamentary structures. Bond et al. (2010) identified individual filamentary structures in SDSS and compared their properties to those produced in cosmological simulations. They found a mean SDSS filament width of 5.5 ± 1.1 or $8.4 \pm 1.4\ h^{-1}$ Mpc, depending on the smoothing length, which in size is comparable to our best-fitting plane ($\sim$ 3 Mpc) when the bottom panel of Fig. 8 is taken as a measure. However, the thickness of the M 101 complex of only rms=67 kpc is remarkable. This is a factor of $\sim$ 40 smaller than the size of the structure.

A direct comparison with simulations is difficult. González & Padilla (2010) used an algorithm to identify and analyze filaments in cosmological simulations. They plotted the filament thickness as a function of the filament length with a bin size of 10 Mpc. In the first bin (0 to 10 Mpc) a median thickness of 1.3 Mpc is estimated. The problem with this result for the purpose of comparison is the low resolution of filament length steps. In their Fig. 8 (upper right panel) they present the count of filaments as a function of thickness. There is a small signal at 0.1 Mpc h^{-1}, but it remains unclear whether this is due to the interpolation between zero and the first point of the function rather than being a real signal. Even when we assume that it is a real signal, the probability of a thickness as small as that observed in the M 101 group complex is essentially zero. If the M 101 group complex is the usual type of a large-scale filamentary structure, its small thickness has to be explained.

One possible explanation for this special configuration is given by the presence of the nearby Local Void (see Courtois et al. 2013). The planar M 101 group complex is well-aligned at the edge of the Local Void and can be seen as part of its boundary. The formation of the flattened structure itself could be induced by the expansion of the Local Void.

Regarding the thin planar structure of the M 101 subgroup itself, with its very small rms thickness of 46 kpc, the question arises of whether this could be a similar phenomenon to the local planes: the Vast Polar Structure (VPOS) of the Milky Way (Pawlowski et al. 2012b) or the Great Plane of Andromeda (GPoA, Ibata et al. 2013). Much of the motivation for finding new faint dwarf galaxies outside the LG is precisely to look for analoguous structures because the local planes are a challenge to the standard ΛCDM scenario of structure formation (e.g., Pawlowski et al. 2014; Cautun & Frenk 2017). However, we believe that the M 101 plane is not the same phenomenon, even though the M 101 plane is only a factor of two or three thicker than the local planes. The scales and the objects that define the planes are different. The local planes are defined by very faint and ultra-faint dwarf satellites in the immediate vicinity of their host galaxies (closer than the virial radius of 250 kpc). In contrast, the M 101 plane is defined by still fairly luminous dwarf galaxies at

separations as large as 1 Mpc. Still, the flattened structure of the M 101 subgroup – and its extension over the whole complex – is remarkable.

How is the galaxy M 101 itself inclined to the group plane? As mentioned in Sect. 4 the spiral galaxy M 101 is seen face-on, which means that our LoS essentially coincides with the direction of the disk normal $\mathbf{n_{M101}} = (0.4107, 0.8267, 0.3845)$ in supergalactic cartesian coordinates. Hence, with an angle of only 3.6° between $\mathbf{n_{M101}}$ and the planar structure of the group, the disk of M 101 is perpendicular and its normal is parallel to the plane. Dubois et al. (2014) studied the alignment of galaxy spins within the Cosmic Web with a large-scale hydrodynamical cosmological simulation and found that more massive galaxies tend to have their spin direction perpendicular to a filament, while less massive galaxies have their spin direction preferentially parallel to a filament with a transition mass around $M_* \approx 3 \times 10^{10}$ $M_\odot$. Tikhonov et al. (2015) calculated a dynamical mass for M 101 of $6.2 \times 10^{11}\,M_\odot$ and gave a mass-to-light (M/L) ratio of 18, thus the stellar mass of M 101 would be $3.4 \times 10^{10}\,M_\odot$, assuming M/L$= 1$ for the stellar component. Hence, the stellar mass of M 101 is just around the Dubois transition mass and either way is in agreement with this work. A follow-up study based on the same simulation framework (Welker et al. 2014) revealed a strong correlation between the merger history and the spin alignment: the more mergers contribute to the mass of a galaxy, the more likely its spin will be perpendicular to the filament. In contrast, the spin of galaxies with no merger is more likely aligned with the filament. This would then suggest that M 101 has undergone few or no mergers in its formation history. This view agrees well with the observation that M 101 has a small (or essentially absent) bulge; in the standard model of bottom-up structure formation, bulges are formed in merger events (e.g., Brooks & Christensen 2016, and references therein).

The lack of a strong bulge in M 101 is an important observation in itself. Kormendy et al. (2010) pointed out the challenge of bulgeless spiral galaxies for hierarchical formation scenarios. How can such massive spiral galaxies like M 101 form out of merger events without growing a prominent bulge? López-Corredoira & Kroupa (2016) showed that there is a correlation between bulge size and the number of tidal dwarf galaxies (N_S). However, in a ΛCDM scenario there should be no correlation between these two quantities because N_S is driven by the dark matter mass of the host galaxy and not by its formation history (Kroupa et al. 2010). In a generalized model of gravity without DM one does expect such a correlation between the bulge and N_S because (tidal dwarf) satellites form in rare fly-by encounters. Bulges themselves would also form in such encounters, making the bulge-to-disk ratio a measure for past interactions (López-Corredoira & Kroupa 2016). What would such a scenario predict for the M 101 group? As M 101 is a spiral galaxy without a bulge, only a few or even no dwarf spheroidals should exist in the group. Karachentsev et al. (2005) reported that bulgeless galaxies generally have no or only a few known dwarf spheroidal companions. To date only three early-type dwarfs have been confirmed

as members of the M 101 group. While in a generalized gravity scenario this missing dSph problem is well explained, the standard model of cosmology needs to find a mechanism for the low abundance of dwarf spheroidals around bulgeless spirals.

How do our new dwarf detections fit into this picture? This can be evaluated by way of a comparison with the Andromeda subgroup. In Chiboucas et al. (2009) the authors show the cumulative luminosity functions (LF) of the Cen A, M 81 and Andromeda satellites. Our survey reached a limiting magnitude of $M_V \sim -10$ mag, assuming a distance of 7 Mpc. Among the three satellite populations, the cumulative LF of the Andromeda subgroup shows the lowest abundance with 15 satellites down to $M_V = -10$ mag. Andromeda and M 101 also have a similar total B-band luminosity ($\Delta B \approx 0.5$ mag), thus a comparison is reasonable. Within a projected virial radius of ≈ 260 kpc around M 101 (Merritt et al. 2014), comparable to Andromeda with 230 kpc, there are seven confirmed members (Holm IV, UGC 08882, DF3, DF1, NGC 5474, NGC 5477, DF2) down to V magnitude of -10 (three early-type and four late-type dwarfs). Additionally, there are five dwarf candidates within this radius (M101 dwD, M101 dwC, M101 dwA, M101 dwB, dw1412+56). Assuming a distance of 6.95 Mpc for all of them, five additional members would contribute to the population, giving a total of twelve, putting the M 101 subgroup almost on a par with the Andromeda subgroup. On the other hand, assuming a positive detection rate of 60 % (14 out of 22 candidates of the M 81 group were confirmed as members (Chiboucas et al. 2013), the rest being background or cirrus) we would gain only three additional members, for a total of ten satellites. This, in turn, would indeed indicate a smaller population of dwarf galaxies in the M 101 subgroup. Using all distance data available and calculating the 3D distances to M 101, only three (NGC 5474, NGC 5477, DF2) of the seven galaxies lying in the projected virial radius are closer than 260 kpc to M 101, drastically increasing the missing-satellite problem in the M 101 subgroup. Similarly, Danieli et al. (2017) draw the same conclusion with their recent publication of HST data for their Dragonfly candidates. The authors also cautiously predict a too-big-to-fail problem for the M 101 subgroup, based on the low abundance of bright dwarf satellites around M 101. Clearly, we need distance measurements for the dwarf candidates in the vicinity of M 101 to answer the question of whether, as claimed, the abundance of dwarf satellites of M 101 is exceptionally low, and hence whether there really is a missing-satellite problem in the M 101 subgroup. In this context it is noteworthy that there are almost no new candidates in the virial radii of all three host galaxies. Could we face similar problems in the M 51 and M 63 subgroups?

The alignment of the spin vector with the planar structure and the low number of M 101 dwarf satellites – if confirmed – lead to the conclusion that M 101 has a weak merger history. Additional evidence for this is given by van Dokkum et al. (2014) who point out a lack of a stellar halo of M 101. Such stellar halos are formed from debris of shredded satellite galaxies (McConnachie et al. 2009), and are an indicator

of previous interaction. Does all this evidence mean that there is no evidence for interaction in the galaxy group? Mihos et al. (2013) studied the faint outskirts of the spiral up to a limiting surface brightness (star density) of $\mu_B \sim 29.5$ mag arcsec^{-2} and found no evidence of extended stellar tidal tails around M 101 or its companions. Such tails should be expected when M 101 had a recent encounter with one of its massive companions. However, two low-surface-brightness features were found in the outer disk. One of them must have formed very recently, due to its blue stellar population. The authors argue that this faint blue feature could have formed in fly-by encounters with NGC 5477 and NGC 5474. The latter galaxy exhibits an off-centered central bulge, suggesting some interaction in the past. The high-velocity gas in the disk of M 101 is another indicator of tidal interaction, possibly with the companion NGC 5477 (Combes 1991).

More prominent than M 101 in terms of interaction is the ongoing merger between M 51 and NGC 5195 (Toomre & Toomre 1972). In Dobbs et al. (2010) this merger was simulated with a hydrodynamical model with a highly elliptical orbit where NGC 5195 passes trough the disk of M 51 twice. A qualitative assessment of the trajectory of NGC 5195 shows that it correlates with our best-fitting plane, which is not surprising, as accretion happens along the filament (Libeskind et al. 2014).

In contrast to more distant dwarf galaxy candidates (e.g., Ordenes-Briceño et al. 2016; Smith Castelli et al. 2016, d > 20 Mpc), the new dwarf galaxy candidates in the M 101 group complex can be resolved into stars with appropriate equipment from the ground (e.g., Subaru) or in space (HST). The task is to confirm these objects as nearby stellar systems, excluding the possibility that they are more distant, unresolved galaxies or Galactic cirrus clouds, Measuring their distances also allows us to assign each of them to one of the three subgroups in the M 101 group complex (or the Canes Venatici I cloud in the foreground). Will the candidates spread along the 3 Mpc sheet or are they clustered around the main galaxies M 101, M 51, and M 63? Accurate distance measurements will be key for the study of the fine structure of large-scale structure in the M 101 group filament.

7. Conclusion

In this work we presented the results of a dwarf galaxy search covering the M 101 group of galaxies and its wider environment including M 51 and M 63 with publicly available data from the Sloan Digital Sky Survey. We searched a sky area of 330 square degrees and found 15 new dwarf candidates. Surface photometry was performed for all candidates in the gr bands and Sérsic profiles were fitted to the surface brightness profiles. We tested the group membership with the classical tools at hand: the central surface brightness–absolute magnitude and effective radius–absolute magnitude relations. The candidates indeed fit in comparison to the structural parameters of known Local Group dwarf galaxies, making them good candidates

of the M 101 group complex. Distance measurements are nevertheless needed to confirm these results. We discussed the possibility that some of the candidates could be dwarf members of the Canes Venatici cloud in the near foreground.

The second part of this work was committed to the 3D spatial distribution of the group and the whole complex. We found that all but one of the galaxies with known distances lie in a thin plane with $rms = 67$ kpc and a length of over 3 Mpc, including M 51 and M 63. The plane was defined by a best fit at the M 101 subgroup alone, i.e., M 101 and its neighbors within 1.5 Mpc, with a rms thickness of only 46 kpc. The recent publication of three additional dwarf galaxies (Danieli et al. 2017) strengthens the picture of a thin, planar structure. This structure happens to be well-aligned with our line of sight, giving us the opportunity to place the new dwarf candidates relative to this plane without knowing their exact distances. For this we defined a M 101 reference frame where the z-axis corresponds to the normal of the plane.

The flattened structure of the M 101 group complex is aligned with the envelope of the Tully Void which could explain its formation by the expansion of the void. There is a clear alignment between the spin direction of M 101 and the planar structure: the spiral disk of M 101 is almost perpendicular to the best-fitting plane. In a ΛCDM scenario this can be explained by a weak merger history. The missing bulge of M 101 also strengthens the case for a steady evolution over long periods of time, rather than via episodic merger events. We discussed the impact of such a formation history with the abundance of dwarf spheroidals in a ΛCDM and a generalized gravity scenario.

Future distance measurements of the candidates in the M 101 group complex will give us answers to the questions of whether the planar structure is only an artifact of small number statistics or a real cosmic structure, and if the latter is true, how thin it is and what the implications are. Will the candidates cluster around the main galaxies or are they more widely distributed along this filament?

Acknowledgements

O.M. and B.B. are grateful to the Swiss National Science Foundation for financial support. H.J. acknowledges the support of the Australian Research Council through Discovery Project DP150100862. The authors thank Marcel Pawlowski and Marina Rejkuba for interesting discussions and helpful input. The authors would like to thank the anonymous referee for the helpful comments that improved the paper.

5.4 The Leo-I group: new dwarf galaxy and UDG candidates

— Oliver Müller, Helmut Jerjen, Bruno Binggeli —

Astronomy & Astrophysics, 2018, accepted for publication

Abstract

The study of dwarf galaxies and their environments provides crucial test beds for predictions of cosmological models and insights into the structure formation on small cosmological scales. In recent years, many problems on the scale of groups of galaxies has challenged the current standard model of cosmology. Our aim is to increase the sample of known galaxies in the Leo-I group, which contains the M 96 subgroup and the Leo Triplet. This galaxy aggregate is located at the edge of the Local Volume at a mean distance of 10.7 Mpc. We employed image enhancing techniques to search for low surface brightness objects in publicly available gr images taken by the Sloan Digital Sky Survey within 500 square degrees around the Leo-I group. Once detected, we performed surface photometry and compared their structural parameters to other known dwarf galaxies in the nearby universe. We found 36 new dwarf galaxy candidates within the search area. Their morphology and structural parameters resemble known dwarfs in other groups. Among the candidates five or six galaxies are considered as ultra diffuse galaxy candidates. If confirmed, they would be some of the closest examples of this galaxy type. We assessed the luminosity function of the Leo-I group and find it to be considerably rich in dwarf galaxies, with twice the number of galaxies as the Local Group at a limiting magnitude of $M_V = -10$ and a steeper faint-end slope.

1. Introduction

More than one thousand galaxies reside in a sphere of 11 Mpc radius around the Milky Way; they are mostly dwarf-type galaxies ($M_B > -17.7$ mag). This so-called Local Volume (Kraan-Korteweg & Tammann 1979; Karachentsev et al. 2004, 2013) contains many prominent galaxy aggregates, e.g., our own Local Group (LG), the Sculptor filament, the Centaurus group, the M 81 group, the Canes Venatici cloud, the M 101 group complex, and the Leo-I group (Tully & Fisher 1988). In recent years many teams have taken up the challenge to search for new dwarf galaxies in the local universe and measure their distances (Chiboucas et al. 2009, 2013; Merritt et al. 2014; Belokurov et al. 2014; Crnojević et al. 2014, 2016; Kim et al. 2015; Müller et al. 2015, 2017a,b; Carlin et al. 2016; Javanmardi et al. 2016; Danieli et al. 2017; Carrillo et al. 2017; Henkel et al. 2017; Park et al. 2017; Makarova et al. 2018). These studies can be used to test the theoretical predictions from the standard model

of cosmology (ΛCDM). For the LG, there is a serious tension between observation and theory represented by the long-standing missing satellite problem (Moore et al. 1999), the too-big-too-fail (TBTF) problem (Kroupa et al. 2010; Boylan-Kolchin et al. 2011), and the plane-of-satellites problem (Kroupa et al. 2005; Pawlowski et al. 2012b; Ibata et al. 2013; Pawlowski 2018), see Bullock & Boylan-Kolchin (2017) for a recent review on small-scale challenges. Such studies are now extended to other nearby galaxy groups, for example to address the plane-of-satellite problem in Cen A (Tully et al. 2015; Müller et al. 2016, 2018b) or the TBTF and missing satellite problems in M 101 (Danieli et al. 2017; Müller et al. 2017b).

Using public data from the Sloan Digital Sky Survey (SDSS) we have started to systematically search for new or hitherto undetected dwarf galaxies in the Local Volume, beginning with the M 101 group complex, covering 330 $\deg^2$ around the spiral galaxies M 101, M 51, and M 63. We found 15 new dwarf galaxy candidates (Müller et al. 2017b). We now continue our optical search for dwarf galaxies in an area that covers 500 $\deg^2$ around the Leo-I group (Fig. 1).

The Leo-I group, with a mean distance of 10.7 Mpc (Karachentsev et al. 2004, 2013), consists of seven bright galaxies, NGC 3351 (= M 95), NGC 3368 (= M 96), NGC 3377, NGC 3379 (= M 105), NGC 3384, NGC 3412, and NGC 3489 (Karachentsev & Karachentseva 2004). Another four bright galaxies, NGC 3632 (= M 65), NGC 3627 (= M 66), NGC 3628 (which make up the Leo Triplet, about six degrees to the east of the main aggregate), and NGC 3593, are possibly also part of the group based on their common distances and systemic velocities (Ferrarese et al. 2000). We note that about eight degrees to the northeast is another quartet of bright galaxies (NGC 3599, NGC 3605, NGC 3607, and NGC 3608), which shares the same systemic velocity but is farther behind and is arguably not associated with the group (Ferrarese et al. 2000).

A spectacular feature of the Leo-I group in HI is known as the Leo ring (Schneider 1985) around NGC 3384/M 105, one of the largest HI structures in the nearby universe. Michel-Dansac et al. (2010) followed this up with a deep optical survey using MegaCam on the CFHT and found no diffuse stellar optical component down to 28 mag arcsec^{-2} surface brightness. The authors suggest an origin based on a collision between NGC 3384 and M 105 using gas and dark matter simulations that can explain the structure of the ring, together with the absence of apparent light. Deeper images ($\mu_V > 29.5$ mag arcsec^{-2}) taken by Watkins et al. (2014) have not yet revealed no optical counterpart of the ring; however, they found some stream-like features associated with the ring that are possibly of tidal origin. In the Leo Triplet another intriguing feature, this time in the optical, is a stellar stream associated with the boxy spiral NGC 3628 (Zwicky 1956), which hosts a tidal dwarf galaxy (Nikiel-Wroczyński et al. 2014) and an ultra compact dwarf galaxy (Jennings et al. 2015).

For the central part of the Leo-I group (i.e., the M 96 subgroup) an initial catalog of 50 dwarf galaxy candidates was produced by Ferguson & Sandage (1990). The authors argued, based on morphological properties, that half of them are group members. Another collection of dwarf galaxies was discovered by Trentham & Tully (2002) who surveyed a 10×10 deg^2 field partially covering the Leo-I group. Using the digitized sky survey, Karachentsev & Karachentseva (2004) refined and extended this list to 50 likely members. For many members HI velocities were derived (Stierwalt et al. 2009), making it possible to distinguish between actual Leo-I members and background galaxies belonging to the more distant Leo cloud (see Fig. 1 in Trentham & Tully 2002 for the difference in velocity space). A very deep but spatially limited image, based on amateur telescopes, was produced for NGC 3628 in the Leo Triplet and revealed another faint dwarf galaxy (Javanmardi et al. 2016).

To follow a consistent naming convention in this paper, from now on we use the term M 96 subgroup to describe the main galaxy aggregate around M 96, and the term Leo-Triplet (Leo-Tr) for the aggregate around M 66. Both subgroups together are called the Leo-I group (see Fig. 1).

In this work we present a search for unresolved dwarf galaxies using publicly available data from the Sloan Digital Sky Survey (SDSS) in 500 deg^2, covering the extended Leo-I group region. In Section 2 we summarize our search strategy, and in Section 3 we present the surface photometry performed for all known and newly found members of the Leo-I group. In Section 4 we discuss our candidate list and potential background contamination. Finally, in Section 5 we draw our conclusions and give a brief outlook.

2. Discovery of new dwarf galaxy candidates

In recent years, different automatic detection approaches have been proposed to search for low surface brightness galaxies (e.g., Merritt et al. 2014; Speller & Taylor 2014; van der Burg et al. 2016; Bennet et al. 2017) with encouraging results. On the other hands, these pipelines were only applied on small areas of the sky (< 10 deg^2) and still have a considerable rate of false detections, or rely on a large number of existing galaxies to study galaxy groups on a statistical basis. It remains to be seen how these methods perform on large-field surveys with areas of several hundred of square degrees and how time-consuming the task of rejecting false-positives will be. We argue, as do other authors (e.g., Park et al. 2017; Wittmann et al. 2017), that a visual search on images is still on par with algorithm-based detections.

In this work, we follow the same methods as described in Müller et al. (2017b) to search for dwarf galaxies in an area of $\sim$500 deg^2 around the Leo-I group using

data taken from the SDSS. In summary this involves the creation of 1 square degree mosaics of g and r images, the use of several image processing algorithms (e.g., binning and Gaussian convolution) to enhance the low surface brightness features within the images, and the final visual search for dwarf galaxies in these processed images. Once an object is detected, surface photometry is applied to derive the structural parameters, which are compared to the properties of known dwarf galaxies of the LG and other groups. Based on this morphological comparison, a detection is considered or rejected as a dwarf galaxy candidate. To estimate our detection rate we conducted an experiment where we induced artificial galaxies into the SDSS images and derived the recovery rate of these objects (Fig. 3 in Müller et al. 2017b).

In Fig. 1 we present the survey footprint, the known galaxies in this field (black and gray dots), and the new dwarf galaxy candidates (red dots) found in our search. In the up-to-date online version[2] of the LV catalog, 63 dwarf galaxies are listed within our footprint, with four (open circle) having a distance estimate smaller than 7 Mpc. In Table 1 we present the coordinates of the 36 dwarf galaxy candidates found in the survey, together with our galaxy type classification and comments on the objects. We indicate whether the objects are found in the vicinity of M 96, in the Leo Triplet, or in the surrounding field. In Figs. 2 and 3 we present images of the newly discovered candidates. Some dwarf galaxy candidates show irregularities. We checked the Galaxy Evolution Explorer (GALEX) survey (in the near- and far-ultraviolet) for extended objects coinciding with our detections. Indeed, the candidates dw1013+18, dw1045+14a, dw1049+15, dw1116+15b, dw1130+20, and dw1148+16 have some UV features, possibly hinting towards star formation. These objects are classified as dIrr/dSph if they possess a smooth profile and are likely transition type dwarfs.

3. Surface photometry

We computed the total apparent magnitude m, the mean effective surface brightness $\langle\mu\rangle_{eff}$, and the effective radius r_{eff} in gr bands for each dwarf galaxy candidate, and for already known group members as many of them do not have accurate photometry. To measure the surface brightness profiles we used a circular aperture (step size of 0.396 arcsec corresponding to 1 pixel). Sérsic profiles (Sersic 1968) were fitted at the derived profiles using the equation

$$\mu_{sersic}(r) = \mu_0 + 1.0857 \cdot \left(\frac{r}{r_0}\right)^n,$$

where μ_0 is the Sérsic central surface brightness, r_0 the Sérsic scale length, and n the Sérsic curvature index. The total extinction corrected absolute magnitude M

[2]last checked: 19 December 2017.

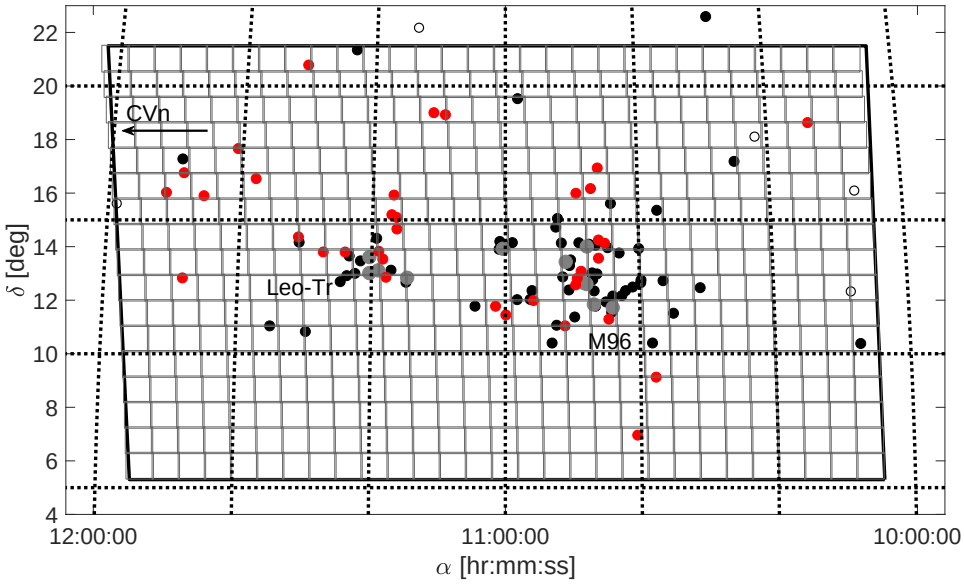

Fig. 1: Survey area of ≈ 500 deg^2 in the Leo-I group region. The squares correspond to the created 1 deg^2 mosaics. The small black dots are previously known members based on their photometric properties, compiled from the Local Volume Catalog (Karachentsev et al. 2004, 2013). The large gray dots are the major galaxies in the M 96 subgroup and Leo Triplet. The red dots indicate the positions of the 36 new dwarf candidates. Open circles are confirmed foreground galaxies (<7 Mpc) taken from the LV Catalog.

is calculated with a distance modulus of $m - M = 30.06$ mag, corresponding to $D = 10.4$ Mpc, as is used for Leo-I members with unknown distance estimates in the LV catalog (see Fig. 4 for all surface brightness profiles in the r band and the associated Sérsic fits). In Table 2 we provide the derived photometry for the new candidates, and in Tables 4 and 5 the previously known (dwarf) members of the Leo-I group.

The magnitude uncertainties are estimated at around ≈ 0.3 mag (Müller et al. 2017b). The main contributions to the error budget are from the uncertainties related to foreground star removal (≈ 0.2 mag) and sky background estimation (≈ 0.2 mag). The uncertainties for $\langle\mu\rangle_{eff}$ are driven by the uncertainties in the measured total apparent magnitude (≈ 0.3 mag arcsec^{-2}). The error for r_{eff} (≈ 1.3 arcsec) is given by the determination of the growth curve. Numerical uncertainties for the Sérsic parameters are provided in the corresponding table.

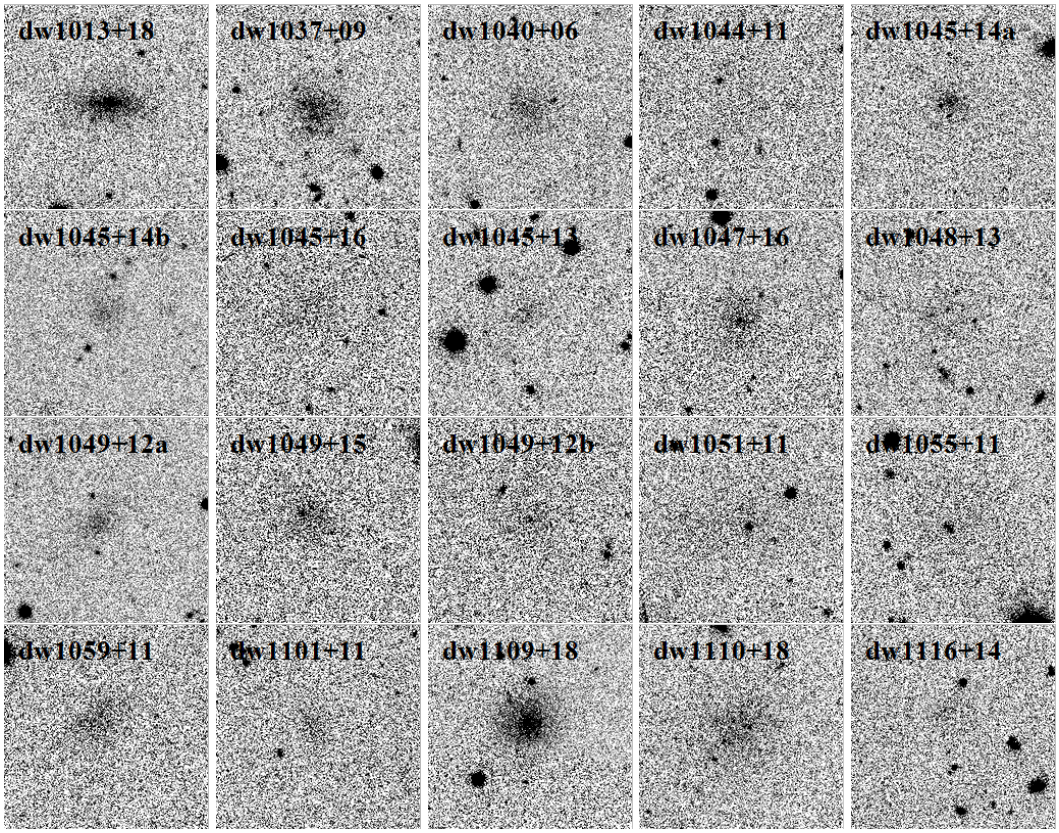

Fig. 2: Gallery showing SDSS r-band images of the new Leo-I group member candidates. One side of an image corresponds to 80 arcsec or 3.88 kpc at the distance of 10 Mpc. North is to the top, east to the right.

4. Discussion

In the following we discuss the membership of the candidates based on their morphological parameters, the contamination of the field by nearby background galaxies, and the potential discovery of ultradiffuse galaxies (UDG).

Membership estimation

The standard approach for establishing membership based on morphological properties is to compare the structural parameters of the candidates with known dwarf galaxies (e.g., Jerjen et al. 2000a; Chiboucas et al. 2009; Merritt et al. 2014; Müller et al. 2017a,b). If the objects fit into the ($\langle\mu\rangle_{eff}$ – M), (r_{eff} – M), (μ_0 – M), and (n – M) scaling relations defined by the known dwarf galaxies in the local Universe, it is reasonable to consider them as dwarf galaxy candidates. The ($\langle\mu\rangle_{eff}$ – M) and (μ_0 – M) are especially crucial because the surface brightness is independent of the assumed distance of the object, therefore making it possible to assess the membership at a certain distance (see Müller et al. 2017a, Fig. 11 for what happens to galaxies with unreasonable distance estimates in those relations). To transform

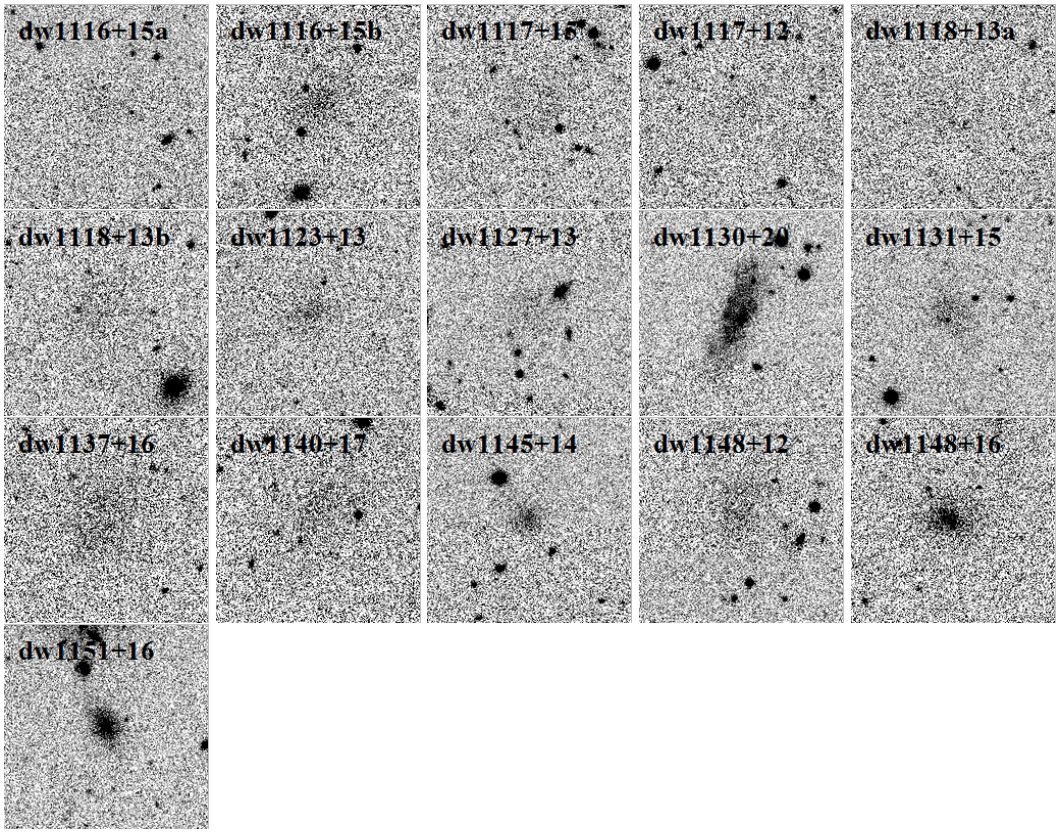

Fig. 3: Fig. 2 continued.

our gr photometry to the Johnson system we used the following equations (Lupton 2005):

$$V = g - 0.5784 \cdot (g - r)_0 - 0.0038$$

$$B = r + 1.3130 \cdot (g - r)_0 + 0.2271$$

The structural parameters of the newly found dwarf candidates, and of the previously discovered Leo-I members and the Local Group dwarf population, are plotted in Fig. 5. The structural parameters of the dwarf candidates fall into the relations defined by the Local Group dwarfs, thus we can assume that the candidates are indeed dwarf members of the Leo-I group. Additionally, we show the 44 UDG candidates in the Coma Cluster discovered by van Dokkum et al. (2015a), who only gave g band photometry and so we assume a color index of $(g - r) = 0.6$ mag to transform them into V-band magnitudes. UDGs typically have an effective radius larger than $r_{eff} > 1.5$ kpc and a central surface brightness fainter than $\mu_g > 24.0$ mag arcsec^{-2} (van Dokkum et al. 2015a).

Dwarf galaxies can also be characterized by their color using the color-magnitude relation (e.g., Lisker et al. 2008; Venhola et al. 2017). Here we compare the $(g - r)_0$ colors of the Leo-I group dwarfs with other well-studied systems in the LV where gr photometry is available, namely the Centaurus group (Müller et al. 2015, 2017a) and the M101 group complex (Müller et al. 2017b). The calculated mean $(g - r)_0$ color

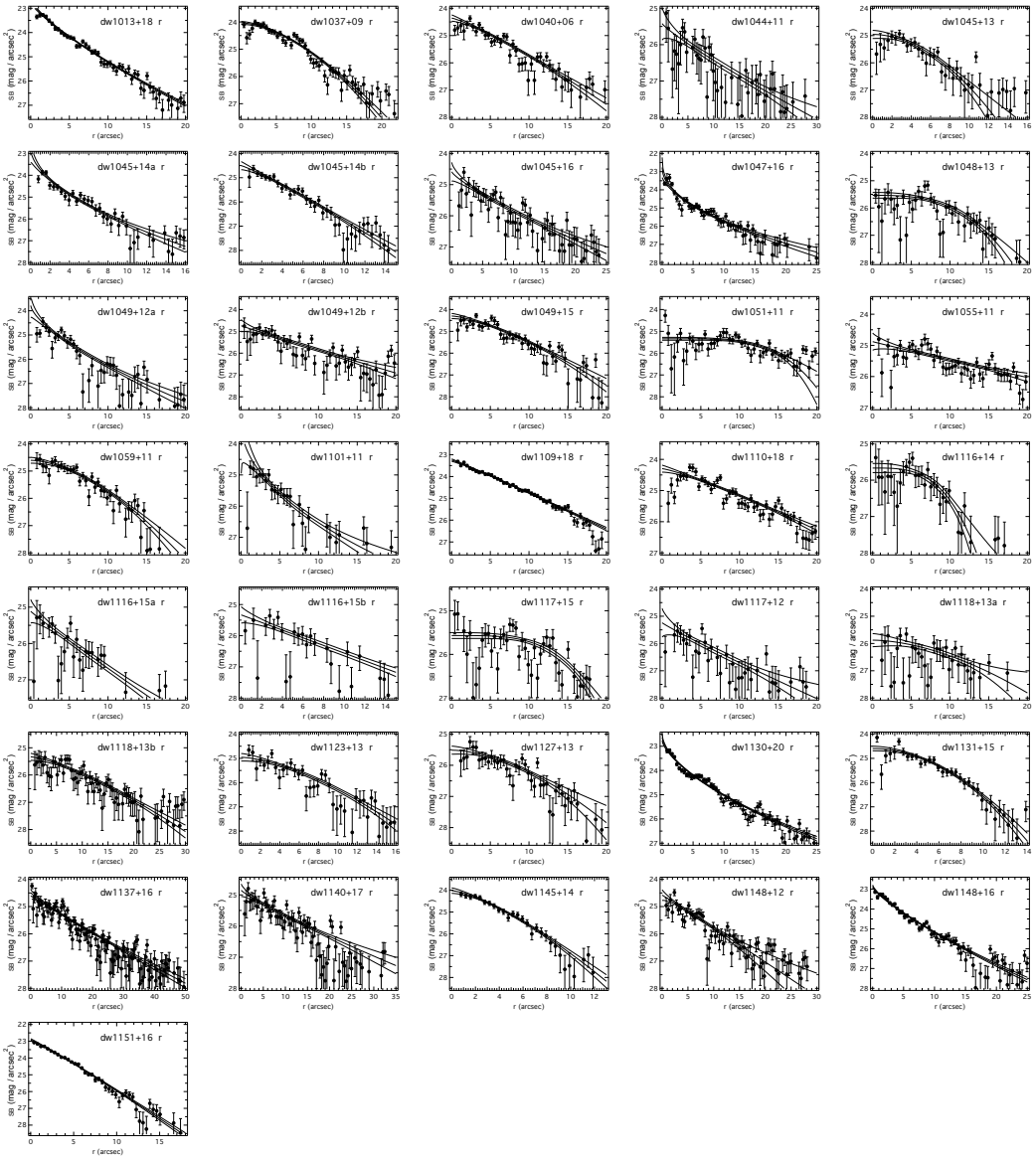

Fig. 4: Surface brightness profiles of all new dwarf galaxy candidates in r and the best-fitting Sérsic profiles with 1σ confidence intervals.

and standard deviation for the three group populations are $(g-r)_{0,Leo-I} = 0.491 \pm 0.282$ mag, $(g-r)_{0,Cen\,A} = 0.463 \pm 0.258$ mag, and $(g-r)_{0,M\,101} = 0.472 \pm 0.190$ mag. In Fig. 6 we show the color distribution as a function of total absolute V-magnitude for these different groups. The dwarfs in the different galaxy groups follow a similar distribution in their colors. We note that the extreme blue colors ($g-r<0$) of some objects, which is uncommon for dwarf galaxies, and the scatter at the faint-end of the scale can arise from the photometric uncertainty.

In the following we discuss some individual candidates that have interesting features.
dw1037+09: This candidate has several knots within and around the galaxy, which could either be bright giant stars or globular clusters (GC).
dw1110+18: Here too there are several knots sprinkled through the object, which

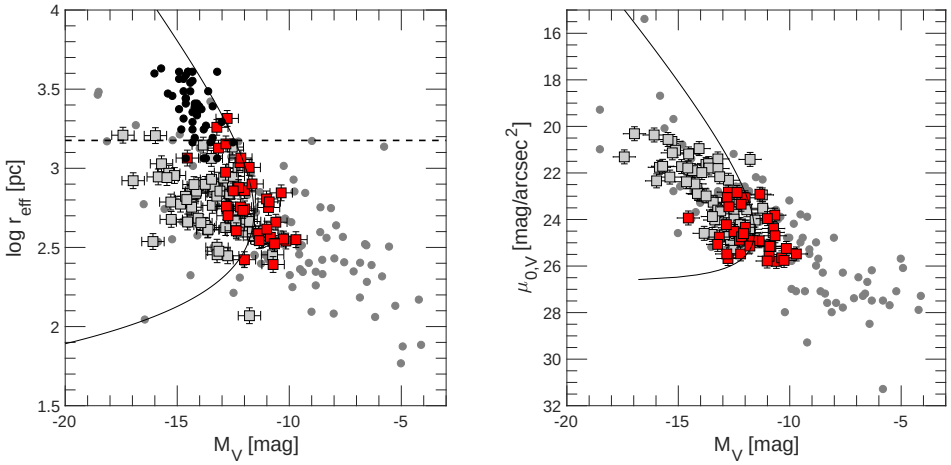

Fig. 5: Scaling relations (r_{eff} – M) and (μ_0 – M) for the newly discovered dwarf candidates (red squares), previously discovered dwarf members (gray squares), and the Local Group dwarf galaxy population (gray dots). The estimated conservative completeness limit, as derived in Müller et al. (2017b), is indicated with the line. The UDG candidates discovered in Coma (van Dokkum et al. 2015a) are overlaid as black dots in the (r_{eff} – M) diagram; also overlaid is the size cut (dashed line) of 1.5 kpc for UDGs.

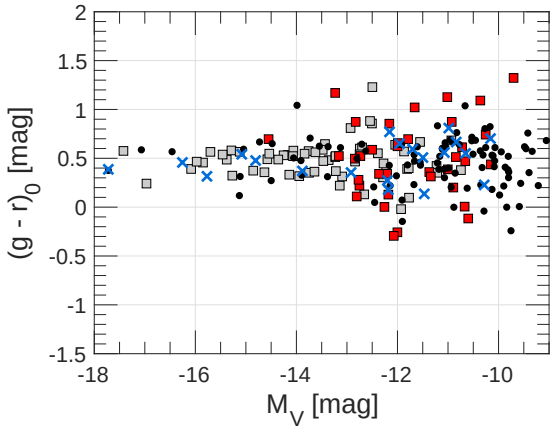

Fig. 6: Color-magnitude relation for the previously known Leo-I dwarf members (gray squares), the new Leo-I members (red squares), the Centaurus group members (black dots, Müller et al. 2015, 2017a), and the M 101 group members (blue crosses, Müller et al. 2017b). Both early- and late-type dwarf galaxies were considered.

could be bright giant stars or GCs.

dw1130+20: This galaxy has some bright knots, which could correspond to HII regions.

Under the assumption that all candidates are members of the Leo-I group, we can determine the galaxy luminosity function (see Fig. 7) and compare it to other nearby galaxy group environments, i.e., the Centaurus group (Müller et al. 2015, 2017a), the LG (McConnachie 2012), the M101 group (Bremnes et al. 1999; Müller et al. 2017b), and the NGC2784 group (Park et al. 2017). Among these five groups, the Leo-I group is the richest galaxy aggregate with approximately 100 galaxies up to an absolute magnitude of $M_V = -10$, in other words if all candidates are confirmed as members. The Leo-I group has approximately twice as many dwarfs as the LG and a steeper faint-end slope of the LF, comparable to that of Cen A. The M 101 and NGC 2784 groups have shallower faint-end slopes. This indicates that galaxy groups

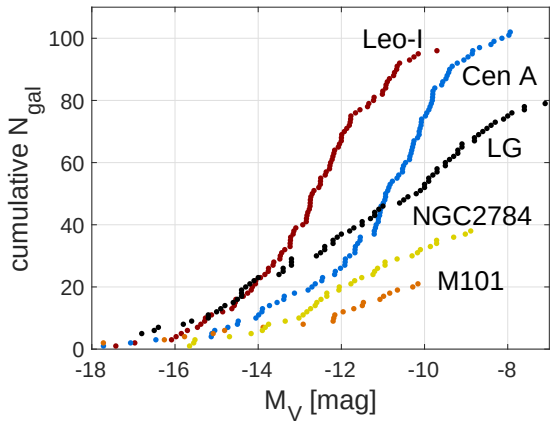

Fig. 7: Cumulative galaxy luminosity functions for different galaxy groups in the Local Volume. Data taken from Leo-I (this work), Centaurus group (Müller et al. 2015, 2017a), LG (McConnachie 2012), NGC 2784 group (Park et al. 2017), and M 101 group (Bremnes et al. 1999; Müller et al. 2017b).

with massive hosts have steeper faint-ends of the LF. While the faint-end slopes of Leo-I and Cen A are comparable, the Leo-I group contains more brighter galaxies in the range from -16 to -14 mag in V-bands, making it more rich (up to $M_V = -10$). In this range (-16 to -14 V mag), the LF of Leo-I is comparable to that of the LG.

Background contamination

One fundamental challenge when searching for new dwarf galaxies is that survey fields are almost always contaminated by galaxy groups in the background. A prime example for such a confusion is the massive elliptical galaxy NGC 5485 with its many dwarf companions (Makarov & Karachentsev 2011) situated ≈20 Mpc behind the Local Volume galaxy M 101 (7 Mpc, Nataf 2015). Figure 8 in Merritt et al. (2016) shows M 101, the background elliptical NGC 5485, and former M 101 dwarf candidates (Merritt et al. 2014) that actually belong to the background galaxy population. Out of the seven dwarf candidates reported by Merritt et al. (2014), only three were confirmed to be M 101 members with HST follow-up observations (Danieli et al. 2017). Recently, more new dwarf candidates were reported around M 101 (Bennet et al. 2017; Müller et al. 2017b), now awaiting confirmation as members by means of distance or velocity measurements. Some will potentially be associated with the background elliptical NGC 5485.
The possibility of contamination prompted us to study the background of the Leo-I group in more detail. In Müller et al. (2017a) we used the Cosmicflows-2 catalog (Tully et al. 2013) to determine the background contamination of the Centaurus group. Here we query the Cosmicflows-2 catalog for bright galaxies with absolute magnitudes M_B<-19 and with radial velocities v_{rad}<2000 km s^{-1} within our survey footprint. Excluding the Leo-I galaxies this search resulted in 24 bright host galaxies potentially contaminating our survey.

To test how these background galaxies will pollute our detections we surveyed for dwarf galaxies within 300 kpc of each such host (approximately the virial radius) with the same methods as used in our search for Leo-I dwarfs, but without removing

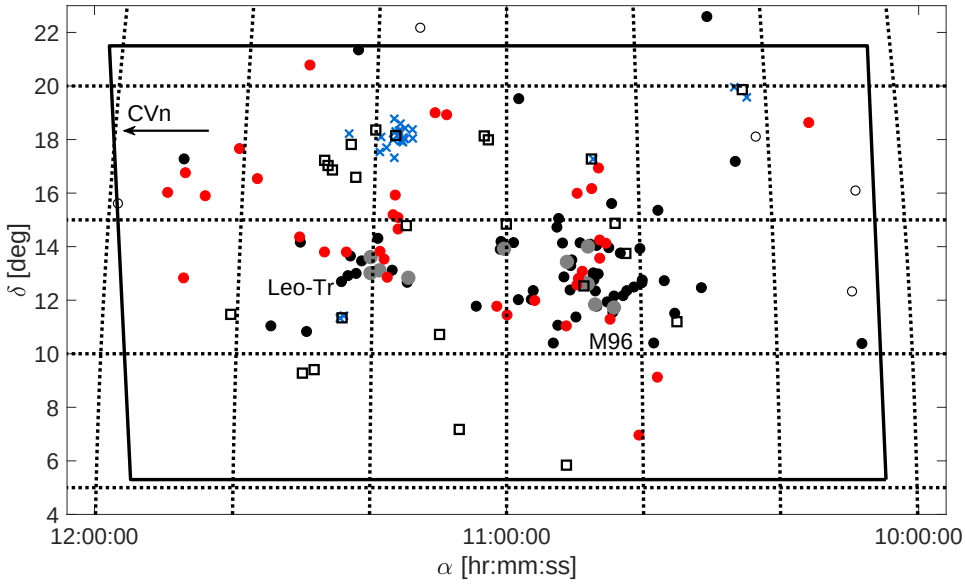

Fig. 8: Same as Fig. 1, but with background host galaxies (black squares) and the background dwarf galaxies (blue crosses) that are clustered around these hosts. The background dwarfs would be considered Leo-I dwarfs (thanks to their morphology) if they were not so close to the background hosts. See Section 5.4 for details.

candidates that are near a background galaxy. Essentially, we search for the candidates we rejected as background sources. In Table 3 we compiled the coordinates for the objects that would be considered as dwarf candidates based on their morphology. In total we found 26 additional dwarf candidates, of which 20 are clustered around NGC 3607 at a distance of $\sim$ 20 Mpc. This indicates that (a) it is not feasible to include every object in the survey footprint as Leo-I dwarf, and (b) that there will probably be some confusion between foreground and background, either by rejecting a foreground dwarf or including a background dwarf.

Some Leo-I dwarf candidates are near both a background host and a Leo-I host. In this case we added a note to Table 1. To the north to the Leo Triplet there are four Leo-I candidates (dw1116+14, dw1116+15a, dw1116+15b, and dw1117+15) clustered around NGC 3596 (15 Mpc). The distribution of the background dwarf galaxies can be seen in Fig. 8. Distance and velocity measurements will be crucial to distinguish their memberships. Until then, the faint-end of the LF will be affected by these uncertain cases.

UDG candidates

Originally discovered by Sandage & Binggeli (1984) and described as "a new type of very large diameter (10,000 pc), low central surface brightness (>25 B mag/arcsec^2) galaxy, that comes in both early (i.e., dE) and late (i.e., Im V) types," this class of galaxies is now called ultradiffuse galaxies (van Dokkum et al. 2015a); these galaxies have been found in many different environments (van der Burg et al. 2016),

for example in clusters (van Dokkum et al. 2015a; Koda et al. 2015), and in groups (Merritt et al. 2016). Different possible formation scenarios have been proposed (e.g., Amorisco & Loeb 2016; Di Cintio et al. 2017) and are under intense debate. van Dokkum et al. (2015a) suggested classifying dwarf galaxies with $r_{eff} > 1.5$ kpc and a fainter central surface brightness than $\mu_g > 24.0$ mag arcsec^{-2} as UDGs; however, this boundary is rather arbitrary and should be considered more as a guideline.
Studying the properties of the Leo-I members we consider dw1055+11, dw1117+15, dw1051+11, KK 96, and ACG 215415 as UDG candidates. With $r_{eff} = 1.3$ kpc dw1137+16 is still considerably large and could be a UDG type. Better photometry is needed to derive the structural parameters more accurately. However, we note that if these objects were more in the foreground (e.g., in the Canes Venatici-I cloud), they would be closer to our point of view and therefore would have smaller intrinsic sizes, making them common-sized dwarf galaxies.
The UDG candidates are distributed in the outskirts of the aggregates and not in the central parts of the group. This is similar to what is found in galaxy clusters: in galaxy clusters the UDG density drops nearly to zero in the central regions because they cannot survive the tidal forces inflicted on them (van der Burg et al. 2016). We note that it is not feasible to assess the UDG distribution in Leo-I with only 5 or 6 candidates.

5. Conclusion

We have surveyed 500 square degrees of gr images taken from SDSS within the extended region of the Leo-I group and found 36 new dwarf galaxy candidates. For every known member and new candidate we derived surface brightness photometry. Based on a comparison of their structural properties with other known dwarf galaxies in the nearby universe and their morphology we consider these candidates to be members of the Leo-I group, lying in the vicinity of the M 96 subgroup, in the Leo Triplet, or in the nearby field. To confirm their membership, follow-ups are required to either measure their radial velocities, their distances, or both. Some of the candidates are exceptionally large with low surface brightness, a characteristic of ultradiffuse galaxies. If these UDGs are confirmed as Leo-I members, they would be some of the closest UDGs to Earth and valuable targets that could be used to improve our understanding of this galaxy type.

Acknowledgements

OM and BB are grateful to the Swiss National Science Foundation for financial support. HJ acknowledges the support of the Australian Research Council through Discovery Project DP150100862. We thank the referee for the helpful comments.

Tab. 1: Names, coordinates, and morphological types of the 36 new dwarf galaxy candidates of the Leo-I group.

Name	α (J2000)	δ (J2000)	Type	Notes
dw1013+18	10:13:29.0	+18:36:44	dIrr/dSph	field
dw1037+09	10:37:40.7	+09:06:20	dIrr	M 96
dw1040+06	10:40:30.3	+06:56:28	dSph	field
dw1044+11	10:44:33.0	+11:16:10	dSph	M 96
dw1045+14a	10:45:00.6	+14:06:20	dIrr/dSph	M 96
dw1045+14b	10:45:56.3	+14:13:37	dSph	M 96
dw1045+16	10:45:56.3	+16:55:00	dSph, bg?	M 96
dw1045+13	10:45:58.1	+13:32:52	dSph	M 96
dw1047+16	10:47:00.0	+16:08:50	dSph,N	M 96
dw1048+13	10:48:35.7	+13:03:34	dSph	M 96
dw1049+12a	10:49:11.4	+12:47:34	dSph	M 96
dw1049+15	10:49:14.3	+15:58:20	dSph/dIrr	M 96
dw1049+12b	10:49:25.8	+12:33:08	dSph/dIrr?	M 96
dw1051+11	10:51:03.8	+11:01:13	dSph, UDG?	M 96
dw1055+11	10:55:43.5	+11:58:05	dSph,N, UDG?	M 96
dw1059+11	10:59:50.9	+11:25:38	dSph	M 96
dw1101+11	11:01:22.5	+11:45:12	dSph	M 96
dw1109+18	11:09:08.5	+18:54:22	dIrr/dSph	field
dw1110+18	11:10:54.9	+18:58:52	dSph	field
dw1116+14	11:16:14.4	+14:38:21	dSph, bg?	Leo-Tr
dw1116+15a	11:16:17.1	+15:04:02	dSph, bg?	Leo-Tr
dw1116+15b	11:16:46.4	+15:54:19	dIrr/dSph, bg?	Leo-Tr
dw1117+15	11:17:02.1	+15:10:17	dSph, UDG?, bg?	Leo-Tr
dw1117+12	11:17:44.2	+12:50:10	dSph	Leo-Tr
dw1118+13a	11:18:15.9	+13:30:53	dSph	Leo-Tr
dw1118+13b	11:18:53.3	+13:48:18	dSph	Leo-Tr
dw1123+13	11:23:56.4	+13:46:41	dSph	Leo-Tr
dw1127+13	11:27:13.0	+13:46:50	dSph	Leo-Tr
dw1130+20	11:30:32.0	+20:45:41	dIrr	field
dw1131+15	11:31:01.0	+15:54:52	dSph	field
dw1137+16	11:37:45.6	+16:31:09	dSph, UDG?	field
dw1140+17	11:40:43.0	+17:38:33	dSph	field
dw1145+14	11:45:32.1	+15:52:50	dSph	field
dw1148+12	11:48:09.1	+12:48:47	dSph	field
dw1148+16	11:48:45.0	+16:44:24	dIrr/dSph	field
dw1151+16	11:51:15.2	+16:00:20	dSph	field

Tab. 2: Photometric and structural parameters of the new dwarf candidates in the surveyed region of the Leo-I group.

Name	g_{tot}	r_{tot}	A_g	A_r	M_r	$(g-r)_{0,tot}$	$\mu_{0,r}$	$r_{0,r}$	n_r	$\langle\mu\rangle_{eff,r}$	$r_{eff,r}$	$\log r_{eff,r}$
	mag	mag	mag	mag	mag	mag	mag arcsec^{-2}	arcsec		mag arcsec^{-2}	arcsec	log pc
(1)	(2)	(3)	(4)	(5)	(6)	(7)	(8)	(9)	(10)	(11)	(12)	(13)
M 96 subgroup												
dw1037+09	17.61	17.09	0.080	0.056	-13.04	0.496	24.04 ± 0.05	9.96 ± 0.38	1.68 ± 0.14	25.44	18.7	2.97
dw1044+11	19.39	19.17	0.088	0.061	-10.97	0.200	25.42 ± 0.45	10.87 ± 5.89	0.87 ± 0.40	26.59	12.1	2.78
dw1045+14a	19.02	18.68	0.097	0.067	-11.46	0.313	22.79 ± 0.63	1.25 ± 1.14	0.56 ± 0.16	24.87	6.92	2.54
dw1045+14b	19.79	19.29	0.094	0.065	-10.85	0.470	24.50 ± 0.17	5.24 ± 0.83	1.13 ± 0.18	25.39	6.61	2.52
dw1045+16	18.50	17.62	0.085	0.059	-12.51	0.854	24.59 ± 0.30	8.39 ± 3.22	0.81 ± 0.24	26.43	23.0	3.06
dw1045+13	18.81	18.08	0.110	0.076	-12.07	0.696	24.96 ± 0.15	7.41 ± 0.70	1.92 ± 0.52	26.59	20.0	3.00
dw1047+16	18.07	17.91	0.091	0.063	-12.23	0.128	22.77 ± 0.55	1.32 ± 1.18	0.49 ± 0.13	25.17	11.2	2.75
dw1048+13	19.83	18.67	0.111	0.077	-11.48	1.126	25.53 ± 0.10	13.63 ± 0.64	2.94 ± 0.78	26.19	12.6	2.80
dw1049+12a	19.39	18.98	0.088	0.061	-11.16	0.386	23.78 ± 0.49	2.92 ± 1.91	0.67 ± 0.19	25.54	8.18	2.61
dw1049+15	18.56	17.88	0.088	0.061	-12.26	0.655	24.30 ± 0.12	9.38 ± 0.90	1.42 ± 0.23	25.08	10.9	2.74
dw1049+12b	19.10	18.05	0.085	0.059	-12.08	1.020	24.74 ± 0.28	9.76 ± 3.03	0.96 ± 0.36	26.04	15.7	2.90
dw1051+11	17.85	16.95	0.092	0.063	-13.19	0.872	25.34 ± 0.07	16.76 ± 0.63	4.15 ± 1.20	26.20	28.2	3.15
dw1055+11	17.59	16.40	0.066	0.046	-13.72	1.169	24.88 ± 0.28	18.86 ± 3.90	0.97 ± 0.54	26.18	36.0	3.25
dw1059+11	18.98	18.60	0.060	0.041	-11.51	0.359	24.61 ± 0.11	9.73 ± 0.72	1.68 ± 0.26	25.02	7.65	2.58
dw1101+11	19.47	19.45	0.058	0.040	-10.66	0.005	23.33 ± 1.62	1.16 ± 2.78	0.50 ± 0.32	25.56	6.64	2.52
Leo Triplet												
dw1116+14	20.33	19.57	0.071	0.049	-10.56	0.742	25.67 ± 0.13	10.63 ± 0.58	3.28 ± 1.11	25.81	7.08	2.55
dw1116+15a	20.26	19.80	0.076	0.052	-10.33	0.437	25.11 ± 0.32	6.79 ± 2.43	0.95 ± 0.28	25.98	6.88	2.54
dw1116+15b	20.42	19.31	0.068	0.047	-10.81	1.091	25.33 ± 0.26	8.85 ± 2.61	1.00 ± 0.32	27.02	13.8	2.84
dw1117+15	17.56	17.25	0.082	0.057	-12.88	0.280	25.57 ± 0.07	17.11 ± 0.51	3.79 ± 0.92	27.31	40.9	3.31
dw1117+12	21.22	19.87	0.073	0.050	-10.25	1.322	25.24 ± 0.52	7.29 ± 4.29	0.93 ± 0.51	26.10	7.02	2.54
dw1118+13a	19.49	19.59	0.077	0.053	-10.54	-0.11	25.88 ± 0.24	14.36 ± 1.94	1.74 ± 1.02	26.36	9.04	2.65
dw1118+13b	18.15	17.78	0.069	0.047	-12.34	0.341	25.33 ± 0.13	15.09 ± 1.66	1.35 ± 0.24	26.45	21.5	3.03
dw1123+13	19.62	19.08	0.079	0.054	-11.05	0.513	24.95 ± 0.16	8.74 ± 1.05	1.55 ± 0.31	25.38	7.26	2.56
dw1127+13	19.76	18.85	0.093	0.064	-11.28	0.872	25.51 ± 0.13	12.85 ± 0.95	1.72 ± 0.52	26.10	11.2	2.75
Field												
dw1013+18	18.02	17.65	0.106	0.073	-12.50	0.340	22.67 ± 0.10	3.29 ± 0.38	0.76 ± 0.04	24.16	7.99	2.60
dw1040+06	17.96	18.22	0.120	0.083	-11.94	-0.29	24.36 ± 0.12	8.18 ± 0.88	1.20 ± 0.17	25.37	10.7	2.73
dw1109+18	17.73	17.18	0.077	0.054	-12.95	0.523	23.25 ± 0.06	7.35 ± 0.41	1.07 ± 0.06	24.17	9.94	2.70
dw1110+18	18.00	17.39	0.077	0.053	-12.74	0.587	24.30 ± 0.11	12.15 ± 1.16	1.20 ± 0.20	25.15	14.2	2.85
dw1130+20	17.53	17.28	0.068	0.047	-12.84	0.220	22.63 ± 0.14	2.75 ± 0.58	0.61 ± 0.05	24.49	10.9	2.74
dw1131+15	19.51	18.87	0.171	0.118	-11.32	0.581	24.59 ± 0.09	7.39 ± 0.42	1.97 ± 0.24	25.22	7.43	2.57
dw1137+16	17.32	16.77	0.097	0.067	-13.37	0.523	24.49 ± 0.12	14.19 ± 1.99	0.89 ± 0.10	25.89	26.6	3.12
dw1140+17	18.54	17.89	0.098	0.068	-12.25	0.623	24.85 ± 0.20	13.96 ± 3.30	0.87 ± 0.23	25.67	14.3	2.85
dw1145+14	19.86	19.20	0.147	0.101	-10.97	0.613	24.02 ± 0.12	4.94 ± 0.49	1.39 ± 0.17	24.65	4.89	2.39
dw1148+12	17.95	17.91	0.119	0.082	-12.25	0.002	24.58 ± 0.20	9.02 ± 1.75	1.02 ± 0.29	25.78	14.9	2.87
dw1148+16	17.49	17.34	0.150	0.104	-12.84	0.109	22.85 ± 0.06	3.77 ± 0.32	0.78 ± 0.04	24.61	11.3	2.75
dw1151+16	18.04	18.27	0.109	0.075	-11.88	-0.25	22.92 ± 0.07	3.92 ± 0.25	1.09 ± 0.05	23.86	5.24	2.42

Tab. 3: Coordinates of the possible background dwarf galaxy in our survey footprint around bright host galaxies with v<2000 km s^2.

Name	α (J2000)	δ (J2000)
NGC 3227_1	10:22:53	+19:34:36
NGC 3227_2	10:24:43	+19:57:16
NGC 3227_3	10:25:50	+19:43:22
NGC 3666_1	11:24:45	+11:20:04
NGC 3666_2	11:24:10	+11:25:12
NGC 3370_1	10:46:47	+17:16:18
NGC 3607_1	11:14:22	+18:02:38
NGC 3607_2	11:14:26	+18:22:30
NGC 3607_3	11:15:35	+18:25:21
NGC 3607_4	11:15:36	+18:01:04
NGC 3607_5	11:15:48	+18:04:40
NGC 3607_6	11:15:52	+17:54:04
NGC 3607_7	11:15:57	+17:56:25
NGC 3607_8	11:16:11	+17:57:04
NGC 3607_9	11:16:18	+18:35:39
NGC 3607_10	11:16:28	+18:11:35
NGC 3607_11	11:16:30	+18:19:27
NGC 3607_12	11:17:01	+18:18:07
NGC 3607_13	11:17:07	+17:19:09
NGC 3607_14	11:17:16	+18:46:27
NGC 3607_15	11:17:22	+17:59:50
NGC 3607_16	11:18:21	+17:41:50
NGC 3607_17	11:19:13	+18:05:47
NGC 3607_18	11:19:21	+17:32:09
NGC 3607_19	11:24:08	+18:13:16
NGC 3607_20	11:31:01	+15:54:48

Tab. 4: Photometric and structural parameters of the previously known Leo-I members.

Name			g_{tot}	r_{tot}	A_g	A_r	M_r	$(g-r)_{0,tot}$	$\mu_{0,r}$	$r_{0,r}$	n_r	$\langle\mu\rangle_{eff,r}$	$r_{eff,r}$	$\log r_{eff,r}$	Ref	D	v
			mag	mag	mag	mag	mag	mag	mag arcsec^{-2}	arcsec		mag arcsec^{-2}	arcsec	log pc		Mpc	km s^{-1}
(1)			(2)	(3)	(4)	(5)	(6)	(7)	(8)	(9)	(10)	(11)	(12)	(13)	(14)	(15)	(16)
M 96 subgroup																	
AGC 205156	10:30:53	+12:26:48	18.65	18.22	0.102	0.071	-11.94	0.398	21.22 ± 0.12	1.80 ± 0.17	1.12 ± 0.08	22.13	2.41	2.08	(AA)	10.43 (LV)	915 (AA)
AGC 202248	10:34:56	+11:29:31	17.17	16.92	0.103	0.071	-13.23	0.220	22.10 ± 0.09	5.15 ± 0.36	1.28 ± 0.07	22.87	6.17	2.49	(AA)		1177 (AA)
NGC 3299	10:36:24	+12:42:25	13.08	12.48	0.082	0.057	-17.66	0.575	21.06 ± 0.02	22.48 ± 0.55	0.77 ± 0.02	22.09	33.3	3.22			604 (AA)
AGC 205165	10:37:05	+15:20:13	15.92	15.39	0.123	0.085	-14.77	0.490	21.85 ± 0.02	7.83 ± 0.16	0.97 ± 0.01	22.97	13.0	2.81	(AA)		724 (AA)
AGC 200499	10:38:08	+10:22:52	14.32	13.90	0.094	0.065	-16.24	0.390	20.25 ± 0.05	5.35 ± 0.19	0.98 ± 0.02	20.15	7.10	2.55	(AA)		1175 (AA)
LeG 04	10:39:40	+12:44:07	18.10	17.53	0.090	0.062	-12.61	0.551	23.10 ± 0.11	4.97 ± 0.59	0.90 ± 0.07	24.43	9.58	2.68	(LV)		
FS 01 (LeG 05)	10:39:43	+12:38:04	16.74	16.14	0.084	0.058	-13.99	0.573	21.50 ± 0.03	4.04 ± 0.15	0.82 ± 0.02	22.91	8.99	2.65	(FS)		780 (AA)
LeG 06	10:39:56	+13:54:33	17.12	16.60	0.117	0.081	-13.56	0.481	23.90 ± 0.03	14.32 ± 0.36	1.50 ± 0.06	24.59	15.7	2.90	(LV)		1007 (AA)
UGC 05812	10:40:56	+12:28:21	15.07	14.56	0.080	0.056	-15.58	0.486	21.97 ± 0.02	13.08 ± 0.22	1.17 ± 0.03	22.97	19.1	2.98			1008 (AA)
FS 04	10:42:00	+12:20:05	15.53	15.13	0.084	0.058	-15.00	0.373	21.55 ± 0.06	7.96 ± 0.42	1.01 ± 0.03	22.57	12.2	2.79	(FS)		772 (AA)
LeG 09	10:42:34	+12:09:02	17.03	16.41	0.082	0.057	-13.72	0.587	24.38 ± 0.08	18.37 ± 1.46	1.05 ± 0.09	25.29	23.8	3.07	(LV)		
LeG 10	10:43:55	+12:08:00	19.16	18.78	0.089	0.061	-11.35	0.352	23.85 ± 0.45	3.86 ± 2.31	0.71 ± 0.22	25.10	7.30	2.56	(LV)		
LeG 11	10:44:02	+15:35:21	18.18	17.78	0.104	0.072	-12.37	0.366	24.13 ± 0.08	10.22 ± 0.57	1.63 ± 0.18	24.53	8.92	2.65	(LV)		
LeG 12	10:44:07	+11:32:03	19.20	18.75	0.098	0.068	-11.40	0.421	23.60 ± 0.75	2.07 ± 2.36	0.57 ± 0.25	25.07	7.33	2.56	(LV)		
AGC 205445	10:44:35	+13:56:22	16.11	15.59	0.103	0.072	-14.56	0.487	21.71 ± 0.03	6.48 ± 0.20	0.92 ± 0.02	22.93	11.7	2.77	(AA)		633 (LV)
FS 09 (LeG 13)	10:44:57	+11:55:00	17.59	17.10	0.073	0.050	-13.03	0.466	23.13 ± 0.11	8.16 ± 0.67	1.39 ± 0.15	23.79	8.70	2.64	(FS)		871 (AA)
FS 13 (LeG 14)	10:46:14	+12:57:38	18.49	17.83	0.081	0.056	-12.31	0.638	24.25 ± 0.05	9.57 ± 0.34	1.70 ± 0.13	24.92	10.4	2.72	(FS)		
FS 14 (KK 93)	10:46:25	+14:01:25	16.99	16.48	0.098	0.068	-13.66	0.471	23.59 ± 0.05	11.06 ± 0.55	1.00 ± 0.04	24.71	17.5	2.94	(FS)		
FS 15 (LeG 16)	10:46:30	+11:45:21	18.63	18.03	0.085	0.058	-12.10	0.569	24.35 ± 0.14	10.64 ± 0.75	2.00 ± 0.49	24.59	8.16	2.61	(FS)		
FS 17 (LeG 17)	10:46:41	+12:19:37	16.44	15.84	0.080	0.055	-14.30	0.578	22.62 ± 0.03	8.74 ± 0.30	1.02 ± 0.03	23.86	16.0	2.90	(FS)		1030 (S+)
LeG 18	10:46:53	+12:44:26	18.05	17.72	0.073	0.051	-12.40	0.304	24.44 ± 0.52	4.65 ± 4.62	0.47 ± 0.16	26.31	20.8	3.02	(TT)		636 (AA)
FS 20 (LeG 19)	10:46:55	+12:47:19	18.37	17.12	0.074	0.052	-13.01	1.228	23.67 ± 0.11	7.00 ± 0.73	1.11 ± 0.11	25.43	18.3	2.96	(FS)		
FS 21 (KK94)	10:46:57	+12:59:54	17.72	16.88	0.098	0.068	-13.26	0.809	24.47 ± 0.05	17.14 ± 0.70	1.37 ± 0.09	25.14	17.9	2.95	(FS)		832 (H+)
Le G21	10:47:01	+12:57:39	18.60	18.18	0.096	0.066	-11.96	0.391	24.46 ± 0.07	10.03 ± 0.46	1.86 ± 0.23	24.90	8.81	2.64	(TT)		843 (AA)
DDO 088	10:47:22	+14:04:15	13.85	13.35	0.114	0.079	-16.16	0.465	22.07 ± 0.02	25.52 ± 0.36	1.14 ± 0.02	22.95	33.1	3.09		7.73 (LV)	573 (H+)
CGCG 066-026	10:48:54	+14:07:28	15.27	14.64	0.132	0.092	-15.52	0.580	20.35 ± 0.02	3.76 ± 0.09	0.73 ± 0.01	22.15	12.6	2.80			541 (LV)
FS 40 (LeG 22)	10:49:37	+11:21:06	17.79	17.16	0.102	0.071	-12.99	0.599	24.40 ± 0.09	13.55 ± 1.03	1.27 ± 0.14	25.20	16.2	2.91	(FS)		
LeG 23	10:50:09	+13:29:02	19.66	19.25	0.104	0.072	-10.89	0.379	24.37 ± 0.19	5.35 ± 0.76	1.44 ± 0.31	25.09	5.85	2.47	(LV)		
UGC 05944	10:50:19	+13:16:18	14.94	14.35	0.099	0.068	-15.93	0.565	21.50 ± 0.01	8.49 ± 0.11	0.79 ± 0.02	23.06	22.0	3.07		11.07 (R+)	1073 (LV)
KK 96	10:50:27	+12:21:34	16.65	16.07	0.084	0.058	-14.06	0.547	24.32 ± 0.06	19.46 ± 1.24	1.05 ± 0.09	25.37	28.8	3.16	(LV)		
LeG 26	10:51:21	+12:50:56	16.30	15.75	0.079	0.054	-14.38	0.534	22.48 ± 0.03	9.52 ± 0.25	1.05 ± 0.02	23.52	14.3	2.85	(LV)		630 (LV)
AGC 205540	10:51:31	+14:06:53	17.75	17.18	0.107	0.074	-12.97	0.540	22.06 ± 0.04	4.27 ± 0.15	1.24 ± 0.04	22.99	5.77	2.46	(AA)		832 (LV)
AGC 205544	10:52:05	+15:01:50	16.86	16.27	0.072	0.050	-13.85	0.561	21.53 ± 0.02	3.94 ± 0.11	0.85 ± 0.01	22.91	8.48	2.63	(AA)		828 (LV)
AGC 202456	10:52:19	+11:02:35	15.94	15.37	0.078	0.054	-14.76	0.547	20.95 ± 0.02	4.88 ± 0.09	0.90 ± 0.01	22.24	9.44	2.67	(AA)		824 (LV)
LeG 27	10:52:20	+14:42:26	18.15	17.27	0.073	0.050	-12.86	0.856	23.40 ± 0.05	7.29 ± 0.33	1.38 ± 0.08	24.52	11.2	2.75	(LV)		
LeG 28	10:53:01	+10:22:43	17.11	16.43	0.083	0.057	-13.70	0.646	23.03 ± 0.04	10.15 ± 0.34	1.17 ± 0.04	23.83	12.0	2.78	(LV)		
LSBCD 640-12	10:55:56	+12:20:22	17.21	16.68	0.060	0.042	-13.44	0.512	23.51 ± 0.08	11.14 ± 0.81	1.15 ± 0.09	24.37	13.7	2.84	(S+)		847 (AA)
LSBCD 640-13	10:56:14	+12:00:35	16.20	15.85	0.065	0.045	-14.27	0.332	22.79 ± 0.03	11.42 ± 0.26	1.59 ± 0.06	23.69	14.7	2.87	(S+)		989 (S+)
LSBCD 640-14	10:58:10	+11:59:53	17.79	17.16	0.055	0.038	-12.95	0.611	24.13 ± 0.06	11.72 ± 0.48	1.68 ± 0.17	24.95	14.3	2.86	(S+)		
AGC 205278	10:58:52	+14:07:47	16.66	16.32	0.060	0.042	-14.07	0.317	21.87 ± 0.03	4.62 ± 0.14	0.87 ± 0.02	23.17	9.35	2.72	(AA)		686 (AA)
LeG 33	11:00:45	+14:10:21	18.98	18.29	0.061	0.042	-11.83	0.667	23.78 ± 0.13	5.69 ± 0.65	1.19 ± 0.16	24.70	7.64	2.58	(LV)		
LSBCD 640-08	11:00:52	+13:52:53	16.19	15.64	0.053	0.037	-14.47	0.530	22.25 ± 0.04	7.25 ± 0.31	0.87 ± 0.02	23.70	16.2	2.91	(S+)		
CGCG 066-109	11:04:26	+11:45:20	15.69	15.31	0.050	0.034	-14.77	0.356	22.26 ± 0.05	11.88 ± 0.43	1.26 ± 0.04	23.00	13.7	2.83			777 (AA)

The quantities listed are as follows: (1) name of candidate; (2–3) total apparent magnitude in the g and r bands; (4–5) galactic extinction in the g and r bands (Schlafly & Finkbeiner 2011); (6) extinction corrected absolute r band magnitude, using a distance modulus of $M - m = 30.06$ mag; (7) integrated and extinction corrected $g - r$ color; (8) Sérsic central surface brightness in the r band; (9) Sérsic scale length in the r band; (10) Sérsic curvature index in the r band; (11) mean effective surface brightness in the r band; (12) effective radius in the r band; (13) logarithm of the effective radius in the r band, converted to pc with a distance modulus of $M - m = 30.06$ mag; (14–16) reference for original discovery, distance measurement, and velocity measurement: (AA) (Haynes et al. 2011), (LV) (Karachentsev & Karachentseva 2004; Karachentsev et al. 2004, 2013), (FS) (Ferguson & Sandage 1990), (S+) (Schombert et al. 1997), (R+) (Rekola et al. 2005), (S+) (Staveley-Smith et al. 1992), (TT) (Trentham & Tully 2002), and (H+) (Huchtmeier et al. 2003). We note that the surface brightness values presented are not extinction corrected.

Tab. 5: Table 4 continued.

Name			g_{tot}	r_{tot}	A_g	A_r	M_r	$(g-r)_{0,tot}$	$\mu_{0,r}$	$r_{0,r}$	n_r	$\langle\mu\rangle_{eff,r}$	$r_{eff,r}$	$\log r_{eff,r}$	Ref	D	v
			mag	mag	mag	mag	mag	mag	mag arcsec^{-2}	arcsec		mag arcsec^{-2}	arcsec	log pc		Mpc	km s^{-1}
(1)			(2)	(3)	(4)	(5)	(6)	(7)	(8)	(9)	(10)	(11)	(12)	(13)	(14)	(15)	(16)
Leo Triplet																	
AGC 202256	11:14:45	+12:38:52	17.26	16.87	0.063	0.044	-13.37	0.368	21.73 ± 0.12	4.07 ± 0.38	1.08 ± 0.06	22.71	5.86	2.49	(AA)	11.0 (LV)	630 (AA)
IC 2684	11:17:01	+13:05:57	15.38	14.79	0.091	0.063	-15.35	0.566	20.91 ± 0.04	3.75 ± 0.18	0.65 ± 0.01	23.12	18.5	2.97			588 (AA)
AGC 215354	11:19:16	+14:17:24	17.23	16.69	0.073	0.051	-13.44	0.522	21.33 ± 0.04	2.92 ± 0.13	0.85 ± 0.02	22.76	6.54	2.51	(AA)		790 (LV)
DGSAT-1*	11:21:37	+13:26:50	19.63	18.92	0.085	0.059	-11.21	0.683	24.81 ± 0.18	8.52 ± 1.23	1.36 ± 0.38	25.27	7.43	2.57	(J+)		
AGC 213436	11:22:24	+12:58:46	16.40	15.85	0.082	0.057	-14.28	0.522	20.78 ± 0.03	2.05 ± 0.08	0.63 ± 0.01	22.85	9.98	2.70	(AA)		626 (LV)
IC 2787	11:23:19	+13:37:47	15.02	14.45	0.085	0.058	-15.68	0.538	20.49 ± 0.02	3.11 ± 0.09	0.60 ± 0.01	22.73	18.0	2.95			708 (LV)
IC 2791	11:23:38	+12:53:46	16.74	16.35	0.088	0.061	-13.79	0.363	21.51 ± 0.06	3.73 ± 0.23	0.87 ± 0.03	22.97	8.40	2.62			666 (AA)
AGC 215415	11:24:34	+12:40:30	18.18	17.26	0.125	0.087	-12.91	0.881	25.63 ± 0.08	21.10 ± 0.88	3.59 ± 1.06	26.49	28.0	3.15	(AA)		1002 (AA)
KKH 68	11:30:53	+14:08:46	16.22	15.83	0.126	0.087	-13.89	0.351	22.84 ± 0.07	11.03 ± 0.64	1.07 ± 0.05	23.89	16.3	2.82	(KKH)	8.50 (LV)	880 (AA)
Field																	
UGC 05456	10:07:19	+10:21:48	13.41	13.13	0.133	0.092	-17.06	0.241	20.31 ± 0.04	10.54 ± 0.51	0.88 ± 0.04	21.31	17.2	2.94		10.52 (LV)	536 (AA)
CGCG 095-078	10:58:02	+19:30:19	15.34	14.99	0.084	0.058	-15.40	0.322	21.03 ± 0.02	6.87 ± 0.12	1.12 ± 0.01	21.95	9.80	2.74		11.70 (LV)	652 (LV)
KKH 67	11:23:03	+21:19:18	17.49	17.34	0.077	0.053	-12.70	0.130	24.75 ± 0.04	18.15 ± 0.48	1.97 ± 0.13	25.08	14.1	2.83	(KKH)		
AGC 213091	11:29:35	+10:48:34	17.68	17.19	0.119	0.083	-12.46	0.447	23.10 ± 0.03	7.71 ± 0.18	1.49 ± 0.04	23.75	8.15	2.51	(AA)	8.22 (LV)	743 (LV)
KKH 69	11:34:53	+11:01:07	16.51	16.17	0.082	0.057	-13.22	0.313	23.54 ± 0.02	16.55 ± 0.27	1.77 ± 0.05	24.02	14.8	2.72	(KKH)	7.4 (LV)	881 (LV)
LV J1149+1715	11:49:06	+17:15:20	17.44	17.43	0.127	0.088	-11.91	-0.02	23.37 ± 0.10	7.03 ± 0.65	1.13 ± 0.10	24.38	9.82	2.52	(LV)	7.11 (LV)	623 (LV)
AGC 215145	11:54:12	+12:26:04	17.95	17.83	0.101	0.070	-11.80	0.096	24.39 ± 0.05	11.36 ± 0.30	2.42 ± 0.20	24.71	9.51	2.57	(HI)	8.20 (i)	1004 (AA)

*: full name: NGC3628-DGSAT-1. The quantities listed are as follows: (1) name of candidate; (2–3) total apparent magnitude in the g and r bands; (4–5) galactic extinction in the g and r bands (Schlafly & Finkbeiner 2011); (6) extinction corrected absolute r band magnitude, using a distance modulus of $M - m = 30.06$ mag; (7) integrated and extinction corrected $g - r$ color; (8) Sérsic central surface brightness in the r band; (9) Sérsic scale length in the r band; (10) Sérsic curvature index in the r band; (11) mean effective surface brightness in the r band; (12) effective radius in the r band; (13) the logarithm of the effective radius in the r band, converted to pc with a distance modulus of $M - m = 30.06$ mag; (14–16) reference for original discovery, distance measurement, and velocity measurement: (J+) (Javanmardi et al. 2016), (AA) (Haynes et al. 2011), (LV) (Karachentsev & Karachentseva 2004; Karachentsev et al. 2004, 2013), (KKH) (Karachentsev et al. 2001), and (HI) (Wong et al. 2006). We note that the surface brightness values presented are not extinction corrected.

5.5 Distances from the tip of the red giant branch to the dwarf galaxies dw1335-29 and dw1340-30 in the Centaurus group

— Oliver Müller, Marina Rejkuba, Helmut Jerjen—

Astronomy & Astrophysics, 2018, accepted for publication

Abstract

The abundance and spatial distribution of dwarf galaxies are excellent empirical benchmarks against which to test models of structure formation on small scales. The nearby Centaurus group, with its two subgroups centered on Cen A and M 83, stands out as an important alternative to the Local Group for scrutinizing cosmological model predictions in a group of galaxies context. We have obtained deep optical images of three recently discovered M 83 satellite galaxy candidates with the FORS2 instrument mounted on the Very Large Telescope. We aim to confirm their group membership and study their stellar population. Deep VI-band photometry was used to resolve the brightest stars in our targets. Artificial star tests are performed to estimate the completeness and uncertainties of the photometry. The color-magnitude diagrams reveal the red giant branch (RGB) stars, allowing us to use the Sobel edge detection method to measure the magnitude of the RGB tip and thus derive distances and group membership for our targets. The mean metallicity of the dwarf galaxies were further determined by fitting BASTI model isochrones to the mean RGB locus. We confirm the two candidates, dw1335-29 and dw1340-30, to be dwarf satellites of the M 83 subgroup, with estimated distances of 5.03 ± 0.24 Mpc and 5.06 ± 0.24 Mpc, respectively. Their respective mean metallicities of $\langle$[Fe/H]$\rangle = -1.79 \pm 0.4$ and $\langle$[Fe/H]$\rangle = -2.27 \pm 0.4$ are consistent with the metallicity-luminosity relation for dwarf galaxies. The third candidate, dw1325-33, could not be resolved into stars due to insufficiently deep images, implying its distance must be larger than 5.3 Mpc. Using the two newly derived distances we assess the spatial distribution of the galaxies in the M 83 subgroup and discuss a potential plane-of-satellites around M 83.

1. Introduction

It is well-known that dwarf galaxies trace the "fine structure of large-scale structure" (Binggeli 1989). The imprinted information in the spatial distribution of dwarf galaxies provides an excellent test bed for structure formation models. Hence the search for optically elusive dwarf galaxies in the Galactic neighborhood is an important contribution to better understand the 3D distribution of baryonic and

non-baryonic matter. Besides using 3D spatial information for cosmology, the census of dwarf galaxies in group environments provides insight into the properties of the local universe (Tully 1988b). The need for such fundamental empirical input makes it necessary to systematically search the sky for hitherto undetected dwarf galaxies. Such an investigation is typically conducted in two steps: (1) find unresolved dwarf candidates in large-field imaging surveys (e.g. Huchtmeier et al. 2001; Chiboucas et al. 2009; Merritt et al. 2014; Müller et al. 2015; Karachentsev et al. 2015; Javanmardi et al. 2016; Müller et al. 2017a,b; Park et al. 2017; Henkel et al. 2017); and then (2) establish distances with ground or space based telescopes (e.g. Jerjen et al. 2001; Jerjen & Rejkuba 2001; Karachentsev et al. 2007; Chiboucas et al. 2013; Danieli et al. 2017; Smercina et al. 2017; Makarova et al. 2018). Alternatively, deep imaging surveys can resolve dwarf galaxies directly into individual stars, especially in the Local Group (Koposov et al. 2015; Kim et al. 2015) and nearby groups (e.g. Sand et al. 2014; Monachesi et al. 2014; Crnojević et al. 2014, 2016). The latter approach, however, can only be done for nearby dwarfs or by a trade-off in the area of the surveyed field.

The nearby Centaurus Group is made up of the Centaurus A (Cen A) subgroup at a mean distance of 3.8 Mpc and the slightly more distant M 83 subgroup at 4.9 Mpc (Karachentsev et al. 2002, 2014; Tully et al. 2015; Tully 2015b). The group has approximately 100 galaxy members, of which approximately 50 percent have accurate distance estimates, mainly based on the HST program conducted by Karachentsev et al. (2007), but also from various ground-based measurements (Jerjen et al. 2000b; Crnojević et al. 2014, 2016). The halo of the Centaurus Group extends over 3.5 Mpc, from 3 Mpc to 6.5 Mpc along our line of sight (see Fig. 11 of Müller et al. 2017a). Behind the group is a vast, empty region devoid of any matter called the Local Void (Tully & Fisher 1987). Because the Cen A subgroup is the most massive, gravitationally bound galaxy aggregate in the Local Volume (LV, Karachentsev et al. 2004, 2013) and the M 83 subgroup is less abundant and further away, it is intrinsically difficult to allocate dwarf galaxies for which we lack accurate distance measurements unambiguously to a subgroup.

In Müller et al. (2015) we reported the discovery of 16 new dwarf galaxy candidates around M 83 using wide-field imaging data collected with the Dark Energy Camera. This survey was subsequently extended to the entire Centaurus Group, leading to the detection of another 41 candidates (Müller et al. 2017a).

An intriguing feature in the dwarf galaxy distribution of the Cen A subgroup has been recently reported by Tully et al. (2015): all but one dwarf galaxy around the host galaxy Cen A (= NGC 5128) known at that time were aligned in two highly flattened planes (vertical scale height $rms \approx 60$ kpc). However, with the addition of the new dwarf galaxies only one of the two planes seems to be statistically significant (Müller et al. 2016). This plane of satellites shows some remarkable similarities to

the planes of galaxies in the Local Group (LG, Pawlowski et al. 2012b, 2013; Ibata et al. 2013) – it is perpendicular to the prominent dust lane of Cen A; it contains an aligned stellar stream from the disrupted dwarf galaxy dw3 (Crnojević et al. 2016), and the extension of the plane is aligned with M 83. However, the most striking feature is the correlation in phase-space. Using the available line of sight velocities measured for half of the confirmed Cen A satellites, Müller et al. (2018b) discovered that most satellites with measured velocities share a coherent motion within the satellite plane, making it the third case discovered of a co-orbiting satellite system in the local universe and the first outside of the LG. A quantitative comparison to cosmological simulations showed that this feature is as unlikely (<1%) as it is in the LG. Hence the Centaurus Group of galaxies is an ideal environment for carrying out cosmological tests outside of the LG.

A fundamental observational ingredient to facilitate such cosmological predictions are accurate distances to dwarf galaxies. At a mean distance of ~ 3.8 Mpc (Karachentsev et al. 2004, 2013) for the Cen A subgroup it is possible to resolve the brightest red giant stars with an 8m class telescope at a good site (e.g. Rejkuba et al. 2001, 2006; Crnojević et al. 2013). In this paper we present deep VI stellar photometry based on the observations taken with the FORS2 instrument mounted at VLT for the three of our dwarf galaxy candidates (dw1325-33, dw1335-29, and dw1340-30), and establish tip of the red giant branch (TRGB) distances for two (dw1335-29 and dw1340-30). The third dwarf candidate dw1325-33 could not be resolved into individual stars.

2. Observations and data reduction

Our targets were the three dwarf galaxy candidates dw1325-33, dw1335-29, and dw1340-30, a subsample from the 16 candidates found by our team in the M 83 subgroup (Müller et al. 2015). In the left column of Fig. 1 we show the discovery images observed with the wide-field Dark Energy Camera mounted at the prime focus of the Blanco 4-m telescope at CTIO. A total of 5.2 hours of VLT time in service mode was subsequently allocated to the follow-up observing run 097.B-0306(A) under excellent observing conditions: dark time and seeing better than 0.6 arcsec, which are necessary to resolve asymptotic giant branch (AGB) and upper red giant branch (RGB) stars at a distance of ~ 5 Mpc. Deep V and I CCD images were taken in 2016/17 with the FOcal Reducer and low dispersion Spectrograph (FORS2) mounted on the UT1 of the Very Large Telescope (VLT) of the European Southern Observatory (ESO). The FORS2 camera has a 6.8×6.8 arcsec field of view and is equipped with a mosaic of two $2k \times 4k$ MIT CCDs, which when used with standard resolution (SR) and 2×2 binning offers a scale of 0.25 arcsec per pixel. The targets were centered on Chip 1, so that Chip 2 is free from the stars of the galaxies and can

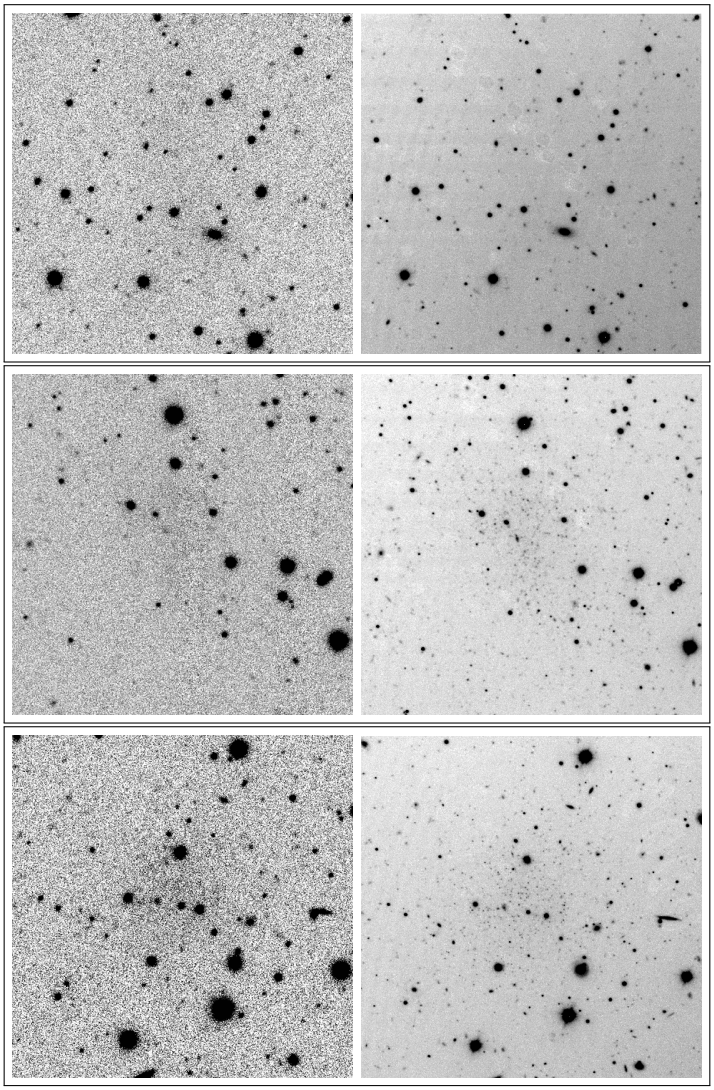

Fig. 1: Left column: r-band DECam images of dwarf galaxy candidates dw1325-33 (top), dw1335-29 (middle) and dw1340-30 (bottom) taken from Müller et al. (2015). Right column: Deep, high resolution FORS2 VLT images of the same objects resolve the brightest stars in the dwarf galaxies, except in the case of dw1325-33 (see section 5.5 for more details). All images are oriented with north up and east to the left. They have 2 arcmin on each side.

be used as reference frame for estimating the contamination of Galactic foreground stars.

In Table 1 we provide a log book of the science observations. The original request was for three V-band frames of 750 sec and 12 exposures in I-band of 231 sec for each target. A first set of V-band images for dw1335-29 was taken under seeing conditions slightly outside the requested constraint of $\lesssim 0.6$ arcsec, and thus was repeated later. In the case of dw1340-30, a single V band exposure was acquired with 0.7 arcsec seeing before the sequence was aborted. The whole sequence was repeated later. These two sets of additional V band images added additional frames and exposure time, which turned out to be useful for the stellar photometry. The combined best seeing FORS2 images produced are shown on the right hand side of Fig. 1.

Tab. 1: Observation summary for the three dwarf galaxy candidates.

α_{2000} (hh:mm:ss) (1)	δ_{2000} (dd:mm:ss) (2)	Observing Date (3)	Instrument (4)	Exposure time (s) (5)	Filter (6)	Airmass (7)	Image quality (arcsec) (8)
dw1325-33							
13:25:41	−33:00:25	8/9 Apr 2016	FORS2	3×750	V	1.01	0.6
		8/9 Apr 2016	FORS2	12×231	I	1.12	0.6
dw1335-29							
13:35:46	−29:43:50	7/8 Apr 2016	FORS2	3×750	V	1.16	0.7
		7/8 Apr 2016	FORS2	12×231	I	1.07	0.5
		8/9 Apr 2016	FORS2	3×750	V	1.02	0.5
dw1340-30							
13:40:19	−30:21:35	13/14 Apr 2016	FORS2	12×231	I	1.05	0.3 - 0.5
		29/30 Apr 2016	FORS2	1×750	V	1.01	0.7
		29/30 Jan 2017	FORS2	3×750	V	1.27	0.6

Data reduction and calibration

Data reduction was carried out within the Image Reduction and Analysis Facility (IRAF) software (Tody 1993). A median combined stack of ten bias frames was used to create a master bias. This was subtracted from all other images. Master flat fields were then created by combining five twilight flats for each filter using an average sigma clipping algorithm to reject any residual faint stars, bad pixels and cosmic rays. These calibration images where then used to process individual science frames and the photometric standard star fields.

The photometric calibration was based on standard star observations from the ESO calibration plan. The photometric standard star fields taken in the VI-bands during each of our observing nights are listed in Table 2[3]. We derived the zero points $ZP_{V,I}$ and extinction coefficients $k_{V,I}$ (Table 3) by comparing our standard star measurements to the values in the Stetson standard star catalog (Stetson 2000), and found them to be consistent with values available from the ESO Quality Control webpages, as well as with an independent cross-calibration based on our DECam images. The photometry was calibrated using the formulae:

$$\begin{aligned} V &= V_{instr} + ZP_V - k_V \cdot X_V - A_V + 2.5 \cdot \log_{10}(t) \\ I &= I_{instr} + ZP_I - k_I \cdot X_I - A_I + 2.5 \cdot \log_{10}(t) \end{aligned}$$

where the exposure time t is given for a single (reference) exposure (750 and 231 seconds for V and I, respectively), A_V and A_I are the Galactic extinction values based on the reddening map by Schlegel et al. (1998) and the correction coefficients from Schlafly & Finkbeiner (2011), and the airmass (X_V, X_I) of a chosen reference exposure is used.

[3] Standard star observations from 29/30 Jan 2017 were not used. We preferred to calibrate both V and I-band images of dw1340-30 with respect to the April 2016 observations, due to the lack of I-band observations after the M1 mirror recoating in August 2016, which would introduce an unknown color-term.

Tab. 2: Observation log for standard star fields.

Date	Field	Airmass	Filters
7/8 Apr	PG 1323	1.07	V & I
2016	IC 4499	1.87	V & I
	NGC 2437	1.02	V & I
8/9 Apr	E5	1.62	V & I
2016	E7	1.27	V & I
	E7	1.08	V & I
13/14 Apr	NGC 5139	1.10	I
2016	IC 4499	1.87	I
29/30 Apr	NGC 2818	1.03	V
2016	NGC 5139	1.78	V
	E7	1.26	V

Tab. 3: Calibration coefficients.

	dw1325-33	dw1335-29	dw1340-30
ZP_V (mag)	27.889 (0.003)	27.887 (0.003)	27.888 (0.004)
ZP_I (mag)	27.334 (0.004)	27.343 (0.004)	27.333 (0.003)
k_V	0.121 (0.003)	0.108 (0.001)	0.132 (0.003)
k_I	0.056 (0.003)	0.068 (0.002)	0.075 (0.002)
X_V	1.011	1.010	1.050
X_I	1.157	1.093	1.065
A_V (mag)	0.147	0.125	0.158
A_I (mag)	0.081	0.069	0.087

Photometry

We carried out photometric measurements for all stars on the bias subtracted and flat-fielded science images using the standalone version of DAOPHOT2 (Stetson 1987) package, which is particularly well suited for crowded fields. The steps carried out include detection of point sources, aperture photometry with a small aperture and then point-spread function (PSF) modeling. We modeled a PSF using 50 isolated bona fide stars across the field on every individual science frame. To check the quality of the PSF model we visually inspected the residual images of all chosen stars and rejected those with a strong residual. From the best V and I frames ($fwhm < 2.3$ px on average for unsaturated stars) a single deep image was produced using MONTAGE2. On this deep image the DAOPHOT2 routines FIND, PHOT and ALLSTAR were run to produce the deepest possible point source catalog. This catalog was then used as input for simultaneous PSF fitting on every science frame using ALLFRAME. The resulting catalogs for each individual image were average combined per filter with the DAOMATCH and DAOMASTER routines keeping only those measurements that had been detected on two thirds of all input

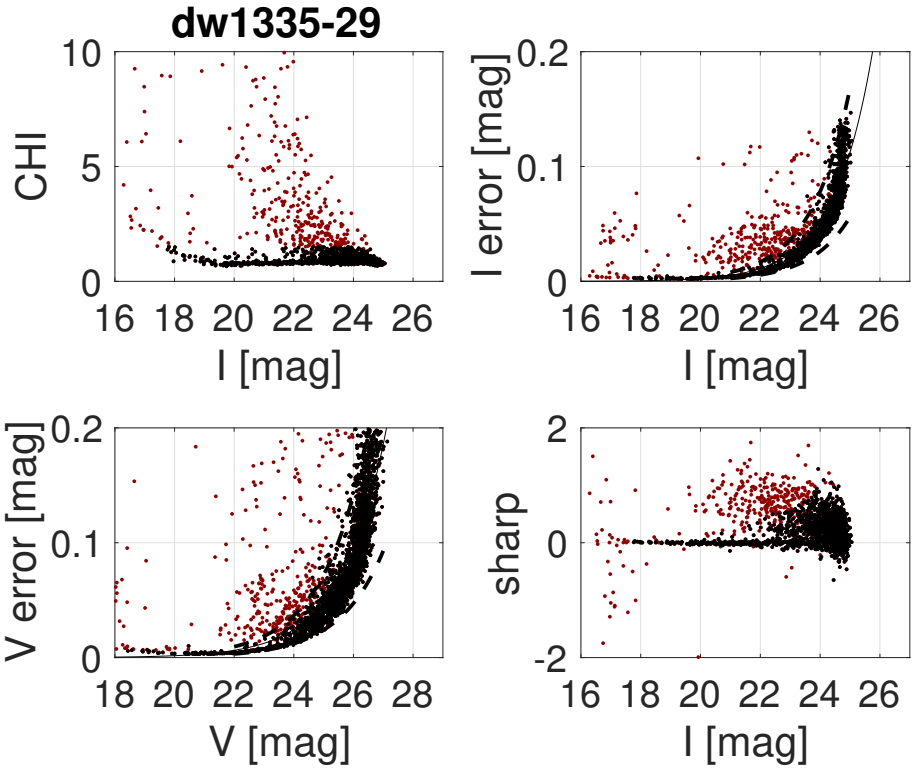

Fig. 2: Selection of bona fide stars from the master catalog of dw1335-29 (see text). The black dots correspond to stars that fulfill all point source constraints and remain in the catalog, while the red dots show rejected objects.

images for the given filter. Finally, stars detected within 1 pix tolerance from both V and I lists were combined to make the master catalog[4].

To further purge the master catalog from non-stellar or blended sources, only stars with good shape parameters were included. The constraints were that the value for χ had to be smaller than 1.5, $sharp$ had to be between -2 and 2, and the magnitude errors were only allowed to deviate 50% from the best fitting value at a given magnitude. We explain this latter constraint more precisely in the following. We fitted an exponential function through the magnitude errors (as function of the measured magnitude) and defined the intervals from 0.5 to 1.5 times the fitted value as the locus within which we keep the detected objects as bona-fide stars. In total a star has to fulfill all these constraints to remain in the master catalog. See Fig. 2 for an illustration of the different constraints in the case of dw1335-29. The plume of objects with high χ values (red symbols in the upper left panel of Fig. 2) and positive $sharp$ values are likely background galaxies and thus are removed from the catalog.

[4]These photometric catalogs are available in electronic form at the CDS via anonymous ftp to cdsarc.u-strasbg.fr (130.79.128.5) or via http://cdsweb.u-strasbg.fr/cgi-bin/qcat?J/A+A/.

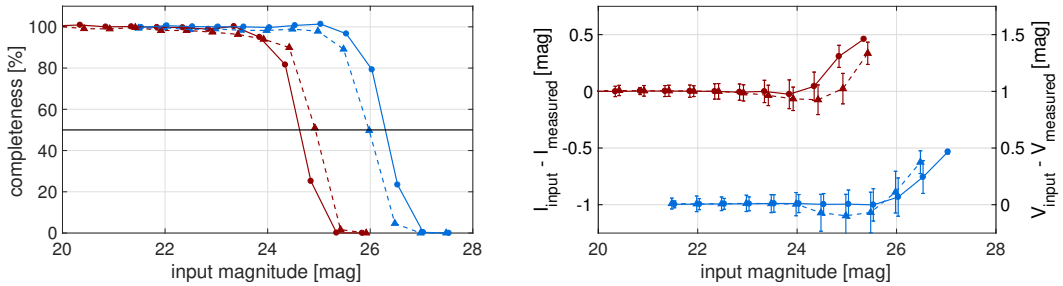

Fig. 3: Results of our artificial star tests for I (red) and V (blue) bands (circles and straight line for dw1335-29, triangles and dashed line for dw1340-30). Left: The recovery rate of the artificial stars induced into the science frames as a function of the input magnitude. The 50% level is highlighted with the black horizontal line. Right: The difference between the input magnitude and measured magnitude as a function of input magnitude.

Completeness and error analysis

We performed artificial star tests to assess the detection completeness and characterize the measurement errors for our PSF photometry. For that purpose, we generated 900 artificial stars, all with the same magnitude for each 0.5 magnitude bin between 20–28 mag. These stars were then uniformly spread over the field and added to every individual science frame, distributing them on a hexagonal grid with a random starting position. The angular separation between stars corresponds to twice the PSF fitting radius, such that the artificial stars do not increase the natural crowding. The dithering offsets between frames were carefully taken into account to ensure that each artificial star is added in every science frame at the exact same sky position. The same PSF photometry pipeline as used before was then applied on every image with artificial stars added for each magnitude iteration of the interval, with the only exception that the PSF model constructed in the scientific photometry is used as there is no need to re-derive it. The recovery rate for the artificially created stars, together with the difference between input and output magnitudes are presented for dw1335-29 and dw1340-30 in Fig. 3. The topmost plot presents the completeness curves of our star detection algorithm, the bottom plot gives the error of our PSF photometry as a function of input magnitude.

For the dw1335-29 data the completeness drops below 50% at 24.6 mag in I and at 26.3 mag in V. The measured PSF-based photometry error starts to grow at 24.0 mag for I, and 25.5 mag for V. For dw1340-30 the completeness drops below 50% at 24.9 mag in I and 25.9 mag in V, the error starts at 24.3 mag in I and 24.9 mag in V, respectively. We note that for dw1340-30 the error drops before the final rise, meaning that we underestimate the measured magnitude. However, within the uncertainty the mean value still agrees with unity. At these magnitude steps we find a systematic dependence of the photometry along the y-axis of the chip which is not apparent within other magnitude steps. We further note that we reach a deeper I band limit for dw1340-30, which is due to better seeing conditions.

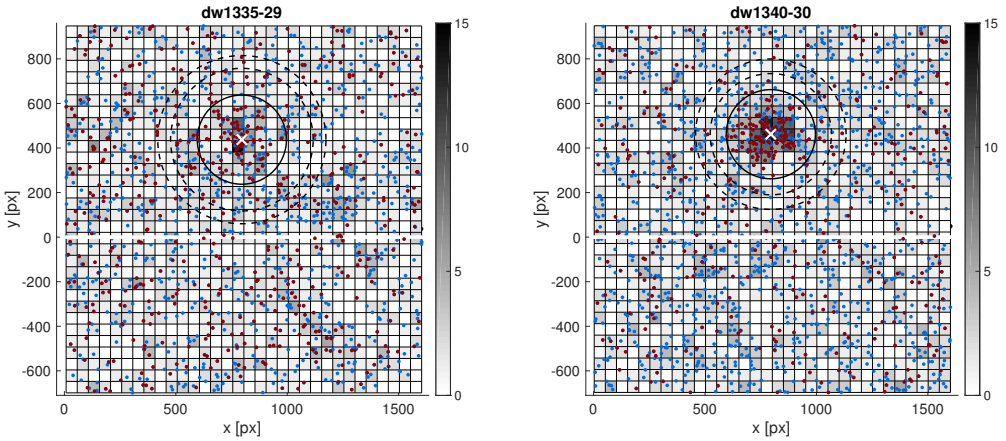

Fig. 4: Distribution of stars (red and blue dots) with I-band magnitudes in the range 24 to 25.5, underlaid by a 2D histogram that represents the local star density (stars per 156 arcsec^2). The cross marks the nominal center of the galaxy and the circle has a radius of 50 arcsec (=200 px). The left panels of Fig. 6 shows the CMD of all stars detected within that radius. The two outer circles (dashed lines) define an annulus with the same area as the inner circle. This area is used for statistical decontamination of the CMDs, and the annulus has the inner radius at the location corresponding to four times the effective radius (Müller et al. 2015) of the corresponding galaxy. Stars in the annulus were used to construct the CMD of Galactic foreground stars in the direction of the dwarf galaxy.

The case of dw1325-33

The third dwarf galaxy candidate, dw1325-33, could not be resolved into individual stars with our data. The reason is not as simple as the candidate not being a nearby dwarf galaxy, although this is also a possible explanation. The presence of a higher underlying sky background (in excess of 16,700 ADU compared to $\sim 13,000$ ADU in the other two galaxies) prevented detection of faint stars in the images. There is also a strong radial gradient in the background light. We modeled this with IRAF's imsurfit command and stacked the resulting images. There is indeed a low-surface brightness feature at the position of the candidate, but the quality of the image is too low to perform reliable photometric measurements. With our current observations we can neither rule out nor confirm the possibility that this candidate is a member of the Centaurus group. We applied our artificial stars analysis to estimate the detection limit within the field of dw1325-33, see Fig. 5 for the results. We are not able to detect stars (10% detection rate) fainter than 24.8 mag, corresponding to a distance of 6.0 Mpc for the TRGB. Considering the steeply dropping completeness below the 50% limit of I=24.4 mag, we conservatively set a lower limit for the dw1325-33 distance to 5.3 Mpc.

3. Results

In the following subsections we redetect the dwarf galaxies as stellar over-densities in the deep CCD images, present their color-magnitude diagrams, and measure the TRGB distance from the I-band luminosity function.

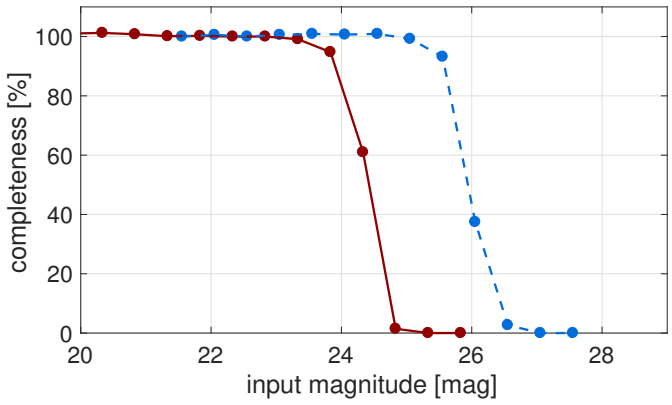

Fig. 5: Results of our artificial star tests for I (red line) and V (blue dashed line) bands for dw1325-33.

Stellar overdensity

When star clusters and nearby dwarf galaxies are resolved into individual stars they can be detected as stellar overdensities superimposed on the Milky Way's foreground star population (e.g. Belokurov et al. 2007; Kim & Jerjen 2015; Kim et al. 2016). Similarly, but given the much smaller spatial extent and thus significantly lower amount of foreground+background contamination, we blindly detected the dwarf galaxy candidates dw1335-29 and dw1340-30 in our CCD images as pronounced stellar overdensities.

In Fig. 4 we show the distribution of all stars within $24 < I < 25.5$ mag. In this magnitude range we expect the TRGB stars at the distance of the M 83 subgroup (see below). The star density is shown in gray scale and sampled on a grid using 50×50 px bins. There are clear overdensities of stars at the positions of the dwarf candidates, as expected if the stars are associated to the galaxies and resolved into individual stars. We note that we find the same overdensity when removing the magnitude constraint for the stars. The estimated radius of the galaxy, where the overdensity is not distinguishable from the foreground population is indicated as solid circle (radius of 50 arcsec corresponding to 200 px), in comparison to the estimated half light radii of 20 arcsec and 17 arcsec for dw1335-29 and dw1340-30, respectively (Müller et al. 2015).

To determine the center of the stellar overdensity we used a k-means algorithm, which samples a set of data into k clusters and minimizes the sum of the distances of each data point to the center of the cluster. Using $k = 1$ we can exploit this algorithms capability to find the center of the galaxy. The centers are at (α_{2000}=13:35:46, δ_{2000}=−29:42:28) for dw1335-29 and (α_{2000}=13:40:19, δ_{2000}=−30:21:31) for dw1340-30, respectively, which agree with the centers estimated in Müller et al. (2015) based on galaxy surface photometry.

Color-magnitude diagrams

Having performed the stellar photometry on Chips 1 and 2 in Section 5.5 and redetected the galaxies as stellar over-densities in Section 5.5 it is possible to establish the color-magnitude diagram (CMD) for each dwarf galaxy. For that purpose, we considered all stars within a circle of radius 50 arcsec (indicated as circle in Fig. 4), corresponding to the approximate extent of the galaxy ($2.5r_h$). Another CMD was created for the reference field area, which has been selected to have the same size by placing an annulus around the galaxy (indicated as dashed ring in Fig. 4), where the stellar population of the dwarf galaxies should not affect the CMD. Both CMDs are presented in Fig 6. Comparing the field CMD to the galaxy CMD it becomes clear that a significant number of foreground stars contaminates the CMD of the galaxy.

To clean the CMD of the galaxy from foreground stars we statistically subtracted stars using the field CMD. For every star in the field CMD the star with the closest matching magnitude and color from the galaxy CMD was removed, but only if it the magnitude difference was smaller than the photometric error at given magnitude (a superposition of the systematic error and its corresponding standard deviation, see Fig. 3). As the field stars are evenly distributed and we use the same area for both CMDs this should statistically clean the galaxy from foreground stars. In the right-hand panel of Fig. 6 we present the remaining stars after the subtraction. In the case of dw1335-29 90 stars remain in the CMD and 42 stars are removed, for dw1340-30 167 stars remain and 51 stars are removed. The high number of subtracted stars is not surprising as the targets are relatively close to the Milky Way plane ($b = 32.2$, and $b = 31.3$). Additionally the projected distance to M 83 is only $\sim$20 kpc, and $\sim$85 kpc for dw1335-29 and dw1340-30, respectively, meaning that there is some contribution of M 83 stars expected in the CMDs. This presence of M 83 extended halo stars that may vary across the field is an additional reason to select the "field" area not too far from the dwarf.

TRGB distance

The tip of the red giant branch (TRGB) method has become the method of choice with which to measure distances in the Local Volume since the method was established in the early 1990s (Da Costa & Armandroff 1990; Lee et al. 1993). There is a sharp cut-off in the luminosity function at the bright end of the first ascent giant branch. This is a well-understood phenomenon: on their evolutionary path the red giants leave the RGB after the helium flash occurs. This physical process can be exploited as a standard candle. The turn-off of the RGB happens at the absolute magnitude of $M_I \sim -4$. The TRGB method is on par with RR Lyrae and Cepheid distance estimates with a typical uncertainty of five percent (Lee et al. 1993; Mould & Sakai 2009; Beaton et al. 2016).

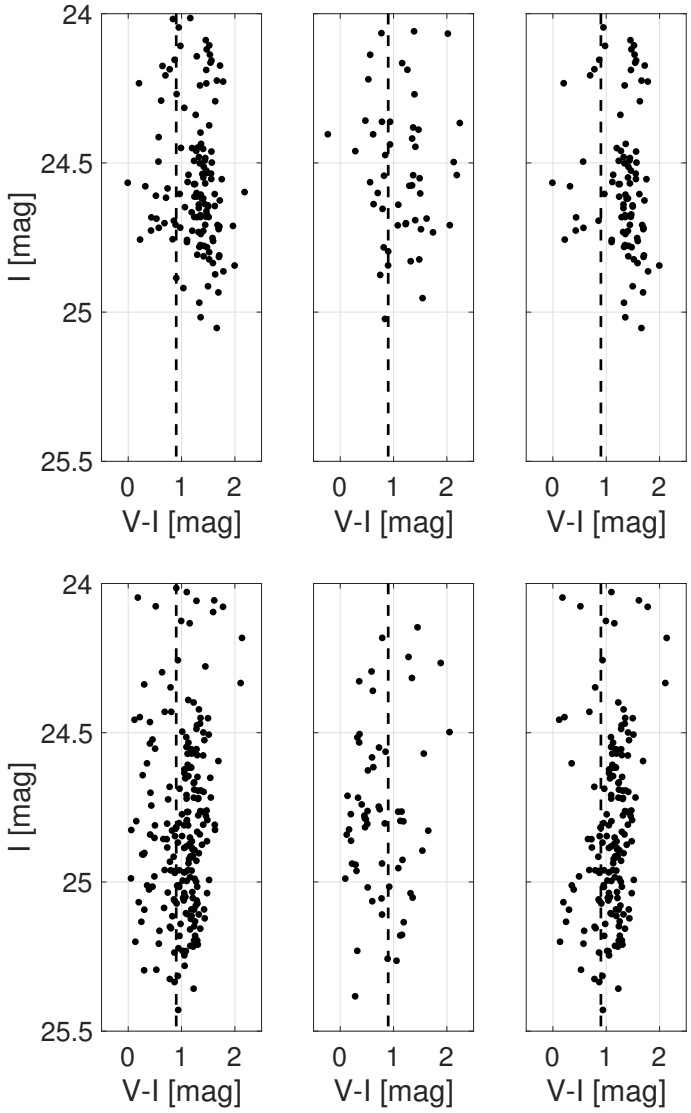

Fig. 6: Extinction-corrected color-magnitude diagrams of dw1335-29 (top) and dw1340-30 (bottom). Indicated with dashed lines is the $V - I < 0.9$ mag boundary. Left: CMD for stars inside a radial aperture of 50 arcsec. Middle: Stars within the reference aperture used for the background subtraction. Right: Stars remaining after statistical cleaning of the CMD.

In practice the tip magnitude of the RGB can be estimated by constructing the I-band luminosity function for all stars in the galaxy ($0.9 < V - I < 2.0$) and convolving it with a Sobel edge kernel $[-2, 0, 2]$ (Lee et al. 1993). The maximum of the convolution indicates the position of the TRGB, while the width of the peak is an estimate of the uncertainty. The LF was constructed using a bin width of 0.05 mag, see Fig. 7. The statistically subtracted CMD was used to construct the LF. The maximum of the edge detection is measured for both galaxies, dw1335-29 and dw1340-30 at $I = 24.425$ mag. We use the middle of the bin to estimate the edge.

To calibrate the derived TRGB magnitudes we used the equations provided by Bellazzini et al. (2004) and Rizzi et al. (2007b):

$$\begin{aligned} M_I^{TRGB} &= -4.05 + 0.217[(V-I)_0 - 1.6] \\ (V-I)_0 &= 0.581[\mathrm{Fe/H}]^2 + 2.472[\mathrm{Fe/H}] + 4.013 \end{aligned}$$

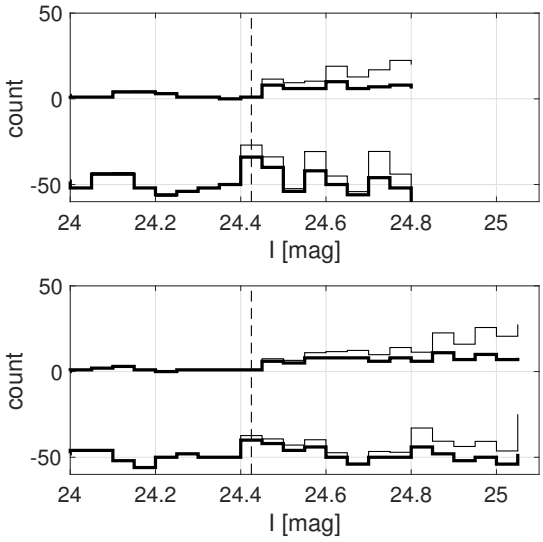

Fig. 7: I-band stellar luminosity function for dw1335-29 (top) and dw1340-30 (bottom). Each panel shows the observed (bold line) and completeness-corrected (thin line) luminosity functions to the point where the completeness drops bellow 30%. The corresponding signals from the Sobel edge detection are shown below the respective luminosity function. The maximum (dashed line) indicates the location of the TRGB.

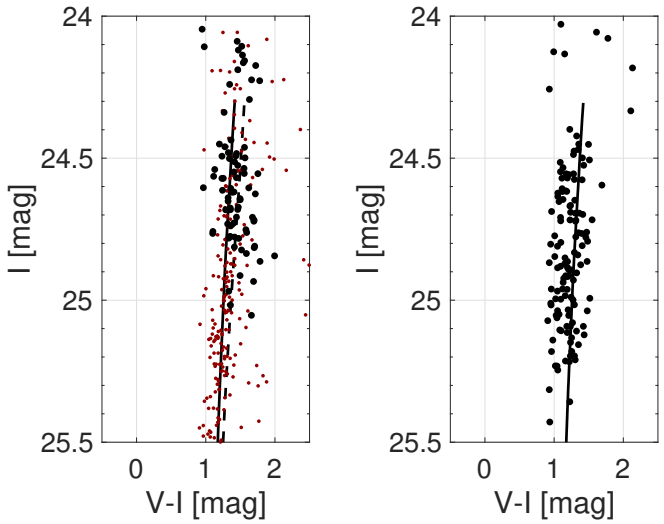

Fig. 8: Cleaned, extinction-corrected color-magnitude diagram with the best-fitting isochrone (line) for dw1335-29 (left) ad dw1340-30 (right). For dw1335-29 we overplot the HST photometry (red) kindly provided by Andreia Carrillo. The dashed line corresponds to the best-fitting isochrone [Fe/H]=-1.266 by Carrillo et al. (2017).

To estimate the mean metallicities [Fe/H] for the dwarfs we fitted theoretical BaSTI isochrones (Pietrinferni et al. 2004) to mean RGB color (Fig. 8). For dw1335-29 a metallicity of $[\mathrm{Fe/H}] = -1.79$ dex is estimated, corresponding to a calibrated absolute TRGB magnitude of $M_I = -4.08 \pm 0.02$ mag, which gives a final distance of 5.03 ± 0.24 Mpc. For dw1340-30 the metallicity is $[\mathrm{Fe/H}] = -2.27$ dex, the calibrated absolute TRGB magnitude of $M_I = -4.09 \pm 0.02$ mag and a final distance estimate of 5.06 ± 0.24 Mpc. These distances put them within the virial radius of M 83 (Müller et al. 2015), making them satellite galaxies of M 83. Information on the dwarfs are shown in Table 4. The estimated metallicities lie well within the metallicity - luminosity relation for dwarf galaxies (McConnachie 2012).

TRGB error estimation

The error budget for the TRGB magnitude comes from different sources, namely the uncertainties in the zero points, the PSF photometry, the TRGB calibration, and

Tab. 4: Properties of the two confirmed dwarf galaxies.

	dw1335-29	dw1340-30
RA (J2000)	13:35:46	13:40:19
DEC (J2000)	−29:42:28	−30:21:31
I_{TRGB} (mag)	24.43±0.10	24.43±0.10
M_I^{TRGB} (mag)	-4.08 ± 0.02	-4.09 ± 0.02
$(m-M)_0$ (mag)	28.51±0.13	28.52±0.03
Distance (Mpc)	5.03±0.24	5.06±0.24
A_V, A_I (mag)	0.125, 0.069	0.158, 0.087
[Fe/H] (dex)	-1.79 ± 0.4	-2.27 ± 0.4
M_V (mag)	-10.25 ± 0.3	-10.79 ± 0.3
L_V (10^6 $M_\odot$)	1.08 ± 0.3	1.77 ± 0.3
$r_{eff,r}$ (pc)	493 ± 32	414 ± 32

the Sobel edge detection. The error in the zero point estimation derives from the standard frames uncertainties (Section. 5.5) and is $I_{ZP,error} = 0.02$ mag. The error in the PSF photometry can be estimated with the results from the artificial star test (Section. 5.5) and is at the position of the TRGB $I_{psf,error} = 0.08$ mag. The uncertainty in the TRGB calibration provided by Rizzi et al. (2007b) together with the contribution of the uncertainty in the metallicity is $I_{calib,error} = 0.02$ mag. The uncertainty of the Sobel edge detection is given by the bin width and is $I_{Sobel,error} = 0.05$ mag. Additionally, Jang et al. (2018) argue that "due to the inability to distinguish the location of the peak within the set binning strategy" 50% of the bin width should be added to the error budget, corresponding to 0.025 mag in our analysis. Overall we obtain a total uncertainty of $I_{err} = 0.10$ mag at the distance of the dwarf galaxies, corresponding to a distance uncertainty of 0.24 Mpc.

4. Discussion

In this section we compare our photometry and results with previous work, and we discuss the spatial distribution of the new M 83 satellites.

Comparison to HST distance of dw1335-29

Carrillo et al. (2017) independently discovered the dwarf galaxy dw1335-29 at the edge of an HST image taken as part of the GHOSTS survey (Radburn-Smith et al. 2011). As the galaxy was only partially covered by the CCD chip they conducted follow-up observations using the VLT/VIMOS instrument to measure its total brightness and structural parameters. They also reported a TRGB distance based on HST photometry of $5.01^{+0.74}_{-0.22}$ Mpc, which is in excellent agreement with our value of 5.03 ± 0.24 Mpc. This agreement demonstrates that high quality images from the VLT can successfully be used to measure TRGB distances out to $\sim 5-6$ Mpc. In Fig. 8 we overlay the HST photometry (kindly provided by Andreia Carrillo) on our VLT

photometry. We note that our estimate of the metallicity is slightly different to that of Carrillo et al. (2017) ([Fe/H]=-1.8 dex opposed to [Fe/H]=-1.3 dex), although they are consistent within the measurement errors. We converted the HST $F606W$ and $F814W$ photometry to VI using a formula provided by Rejkuba et al. (paper in preparation). Using the the metallicity of [Fe/H]=-1.3 dex provided by Carrillo et al. (2017) we estimate a TRGB distance of 4.87$\pm$0.24 Mpc, still well within the error estimate.

Tidal features?

The dwarfs are close to M 83 and are potentially tidally disturbed. In Fig 4 we plotted the star map between I=24.0 mag and I=25.5 mag. Additionally, we color code the stars corresponding to a mask around the best fitting isochrone of the respective dwarf galaxy in red, i.e. the expected RGB stars. In the field around the galaxies we find no significant stellar overdensity. However, within the galaxy dw1340-30 there is a small lopsidedness of RGB stars in the southeast direction. Re-estimating the center with only the RGB stars gives a deviation from the previous established center of 3.2 arcsec. Interestingly, this lopsidedness is aligned with the connection line between M 83 (to the North-West) and dw1340-30.

Spatial distribution

Both dw1335-29 and dw1340-30 lie inside the virial radius of M 83 (210 kpc; Müller et al. 2015) with a 3D separation of 130 kpc and 180 kpc to M 83, respectively, making them satellites of the M 83 subgroup and members of the Centaurus group.

Carrillo et al. (2017) find in dw1335-29 a relatively small but significant number of blue stars that are statistically consistent with being young upper main sequence members of the dwarf resulting from a constant star formation history. Hence dw1335-29 is either a dwarf irregular or transition type dwarf. Carrillo et al. (2017) note that the presence of young stars is puzzling given the close proximity with only $\sim$26 kpc projected distance to M 83, and provided two possible explanations: either the real separation is larger than the projected or M 83 is extremely inefficient in quenching star formation. The former idea is supported by the lack of tidal features within the dwarf galaxy, and consistent with our estimate of the 3D separation of 130 kpc. We further note that if there is ongoing star formation there must be gas. However, none of the candidates were detected in HI (with an upper limit of $M_{HI} < 8.5 \times 10^6\, M_\odot$, Müller et al. 2017a).

In Fig. 9 we present the 3D distribution of the M 83 subgroup in supergalactic coordinates. Noteworthy is the physical separation between dw1335-29 and KK208 of only 28 kpc. This is indeed remarkably close. KK208 is a peculiar object, as it lacks a well defined center and is stretched over 10 arcmin (corresponding to 15 kpc at a distance of 5 Mpc). It was resolved into individual stars with HST (Karachentsev

et al. 2002). The authors suggest that this object is tidally disrupted by M 83 similar as the Sagittarius galaxy by the Milky Way (Ibata et al. 1994). In Fig. 10 we show a DECam image that includes dw1335-29, KK208, and M 83. We note that Carrillo et al. (2017) refer to KK208 as a tidal stream. We follow the same conclusion that there is no visible connection between the two objects.

As there is strong evidence that the Cen A subgroup hosts a plane of satellites (Tully et al. 2015; Müller et al. 2016) one may wonder if such an arrangement is found also in the M 83 subgroup. However, there are two major caveats that make it rather difficult to answer this question – the virial radius of M 83 is only 210 kpc compared to ≈ 300 kpc of Cen A, meaning that a plane-of-satellites around M 83 would be smaller compared to Cen A's plane (rms major axis length of 309 kpc Müller et al. 2016), and M 83 is 1.2 Mpc farther away, systematically increasing the error in the distance measurements (around 40 percent in absolute distance uncertainties). At the distance of M 83, a typical distance uncertainty of $\pm$0.3 Mpc already covers the full virial radius. In Fig. 9 we projected the dwarf satellites onto the galactic plane. Using a singular value decomposition as described in Müller et al. (2016) we fit a plane through the M 83 subgroup and estimate an rms thickness of 20.4 kpc, considering all six galaxies (KK 208, M 83, NGC 5264, KK 218, dw 1340-30, and dw 1335-29) within 210 kpc (= the virial radius of M 83 Müller et al. 2015) and $rms = 55$ kpc for galaxies within 600 kpc (while removing HIDEEP J1337-33 from the analysis as this dwarf is $\approx$300 kpc away from the estimated plane). In comparison, the Milky Way plane has a rms thickness of 19.9 kpc , the Andromeda plane a rms thickness of 13.6 kpc (Pawlowski et al. 2013), the Cen A plane a rms thickness of 69 kpc (Müller et al. 2016), and the plane around M 101 a rms thickness of 46.0 kpc (Müller et al. 2017b).

5. Summary and conclusions

We have resolved the two dwarf galaxy candidates dw1335-29 and dw1340-30 (Müller et al. 2015) into individual stars, using the FORS2 instrument mounted at the VLT. With these deep images we derived their distances and mean metallicities and confirmed them to be members of the M 83 subgroup in the Centaurus group. The third dwarf candidate dw1325-33 could not be resolved into individual stars, due to increased sky brightness preventing sufficiently deep photometry. When comparing to similar group studies, such as the M 81 group (Chiboucas et al. 2009; Crnojević et al. 2014) or the M 101 group (Merritt et al. 2014; Danieli et al. 2017), a confirmation rate of $\sim$67% is expected and achieved.

Future follow-up observations for the numerous remaining dwarf galaxy candidates are necessary to create a complete picture of the Centaurus group. As most of the remaining dwarf galaxy candidates will be associated to the closer Cen A subgroup, resolving their individual RGB stars will be easier to achieve assuming a similar

observation strategy we used with the VLT. At the Centaurus A distance the RGB tip magnitude is approximately 0.4 mag brighter at $M_{I,TRGB} = 24.05 \pm 0.05$ (Rejkuba et al. 2005). The other members of this subgroup are expected at a similar distance, implying that their RGB tip is well within our detection and completeness limits.

Why is it important to aim for a well sampled census of the Centaurus group dwarfs? Apart from studying the star formation history and the metallicity distribution of the group (Rejkuba et al. 2006; Crnojević et al. 2010, 2011b,a, 2012), which is in itself an interesting topic, the Centaurus group provides an excellent testbed to study cosmological model predictions, for example the phase-space correlation of the Cen A satellite galaxies (Müller et al. 2018b). Such results rest fundamentally on the number of accurate distance measurements and can be affected by small number statistics. However, if the corotating planar structure is true, the addition of new data will increase its significance and further support this finding. It is therefore crucial to continue measuring distances for as many candidates as possible.

Acknowledgements

OM is grateful to the Swiss National Science Foundation for financial support. HJ acknowledges the support of the Australian Research Council through Discovery project DP150100862. We thank Andreia Carrillo for providing the HST photometry for dw1335-29 and the referee for helpful comments, which improved the clarity of the paper.

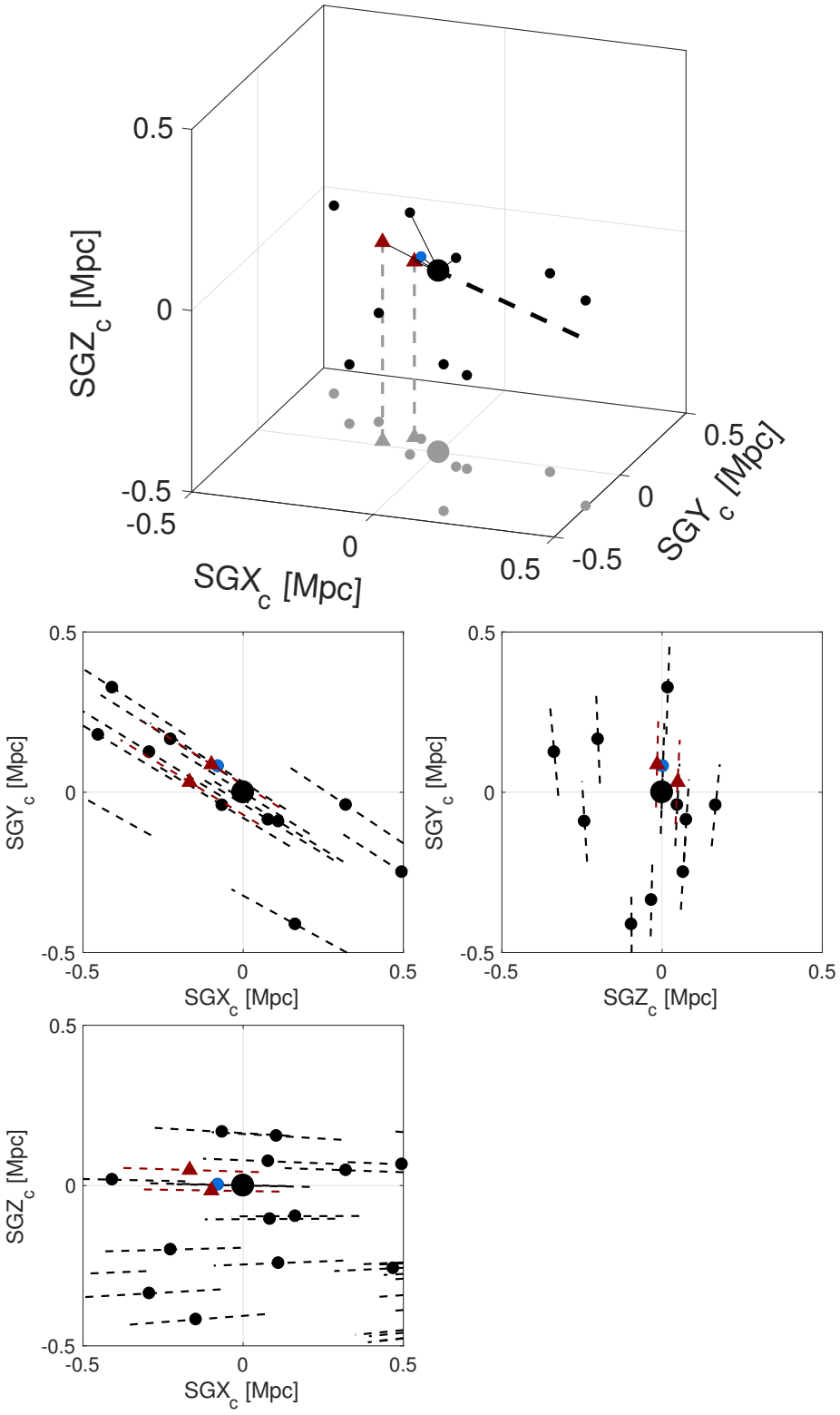

Fig. 9: Distribution of the M 83 subgroup in supergalactic coordinates, centered at M 83. Data taken from to the LV catalog. The big black dot is M 83, the small dots are dwarf galaxies. Top: satellites within the virial radius (210 kpc) are connected to M 83 with a thin black line. The dwarfs are projected onto the galactic plane (SGX-SGY plane). The position of the two confirmed dwarf galaxies (red triangles) are indicated with the gray dashed line. The position of KK208 is color-coded in blue. The black dashed line corresponds to our line-of-sight to M 83. Bottom: the projections onto the SGX-SGY, SGZ-SGY, and SGX-SGZ planes, respectively, together with their 5% distance uncertainty (dashed lines).

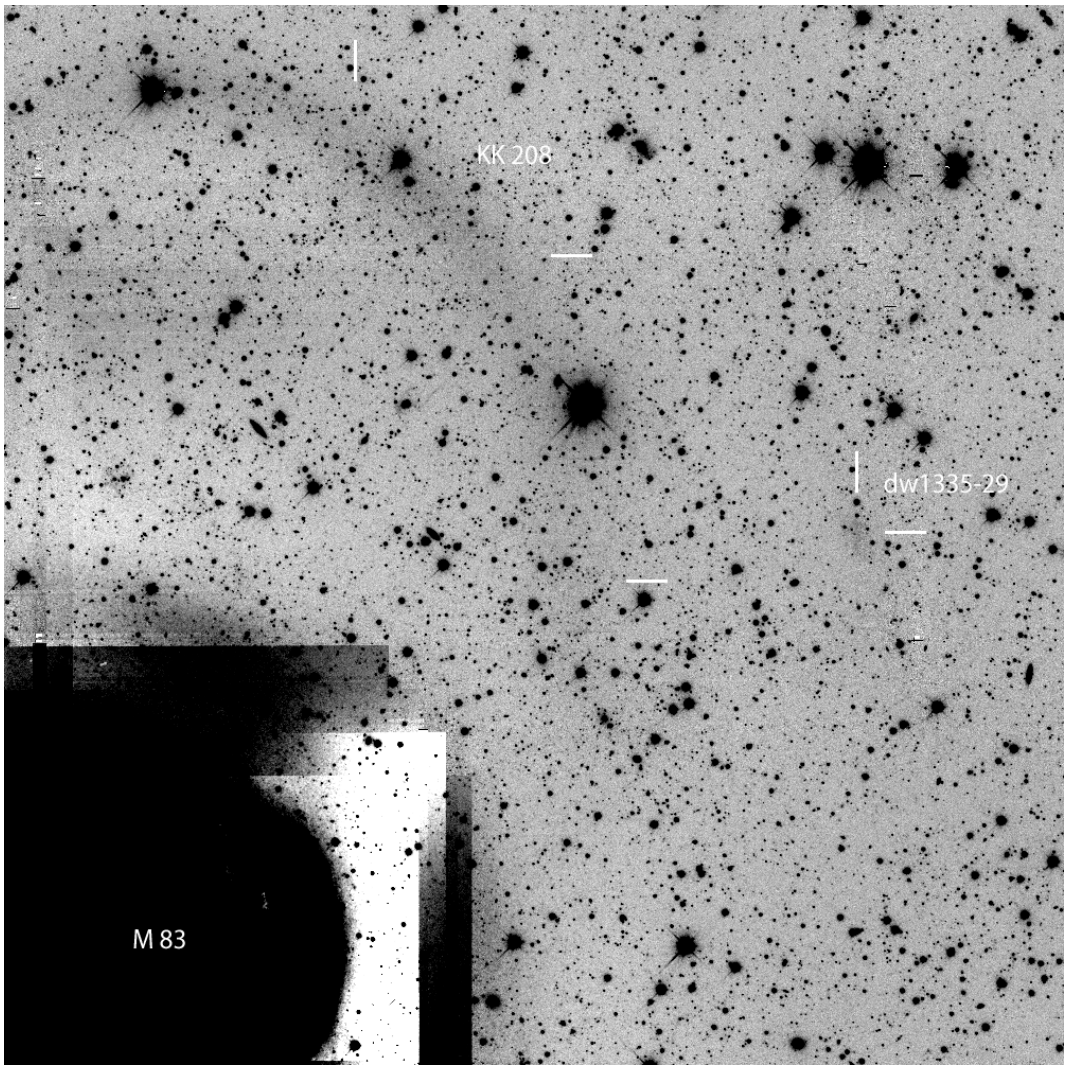

Fig. 10: DECam field in r around M 83 (Müller et al. 2015), containing the tidally disrupted dwarf KK208 and dw1335-29. In the bottom left corner is M 83.

5.6 Testing the two planes of satellites in the Centaurus group

— Oliver Müller, Helmut Jerjen, Marcel S. Pawlowski, Bruno Binggeli —

Astronomy & Astrophysics, 2016, 595, A119

Abstract

The existence of satellite galaxy planes poses a major challenge for the standard picture of structure formation with non-baryonic dark matter. Recently Tully et al. (2015) reported the discovery of two almost parallel planes in the nearby Cen A group using mostly high-mass galaxies (M_B < -10 mag) in their analysis. Our team detected a large number of new group member candidates in the Cen A group. This dwarf galaxy sample, combined with other recent results from the literature, enables us to test the galaxy distribution in the direction of the Cen A group and to determine the statistical significance of the geometric alignment. Taking advantage of the fact that the two galaxy planes lie almost edge-on along the line of sight, the newly found group members can be assigned relative to the two planes. We used various statistical methods to test whether the distribution of galaxies follows a single normal distribution or shows evidence of bimodality as has been reported earlier. We confirm that the data used for the Tully et al. (2015) study support the picture of a bimodal structure. When the new galaxy samples are included, however, the gap between the two galaxy planes is closing and the significance level of the bimodality is reduced. Instead, the plane that contains Cen A becomes more prominent. We found evidence that the galaxy system around Cen A is made up of only one plane of satellites. This plane is almost orthogonal to the dust plane of Cen A. Accurate distances to the new dwarf galaxies will be required to measure the precise 3D distribution of the galaxies around Cen A.

1. Introduction

The mere abundance and spatial distribution of faint dwarf galaxies provide a powerful testbed for dark matter and structure formation models on Mpc and galaxy scales. The standard picture of structure formation with dark matter is heavily challenged by the highly asymmetric features found in the distributions of dwarf galaxies in the Local Group, which was first noted by Kroupa et al. (2005). There is the vast polar structure (VPOS; Pawlowski et al. 2012b, 2015b; Pawlowski 2016), a thin (rms height $\approx$ 30 kpc) highly inclined, co-rotating substructure of faint satellite galaxies, young globular clusters, and stellar streams, spreading in Galactocentric distance between 10 and 250 kpc. A similar feature was found in the Andromeda galaxy surroundings, the so-called Great Plane of Andromeda (GPoA; Koch & Grebel

2006; Metz et al. 2007; Ibata et al. 2013). On a slightly larger scale, two dwarf galaxy planes containing all but one of the 15 non-satellite galaxies have been identified in the Local Group (Pawlowski et al. 2013). Such extreme satellite planes are found in only $< 0.1\%$ of simulated systems in cosmological simulations (e.g., Ibata et al. 2014b; Pawlowski et al. 2014), making them difficult to accommodate in a standard ΛCDM scenario. An alternative analysis of cosmological simulations, based on including the look elsewhere effect but ignoring observational uncertainties and the non-satellite planes (Cautun et al. 2015a), finds that only about 1 per cent of Local Group-equivalent environments should host similarly extreme satellite structures.

The fundamental question arises whether the relative sparseness and asymmetric distribution of low-mass dwarf galaxies encountered in the Local Group is a statistical outlier or a common phenomenon in the local universe. Ibata et al. (2014a) have approached this question with a statistical study of velocity anticorrelations among pairs of satellite galaxies on opposite sides of their host, using data from the SDSS survey. They found a strong excess in anticorrelated velocities, which is consistent with co-orbiting planes, but their conclusions were based on a small sample of only 22 systems, and have been challenged since (Phillips et al. 2015; Cautun et al. 2015b, but see Ibata et al. 2015). A different approach to address the question of satellite planes is to extend searches for such structures to satellite populations in other galaxy groups in the nearby universe. For example, Chiboucas et al. (2013) have found that dwarf spheroidal galaxies in the M81 group lie in a flattened distribution.

Most recently, Tully et al. (2015), hereafter T15, reported evidence for a double-planar structure around Centaurus A (Cen A, NGC5128) in the nearby Centaurus group of galaxies, with properties reminicent of the two Local Group dwarf galaxy planes (Pawlowski et al. 2013). Furthermore, Libeskind et al. (2015) found that the Local Group and the Cen A group reside in a filament stretched by the Virgo Cluster and compressed by the Local Void and smaller voids. Four out of five planes of satellites (including the two galaxy planes around Cen A) align with this filament with the normal vectors pointing in the direction of the Local Void and the planes almost parallel to the minor axis of the filament. These results demonstrate that systematic studies of the spatial distribution of low luminosity galaxies in nearby groups can provide important observational constraints for further testing of structure formation models outside of the Local Group.

The aim of the present study is to test how recently discovered dwarf galaxies in the Centaurus group (Sand et al. 2014; Crnojević et al. 2014, 2016; Müller et al. 2015, 2017a) are distributed in the double planar structure reported by Tully and collaborators. Comparing the footprint of the two planes, 20 of these dwarf candidates are located in that region of the sky. It is important to note that this analysis is feasible without distance information because of special geometry: the

normal vectors of the two planes are almost parallel and perpendicular to the line of sight. Consequently, any distance uncertainties for the new galaxies does not move them in or out of the two planes.

In section 2 we present the four different galaxy samples used in our analysis. In section 3 we show the transformation between the equatorial coordinate system to the Cen A reference frame and fit the two planes of satellites. Section 4 follows a discussion of the geometrical alignment of the planes and the distribution of galaxies. We test the statistical significance of the two planes in Section 5, followed by Section 6 where we summarize the results.

2. Sample description

In recent years several untargeted imaging surveys were dedicated to search for low surface brightness dwarf galaxies in the nearby universe (e.g., Chiboucas et al. 2009, 2013; Merritt et al. 2014; Javanmardi et al. 2016). In particular, the richest galaxy aggregate in the Local Volume, the Centaurus A (Cen A) group of galaxies received attention. The Panoramic Imaging Survey of Centaurus and Sculptor (PISCeS; Sand et al. 2014; Crnojević et al. 2014, 2016) revealed 13 extremely faint dwarf galaxies in the vicinity ($\sim 11\,\mathrm{deg}^2$) of Cen A. Group memberships of nine dwarfs have been confirmed with the tip of the red giant branch (TRGB) method. Our team conducted a survey of 550 square degrees around the Centaurus group, including the Cen A and M 83 subgroups, discovering 57 potential group member dwarf galaxies (Müller et al. 2015, 2017a).

The Centaurus group is the largest concentration of galaxies in the Local Volume (Distance < 10 Mpc). Before our study there were about 60 group members known (Karachentsev et al. 2004, 2013). Similar to the Local Group, the Centaurus group has two gravitational centers consisting of a larger galaxy population around the massive, peculiar galaxy NGC 5128 (Cen A) at a mean distance of 3.8 Mpc, and a smaller concentration around the giant spiral M 83 at a mean distance of 4.9 Mpc (Karachentsev et al. 2004, 2013; Tully et al. 2015; Tully 2015b).

This work makes use of four different galaxy samples; these are listed in Table 1. The first sample (1), hereafter called T15 sample, is almost identical to the sample of T15 as given in their Table 1. The authors subdivided their galaxies into six subsamples: Plane 1, Plane 2, Plane 1?, Plane 2?, other and other?. The Plane 1 subsample consists of 14 galaxies. Following T15, we exclude the extremely faint dwarf galaxies Dw-MM-Dw1 and Dw-MM-Dw2 (Crnojević et al. 2014) to avoid any selection bias. The Plane 2 subsample contains 11 galaxies. In the other four subsamples six galaxies lack measured distance information, meaning that they are considered Cen A members based on morphological and/or surface brightness grounds. We exclude PGC 45628 from these because its projected distance from

Tab. 1: Galaxy numbers in the four samples. Members and candidates are galaxies with and without distance measurements, respectively.

Sample name	Members (N)	Candidates (N)	Total (N)
T15 sample (1)	14+11	5	30
LV sample (2)	34	0	34
Candidate sample (3)	0	25	25
Complete sample (4)	34	25	59

Cen A is larger than 1 Mpc. Three other galaxies (ESO 219-010, ESO 321-014, and PGC 51659) have measured distances but cannot be unambiguously assigned to one of the two planes; we exclude these galaxies from the sample. In summary, our T15 sample contains 25 galaxies that have measured distances (members) and five without (candidates).

The second sample (2) includes the 25 members from the T15 sample and the nine newly discovered dwarf galaxy members from Crnojević et al. (2014, 2016), including the two PISCeS dwarfs that were excluded in the first sample. Hereafter we call it the LV sample because all of these 34 galaxies with distances are part of the Local Volume (LV) sample listed in the online version of the Updated Nearby Galaxy Catalog (Karachentsev et al. 2013).

The third sample (3) comprises all candidate members of the Cen A subgroup known to date between $197.5^\circ < \alpha_{2000} < 207.5^\circ$ and $-46^\circ < \delta_{2000} < -36^\circ$. This sample, called hereafter the Candidate sample, consists of 25 dwarf candidates in the vicinity of Cen A, including the new dwarf candidates from Müller et al. (2017a) and the four candidates without distances from Crnojević et al. (2016). All of these candidates are considered likely members of the Cen A subgroup based on morphological and/or surface brightness grounds.

The fourth sample (4) contains all Cen A group members and candidates known to date, hereafter called the Complete sample. It is the combination of the 34 galaxies with distances (LV sample) and the 25 candidates from the Candidate sample. The LV sample and the Complete sample contain only galaxies with radial distances smaller than 1 Mpc from Cen A (3.68 Mpc). See Table 2 for a complete list of galaxies (names, coordinates, and distances) included in our analysis.

3. Transformation between coordinate systems

To compare our results with those of T15 we need to transform the 3D positions of all sample galaxies from the equatorial system to the Cen A reference frame. This is carried out in three steps: (i) a transformation from equatorial (RA, DEC) to the Galactic (l, b) coordinates, (ii) a transformation to the supergalactic (SGL, SGB)

Tab. 2: Members and possible members of the Cen A subgroup.

Galaxy Name	α_{2000} (deg)	δ_{2000} (deg)	D (Mpc)	Sample
ESO269-037[1]	195.8875	-46.5842	3.15	(1)(2)(4)
NGC4945[1]	196.3583	-49.4711	3.72	(1)(2)(4)
ESO269-058[1]	197.6333	-46.9908	3.75	(1)(2)(4)
KKs53[1]	197.8083	-38.9061	2.93	(1)(2)(4)
KK189[1]	198.1875	-41.8319	4.23	(1)(2)(4)
ESO269-066[1]	198.2875	-44.8900	3.75	(1)(2)(4)
NGC5011C[1]	198.2958	-43.2656	3.73	(1)(2)(4)
KK196[1]	200.4458	-45.0633	3.96	(1)(2)(4)
NGC5102[1]	200.4875	-36.6297	3.74	(1)(2)(4)
KK197[1]	200.5042	-42.5356	3.84	(1)(2)(4)
KKs 55[1]	200.5500	-42.7308	3.85	(1)(2)(4)
NGC5128[1]	201.3667	-43.0167	3.68	(1)(2)(4)
KK203[1]	201.8667	-45.3525	3.78	(1)(2)(4)
ESO324-024[1]	201.9042	-41.4806	3.78	(1)(2)(4)
NGC5206[2]	203.4292	-48.1511	3.21	(1)(2)(4)
NGC5237[2]	204.4083	-42.8475	3.33	(1)(2)(4)
NGC5253[2]	204.9792	-31.6400	3.55	(1)(2)(4)
KKs 57[2]	205.4083	-42.5819	3.83	(1)(2)(4)
KK211[2]	205.5208	-45.2050	3.68	(1)(2)(4)
KK213[2]	205.8958	-43.7691	3.77	(1)(2)(4)
ESO325-011[2]	206.2500	-41.8589	3.40	(1)(2)(4)
KK217[2]	206.5708	-45.6847	3.50	(1)(2)(4)
CenN[2]	207.0375	-47.5650	3.66	(1)(2)(4)
KK221[2]	207.1917	-46.9974	3.82	(1)(2)(4)
ESO383-087[2]	207.3250	-36.0614	3.19	(1)(2)(4)
KK198	200.7342	-33.5728	3.68*	(1)(3)(4)
KKs54	200.3850	-31.8864	3.68*	(1)(3)(4)
KKs59	206.9920	-53.3476	3.68*	(1)(3)(4)
KKs58	206.5042	-36.3281	3.68*	(1)(3)(4)
KKs51	191.0896	-42.9397	3.68*	(1)(3)(4)

Galaxy Name	α_{2000} (deg)	δ_{2000} (deg)	D (Mpc)	Sample
CenA-MM-Dw5	199.9667	-41.9936	3.42	(2)(4)
CenA-MM-Dw4	200.7583	-41.7861	3.91	(2)(4)
CenA-MM-Dw6	201.4875	-41.0942	3.61	(2)(4)
CenA-MM-Dw7	201.6167	-43.5567	3.38	(2)(4)
CenA-MM-Dw2	202.4875	-41.8731	3.60	(2)(4)
CenA-MM-Dw1	202.5583	-41.8933	3.63	(2)(4)
CenA-MM-Dw3	202.5875	-42.1925	4.61	(2)(4)
CenA-MM-Dw9	203.2542	-42.5300	3.81	(2)(4)
CenA-MM-Dw8	203.3917	-41.6078	3.47	(2)(4)
dw1315-45	198.9833	-45.7506	3.68*	(3)(4)
dw1318-44	199.7417	-44.8947	3.68*	(3)(4)
CenA-MM-Dw11	200.4167	-43.0825	3.68*	(3)(4)
dw1322-39	200.6333	-39.9060	3.68*	(3)(4)
dw1323-40c	200.9042	-40.7214	3.68*	(3)(4)
dw1323-40b	200.9792	-40.8358	3.68*	(3)(4)
CenA-MM-Dw12	201.0417	-42.1397	3.68*	(3)(4)
dw1323-40	201.2208	-40.7614	3.68*	(3)(4)
dw1326-37	201.5917	-37.3856	3.68*	(3)(4)
CenA-MM-Dw10	201.7042	-43.0000	3.68*	(3)(4)
dw1329-45	202.2917	-45.1753	3.68*	(3)(4)
CenA-MM-Dw13	202.4625	-43.5194	3.68*	(3)(4)
dw1330-38	202.6708	-38.1675	3.68*	(3)(4)
dw1331-40	202.8583	-40.2631	3.68*	(3)(4)
dw1331-37	202.8833	-37.0581	3.68*	(3)(4)
dw1336-44	204.1833	-44.4472	3.68*	(3)(4)
dw1337-44	204.3917	-44.2186	3.68*	(3)(4)
dw1337-41	204.4792	-41.9031	3.68*	(3)(4)
dw1341-43	205.4042	-43.8547	3.68*	(3)(4)
dw1342-43	205.6633	-43.2553	3.68*	(3)(4)

Galaxies with unknown distances are denoted with a *. We adopted the distance of Cen A (3.68 Mpc) for them. Galaxies that are members of Plane 1 or 2 are denoted with [1] or [2], respectively, according to T15. Galaxies denoted with (1) belong to the T15 sample, (2) are from the LV sample, (3) belong to the Candidate sample, and (4) are in the Complete sample.

coordinates, and (iii) a translation and rotation to the Cen A reference frame (CaX, CaY, CaZ). In the latter reference system, Cen A is located at the origin, and the two nearly parallel galaxy planes, represented by an averaged normal direction, lie in the XY projection. The two planes are then visible edge-on in the XZ projection (see our Sect. 4 and Fig. 2 in T15).

The transformation between polar coordinates and Cartesian coordinates is given by

$$x = d \cdot \cos(\delta) \cdot \cos(\alpha)$$

$$y = d \cdot \cos(\delta) \cdot \sin(\alpha)$$

$$z = d \cdot \sin(\delta),$$

where d is the heliocentric distance to the galaxy. To rotate from equatorial coordinates to Galactic coordinates, the Cartesian coordinates $v = (x, y, z)$ (equatorial system) have to be multiplied from the left by the rotation matrix

$$\boldsymbol{R_G} = \begin{bmatrix} -0.0549 & -0.8734 & -0.4839 \\ +0.4941 & -0.4448 & +0.7470 \\ -0.8677 & -0.1981 & +0.4560 \end{bmatrix}.$$

From galactic coordinates to supergalactic coordinates, the rotation is given by the matrix

$$\boldsymbol{R_{SG}} = \begin{bmatrix} -0.7357 & +0.6773 & +0.0000 \\ -0.0746 & -0.0810 & +0.9940 \\ +0.6731 & +0.7313 & +0.1101 \end{bmatrix}.$$

Therefore the transformation from equatorial to supergalactic coordinates is:

$$v_{SG} = \boldsymbol{R_{SG}} \boldsymbol{R_G} v.$$

In T15 the authors transformed the supergalactic coordinates into the Cen A reference frame. To do this, they applied a translation to the coordinate system such that Cen A is at the origin (0,0,0)

$$v_{SG,CenA} = v_{SG} + \begin{pmatrix} +3.41 \\ -1.26 \\ +0.33 \end{pmatrix} \text{ [Mpc]}$$

and then rotate into the new coordinate system with

$$\boldsymbol{R_{Ca}} = \begin{bmatrix} +0.994 & -0.043 & +0.102 \\ -0.001 & +0.919 & +0.393 \\ -0.111 & -0.391 & +0.914 \end{bmatrix}.$$

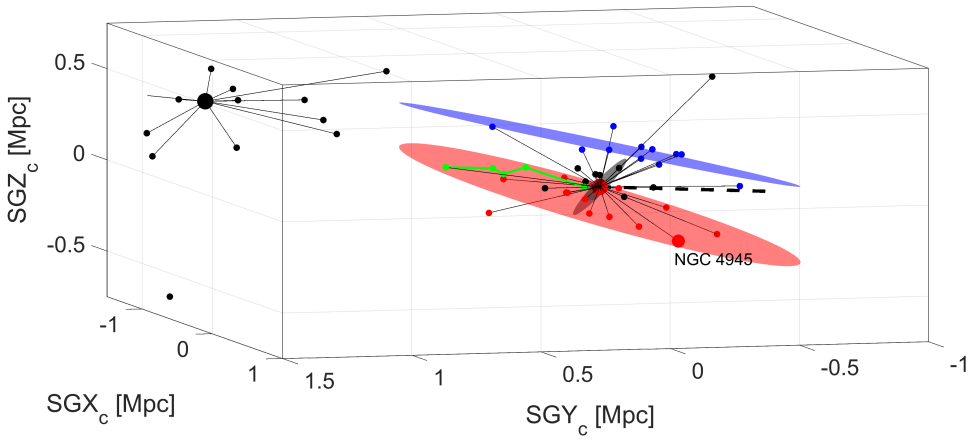

Fig. 1: Three-dimensional distribution of known Centaurus group members in supergalactic coordinates centered on Cen A. The large red dot is Cen A, the large black dot is M 83, and the intermediate-size red dot is the late-type spiral NGC 4945. The small red dots are plane 1 dwarf satellite members, the blue dots plane 2 members from T15, the black dots are additional (non-plane) members of the Cen A group. The best-fitting planes 1 and 2 are illustrated by the red and blue disks, respectively. The smaller gray disk that stands almost orthogonally to the two satellite planes represents the dust lane of Cen A. The dashed black line corresponds to the line of sight toward Cen A. The green line connects the five regions in the tail of the tidally disrupted dwarf CenA-MM-Dw3 where distances could be measured (Dw3, Dw3 S, Dw3 SE, Dw3 N, and Dw3 NW, Crnojević et al. 2016).

The final transformation to the Cen A reference frame is

$$v_{Ca} = \boldsymbol{R_{Ca}} v_{SG,CenA.}$$

We note that T15 uses 3.66 Mpc as distance for Cen A, while their given translation from v_{SG} to $v_{SG,CenA}$ only adds up to 3.65 Mpc. In this work we use an updated distance value of 3.68 Mpc taken from the LV catalog. These small differences place Cen A with a minor offset to the center of the reference frame.

4. Geometrical alignment of the satellites

We used two different algorithms to fit the two planes of satellites in three dimensions: a singular value decomposition (svd; Golub & Kahan 1965) and the tensor of inertia (ToI; e.g., Pawlowski et al. 2015a). The 14 galaxies used for fitting plane 1 are labeled [1] in Table 2 and the 11 galaxies for plane 2 are labeled [2]. The normal vectors of the best-fitting planes given in supergalactic coordinates are $\mathbf{n_1} = (-0.1576, -0.4306, 0.8886)$ and $\mathbf{n_2} = (0.0875, 0.3225, -0.9425)$ for plane 1 and 2, respectively. Both algorithms return the same results. The angle between the two normal vectors is found to be 8.0°, which is in good agreement with 7° published by T15. We cannot evaluate why there is a difference between our results and T15, as neither the plane-fitting method nor the exact sample of galaxies used for the fits were stated in T15. The measured angles between $\mathbf{n_1}$, $\mathbf{n_2}$, and the normal vector of the supergalactic plane are 16.9° and 24.6°, respectively, meaning that the

two planes are not far from being parallel to the supergalactic plane. Using the ToI algorithm we further calculated that plane 1 has a root-mean-square (rms) thickness of 69 kpc and a major-axis rms length of 309 kpc, while plane 2 has a thickness of 48 kpc and a length of 306 kpc.

As the prominent dust lane of Cen A itself represents a reference plane, one can further ask how the satellite planes are spatially arranged with respect to Cen A. The orientation of the dust lane was studied by Hui et al. (1995) who give an inclination of 17° to the line of sight and a position angle for the disk angular momentum of 35° in the sky (counting from N through E). This latter angle also coincides with the position angle of the photometric major axis (Dufour et al. 1979). From these two angles we calculated the normal vector of the Cen A dust plane in supergalactic coordinates to be $\mathbf{n_{dust}} = (-0.0305, 0.8330, 0.5525)$. The resulting angular difference to the normal vectors of the satellite planes 1 and 2 amounts to 82.1° and 104.8°, respectively. This means that the satellite planes are almost orthogonal to the dust plane of Cen A (see Fig. 1), which is reminiscent of the local situation where the VPOS is essentially perpendicular to the plane of the Milky Way. Furthermore, the angle between the connection line of Cen A and M 83 and the normal of the dust plane is only 30°, meaning that $\mathbf{n_{dust}}$ almost points toward M 83.

Crnojević et al. (2016) discovered the tidally disrupted dwarf galaxy CenA-MM-Dw3 with tails spanning over 1°.5 (~ 120 kpc). They measured distances at five separate high surface brightness locations along the elongation. Defining the directional vector of CenA-MM-Dw3 as the vector between CenA-MM-Dw3 and CenA-MM-Dw3-SE, the vector is $\mathbf{e_{Dw3}} = (0.8983, -0.4266, 0.1056)$ in supergalactic coordinates. Astonishingly, we find that angles between this vector and the plane 1 and 2 normal vectors are 82° and 99°, respectively, meaning that the tidally disrupted dwarf is almost parallel to the two planes. This is again reminiscent of the Local Group where the Magellan Stream aligns with the VPOS. In contrast to the Local Group the angle between $\mathbf{e_{Dw3}}$ and the normal of the dust plane is 109°, meaning that the tidal dwarfs is almost parallel to the dust plane. The tail itself lies along the line of sight, having the positive effect that the distance errors only move along this direction, hence the uncertainties do not change the angles between the tail and the planes. In Table 3 we compile the calculated vectors in supergalactic coordinates.

Tab. 3: Directions in supergalactic coordinates.

		(SGX, SGY, SGZ)
normal plane 1	$\mathbf{n_1}$	$(-0.1576, -0.4306, +0.8886)$
normal plane 2	$\mathbf{n_2}$	$(+0.0875, +0.3225, -0.9425)$
normal Cen A dust plane	$\mathbf{n_{dust}}$	$(-0.0305, +0.8330, +0.5525)$
elongation CenA-MM-Dw3	$\mathbf{e_{Dw3}}$	$(+0.8983, -0.4266, +0.1056)$

Fig. 1 shows the 3D galaxy distribution of the Centaurus group in supergalactic coordinates with Cen A at the origin. Data are drawn from the online version of the LV catalog (Karachentsev et al. 2013). The primary double structure of the group is defined by the Cen A (big red dot) subgroup and the M 83 (big black dot) subgroup, and the secondary double-plane structure around the Cen A subgroup. The 14 Plane 1 satellites are shown as red dots, the 11 Plane 2 satellites as blue dots according to the T15 sample. The intermediate-size red dot is NGC 4945. The best-fitting planes are also indicated (shown as red and blue disks; for details on the fitting procedure see above), the alignment of the tidal features of CenA-MM-Dw3 (green line with dots), and the dust plane of Cen A (in gray).

5. Mapping the new dwarf candidates

We now switch to the Cen A reference frame (CaX, CaY, CaZ) that was introduced by T15. The top panels of Fig. 2 show the distribution of the Cen A group members in the CaX – CaZ projection; this plot is directly comparable to Fig. 2 of T15. Here, the two galaxy planes are seen edge-on. The bottom panels show the CaX – CaY projection, presenting the planes in a face-on view. As has already been noted in T15, our line of sight lies almost in the direction of the two planes. The angle between the best-fitting planes and the line of sight at the distance of Cen A is only 14.6° and 12.8° (with a different sign), respectively, for plane 1 and 2. As a consequence of this geometry, any distance uncertainties move galaxies essentially along the two planes and thus have little bearing on the bimodal structure. On the other hand, for the same reason one might surmise that the planes are an artifact produced by the spread of distance errors. This is unlikely to be the case, however, as the planes are significantly more extended than the distance errors. T15 came to the same conclusion.

The special geometrical situation allows us to put the two planes of satellites to the test with the help of our new dwarf candidates around Cen A (Müller et al. 2017a). Given the celestial position (i.e., equatorial coordinates) of a dwarf candidate, its relative position to the planes is essentially given as well. There are three possibilities for a candidate: (1) it lies in one of the two planes, (2) it lies between the planes, or (3) it lies outside of the bimodal structure. Again, the key point is that this test can be conducted without knowing the distances of the candidates, deferring, at least in this preliminary manner, the observationally challenging task of distance measurements.

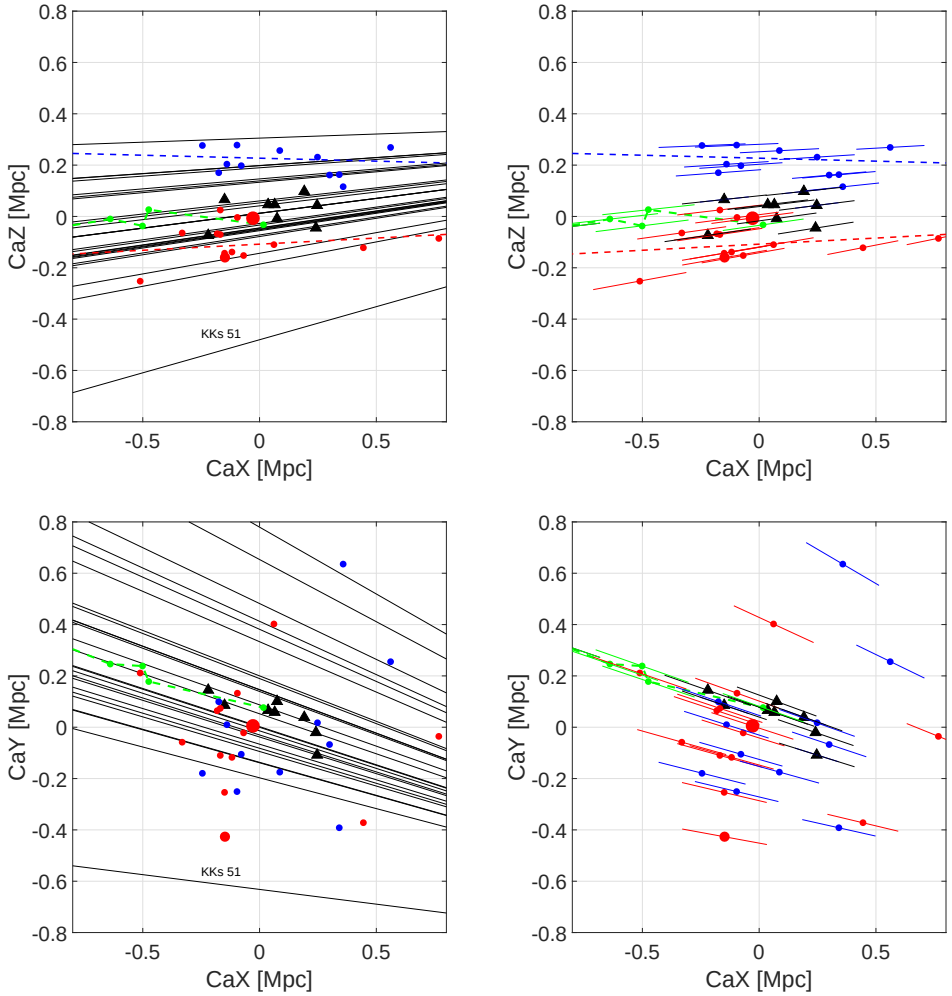

Fig. 2: Top left: edge-on view of the two galaxy planes. Red dots are satellites in plane 1, blue dots are satellites in plane 2, and black triangles are new dwarfs from the PISCeS survey. The green dotted line corresponds to the tidally disrupted dwarf CenA-MM-Dw3 where the dots themselves are regions in the tail where distances were measured (Dw3 S, Dw3 SE, Dw3 N, and Dw3 NW). CenA-MM-Dw3 itself falls outside the frame. The red and blue dashed lines are the best-fitting planes. The 25 thin black lines indicate the possible locations of new dwarf candidates without distance measurements. Top right: same as top left but without the possible group members, giving instead an indication of the distance uncertainties of the known members. The colored lines correspond to 5 percent distance errors, projected onto the CaX - CaZ plane. Bottom left: galaxy distribution in the CaX - CaY plane, where we see the two planes superimposed and face-on. Bottom right: same as bottom left, only showing the galaxies with known distances. As in Fig. 1, the large red dot is Cen A and the intermediate-size red dot is the giant spiral NGC 4945.

In the top panels of Fig. 2 all known Cen A group members with distances are plotted in the CaX - CaZ projection. Red dots are the galaxies in plane 1, blue dots are galaxies in plane 2 according to T15, and black triangles are the newly found galaxies by Crnojević et al. (2014, 2016). The best-fitting planes, i.e., their lines of intersection with the orthogonal CaX - CaZ plane, are shown in the top left panel. In the top right panel the 5 percent distance uncertainties for the galaxies are added, showing the distance range along the line of sight. Likewise, the thin black lines in the top left panel indicate the lines of sight for the candidate Cen A group members,

nicely illustrating the near parallelism between the satellite planes and our line of sight. The bottom panels show the CaX - CaY projection, looking at the plane face-on.

From the CaX - CaZ projection it becomes clear that the 25 dwarf galaxy candidates, provided they are Cen A group members, can be assigned almost unambiguously to one of the two planes because there is no double plane crossing along the line of sight at the distance of Cen A. In fact, of the 25 lines of sight (= possible positions of the candidates) none are crossing both planes within the distance range considered ($D_{Cen\,A} \pm$ 0.75 Mpc); see Fig. 2, top left. One candidate, KKs 51, clearly misses both planes. For example, to be a member of plane 1, it would have to be 2 Mpc from the Milky Way (or 1.9 Mpc from Cen A) where the line of sight and plane 1 intersect. In T15, this candidate is indicated as other?. We conclude that KKs 51 is not a member of the planes and therefore should count as other. Looking solely at the CaX-CaZ projection, there remains the possibility that the lines of sight are only projected into the region of the planes, while in the 3D reality they could lie way off the planes. The CaX-CaY projection (face-on view) in the bottom panels shows that this is not the case. Only the line of KKs 51 is far from the Cen A galaxy aggregation.

Interestingly, the nine PiSCeS dwarfs (black triangles in Fig. 2) seem to fill the gap between the two planes. This raises the question what will happen when the large sample of our new dwarf candidates comes into play. Will the bimodal structure be lost altogether, unmasking the double-plane structure of the Cen A subgroup as an effect of small-number statistics, or will the case for a double plane be strengthened?

The Cen A subgroup members and candidates can now be sampled along the CaZ axis. In T15 this is carried out in their Fig 2 by plotting a histogram of CaZ coordinates for members with their individually measured distances and for possible members (the dwarf candidates) assuming a distance of 3.68 Mpc (the distance of Cen A). We binned our galaxy samples as in Fig 3. The red and blue bins correspond to the plane galaxies from the T15 sample, colored as before. The bimodal structure is clearly visible. If we add the nine satellites (in black) from the PISCeS survey (Crnojević et al. 2014, 2016) the gap starts to fill up. A limitation of the PiSCeS survey, however, is the relatively small area of 11 deg^2 covered (see Fig. 2 in Müller et al. 2017a). Nevertheless, despite this possible bias, every dwarf that is found between the two planes reduces the significance of the bimodality. Finally, when including the more homogeneous and bias-free sample of 25 candidates (gray bins) that covers most of the vicinity of Cen A from the Candidate sample (Müller et al. 2017a; Crnojević et al. 2016) the bimodality in the distribution increases slightly again and the population of plane 1 becomes dominant.

However, this representation of the CaZ distribution as a histogram is somewhat problematic. Not only does a histogram depend on the chosen starting point and bin

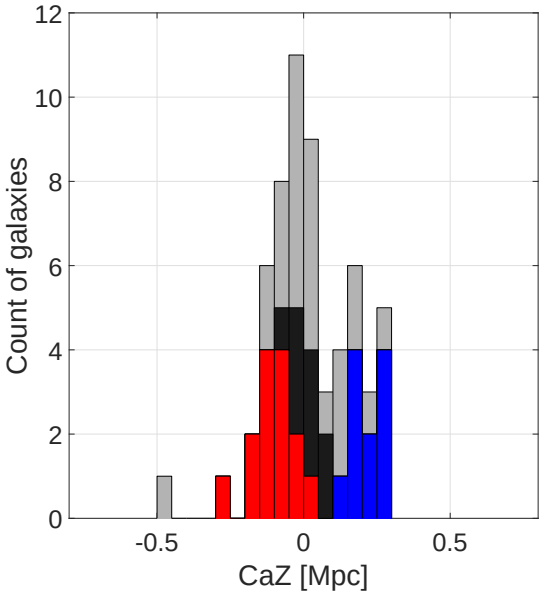

Fig. 3: Histogram of the Cen A satellite distribution along the CaZ axis. The red and blue bins correspond to the (14+11) plane 1 and 2 members, respectively, from the T15 sample. The gray bins are the 25 Cen A subgroup member candidates assuming a distance of 3.68 Mpc (Cen A).

width, we also adopted the same fixed distance for all candidates. Although there is only a weak dependence of CaZ on the distance, owing to the fact that the line of sight is almost perpendicular to the CaZ axis, the mean CaZ range covered by a group member candidate is around 0.11 Mpc in the distance interval $2.93 < D < 4.43$ Mpc, which can shift a candidate back and forth by up to two bins of 0.05 Mpc width. A better representation of the data can be achieved using the adaptive kernel density estimation. In this technique, the galaxies (members and candidates) are represented by standard normal curves with μ as the measured or assumed distance and σ as the distance uncertainty amounting to 5 percent for members, accounting for measurement errors, and 0.5 Mpc for candidates, accounting for the depth of the subgroup. The standard normal curves are then projected onto the CaZ axis, resulting in standard normal curves with different σ values, which depend on the projection angle, i.e., the angle between the line of sight and CaZ. This angle varies systematically over CaZ (see Fig. 2, top left), from close to orthogonal at positive CaZ values (CaZ~ 0.2 Mpc), giving very narrow standard curves, to ever smaller acute angles toward negative CaZ values (CaZ~ -0.3 Mpc), giving broader standard curves. The combined density distribution of the galaxies along the CaZ axis, by co-adding the projected normal curves, is given in Figs. 4 and 5.

In Fig. 4 the T15 sample (black solid line) and all candidate galaxies without distances from the Candidate sample (red dashed line) are plotted differentially. For the galaxies without distance measurements a distance of 3.68 Mpc and a distance uncertainty of ± 0.5 Mpc is assumed. These standard normal curves are plotted in gray. The bimodality is visible, albeit the peak around plane 1 is higher than the peak around plane 2.

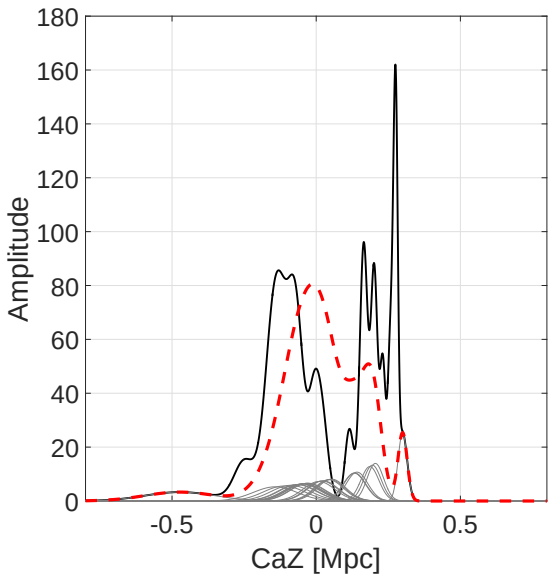

Fig. 4: Adaptive kernel for the Cen A subgroup members. Shown is the density distribution of satellite galaxies along the CaZ axis from a superposition of projected standard normal curves accounting for distance uncertainties (see text). The black line corresponds to the T15 sample (members and candidates), and the red dotted line to the Candidate sample, assuming a distance of 3.68 Mpc (Cen A) and an uncertainty due to the depth of the subgroup of ± 0.5 Mpc. The standard normal curves of the candidates are shown in gray.

Fig. 5 shows the same data as the histogram in Fig. 3. This plot contains all the information up to date. The gray line corresponds to the plane satellites from the T15 sample, the black line to the LV sample, and the red dashed line to the Complete sample. In all three samples the gap is visible. It is now important to test the significance of the planar structures.

6. Statistical analysis

Is the seemingly bimodal structure of the Cen A subgroup statistically significant? To answer this question we performed two different statistical tests, the Anderson-Darling test (D'Agostino & Stephens 1986) and the Hartigan dip test (**?**). The null hypothesis is that the observed galaxy distribution can be described by a unimodal normal distribution. Basically, we ask whether or not the galaxy distribution in the edge-on view, sampled along the CaZ axis, can be explained by a single normal distribution. If the null hypothesis is rejected, there must be evidence of multimodality in the Cen A subgroup, or the assumption of an underlying normal distribution is incorrect. We test the four samples listed in Table 1: (1) the T15 sample, (2) the LV sample, (3) the Candidate sample, and (4) the Complete sample.

The Anderson-Darling test is an improved version of the Kolmogorov-Smirnov test. Both of these tests compare the standard normal cumulative distribution function (CDF) with the empirical cumulative distribution function (ECDF) created from the data. If the difference between the ECDF and CDF becomes larger than a critical value, the hypothesis of normality is rejected with some significance level. In contrast to Kolmogorov-Smirnov, the Anderson-Darling test weights the tails of a distribution higher than the center. We use the implementation of the Anderson-Darling test provided by MATLAB.

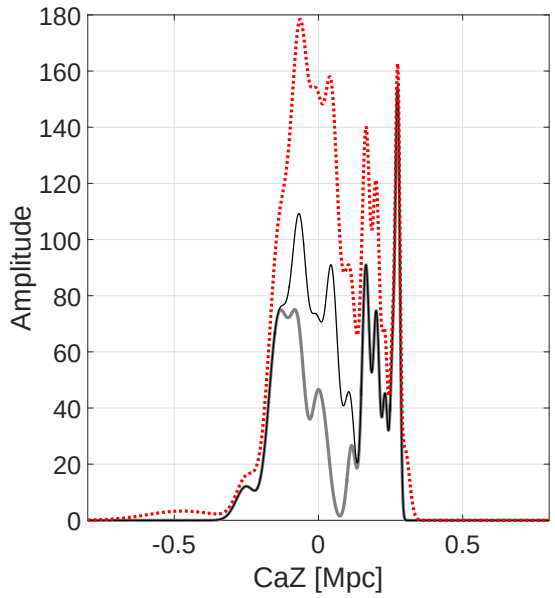

Fig. 5: Same as Fig. 4 but including the PISCeS dwarfs and shown as density distribution, analoguous to the histogram of Fig. 3. The gray line corresponds to the members of the two planes from the T15 sample. The black line corresponds to the LV sample, comprising the T15 sample plus the nine new dwarfs from the PISCeS survey, thus representing all known galaxies with distances < 1 Mpc from Cen A. The red dotted line is the grand total, i.e., the superposition of the black line and all the possible members of the Cen A subgroup from the Candidate sample (Müller et al. 2017a; Crnojević et al. 2016), assuming a distance of 3.68 Mpc (Cen A) and an error of ± 0.5 Mpc. The galaxy Cen A itself is located at CaZ=0.

The results for the Anderson-Darling test are presented in Table 4: samples (2), (3), and (4) pass the test for normality at the significance level of 5% with p_{AD}-values of 0.18, 0.07, and 0.15, respectively. With a p_{AD}-value of 0.07 the candidates-only sample (3) has still a marginal probability of not being unimodally distributed. Sample (1) is inconsistent with being drawn from a normal distribution with a p_{AD}-value of 0.02, an expected result given the finding of T15. Taking all the recently added data into account, however, the distribution of galaxies along the CaZ axis becomes consistent with being normally distributed.

There is a possible caveat. The footprint of the PISCeS survey does not cover the whole area on the sky taken by the two planes, see Fig. 2 of Müller et al. (2017a), which could lead to a selection bias. Disregarding the findings of the PISCeS survey: Dw1, Dw2, Dw4, Dw8, and Dw9 would have been detected in the data of our Centaurus group survey, but not the extremely faint and diffuse objects Dw5, Dw6, and Dw7. Furthermore, the photometric properties of the tidally disrupted dwarf Dw3 does not conform with our search criteria and would have remained undetected as well. We also assume that Dw10, Dw11, Dw12, and Dw13 would not have been detected (no photometry was performed in Crnojević et al. (2016) for these candidates). In total, only five Dw galaxies would then feature in the Candidate sample and Complete sample with an assumed distance of 3.68 Mpc. Do the significance tests return different results with these conservative assumptions? We repeated the Anderson-Darling test with the following results: the null hypothesis is rejected for samples (1) and (2), while samples (3) and (4) are consistent with a normal distribution at the 5% confidence level. Sample (2) is rejected because it now contains only the galaxies with distances from the T15 sample. We therefore conclude that the outcome of the Anderson-Darling is little affected by a selection bias from including the PISCeS dwarfs in the analysis.

The Hartigan dip test provides another method to test for bimodality. It measures the maximum difference between the empirical distribution function and the unimodal distribution function that minimizes that maximum difference. We use an implementation originated by Hartigan (1985), which was translated into MATLAB by Ferenc Mechler.

The results for the Hartigan dip test are as follows: samples (2), (3), and (4) pass the test at the significance level of 5% with p-values of 0.61, 0.72, and 0.84, respectively. Only sample (1) fails the test with a p-value of 0.00. This is the same result as before. Again we checked for a change of the results by the exclusion of the five candidates from the T15 sample. With a p-value of 0.08 the result for this plane-members-only subsample changes indeed. It now has a marginal probability of not being unimodally distributed, and when testing at a 10% significance level it is clearly rejected from unimodality. Overall the conclusion is hence the same: while the galaxy data used in the original analysis by Tully and collaborators support the picture of a multimodal distribution (two planes), adding the new galaxies, and thereby doubling the sample, presents a picture that is consistent with a unimodal normal distribution.

Until now no distance uncertainties were taken into account when testing for the significance of the planes. To test whether these results are indeed representative of the data and their uncertainties, we performed Monte Carlo simulations where the distance of a galaxy is randomly taken from a normal distribution with μ given by the galaxy position and σ by the distance error of 5 %. Remember that we sample along the CaZ axis, which means that we only count the CaZ component of the distance uncertainty. For galaxies without distance measurements a conservative distance uncertainty of $\pm$0.5 Mpc, accounting for the depth of the Cen A subgroup, is taken. We calculated 10000 realizations of all samples and applied both the Anderson-Darling and the Hartigan dip test on them. The resulting probabilities that the null hypothesis (= normal distributed) is rejected for the Anderson Darling and the Hartigan dip test are as follows: (1) is rejected in 66 and 62 percent of the draws, (2) in 2 and 0 percent, (3) in 21 and 0 percent, and (4) in 5 and 0 percent.

In this analysis all candidates are considered to be satellites of Cen A. But what if some of these candidates are not members of the Cen A subgroup but lie in the background? To check this possibility, we broadened the distance uncertainty to $\pm$1.5 Mpc and repeated the MC runs. Remember that we exclude all galaxies with radial distances to Cen A larger than 1 Mpc. When we rerun the simulations with this setup, (1) gets rejected in 65 and 56 percent of the cases, (3) in 18 and 2 percent, and (4) in 5 and 0 percent. Hence this wider spread essentially lowers the rejection rate.

The results of these tests are summarized in Table 4. Column 1 lists the test sample name. Columns 2 and 3 gives the accepted hypothesis and p-value from the Anderson-

Tab. 4: Anderson-Darling and Hartigan dip test results.

Sample	h_{ad}	p_{AD}	$P_{AD,MC}$	h_{dip}	p	$P_{dip,MC}$
(1)	h_1	0.02	0.66 (0.65)	h_1	0.00	0.62 (0.56)
(2)	h_0	0.18	0.02	h_0	0.61	0.00
(3)	h_0	0.07	0.21 (0.18)	h_0	0.72	0.01 (0.02)
(4)	h_0	0.15	0.05 (0.06)	h_0	0.84	0.00 (0.00)

Darling test. Column 4 lists the probability for a rejection of h_0 estimated with the Anderson-Darling test from Monte Carlo simulations. The results from the test with a distance uncertainty of $\pm$ 1.5 Mpc are indicated in brackets. Columns 5 and 6 gives the accepted hypothesis and p-value from the Hartigan dip test. Column 7 lists the probability for a rejection of h_0 estimated with the Hartigan dip test from Monte Carlo simulations. In brackets The results from the test when adopting a distance uncertainty of 1.5 Mpc are indicated in brackets.

From all our results, we conclude that with the addition of the new data the significance against a unimodal distribution of the satellites around Cen A rises, i.e., the significance for bimodality is weakened, even though the case for a double-plane structure, as suggested by T15, is not completely ruled out.

We performed one last test. What would happen if the new candidates were lying exactly in (one of) the two planes? To find out, we calculated the intersection point between the line of sight and the planes, and thus a new (hypothetical) distance d_{inter} for each candidate from the Candidate sample and the Complete sample. To account for the thickness of the planes, we also calculated the intersection points at $\pm$ the r.m.s. thickness of the planes, giving a minimal (d_{min}) and maximal (d_{max}) value for the distance. We only take galaxies into account where the radial distance between the galaxy and Cen A is less than 1 Mpc. In Table 5 we present the estimated distances for all galaxies, where at least one of the three intersection points is closer than 1 Mpc to Cen A. Distances indicated with an asterisk are outside of this 1 Mpc radius. The following eight candidates miss the two planes in the 1 Mpc vicinity of Cen A and are therefore removed from the modified Candidate and Complete samples: dw1329-45, CenA-MM-Dw13, dw1331-40, dw1337-41, KK198, KKs54, KKs59, and KKs51. Applying the Anderson-Darling and Hartigan dip tests to the modified Candidate sample and Complete sample leads to the following changes: (3) and (4) are now rejected by the Anderson-Darling test both with a p_{AD}-value of 0.00. The same is true when testing with d_{min} and d_{max}. On the other hand, the Hartigan dip test still accepts the null hypotheses for samples (3) and (4), as before, but the p-values are lowered to 0.08 and 0.66, respectively. Again, we get the same result when testing with d_{min} and d_{max} instead of d_{inter}. With a p-value of 0.08, the modified Candidate sample is now marginally significant that is not

Tab. 5: Predicted distances for the candidates.

Name	d_{inter} [Mpc]	d_{min} [Mpc]	d_{max} [Mpc]
Plane 1			
dw1315-45	3.84	3.53	4.15
dw1318-44	4.07	3.75	4.40
CenA-MM-Dw11	4.15	3.82	4.45
dw1322-39	3.83	3.52	4.13
dw1323-40c	4.07	3.75	4.40
dw1323-40b	4.13	3.80	4.46
CenA-MM-Dw12	4.37	4.02	4.72*
dw1323-40	4.26	3.92	4.60
dw1326-37	4.01	3.70	4.33
CenA-MM-Dw10	4.99*	4.59	5.39*
dw1330-38	4.86*	4.47	5.25*
dw1331-37	4.85*	4.46	5.23*
Plane 2			
dw1336-44	2.26*	1.78*	2.74
dw1337-44	2.36*	1.86*	2.87
dw1341-43	3.29	2.59*	4.00
dw1342-43	3.51	2.76	4.26
KKs58	3.02	2.38*	3.67

unimodal, whereas the modified Complete sample gives a strong hint for unimodality, in contrast to the Anderson-Darling test.

Hypothetically, putting the new candidates onto the best-fitting planes must of course strengthen the case for the planes. But as we cannot exclude the possibility that the dwarfs are indeed lying in the planes without accurate distance measurements, we also cannot conclusively rule out the reality of the planes.

7. Discussion and conclusions

The discovery of a large number of new dwarf galaxies in the nearby Centaurus group (Crnojević et al. 2014, 2016; Müller et al. 2015, 2017a) opened the opportunity to conduct a significance test of the two planes of satellites reported by Tully et al. (2015). While this normally requires follow-up observations to measure galaxy distances, in the case of the Cen A subgroup, owing to the special geometric situation, one can take advantage of the fact that the line of sight from our vantage point runs along the postulated planes of satellites. Therefore, galaxies even without distance measurements can be used for the test, as distance uncertainties move galaxies along or parallel to the planes. In other words, distance uncertainties produce only little crosstalk between the planes and the space around them. This allows us to include

all Cen A member candidates in the analysis, which doubles the sample size from 30 to 59.

Sampling galaxy positions along an edge-on projection of the planes, we studied the distribution of Cen A subgroup members by two different techniques: a histogram and a more sophisticated adaptive kernel density estimation. A gap, or dip in the distribution marking the two planes, is visible in both representations of the data. However, it is also very evident that with the inclusion of the new galaxy data the gap between the two planes starts to be filled, raising the conjecture that the two plane scenario around Cen A might be an artifact of low number statistics. To put this under statistical scrutiny, we performed an Anderson-Darling test and a Hartigan dip test to see whether the distribution is in agreement with a unimodal normal distribution. We find that both tests fail with the sample used by Tully et al. (2015), rejecting the unimodal normal hypothesis for that orginal sample. This result is consistent with their finding that the satellites can be split into two planes. However, with the addition of the new dwarf members and candidates of the Cen A subgroup, the deviation from a normal distribution loses statistical significance in the sense of the two tests applied. Hence it is now conceivable that the satellites follow a normal distribution and the gap between the two planes is indeed an artefact from small number statistics. We performed Monte Carlos simulations to further strengthen these results by taking distance uncertainties into account and find that the results change only marginally.

Given that distance measurements for the candidate galaxies are unavailable at the moment, it is theoretically possible to allocate 17 out of 25 galaxies to one of the two planes each by moving them along the line of sight. That means that technically the existence of the two planes cannot be completely ruled out at this point. Only distance measurements will tell whether the candidates lie on or near the planes. All we can say is that the case for two planes around Cen A is weakened by including the currently available data for 29 new dwarfs and dwarf candidates.

At first glance, another secondary result of our testing is that in parallel with the weakening of the significance for bimodality, the galaxy population in plane 1 has now become dominant. This is not surprising: Cen A lies closer to plane 1 in projection (CaZ=0 in Fig. 5), such that any newly discovered satellite galaxy in a distribution that is radially concentrated on Cen A will necessarily result in an additional member of plane 1. However, this amassing of Cen A satellites in the proposed plane 1 is important, as the planarity of Plane 1 has not been destroyed by adding the candidates. The alignment of the tidally disrupted CenA-MM-Dw3 with plane 1 (see Figs. 1 and 2) is intriguing too. The Cen A plane 1 is certainly a good candidate analog of the local thin planes detected around the Milky Way (VPOS) and the Andromeda galaxy (GPOA). Future distance measurements for the many

new Cen A subgroup member candidates will be able to tell how far the analogy will take us.

Acknowledgements

OM, HJ, and BB are grateful to the Swiss National Science Foundation for financial support. HJ acknowledges the support of the Australian Research Council through Discovery projects DP120100475 and DP150100862. MSPs contribution to this publication was made possible through the support of a grant from the John Templeton Foundation. The opinions expressed in this publication are those of the authors and do not necessarily reflect the views of the John Templeton Foundation. The authors like to thank the anonymous referee for helpful comments that improved the paper.

5.7 A whirling plane of satellite galaxies around Centaurus A challenges cold dark matter cosmology

— Oliver Müller, Marcel S. Pawlowski, Helmut Jerjen, Federico Lellii —

Science, 2018, 359, 534

Abstract

The Milky Way and Andromeda galaxy are each surrounded by a thin plane of satellite galaxies that may be corotating. Cosmological simulations predict that most satellite galaxy systems are close to isotropic with random motions, so those two well-studied systems are often interpreted as rare statistical outliers. We test this assumption using the kinematics of satellite galaxies around the Centaurus A galaxy. Our statistical analysis reveals evidence for corotation in a narrow plane: of the 16 Centaurus A's satellites with kinematic data, 14 follow a coherent velocity pattern aligned with the long axis of their spatial distribution. In standard cosmology simulations, $< 0.5\%$ of Centaurus A-like systems show such behavior. Corotating satellite systems may be common in the Universe, challenging small-scale structure formation in the prevailing cosmological paradigm.

1. Introduction

The presence of planes of satellite dwarf galaxies around the Milky Way (Kunkel & Demers 1976; Lynden-Bell 1976; Pawlowski et al. 2012b, 2013) and Andromeda (McConnachie & Irwin 2006; Koch & Grebel 2006; Ibata et al. 2013) galaxies have challenged our understanding of structure formation on galactic and subgalactic scales. Similar structures are rare in galaxy formation simulations based on the standard Lambda Cold Dark Matter (ΛCDM) cosmological model, which predicts close to isotropic distributions and random kinematics for satellite systems (Kroupa et al. 2005). The existence of planes of satellite galaxies around these two largest galaxies in the Local Group is difficult to explain within the ΛCDM framework. Some authors have argued that preferential accretion of satellites along filaments may explain such flattened structures (Zentner et al. 2005). Others suggest that the Local Group should be considered a rare exception in an otherwise successful cosmological model (Ostriker & Steinhardt 1995; White et al. 1993; Eisenstein et al. 2005). This interpretation, however, has been challenged by emerging evidence for anisotropic satellite distributions around massive galaxies beyond the Local Group (Müller et al. 2017b; Chiboucas et al. 2013).

The cosmic expansion of the Local Void (a vast, empty region of space adjacent to the Local Group) has been suggested as a possible origin for the formation of these planar structures (Libeskind et al. 2015). An issue which is mostly ignored in this context is the coherent kinematics of the satellite galaxies, which are likely corotating around their host. This is clear for the Milky Way (Pawlowski & Kroupa 2013; Pawlowski et al. 2015b) where accurate proper motions are available for several satellites, but it remains more uncertain for Andromeda (Ibata et al. 2013) because only velocities projected along the line of sight (LoS) are measurable. Such orderly kinematic motions are extremely rare in high-resolution cosmological N-body simulations (Pawlowski et al. 2014) and statistically should not be observed in typical galaxy groups. It remains unclear whether such planes of satellites are unique to the Local Group, or ubiquitous in the nearby Universe.

In this Research Article, we study the galaxy group in the constellation Centaurus. The Centaurus Group is the richest assembly of galaxies within a distance of 10 megaparsecs (Mpc) from the Milky Way, the so-called Local Volume (Karachentsev et al. 2004, 2013). It comprises two concentrations: the Cen A subgroup dominated by a radio-active elliptical galaxy Centaurus A (Cen A, NGC 5128) at a distance of 3.8 Mpc, and the M 83 subgroup dominated by a late-type spiral galaxy M 83 (NGC 5236) at a distance of 4.9 Mpc (Karachentsev et al. 2004, 2013). The galaxies which are gravitationally bound to Cen A were claimed to be distributed in two parallel planes (Tully et al. 2015). The discovery of additional satellite galaxies in the group weakened the case for a double-planar structure, whilst a single-plane interpretation has become more statistically significant (Müller et al. 2015, 2017a; Crnojević et al. 2016). This plane has a small scale height with a root-mean-square (rms) thickness of 69 kiloparsecs (kpc) and a major axis rms length of 309 kpc (Müller et al. 2016). We investigate the kinematics of this planar structure and compare it with galaxy formation simulations in ΛCDM cosmology.

2. Dynamics of the Cen A satellite system

From Earth the satellite plane around Cen A is seen nearly edge-on at an inclination of 14.6 degrees (Müller et al. 2016). This coincidental geometrical alignment allows us to scrutinize the kinematics of the plane. We use all available heliocentric velocities for the Cen A satellites, taken from the Local Volume catalog (Karachentsev et al. 2004, 2013). The vast majority of satellites have accurate distances derived from the tip magnitude of the red giant branch (TRGB) method with a typical uncertainty of ≈ 5 percent. There are 31 confirmed satellites of Cen A with accurate distance measurements. Half of them have measured LoS velocities. One sample galaxy (KKs 59) has a measured velocity but lacks a TRGB distance: we adopt the same distance as for Cen A; excluding this galaxy does not change our results. The adopted data are listed in Table S1.

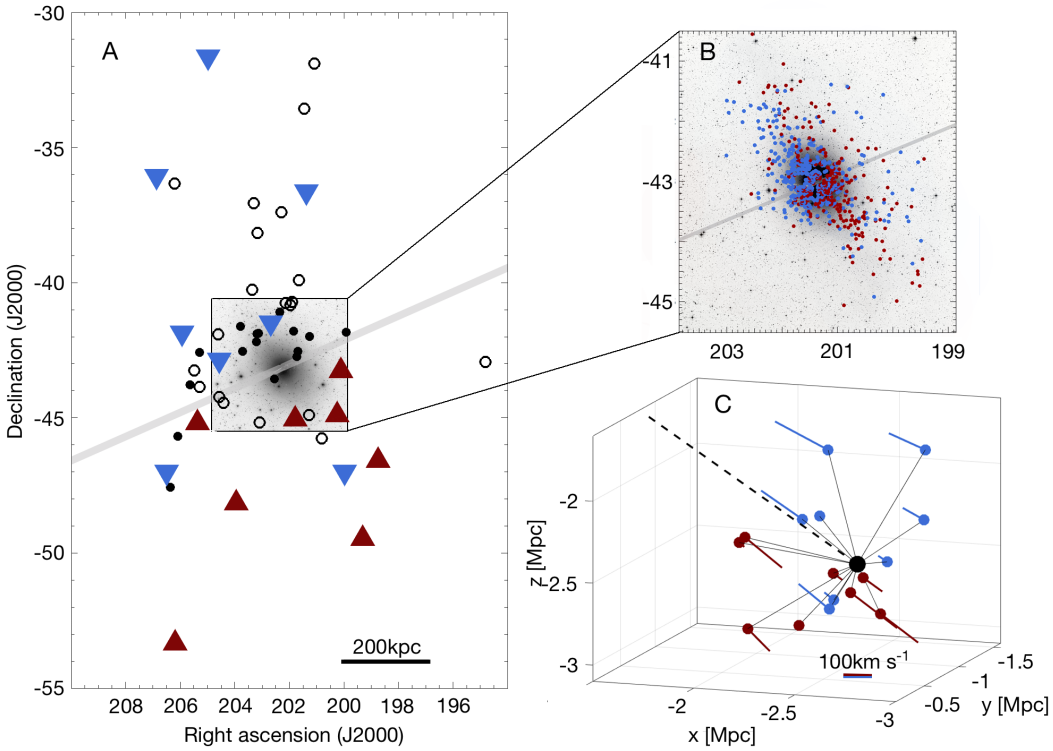

Fig. 1: On-sky and 3D distribution of the satellite system. A: The on-sky distribution of the Cen A subgroup. The central image of Cen A has been scaled up by a factor of five to illustrate the features of the host galaxy. Blue downwards and red upwards pointing triangles show approaching and receding satellite galaxies with respect to Cen A velocity, respectively. Open circles are group member candidates, filled circles are confirmed satellites without velocity measurements. The line that optimally separates the approaching/receding satellites is indicated with the wide grey band; it coincides with the dust lane of Cen A. B: The kinematic distribution of 1239 planetary nebulae (Walsh et al. 2015). Blue PNs are approaching, red PNs are receding relative to Cen A. C: 3D representation of the spatial distribution of the Cen A satellite galaxies in equatorial Cartesian coordinates (the Earth is at $x = y = z = 0$). The length of the colored lines is proportional to the observed velocity, the dashed line is our line of sight towards Cen A.

The on-sky distribution of the satellites is plotted in Fig. 1 together with their motions relative to Cen A. Figure 1 also shows the positions and kinematic information for 1239 planetary nebulae (Walsh et al. 2015) and the 3D distribution of the satellites with measured velocities. The mean velocity of the Cen A satellite system (555 km s^{-1}) is equal to the recession velocity of Cen A (556$\pm$10 km s^{-1}) within the measurement uncertainties. Hereafter, the recession velocity of Cen A is used as a zero-point reference and the terms approaching/receding are intended with respect to this velocity. The dust lane of Cen A serves as a natural dividing line: its position angle ($PA = 110°$) roughly coincides with the geometrical minor axis of the satellite plane (Müller et al. 2016). Clearly, approaching and receding satellites tend to lie to the South-West and North-East of the dividing line, respectively, indicating a kinematically coherent structure.

To determine the statistical significance of the kinematic coherence, we compare the velocities of Cen A satellites to a random phase-space distribution. Every galaxy has

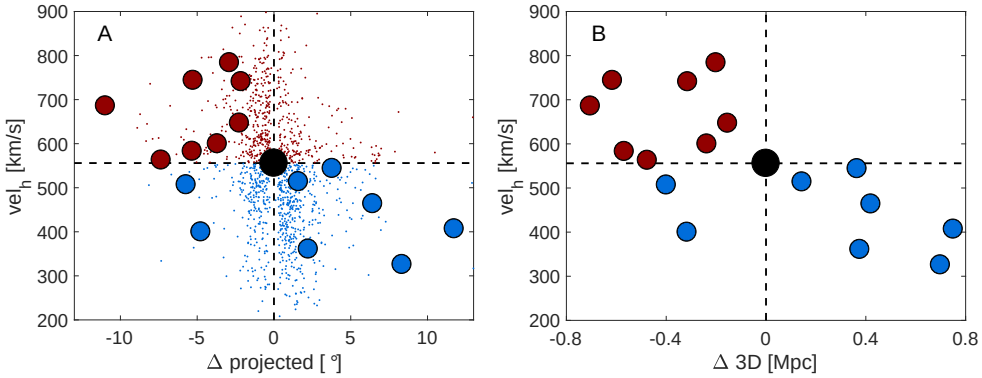

Fig. 2: Velocities and separations to Cen A. Heliocentric velocities versus angular (A) and 3D (B) distances from Cen A (black dot), in the North (positive Δ) or South (negative Δ) of the dust lane. Large and small dots show, respectively, satellite galaxies and planetary nebulae. Blue and red colors indicate, respectively, approaching and receding objects with respect to the Cen A velocity. The angular distances of the PNs are scaled up by a factor of ten.

a 50% chance of approaching or receding along the LoS. The probability of finding at least 14 out of 16 galaxies with coherent velocity movement is 0.42%. Consequently, the observed velocity pattern of the Cen A satellites is statistically different from a random phase-space distribution at the 2.6σ confidence level.

Figure 2 shows the heliocentric velocities of the satellite galaxies as a function of their distances to Cen A. The geometrical minor axis of the plane (or equivalently the dust lane) is used to assign a positive or negative sign to the distance between satellite galaxies and Cen A. Figure 2 shows a clear trend: galaxies to the South of Cen A are approaching, whereas galaxies to the North are receding. This is to be expected if the satellites are rotating around Cen A. Only two satellite galaxies (KK 221 and ESO 269-058) deviate from this trend and may potentially be counter-rotating, analogous to the Sculptor dwarf in the Milky Way halo (Pawlowski et al. 2011). An inspection of their properties and alignment inside the plane does not reveal any peculiar characteristics (e.g., they are not more massive or luminous than other satellites). The velocity field of the planetary nebulae within Cen A follows a similar trend: planetary nebulae in the northern and southern hemisphere are (on average) systematically blue and red shifted, respectively.

To explore the observed velocity pattern for the satellite galaxies, we ran three statistical tests, namely Pearson's R, Spearman's Rho, Kendall's Tau. These are standard methods to test correlations between independent variables. While the Pearsons's method tests for a strictly linear correlation, the Spearman's Rho and Kendall's Tau methods test for a general correlation between the variables. The null hypotheses is that velocities and separations are uncorrelated. The velocity pattern is significant within a confidence interval of 2σ (p-value < 0.03) for the projected separation and 3σ (p-value < 0.01) for the 3D separation (see Supplementary Materials). These low p-values lead us to reject the null hypothesis, implying a

small chance of finding such a correlation in random, normal distributed data. We further consider how much more likely the hypothesis of correlated data is in respect to the hypothesis of uncorrelated data. We applied a Bayesian correlation test (Wetzels & Wagenmakers 2012) and found that the scenario of coherently moving satellites is 4.5 times more likely using the projected separation and 16.5 times more likely using the full 3D information than uncorrelated satellite movements (see Supplementary Materials). Projected separations consistently give lower statistical significance than 3D distances because they contain less physical information: this highlights the importance of having TRGB distance measurements for dwarf galaxies in Centaurus.

3. Implications for galaxy formation

The satellite galaxies in the Cen A subgroup collectively form a coherent kinematical structure. Comparable structures have been discovered in the Milky Way halo, where the majority of the 11 classical satellites share a coherent orbital motion (established with proper motion measurements of individual stars from the satellites) (Pawlowski & Kroupa 2013), and for the Andromeda galaxy, for which 13 out of 15 satellites follow a coherent LoS velocity trend (Ibata et al. 2013).

While we find that the kinematics of the Cen A satellites are unlikely to occur by chance, this does not immediately allow us to draw conclusions about its agreement with predictions from ΛCDM cosmology. Satellite galaxy systems in cosmological simulations generally exhibit some degree of phase-space coherence, due to the accretion of sub-halos from preferred directions, along filaments and in groups (Zentner et al. 2005). To judge whether this effect is sufficient to explain the observed coherence in the Cen A satellites, we determined the occurrence of such extreme structures in two cosmological simulations: Millennium II (Boylan-Kolchin et al. 2009) and Illustris (Vogelsberger et al. 2014). Millennium II is a dark-matter-only N-body simulation that includes gravitational effects such as sub-halo accretion from filaments, but neglects baryonic effects such as stellar and black-hole feedback and possible destruction of satellite galaxies due to the enhanced tidal effects from the baryonic disk (Garrison-Kimmel et al. 2017). The relative importance of these effects is highly debated (Buck et al. 2016; Gillet et al. 2015; Bahl & Baumgardt 2014; Bullock & Boylan-Kolchin 2017). Hence, we also analyze the hydrodynamical Illustris simulation (Vogelsberger et al. 2014), which additionally includes gas physics, star formation, and feedback processes.

Our approach is analogous to recent studies of the frequency of the satellite planes around the Milky Way and the Andromeda galaxy (Pawlowski et al. 2014; Cautun et al. 2015a). We identify Cen A analogs within the simulations by selecting dark matter halos with masses between $4 - 12 \times 10^{12}$ solar masses ($M_\odot$) and by rejecting any candidate hosts that have a companion galaxy with dark matter halo mass

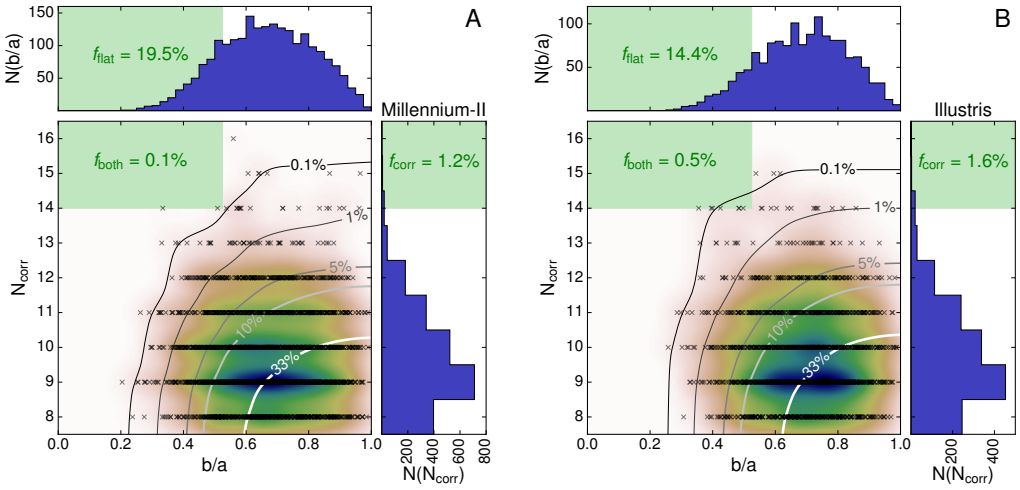

Fig. 3: Comparison to ΛCDM cosmological simulations. The number of kinematically correlated satellites $N_{\rm corr}$ and the on-sky axis-ratio flattening b/a are plotted for Cen A analogs from the Millennium II (panel A) and Illustris (panel B) simulations. The density of simulated systems is indicated by the color map. The contours show the frequency of more extreme realizations, i.e., the number of points to the upper left of each position divided by the total number of realizations. The top and right histograms show the number of realizations with a given axis ratio $N(b/a)$ and a given number of correlated velocities $N(N_{\rm corr})$, respectively. The green areas delineate the regions in which systems are as or more extreme than the observed one: $f_{\rm flat}$, $f_{\rm corr}$, and $f_{\rm both}$ give the frequency of realizations that are, respectively, at least as flattened as the observed system, at least as kinematically correlated, or both. A system has to fulfill both conditions simultaneously to reproduce the observed properties of the Cen A satellite system.

$\geq 1 \times 10^{12} M_{\odot}$ within 1.4 Mpc distance. We require a simulated galaxy-satellite system to fulfill two simplified criteria to be considered similar to the observed system: (i) the projected on-sky axis ratio of the system must be $b/a \leq 0.52$, where a and b are the semi-major and semi-minor axes, respectively, and (ii) the kinematic coherence along the long axis is at least 14 out of 16 satellites. We find that the occurrence of arrangements similar to Cen A in the cosmological simulations is 0.1 per cent for Millennium II and 0.5 per cent for Illustris (Fig. 3). These estimates must be considered upper limits, since we do not take into account the full 3D distribution of satellite galaxies. Even though the hydrodynamical Illustris simulation does contain a higher frequency of systems analogous to Cen A than the dark-matter-only Millennium II simulation, they are rare cases in both. The observed Cen A satellite system is thus in serious tension with the expectations from these ΛCDM simulations, to a similar degree as the satellite planes in the Local Group.

Could the coherent motion be the result of cosmic expansion? If that were the case, a correlation between the velocities of the satellites and their distances to the Milky Way would be expected. This is not found for the sample of Cen A satellite galaxies (Figure 1, C). We thus can rule out that the cosmic expansion is responsible for the observed velocity field. Another possible origin of a velocity gradient is a perspective effect. For angular offsets δ along the direction of motion, a fraction $\sin(\delta)$ of a system's bulk tangential velocity is projected along the line of sight (van der Marel &

Guhathakurta 2008; Salomon et al. 2016). The velocity gradient found for the Cen A system in Fig.2 implies a tangential velocity of the order of 1,000 km s^{-1}, comparable to what would be required for the Andromeda satellite plane (Ibata et al. 2013). This is unphysically high given that it exceeds the cosmic expansion at the distance of Cen A by a factor of 3.7. Such an interpretation of the velocity gradient would imply that the Cen A group moves in the direction defined by the satellite plane, which is unlikely. Another potential systematic issue is the contribution to the LoS velocity by the motion of the Sun around the Galactic centre. However, we found that this contribution is negligible: -2 to -4 km s^{-1}, depending on the sky position, well within the uncertainties of the heliocentic velocity measurements (Table S1).

The coherent kinematics of the Cen A satellites, instead, is best explained by corotation within the plane. We explored a toy model with purely circular orbits and tried to deproject the LoS velocities into circular velocities (see Supplementary Materials). The results were unsatisfactory as many satellites would have unrealistic circular velocities, which randomly vary with the distance from Cen A. This suggests that the satellites must be on elliptical orbits, as expected for collisionless objects. Two galaxies do not follow the general trend: they may be counter-rotating, or on highly elliptical orbits, or simply unrelated to the planar structure. PNe provide additional evidence (Peng et al. 2004): they also show coherent motion albeit this is less pronounced than for the dwarf satellites, only 65% of PNe partake in the common motion (Figure 1). Since the same trend is present in two independent populations of objects with different orbital times, we can expect this correlation to be long lived and thus indicative of corotation within the planes.

Corotation outside the Local Group has been investigated using satellite galaxy pairs on opposite sides of their hosts (Ibata et al. 2014a). The LoS velocities of satellite pairs are preferentially anti-correlated, suggesting a high incidence ($> 50\%$) of corotating satellite pairs in the Universe (Ibata et al. 2014a), although that result remains controversial (Phillips et al. 2015; Cautun et al. 2015b; Ibata et al. 2015). For the Cen A subgroup, the presence of a plane of satellite galaxies is known independently of velocity information and is established using multiple group members. This is unlike previous studies, which were unable to determine whether specific pairs of satellites actually lie in a plane (Ibata et al. 2014a).

In alternative frameworks for the formation of dwarf galaxies, co-rotating planes of satellites could be a consequence of past interactions and mergers between disk galaxies (Pawlowski & Kroupa 2013). During galaxy mergers, tidal tails form from disk material due to angular momentum conservation and can collapse into tidal dwarf galaxies (Hibbard et al. 2001; Bournaud et al. 2007; Lelli et al. 2015). Hydrodynamical simulations show these may survive the interaction and begin orbiting around the central merger remnant as dwarf satellites (Bournaud & Duc 2006; Ploeckinger et al. 2015). In the Local Group, a major merger forming the

Andromeda galaxy has been proposed as a possible origin of the observed satellite galaxy planes around both the Milky Way (Fouquet et al. 2012) and the Andromeda galaxy (Hammer et al. 2013). The recent finding of a correlation between the size of spiral galaxy bulges (thought to form via major mergers) and the number of satellites is in agreement with this picture (López-Corredoira & Kroupa 2016). Even the existence of some counter-rotating satellites can be understood in this framework (Pawlowski et al. 2011).

In summary, we find evidence for a kinematically coherent plane of satellite galaxies around Cen A, demonstrating that the phenomenon is not restricted to the Milky Way and Andromeda galaxies The kinematic coherence can be understood if the satellites are co-rotating within the plane, as seen around the Milky Way. Considering that the likelihood of finding a single kinematically coherent plane is $\lesssim$0.5% in cosmological ΛCDM simulations, finding three such systems in the nearby Universe seems extremely unlikely.

Acknowledgments

The authors thank Bruno Binggeli and Marina Rejkuba for interesting discussions and helpful inputs. O.M. thanks Eva Schnider for inputs concerning the figures. O.M. is grateful to the Swiss National Science Foundation for financial support. M.S.P. acknowledges that support for this work was provided by NASA through Hubble Fellowship grant #HST-HF2-51379.001-A awarded by the Space Telescope Science Institute, which is operated by the Association of Universities for Research in Astronomy, Inc., for NASA, under contract NAS5-26555. H.J. acknowledges the support of the Australian Research Council through Discovery Project DP150100862. The work of F.L. is supported by an ESO postdoctoral fellowship. The Millennium-II Simulation databases used in this paper and the web application providing online access to them were constructed as part of the activities of the German Astrophysical Virtual Observatory (GAVO). The Illustris Simulation databases are provided by the Illustris Collaboration. The observational data we used are given in Table S1. The software for our Monte Carlo analysis is provided in Data S1, and the catalogues of Cen A analogues in the simulations are in Data S2 and S3. The authors thank the anonymous referees for the helpful comments that improved the paper.

Supplementary Materials
www.sciencemag.org

- Materials and Methods
- Supplementary online text
- Figs. S1, S2
- Tables S1, S2
- References (53-70)
- Movie S1
- Data S1, S2

Supplementary Materials

Materials & Methods

The coordinates, distances and heliocentric velocities of the galaxies used in this work are compiled in Table S1. The coordinates and distances are adopted from (Tully et al. 2015; Müller et al. 2016). The heliocentric velocities are taken from the online version[5] of the Local Volume catalog (Karachentsev et al. 2004, 2013), a compilation of objects within 11 Mpc from the Local Group (Tully et al. 2015). The main source of distance estimates are TRGB measurements using the Hubble Space Telescope. This method uses the sharp upturn in the stellar luminosity function produced by the red giant stars leaving the red giant branch during the explosive onset of the helium burning phase of evolution. The velocities were measured using either the 21-cm hydrogen emission line (H I line) as part of the blind H I Parkes All Sky Survey (HIPASS) (Barnes et al. 2001), or via dedicated optical spectroscopy of individual targets using various absorption lines (e.g. Balmer lines and Ca II).

General test of kinematic coherence for a planar satellite distribution

If the heliocentric velocities of satellite galaxies are related to their planar distribution, the split between approaching and receding satellites should be maximal when the separation line is equal to the geometrical minor axis of the plane. To test this hypothesis we separate the satellite population with dividing lines centered on Cen A and PA in the range $0^\circ - 180^\circ$ (North to East). Fig. S1 shows that the number of satellite galaxies with coherent velocities is highest (14 coherent moving satellites out of 16, or 88%) when the separation line corresponds to the geometrical minor axis of the Cen A system and smallest when it is close to the major axis ($0^\circ < PA < 20^\circ$ and $175^\circ < PA < 180^\circ$). The maximum coherence is actually achieved within two broad PA ranges ($85^\circ < PA < 110^\circ$ and $125^\circ < PA < 155^\circ$). There is no a-priori reason why these intervals should include the geometric minor axis of the plane. This demonstrates that both satellite positions and velocities are consistent with a co-rotating plane. We performed the same test with the available kinematic data for planetary nebulae and found agreement within 5 percent.

Tests of correlation between LoS velocities and separations to Cen A

To explore the relation between the line-of-sight velocities of satellite galaxies and their separations to Cen A, we applied three different correlation tests to the data: the Pearson's R test, the Spearman's Rho test, and the Kendall's Tau test. The

[5] last checked: 11 December 2017

resulting correlation coefficient is a number between -1 and 1, where ± 1 indicates a perfect positive or negative correlation, while 0 means no correlation. We used the algorithms implemented in the statistics toolbox of Matlab. The tests were applied on the velocities and projected/3D separations of all galaxies. Every test finds a correlation within a 95% confidence level. The correlation values (and corresponding p-values) for the projected separations are -0.599 (0.011), -0.529 (0.031), and -0.382 (0.034), respectively. For the 3D separation we find correlation within a 99% confidence level, the values are are -0.682 (0.003), -0.618 (0.010), and -0.485 (0.006), respectively. Overall, there is strong evidence for correlated motion.

Monte Carlo simulations of the kinematic coherence

To further assess the kinematic coherence, we performed Monte Carlo simulations where we shuffled the measured velocities and randomized the sign of the 3D separation. Hence, every galaxy is assigned a new but measured velocity value. Its relative position to Cen A (north or south) is decided by a fair coin flip. As we measure the separation of Cen A to its satellites, this coin flip corresponds to randomizing the angles and keeping the radius fixed (in 50% of the cases the satellite will lie to the north of Cen A, in 50% to the south). On this new dataset, the three correlation tests were applied. This was repeated 100,000 times. The measured p-values follow uniform distributions, meaning that there is no favorite setup for correlated satellites. Figure S2 shows a histogram of all correlation values in the Monte Carlo simulation. The correlations follow normal distributions with the mean around 0 (= no correlation). Our observed correlation values lie in the 3σ tail.
We repeated this Monte Carlo method for the projected separation and confirm the previous results. As we used fixed distances we further investigated how the distance uncertainties affect our results by repeating the test, but this time randomizing the distance within a normal distribution (mean $\mu = D$ and standard deviation $\sigma = 5\%$ uncertainty) for every run. This again confirms our prior results.

Bayesian analysis

P-values smaller than 0.01 indicate a small chance of finding such a correlation in random, normal distributed data. We therefore consider how much more likely the hypotheses of correlated data is in respect to the null hypothesis of uncorrelated data. The Bayes Factor BF quantifies the evidence of a model M_1 in favor of an alternative model M_0. Here M_1 will correspond to correlated data, M_0 to uncorrelated data. The Bayes Factor is (Wetzels & Wagenmakers 2012):

$$BF = (n/2)^{1/2} \cdot \Gamma(1/2)^{-1} \cdot \int_0^\infty (1+g)^{(n-2)/2}[1+(1-r^2)g]^{-(n-1)/2} g^{-3/2} \mathsf{e}^{-n/(2g)} dg \tag{5.3}$$

where n is the number of data points, Γ is the Gamma function, g is the g-prior, and r is Pearson's correlation value. A value of BF larger than 1 favors the model M_1, otherwise it favors the model M_0. This numerical integration gives $BF = 4.53$ and $BF = 16.56$, respectively, meaning that with the given data the model M_1 is more likely than M_0, hence coherent moving satellites are indeed the statistically-favoured model.

Test of circular orbits within the satellite plane

We tested whether the satellite galaxies are on circular orbits within the plane. In such circumstance, the circular velocity $V_{\rm c}$ of the satellite is related to its line-of-sight velocity $V_{\rm LoS}$ via the following equation:

$$V_{\rm LoS} = V_{\rm Cen\,A} + V_{\rm c} \sin(i) \cos(\theta) \tag{5.4}$$

where $V_{\rm Cen\,A}$ is the systemic velocity of Cen A, i is the inclination of the plane with respect to the sky, and θ is the azimuthal angle of the satellite within the plane. The azimuthal angle can be easily estimated by choosing a face-on orientation for the satellite plane.

The circular velocities of the satellites are expected to either decrease with distance from Cen A (like planets in the Solar System) or to reach a constant value (like gas and stars within galaxies). Instead, we find that the values of $V_{\rm c}$ vary randomly from galaxy to galaxy, suggesting that the orbits cannot be circular. Varying the distance of satellites within the uncertainties does not improve the result, hence we conclude that the orbits must be elliptical.

Comparison to ΛCDM simulations

To determine how common the Cen A's satellite system is in ΛCDM simulations, we compare to two publicly available simulations: the dark-matter-only Millennium II simulation (Boylan-Kolchin et al. 2009) and the hydrodynamical Illustris simulation (Vogelsberger et al. 2014; Nelson et al. 2015) which includes prescriptions for gas physics, star formation, and feedback processes. Specifically, for Millennium II we adopt the redshift zero galaxy catalogue (Guo et al. 2013) which re-scales the simulation to Wilkinson Microwave Anisotropy Probe 7 (WMAP) cosmological parameters, while for Illustris we use the redshift zero catalog of the highest-resolution Illustris-1 run (Nelson et al. 2015). We select as possible host galaxies all dark matter halos with a virial mass in the range of $4.0 \text{ to } 12.0 \times 10^{12}\,M_{\odot}$. This mass range is selected to be consistent with several different halo mass estimates for Cen A (Woodley 2006; Woodley et al. 2007; Karachentsev et al. 2007; Woodley et al. 2010). Cen A is an isolated galaxy: its closest massive neighbor is M 83 which lies 1.1 Mpc behind Cen A and $\sim$13° degrees away. Thus, to make sure our host halos are similarly isolated as

Cen A, we reject all possible hosts which have another halo of mass $\geq 1.0 \times 10^{12}\,M_{\odot}$ within a distance of 1.4 Mpc. This leaves us with 222 (Millennium II) and 146 (Illustris) isolated host galaxies.

For each host, 10 randomly oriented sight-lines are chosen, and the host and its surrounding galaxies are placed at Cen A's distance of 3.68 Mpc from the observer's point of view. We then mock-observed the galaxy systems from this orientation, by projecting the angular positions relative to the host as well as the line-of sight velocities. All galaxies within 12° and separated by less then 0.8 Mpc from the host are recorded as satellite galaxies. This is independent of whether they are actually within the virial radius of the simulated host halos. Nevertheless, in the following we will refer to them as satellites for simplicity. We also reject all satellites within 1° of the LoS to the host, since these would be unobservable in front of Cen A (the closest Cen A satellite with a measured line-of-sight velocity is ESO324-024 at an angular distance of $\sim$1.6°). Only satellites with an r-band magnitude of -9 or brighter are considered in Illustris. This avoids selecting dark sub-halos that did not form any stars. We rank these satellites by their peak virial mass (Millennium II) or r-band magnitude (Illustris), and select at random 16 satellites ($N_{\rm kine}$) out of the top 30 satellites ($N_{\rm sat}$). This is because kinematics (line-of-sight velocities) are only known for 16 out of the $\sim$30 Cen A satellites with measured distances (Tully et al. 2015). To test whether this selection affects the results we also repeat the analysis while selecting only the top $N_{\rm sat} = 16$ satellites. For Millennium II, in all cases a sufficient number of satellites was found within the mock survey volume. This leaves 2220 realizations of satellite systems ($N_{\rm realizations}$). In Illustris, a few realizations do not contain a sufficient number of satellites and are excluded, such that $N_{\rm realizations} = 1441$ (if the top 30 satellites are chosen) and $N_{\rm realizations} = 1459$ (if the top 16 satellites are chosen) are included in the analysis out of 1460 generated systems.

To avoid the look-elsewhere-effect, we apply some simplified criteria which the simulated satellite system has to fulfill to be counted as comparably correlated to the observed Cen A system. This effectively results in an upper limit on the frequency of satellite systems as correlated as that of Centaurus A, i.e., we underestimate any tension with the ΛCDM simulation. We measure the overall flattening of the 16 satellite system on the sky and its kinematic coherence. By considering only the overall two-dimensional (projected) flattening, we avoid uncertainties based on distance measurements and the possibility of there being two parallel planes (see (Tully et al. 2015; Müller et al. 2016) for discussion). We measure the flattening b/a by finding the short and long axes of the distribution using the tensor of inertia method (Pawlowski et al. 2015b) and calculating the root-mean-square extend of the satellites along these axes. The kinematic coherence $N_{\rm corr}$ is measured as for the observed system, along the direction defined by the long axis of the satellite distribution. Applying the algorithm to the 16 observed Cen A satellites with

measured kinematics, we obtain $b/a = 0.52$ and $N_{\rm corr} = 14$. The results are compiled in Table S2, and illustrated in Fig. 3. In the following we study the frequency of finding Cen A like analogues in the cosmological simulations as flattened as the observed system ($f_{\rm flat}$); as kinematically correlated as the observed system ($f_{\rm corr}$); and fulfilling both criteria simultaneously ($f_{\rm both}$).

For Millennium II, we find that 433 out of 2220 realizations contain satellite systems that are at least as flattened ($b/a \leq 0.52$) as Cen A on the sky ($f_{\rm flat} = 19.5$ per cent) and 26 that are sufficiently kinematically correlated ($N_{\rm corr} \geq 14$; $f_{\rm corr} = 1.17$ per cent). This is in line with earlier findings (Pawlowski et al. 2012a) indicating that satellite systems in ΛCDM simulations are somewhat, but not strongly, more correlated than perfectly isotropic systems (for which the frequency of equally strong kinematic correlation would be 0.42 per cent). Only 2 out of our 2220 realizations are simultaneously sufficiently flattened and sufficiently kinematically correlated to match the observed Cen A satellite system ($f_{\rm both} = 0.09$ per cent). This makes the Cen A system a $\geq 3.3\sigma$ outlier, indicating that it is a rare exception in ΛCDM. This low frequency is comparable to those reported for the satellite planes around the Milky Way and Andromeda (Ibata et al. 2014b; Pawlowski et al. 2014). Even if we pre-select only those simulated satellite systems which are at least as extremely flattened as the observed system, only 0.46 per cent of these (2 of 433) display a kinematic coherence at least as extreme as that observed for Cen A. This number is consistent with that expected from random velocities.

The Millennium II galaxy catalogue contains so-called orphan galaxies: objects that are tracked even after their host dark matter halo has been disrupted. Their positions may be unreliable. Excluding these objects from our analysis reduces the frequency of sufficiently flattened (to 289 or 13.0 per cent) and sufficiently kinematically coherent (to 17 or 0.77 per cent) systems. The frequency of realizations fulfilling both criteria simultaneously stays the same (2 or 0.09 per cent).

For Illustris, 207 out of 1441 realizations are as flattened as Cen A on the sky ($f_{\rm flat} = 14.4$ per cent), which is lower than for Millennium II ($f_{\rm flat} = 19.5$ per cent). On the other hand, Illustris results in slightly higher frequencies of kinematically correlated satellite systems (23 out of 1441 realizations, or $f_{\rm corr} = 1.6$ per cent) and of systems fulfilling both the flattening and the correlation criteria (7 out of 1441 realizations, or $f_{\rm both} = 0.49$ per cent). The sample sizes of satellite systems in both simulations are too small to decide whether these are genuine effects of the modelling of baryonic physics in the Illustris simulation, or simply stochastic fluctuations.

Two of the observed satellite galaxies have line-of-sight velocities that overlap with that of Cen A within the uncertainties: NGC 4945 and NGC 5011C. In the unlikely case that both satellite velocities are revised to a lower value while Cen A's velocity is also revised to a higher value, this could in principle reduce the number of satellites

with coherent velocities from $N_{\rm corr} = 14$ to $N_{\rm corr} = 12$. In that case, finding a similar coherence in the simulations is more likely ($f_{\rm corr} = 11.2$ and $f_{\rm corr} = 11.5$ per cent for Millennium II and Illustris, respectively). Consequently, the frequency of systems fulfilling both the flattening and the velocity coherence criteria is increased to $f_{\rm both} = 2.16$ per cent for Millennium II and to $f_{\rm both} = 1.67$ per cent for Illustris.

In the previous analysis we randomly selected 16 out of 30 top-ranked satellites to mimic the fact that velocities are only known for a subset of the confirmed Cen A satellites. To test this selection, we have repeated the previous analysis by using only the 16 top-ranked satellites. The results are also shown in Table S2. The resulting frequencies do not differ substantially or systematically from those previously found. This indicates that our selection does not bias our results.

Supplementary Text

Hydrodynamic simulations model baryonic processes such as gas cooling, star formation, stellar and nucleosynthetic evolution, supernova and black hole feedback. These simulations have been used to address discrepancies between ΛCDM and observations on small-scales, which were first identified in dark-matter-only simulations (Bullock & Boylan-Kolchin 2017). Modelling of baryons most directly affect the inner regions of dark matter halos ($\lesssim$10 kpc), since this is where most stars form and eventually explode as supernovae, injecting energy in the surrounding medium. The overall distribution and motion of satellite galaxies concern much larger spatial scales (> 100 kpc), thus they are less directly affected by baryonic effects. However, these may not be entirely negligible. Baryonic effects can change the halo potential relative to a dark-matter-only case if they, for example, lead to the formation of a dark matter core. The formation of a central disk galaxy and resulting potential can furthermore enhance the tidal stripping of satellites. This can bias the distribution of satellite galaxies since the innermost satellites are preferentially destroyed, resulting in radially more extended satellite systems (Garrison-Kimmel et al. 2017). Satellites on more radial orbits are expected to be more affected by tidal stripping, such that the orbital properties of the whole satellite system can also be affected.

In our analysis we find agreement with this tendency of more radially extended satellite systems for hydrodynamical simulations. Even though the same selection cuts are applied (satellites between 1° and 12° from their host, and within 800 kpc), the Cen A analog systems have an average root-mean-square radial extent $\langle R_{\rm rms}\rangle = 5.1^\circ$ in the Millennium II simulation but are more extended in the Illustris simulation with an average $\langle R_{\rm rms}\rangle = 5.9^\circ$. The latter is close to the observed Cen A system, for which we measure $R_{\rm rms} = (6.1 \pm 0.8)^\circ$ with the uncertainty estimated via bootstrap resampling.

The overall flattening and kinematics of satellite systems, however, do not show substantial differences between the dark-matter-only Millennium II and the hydro-

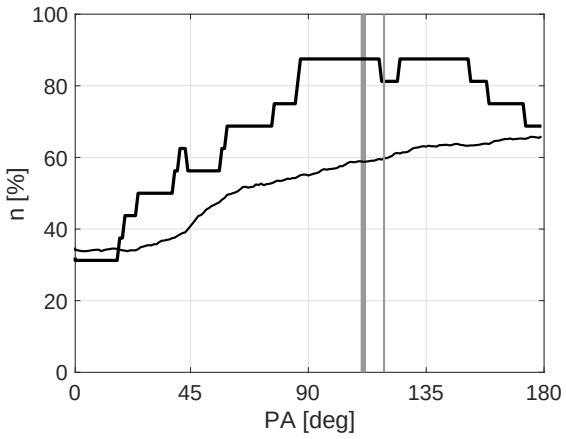

Fig. 1: Alignment of the kinematic coherence. The fraction of approaching/receding satellite galaxies (thick black line) and planetary nebulae (thin black line) with respect to a separation line with variable position angle (PA) centered on Cen A. The thick vertical gray line indicates the position angle of Cen A dust lane ($PA = 110^{\circ}$). The thin gray lines is the position angle ($PA = 119^{\circ}$) of the satellite plane projected minor axis.

dynamic Illustris simulation. Hence, we conclude that there is no evidence that baryonic effects are sufficient to result in a substantially increased fraction of extreme satellite planes comparable to the observed Cen A system.

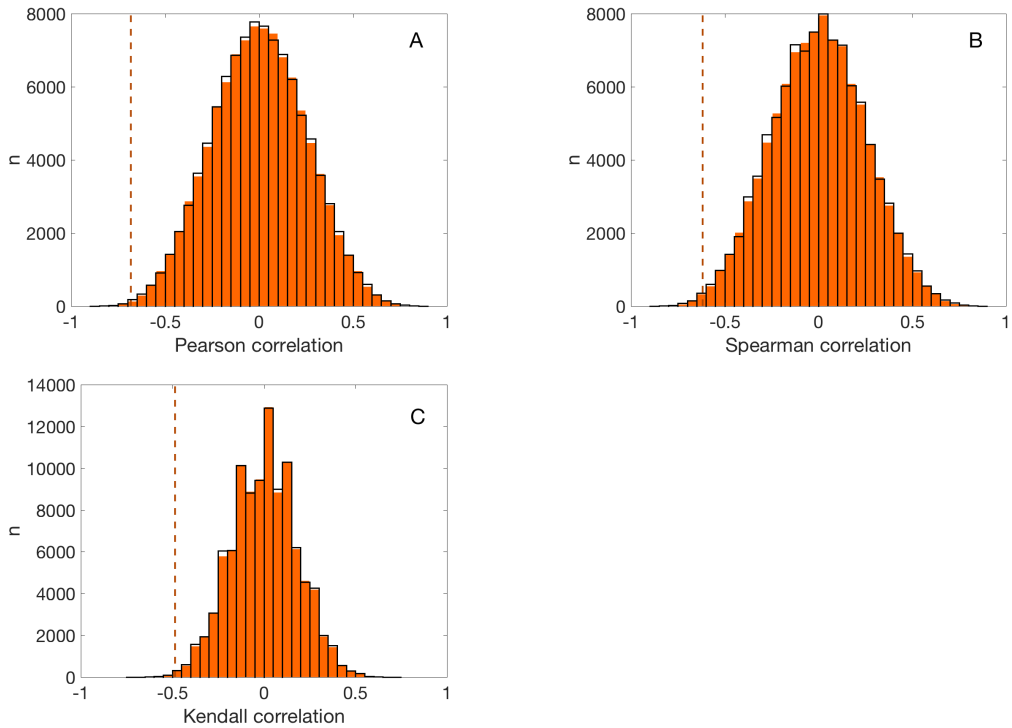

Fig. 2: Monte Carlo simulations. Results from Monte Carlo simulations for the three different correlation tests without (orange bins) and with (black line) considering the distance uncertainties. A correlation value of ± 1 corresponds to fully correlated data in positive or negative direction, respectively. The vertical dashed lines correspond to the measured correlation in the observed data. The bin width is 0.05.

Caption for Movie S1

The movie starts by showing the 3D spatial distribution of all confirmed satellites of Cen A (black dots) and the candidate members (open circles) with their predicted distances (Müller et al. 2016) in equatorial cartesian coordinates. The dashed line is our line-of-sight towards Cen A. The plane of satellites (gray) is faded in. Then, the satellites without measured velocities are faded out and the kinematic information of the satellites is presented by a color and a line (red and blue for receding and approaching, respectively). The length of the lines is proportional to the observed velocity.

Tab. 1: Data used in this work. Members of the Cen A subgroup (Karachentsev et al. 2004, 2013; Tully et al. 2015; Müller et al. 2016) with known distances and radial velocities. For KKs 59 we adopted the same distance as Cen A because there is no accurate TRGB distance available. (a): galaxy name, (b): right ascension in epoch J2000, (c): declination in epoch J2000, (d) galaxy distance, (e): reference for the distance measurement, (f): galaxy heliocentric velocity, and (g): reference for the velocity measurement.

Galaxy Name	α_{2000} (degrees)	δ_{2000} (degrees)	D (Mpc)	Reference	v_h (km s^{-1})	Reference
(a)	(b)	(c)	(d)	(e)	(f)	(g)
ESO 269-037	195.8875	−46.5842	3.15±0.09	(Karachentsev et al. 2004, 2013)	744±2	(Karachentsev et al. 2004, 2013)
NGC 4945	196.3583	−49.4711	3.72±0.03	(Tully et al. 2015)	563±3	(Koribalski et al. 2004)
ESO 269-058	197.6333	−46.9908	3.75±0.02	(Karachentsev et al. 2004, 2013)	400±18	(Banks et al. 1999)
ESO 269-066	198.2875	−44.8900	3.75±0.03	(Karachentsev et al. 2004, 2013)	784±31	(Jerjen et al. 2000b)
NGC 5011C	198.2958	−43.2656	3.73±0.03	(Karachentsev et al. 2004, 2013)	647±96	(Saviane & Jerjen 2007)
KK 196	200.4458	−45.0633	3.96±0.11	(Karachentsev et al. 2004, 2013)	741±15	(Jerjen et al. 2000a)
NGC 5102	200.4875	−36.6297	3.74±0.39	(Tully et al. 2015)	464±18	(Doyle et al. 2005)
Cen A	*201.3667*	*−43.0167*	*3.68±0.05*	(Karachentsev et al. 2004, 2013)	*556±10*	(Koribalski et al. 2004)
ESO 324-024	201.9042	−41.4806	3.78±0.09	(Karachentsev et al. 2004, 2013)	514±18	(Doyle et al. 2005)
NGC 5206	203.4292	−48.1511	3.21±0.01	(Karachentsev et al. 2004, 2013)	583±6	(Peterson & Caldwell 1993)
NGC 5237	204.4083	−42.8475	3.33±0.02	(Karachentsev et al. 2004, 2013)	361±4	(Koribalski et al. 2004)
NGC 5253	204.9792	−31.6400	3.55±0.03	(Tully et al. 2015)	407±3	(Koribalski et al. 2004)
KK 211	205.5208	−45.2050	3.68±0.14	(Karachentsev et al. 2004, 2013)	600±31	(Puzia & Sharina 2008)
ESO 325-011	206.2500	−41.8589	3.40±0.05	(Karachentsev et al. 2004, 2013)	544±1	(Kirby et al. 2012)
KK 221	207.1917	−46.9974	3.82±0.07	(Karachentsev et al. 2004, 2013)	507±13	(Puzia & Sharina 2008)
ESO 383-087	207.3250	−36.0614	3.19±0.03	(Karachentsev et al. 2004, 2013)	326±2	(Koribalski et al. 2004)
KKs 59	206.9920	−53.3476	3.68*		686±1	(Kirby et al. 2012)

Tab. 2: Comparison to ΛCDM simulations. Frequencies of realizations of satellite systems in the Millennium II and Illustris simulations being as flattened ($f_{\rm flat}$) and as kinematically correlated ($f_{\rm corr}$) as the observed Cen A system, or fulfilling both criteria simultaneously ($f_{\rm both}$).

Simulation sample	$N_{\rm realizations}$	$N_{\rm kine}/N_{\rm corr}$	$f_{\rm flat}$ (%)	$f_{\rm corr}$ (%)	$f_{\rm both}$ (%)
16 out of top 30 satellites					
Millennium II	2220	14/16	19.5	1.17	0.09
Illustris	1441	14/16	14.4	1.60	0.49
Millennium II	2220	12/16	19.5	11.2	2.16
Illustris	1441	12/16	14.4	11.5	1.67
Top 16 satellites					
Millennium II	2220	14/16	17.5	0.50	0.18
Illustris	1459	14/16	15.9	1.30	0.27
Millennium II	2220	12/16	17.5	10.7	2.34
Illustris	1459	12/16	15.9	13.6	2.26

Conclusion

5

In the last Chapter I have presented the papers I have published as first-author during my PhD studies. Let me briefly review the main findings and finally provide an outlook on how to continue from hereon.

5.1 Summary of this thesis

In Sections 5.1 - 5.4 we reported the discovery of 108 new dwarf galaxies in the Local Volume – which is ∼10% of its currently known dwarf galaxy population – using dedicated time at the Dark Energy Camera and publicly available data from the Sloan Digital Sky Survey. Their morphology and structural parameters suggest memberships of the corresponding galaxy groups, i.e. the Centaurus group, the M 101 group, and the Leo-I group. We have started to follow up the dwarf galaxies in the Centaurus group with the Very Large Telescope – the largest optical telescope in the southern hemisphere – by resolving their red giant branch population and confirmed two dwarf galaxies to be associated to M 83 (Section 5.5). These dwarfs, together with the other known dwarf galaxies around M 83, suggest another planar structure in the Centaurus group with geometric properties similar to those of the Local Group. The dwarf galaxies in the M 101 group again seem to be aligned in a flattened structure, extending over several Megaparsec (Section 5.3).

With the addition of new dwarf galaxies around Cen A we have shown that there is likely only one plane-of-satellites (Section 5.6), in contrast to the two planes proposed by Tully et al. (2015). Using archival line-of-sight velocities we have studied the motion of these satellites around Cen A and have found strong evidence that the satellites follow a common movement pattern (Section 5.7) – similar to the dwarfs around the Milky Way and the Andromeda galaxy. The satellites to the north are blue-shifted, the satellites to the south are red-shifted, in respect to the mean velocity of the subgroup. With 14 out of 16 satellites being phase-space correlated, this arrangement seems unlikely to be of random occurrence. We have studied this coherently moving plane-of-satellites within the ΛCDM standard model of cosmology, using the best high-resolution N-body simulations available to the public (the Millennium-II and Illustris simulations) and found that this arrangement is highly unlikely, with only 0.1% - 0.5% of the Cen A-analogue systems having a similar phase-space correlation. This, together with the Local Group planes-of-satellites – which have each a similar probability to occur in these simulations – poses a major challenge to our understanding of structure formation in the universe. How is it possible that we observe such rare configurations so frequently? This warrants

further explanations from the cosmology community. Maybe this even points out towards a new paradigm of structure formation.

5.2 New dwarf galaxies in the Local Volume

In Sections 5.1 - 5.4 we have presented new dwarf galaxy candidates in the Local Volume galaxy groups of Centaurus, M 101, and Leo-I. In the following Figure 5.1 the cumulative luminosity distribution[1] is presented for these galaxy groups, with and without our newly detected dwarf galaxies. The cumulative luminosity distribution counts the number of galaxies brighter than a given absolute magnitude. For galaxies, for which no distance measurements are available, a distance corresponding to the group is assumed.

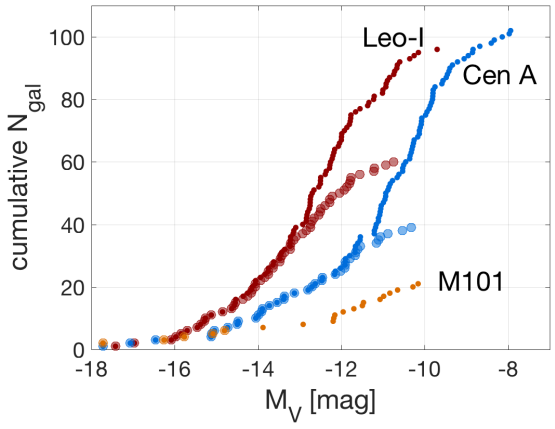

Fig. 5.1: Cumulative galaxy luminosity distribution for the surveyed galaxy groups in the Local Volume. Light points correspond to the luminosity distribution with only previously known dwarf members, filled points to the updated luminosity distribution including our new detections.

In each group we have significantly increased the census of dwarf galaxies over several magnitudes. This is expected as we had deeper imaging data available for our search. As I will discuss in Section 5.4 this is only the first step to map the Local Volume. Surveys in more groups and follow-ups will be needed to compare the several nearby galaxy groups. Still, it is already evident that the different groups have different abundances (see Section 5.4 Figure 7 for the luminosity functions of other galaxy groups in the Local Volume), i.e. different steepnesses at the faint end of the luminosity function. For example: the Leo-I and Centaurus groups have almost twice the number of dwarf galaxies as the Local Group (up to an absolute magnitude of $V = -10$), this is, if the new candidates are confirmed. Moreover, the SDSS studies show that we are able to detect dwarf galaxies up to $V = -10$ mag – the regime of the classical dwarfs.

[1] In Section 5.4 we refereed to this distribution as luminosity function, which is strictly speaking not correct (Schechter 1976). The luminosity function is additionally normalized by the volume the galaxies reside in, while the luminosity distribution only takes the abundance of galaxies per luminosity interval into account. However, if the covered volume is the full extend of the galaxy group, the luminosity distribution corresponds to the luminosity function.

Tab. 5.1: Planar structures in the Local Volume.

Name	rms [kpc]	radius [kpc]	members	Ref.
MW, VPOS	∼20	∼250	25	Pawlowski et al. (2013)
M 31, GPoA	∼15	∼270	19	Pawlowski et al. (2013)
LG plane 1	∼60	∼1000	9	Pawlowski et al. (2013)
LG plane 2	∼70	∼500	5	Pawlowski et al. (2013)
M 81 group	?	∼300	∼20	Chiboucas et al. (2013)
Cen A plane 1	∼70	∼500	∼30	Section 5.6
M 83 plane	∼20	∼210	6	Section 5.5
M 101 plane	∼50	∼260	8	Section 5.3
M 101 wall	∼70	∼1500	13	Section 5.3

5.3 Planes-of-satellites in the Local Volume

While for many galaxy groups in the Local Volume the data is too sparse to study the 3D structures, we already have an idea of how apparent dwarf galaxy planes in the local neighbourhood are with the few systems available for such studies. In Table 5.1 all known planar structures and their properties are compiled.

In the Local Group, the VPOS and the GPoA are thin co-rotating structures surrounding their host galaxies – with a rms thickness smaller than 20 kpc and extents of roughly 250 kpc, corresponding to the virial radii of these systems. Furthermore, between the Milky Way and the Andromeda galaxy there are two extended planar structures – the LG plane 1 and LG plane 2 – which are thicker ($\sim$ 60 kpc) and more extended than the VPOS and GPoA. Intriguingly the LG plane 1 is aligned with the VPOS, pointing towards a common formation history.

Outside the Local Group, Chiboucas et al. (2013) reported a flattened, albeit not flat, structure in the M 81 group of galaxies. However, no rms thickness measurement is given in their paper. A re-analysis of this group could be worth a try, especially in terms of ΛCDM predictions. In Section 5.6 we discussed the two planar structures around Cen A and concluded that it is likely only one thick plane with rms of ∼70 kpc and a radial extent of 500 kpc. Furthermore, we showed that the dwarf galaxies in this plane are again phase-space correlated to the VPOS and GPoA dwarf galaxies (Section 5.7). These three known phase-space correlated planes-of-satellites are shown in Figure 5.2. The similarity is clearly visible, with most of the satellites occupying two of the four quadrants. The second major galaxy in the Centaurus group, the M 83 galaxy, potentially hosts another plane-of-satellites as discussed in Section 5.5. Future measurements will reveal if this is significant. The last group of galaxies known in the Local Volume possessing a flattened structure is the M 101 group. There the satellites of M 101 follow a planar alignment, which extends to M 51 and M 63, well over 3 Mpc. This filamentary wall is extraordinarily thin, with the satellites around M 101 having a rms thickness of only 50 kpc and the extended

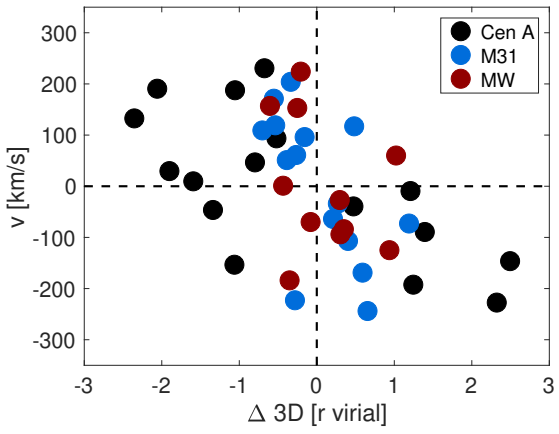

Fig. 5.2: The phase-space correlation of the Milky Way, the Andromeda galaxy, and the Cen A dwarf galaxies. The 3D separation is taken from Pawlowski et al. (2013) and Müller et al. (2018b), the line-of-sight velocities from Karachentsev et al. (2013) and Müller et al. (2018b). For the Milky Way, the line-of-sight velocities were constructed from the 3D velocities by transforming the system such that an observer would see the Milky Way disc and the planar structure edge on (see Figure 1 in Pawlowski 2018). The data was kindly provided by Marcel Pawlowski. The radial extent was scaled to the virial radii of the galaxies, i.e. $r_{virial} = 250$ kpc for the Milky Way, $r_{virial} = 270$ kpc for the Andromeda galaxy, and $r_{virial} = 300$ kpc for Cen A.

wall being marginally thicker with only 70 kpc, by at least a factor 4 thinner than expected from the filaments in the Cosmic Web.

Comparisons to cosmological simulations were only drawn for three galaxy systems, the Milky Way, the Andromeda, and the Centaurus subgroups. For each of these systems the appearance of co-rotating structures in such simulations is around 0.1-1.0%. When we naively multiply these probabilities we obtain a chance between 1 to 10^9 and 1 to 10^6, astronomically small probabilities. However, before we jump to conclusions we need to put this result into perspective and be aware of the underlying assumption going into this probability estimate: each system has an independent formation history and therefore corresponds to an independent random variable. The Milky Way and the Andromeda galaxy are making up the Local Group and are separated by less than 1 Mpc, so their formation will not be completely independent and a simple multiplication of the probabilities is hence not allowed. The Centaurus group on the other hand is four times farther away than the Andromeda galaxy and is isolated in respect to the Local Group, but it resides within the same filament as the Local Group – the Local Sheet. The formation may not be as independent as naively assumed. And more, I ask specifically about the probability of finding Milky Way, Andromeda, and Centaurus like systems, which probably doesn't cover the full possible planar arrangements in the universe and introduces a bias. Still, the individual results tell us that such co-rotating planes-of-satellites are a fairly rare configuration in the cosmological models but a seemingly frequent observation in the nearby universe, warranting an explanation.

To further study a connection between the formation of these structures, a dependence on the local filament should be investigated. The work by Libeskind et al. (2015) already suggests a connection between the planes-of-satellites and the Cosmic Web. The community should start to examine the appearance of planes-of-satellites within their environments in cosmological high-resolution simulations. Do we find

several close-by planes-of-satellites, perhaps within in a thin filament? Such a question should be possible to answer with current studies and available simulations by correlating the appearing Milky Way, Andromeda, and Centaurus analogues in 3D positions and looking for apparent over-densities of such structures.

5.4 Future Work

Here I discuss several projects, some of which have already started, others which are in the planning phase, which will continue the results from this thesis.

Deep optical follow-up: The immediate goal is now to confirm the newly discovered dwarf galaxy candidates and establish their membership by measuring their distances. We have already started such a project using the Very Large Telescope as discussed in Section 5.5, where we were able to resolve the red giant branch stars for two out of three dwarf candidates, therefore confirming their membership in the Centaurus group. Moreover, for 15 more dwarf galaxy candidates in the immediate vicinity of Cen A, we were a granted more time at the Very Large Telescope with FORS2 in ESO's observation period P101, which will be conducted between April and September 2018. This will test the bimodal planar structure suggested by Tully et al. (2015) but challenged by us (Müller et al. 2016) and will further underline whether the planarity is real or not. It will also help to re-establish the exact alignment of the plane, as well as the rms thickness. Another VLT observation proposal for the remaining dwarf galaxy candidates in the Centaurus group was submitted for P102. This will help us to study the whole 3D structure of the galaxy aggregate. In the Local Group, there are dwarf galaxies forming a bridge between the Milky Way and the Andromeda galaxy. Do we find something similar in the Centaurus group? And how about the planar structure we proposed around M 83, is this real or just a statistical fluke?

While it is still possible to resolve the dwarf galaxies up to 5 Mpc with ground-based telescopes (within reasonable exposure times), when going farther away only space-based measurements with the Hubble Space Telescope are feasible. In collaboration with Igor Karachentsev and Brent Tully we have written a proposal to measure the distances of the candidates in the M 101 group, which is at 7 to 9 Mpc. While unsuccessful in the last call for proposals, we aim to resubmit an improved version. The M 101 group is an interesting target due to its apparent lack of galaxies. Its luminosity function is significantly low, as seen in Section 5.4 Figure 7. Sorting out the actual members from contaminants is therefore the next task before a thorough analysis of the dwarf galaxy abundance in this group can be made.

And what about the Leo-I group candidates? At 10 to 11 Mpc, again only space based observations can confirm their memberships. While the M 101 group has the lowest abundance of dwarfs in the Local Volume, the Leo-I group has the highest. This is not surprising, because the Leo-I group hosts many bright galaxies and therefore

has a dense environment. Following up this group will be very expensive due to the many candidates in this group, making it unlikely that such a project will see the light of the day. On the other hand, 5 to 6 of the candidates fall into the regime of the ultra diffuse galaxies – a recent hot topic in the cosmology community[2]. Those candidates are some of the closest objects discovered of this special type of dwarf galaxy and provide an unique testbed to study their stellar population.

MUSE follow-up: The low number of satellites with velocity measurements in the plane-of-satellites around Cen A is a a reason for concern. While it is unlikely that 14 out of 16 satellites share a coherent motion by chance, it is still a possibility. Therefore, we were granted follow-ups for additional 14 dwarf galaxies within the plane-of-satellite around Cen A with MUSE at the Very Large Telescope in ESOs observation Period P101. MUSE is one of the most powerful Integral Field Units in the world – able to measure multiple spectra on a large field of view simultaneously. With one pointing we will be able to get spectra in 2D over large parts of the target galaxies. Using these spectra we can derive the line-of-sight velocities of the galaxies, as well as the internal kinematics and with that their dark matter content for the brightest objects in our target list. We hope to be able to rule out the possibility of a statistical fluke and get a complete sample of velocity measurements for this structure, especially in the immediate vicinity ($\leq$ virial radius). This will help to improve the comparison to cosmological simulations, as well as to the VPOS and GPoA.
On a different note, this project is one of the first of its kind to study low surface brightness objects with MUSE and will provide a benchmark on how far this instrument can be pushed in terms of such low S/N objects. This will be interesting for future studies of the ultra diffuse galaxy population and dwarf galaxies in the nearby universe.

Dwarf galaxy surveys: The Local Volume is still mainly uncharted territory if it comes down to the low-surface brightness population, especially the gas-poor dSph which will remain undetected in large-scale radio surveys. The last thorough search for dwarf galaxies was made with digitized photo plates almost 20 years ago. Since then, with the advance of CCD cameras, multiple public available surveys were conducted covering large areas of the sky, as well as dedicated searches for dwarf galaxies around major galaxies. With the Dark Energy Camera and the SkyMapper telescope we have mapped most of the nearby Sculptor group, and together with the public Dark Energy Survey we will be able to put together an almost complete picture of this loose galaxy aggregate – the first of its kind with the CCD technology.

[2]As a comparison: Merritt et al. (2014) discovered 7 dwarf galaxy candidates in the M 101 group and followed them up with the Hubble Space Telescope. Only 3 candidates were confirmed as dwarf members of M 101 (Danieli et al. 2017) and 4 were false positives and are actually background ultra diffuse galaxies (Merritt et al. 2016). The SAO/NASA ADS Astronomy Abstract Service counts 9 citations for the M 101 HST paper on the resolved dwarf galaxies (i.e. the successful project) and 31 citations for the unresolved ultra diffuse galaxies in the background.

Additionally, surveys like the Dark Energy Survey and the Sloan Digital Sky Survey will allow us to continue our search for dwarf galaxies in publicly available data, as we did for the M 101 and Leo-I groups. Of special interest will be the Canes Venatici cloud with its many dwarf members. The Canes Venatici cloud, together with the Local Group, the Sculptor group and the Centaurus group, forms the so-called Local Sheet, the large-scale filament going through the Local Volume. What will we uncover in such a survey? Will we find ultra diffuse galaxies there? Such dwarf galaxy surveys will lay the foundation for future studies.

The presented projects are all of observational character. To improve our understanding of structure formation these studies need to be accompanied by cosmological studies, to put them into a bigger picture. To rephrase it in Hubble's words: "Yet observation and theory are woven together, and it is futile to attempt their complete separation.".

6 Zusammenfassung der Doktorarbeit

"Die Astronomie ist vielleicht diejenige Wissenschaft, worin das wenigste durch Zufall entdeckt worden ist, wo der menschliche Verstand in seiner ganzen Grösse erscheint, und wo der Mensch am besten kennen lernen kann, wie klein er ist."

— Professor Georg Christoph Lichtenberg
Deutscher Naturwissenschaftler, Schriftsteller und Philosoph der Aufklärung

In unserem Universum gibt es unzählige Galaxien – von riesigen elliptischen Galaxien, die Milliarden von Sternen enthalten, bis hin zu den kleinsten sogenannten Zwerggalaxien, welche nur aus einigen tausend Sternen bestehen. Zahlenmässig sind die Zwerggalaxien die häufigsten Galaxien im Universum. Ihr abgestrahltes Licht reicht meist gerade noch aus, um nicht im Rauschen des Nachthimmels zu versinken. Zwerggalaxie ist jedoch nicht gleich Zwerggalaxie, im Gegenteil, es gibt einen ganzen Zoo vielfältiger Zwerge, die sich hinsichtlich ihrer Masse, Grösse, Helligkeit, und schlussendlich in ihrem Aussehen deutlich unterscheiden. In dieser Doktorarbeit sind in ersten Linie die zwergelliptischen Galaxien von Interesse, die sich durch eine regelmässige Helligkeitsverteilung ohne grosse Irregularitäten auszeichnen. Dieser Typ von Zwerg kommt hauptsächlich in Galaxiengruppen und Galaxienhaufen vor und wir vermuten, dass diese Zwerge die ältesten Objekte des Universums sind.

Warum sind diese astronomischen Objekte für die Wissenschaft von Interesse? Die Antwort liegt in ihrer Konzentration an Dunkler Materie – Zwerggalaxien sind von Dunkler Materie dominiert. Besitzen gewöhnliche Spiralgalaxien ein Masse zu Leuchtkraft Verhältnis von etwa zwei, so geht dies bei den Zwerggalaxien in Richtung eintausend und mehr. Unter der Annahme, dass das abgestrahlte Licht von Galaxien ausschliesslich von Sternen stammt, gibt dieses Verhältnis somit an, wie viel nicht-sichtbare Masse in einer Galaxie steckt.

Die Dunkle Materie können wir zwar nicht direkt sehen, aber dennoch durch ihren gravitationellen Einfluss erahnen. Nach dem Standardmodell der Kosmologie existiert fünfmal mehr Dunkle Materie als normale – sogenannte baryonische – Materie, also Sterne, Gas, die Elemente, Planeten – einfach alles, was wir aus unserem

täglichen Leben kennen. Das Universum hingegen besteht hauptsächlich aus Dunkler Materie und ist im wahrsten Sinne des Wortes dunkel.

Mithilfe von Supercomputern können wir die Entwicklung der Dunklen Materie im Universum simulieren und somit mitverfolgen. Zuerst formen sich kleine Verklumpungen aus Dunkler Materie, welche im Laufe der Zeit immer grössere Strukturen bilden. Die kleinsten Strukturen entsprechen den Zwerggalaxien, welche allmählich miteinandern verschmelzen und somit zu grösseren Galaxien anwachsen. Diese wiederrum ordnen sich zu komplexen Gebilden an, wie etwa Galaxiengruppen oder Galaxienhaufen. Durch die immer besser werdenden technischen Möglichkeiten können wir also die Entwicklung der Zwerggalaxien am Computer mitverfolgen und einige Vorhersagen machen – zum Beispiel über die Anzahl an Zwerggalaxien, deren Verteilung und Bewegungen. Eine solche Vorhersage ist, dass in der Nachbarschaft unserer Milchstrasse tausende von Zwerggalaxien anzutreffen seien, entdeckt wurde bislang aber nur eine Handvoll – dies ist das sogenannte *missing-satellite* Problem (zu Deutsch: das fehlende Satelliten Problem). Auch die Verteilung und Bewegung sind nicht so wie erwartet: während die Zwerggalaxien in den Simulationen wie Bienen um die Zentralgalaxie schwirren, sie also fast gleichmässig verteilt sind und sich zufällig bewegen, gibt es in Tat und Wahrheit eine erstaunliche Ordnung der Zwerggalaxien um die Milchstrasse. Die beobachteten Zwerge sind in einer dünnen Scheibe angeordnet und rotieren im selben Drehsinn um die Milchstrasse – ähnlich wie die Planeten um die Sonne. In den Simulationen sind solche Strukturen sehr selten und kommen nur mit einer 0.1-prozentigen Wahrscheinlichkeit vor.

Nun bestand lange Zeit der Konsens darüber, dass die Milchstrasse ein Spezialfall sei, doch diese Vorstellung musste revidiert werden, als das gleiche Phänomen im Jahre 2013 im Umfeld der Andromeda Galaxie gefunden wurde. Die Andromeda Galaxie, zusammen mit der Milchstrasse, gehört zur Lokalen Gruppe. Nun wurde also schon zweimal ein solcher Ausnahmefall gefunden, was unwahrscheinlich, aber dennoch möglich ist. Diese Diskrepanz von Theorie und Beobachtung ist als das *planes-of-satellites* Problem (zu Deutsch: Satellitenebenen Problem) bekannt. Die Hauptfrage, die ich mit meiner Doktorarbeit zu beantworten versuche, lautet wie folgt: Ist die Lokale Gruppe nur ein statistischer Aussreisser im sonst erfolgreichen Standardmodell der Kosmologie, oder finden wir solche Diskrepanzen häufiger?

Um eine Antwort auf diese Frage zu finden, müssen wir Galaxiengruppen ausserhalb unserer eigenen studieren. Zuerst einmal muss eine genügend grosse Anzahl von Zwerggalaxien in den anderen Gruppen bekannt sein. Es muss also sozusagen eine Volkszählung durchgeführt werden. Deshalb haben wir mit der Dark Energy Camera in Chile nach unentdeckten Zwergen in der nahen Centaurus Gruppe gesucht. Die Centaurus Gruppe ist unser nächster Nachbar am südlichen Firmament und ist etwa 4 Megaparsec von uns entfernt (was etwa 13 Millionen Lichtjahren oder 120 Trillionen Kilometern entspricht). Mit diesem Vier-Meter-Teleskop konnten wir 56

neue Zwerggalaxien entdecken – was einer Verdoppelung der Anzahl bekannter Galaxien in der Centaurus Gruppe nahekommt.

Nun wird es spannend: Während wir uns auf die Suche nach neuen Zwergen begaben, wurde gleichzeitig von einem Team um Brent Tully eine Studie veröffentlicht, welche die Verteilung der Zwerggalaxien um Cen A – der Hauptgalaxie der Centaurus Gruppe – untersuchte. Die Autoren schlugen vor, dass sich die Zwerggalaxien in zwei parallelen Ebenen anordneten. Mit unseren neu gefundenen Zwergen stellten wir hingegen fest, dass es sich wahrscheinlich nur um eine einzelne Ebene handelt, in dem wir statistische Tests anwendeten. Weiter haben wir herausgefunden, dass diese Ebene erstaunliche Ähnlichkeiten zu den Ebenen der Lokalen Gruppe aufweist: Sie steht senkrecht zur Staubebene von Cen A, sie zeigt auf M 83 – die zweite Hauptgalaxie in der Gruppe – und sie enthält einen stellaren Strom. Da die genauen Distanzen der neuen Zwerge noch nicht bekannt sind, haben wir mit dem Very Large Telescope – dem grössten optischen Teleskop in der südlichen Hemisphäre – ein Pilotprojekt gestartet um ihre Distanzen zu messen. Von drei Kandidaten konnten wir zwei Zwerggalaxien bestätigen, der dritte Kandidat im Bunde ist wohl eine Hintergrundsgalaxie. Mit diesen beiden neuen Zwergen, zusammen mit den vorher bekannten, vermuten wir auch um M 83 eine Scheibenstruktur – mehr Daten sind jedoch nötig, um dies zu bestätigen.

Auch in in anderen Gruppen haben wir den Zensus der Zwerggalaxien vorangebracht. In öffentlich verfügbaren Daten des Sloan Digital Sky Survey (SDSS) konnten wir 15 Zwerggalaxien Kandidaten in der M 101 Gruppe und 36 Kandidaten in der Leo-I Gruppe ausfindig machen. Auch um M 101 scheint die Verteilung der Zwerggalaxien dünner als erwartet. In Leo-I hingegen ist die Verteilung zufällig – also so wie im Standardmodell vorhergesagt. Wir konnten dafür eine andere Entdeckung in Leo-I machen. Eine Handvoll der Zwerge sind sogenannte Ultra-Diffuse Galaxien (UDG). Dieser Typ von Galaxie ist in etwa so gross wie die Milchstrasse, enthält aber nur soviel Materie wie eine Zwerggalaxie. Ihre Entstehung ist noch nicht verstanden und Gegenstand hitziger Debatten. Unsere neu entdeckten UDGs sind einige der nächstgelegenen UDGs im bekannten Universum und somit ideal, um ihre Entstehung genauer zu untersuchen.

Um nochmals zur Frage zurückzukommen, ob die Lokale Gruppe speziell sei, haben wir uns die Bewegungen in der Satellitenscheibe um Cen A angeschaut. Da die Ebene in unserer Sichtlinie liegt – sprich, wir sie von der Kante aus sehen – können wir eine Kohärenz der Bewegung studieren, indem wir betrachten, wie sich die Zwerge im Gegensatz zu Cen A bewegen. Besitzen die Zwergen denselben Drehsinn, so müssen sie sich auf der einen Seite von uns aus gesehen wegbewegen – rotverschoben sein – und sich auf der anderen Seite auf uns zu bewegen – blauverschoben sein. Genau dies haben wir festgestellt: 14 von 16 Satelliten folgen einer solchen Bewegung, die am besten durch eine gemeinsame Rotation um Cen A erklärt wird. Die Lokale

Gruppe ist also kein Einzelfall, wir haben das gleiche Phänomen in der Centaurus Gruppe nachgewiesen! Wir haben die Centaurus Gruppe mit Dunkle Materie Simulationen verglichen und festgestellt, dass auch hier die Wahrscheinlichkeit, eine derartige Konstellation zu finden im Bereich von 0.1 bis 1.0 Prozent liegt. Dies stellt eine grosse Herausforderung für das Dunkle Materie Modell dar, da wir solche Strukturen häufiger beobachten als sie statistisch gesehen vorkommen sollten. Dies könnte darauf hindeuten, dass wir etwas in der Entstehung solcher Galaxiengruppen noch nicht verstanden haben, oder eventuell sogar, dass die zugrundeliegende Gravitationstheorie unvollständig ist.

Acknowledgement

"I'm not a hugging person."

— Doctor Who
Time Lord

You should always start at the end, so the first words written in this thesis are the last to appear. There are many people worth mentioning here as I have met a lot of wonderful human beings during my PhD studies.

First and foremost I thank my advisor Bruno Binggeli. In todays publish-or-perish climate, you made it possible to provide a creative working environment, where ideas could be pursued without the worry of deadlines or the impact of them. Giving me a lot of individual freedom was the perfect setting to start thinking outside of the box, to challenge myself and others. The most important thing I learned during my studies was not about dwarf galaxies, cosmology, or astronomy in general, but what it means to be a scientist. I enjoyed and tried to implement the anecdotes from back in the days, where scientific discoveries were pursued in the name of science. I learned that being a scientist is not just a profession, but a lifestyle.

Next I want to thank my co-advisor Helmut Jerjen, who pushed me towards the forefront of todays research. Your working-ethics and critical mind are a great inspiration and you taught me how survive in the minefield of science. I am very grateful for your hospitality during my five week stay down under – I will be back! I also want to thank Marina Rejkuba for opening a new world for me: the realm of resolved stars. My visits to ESO are one of my most memorable experiences during my studies.

Then I thank my collaborators: Mr. VPOS, aka Marcel S. Pawlowski, and Federico Lelli for the enojoyable meetings we had all around the world (Teneriffe, Obergurgl, Basel, Garching, Cleveland, and Mainz). I certainly hope there are more meetings and discussions to follow. Perhaps we find ourselves at the same institute one day – I would enjoy that.

There are a lot of friends I am happy to have met at university: my good friends Eros Cazzato, Francesco Cefala, and Oliver Heinimann, whom I spent a lot of time

together; my number one fan-girl, Migle Graužinytė, whose last name I still can't properly pronounce; and the former people from Friedl's astro-physics group, who adopted me as one of their own.

I also thank the scientists who took interest in my research: Denija Crnojevic, who supported me with both scientific and personal advices during the years; Pavel Kroupa, whose tremendous work influenced me to take interest in cosmology; and Marius Cautun, for interesting discussions per mail and in person. Of course there are many more scientists I am grateful to have met in person or have corresponded by e-mail. And more, I am truly humbled to have started collaborating with Igor Karachentsev and Brent Tully, whom I admire as role models in dwarf galaxy research.

Proof-reading was done by Eva Schnider and Jerome Meier, so if the careful reader finds any overlooked typos, they are the ones to blame. In other words: Thank you very much for the careful revision, comments, and suggestions which improved the quality of the manuscript.

Lastly I thank my long-term girlfriend Eva Schnider – it's been more than ten years – for being the wonderful person you are, enduring all the times I thought after-work hours and weekends are meant to do more science. I'm sorry for getting angry while you were pointing out that most – albeit not all – of the work can and should be done during office hours.

"Who are you, who are so wise in the ways of science?"

— Jean-Luc Picard
Monty Python and the Holy Grail

Bibliography

Ahmed, S. H., Brooks, A. M., & Christensen, C. R. 2017, MNRAS, 466, 3119

Ahn, C. P., Alexandroff, R., Allende Prieto, C., et al. 2014, ApJS, 211, 17

Alam, S., Albareti, F. D., Allende Prieto, C., et al. 2015, ApJS, 219, 12

Amorisco, N. C. & Loeb, A. 2016, MNRAS, 459, L51

Angus, G. W. 2008, MNRAS, 387, 1481

Angus, G. W. 2009, MNRAS, 394, 527

Angus, G. W., Diaferio, A., & Kroupa, P. 2011, MNRAS, 416, 1401

Aubert, D., Pichon, C., & Colombi, S. 2004, MNRAS, 352, 376

Babcock, H. W. 1939, Lick Observatory Bulletin, 19, 41

Bahl, H. & Baumgardt, H. 2014, MNRAS, 438, 2916

Banik, I., O'Ryan, D., & Zhao, H. 2018, MNRAS

Banks, G. D., Disney, M. J., Knezek, P. M., et al. 1999, ApJ, 524, 612

Barnes, D. G., Staveley-Smith, L., de Blok, W. J. G., et al. 2001, MNRAS, 322, 486

Beaton, R. L., Freedman, W. L., Madore, B. F., et al. 2016, ApJ, 832, 210

Bellazzini, M., Ferraro, F. R., Sollima, A., Pancino, E., & Origlia, L. 2004, A&A, 424, 199

Belokurov, V., Irwin, M. J., Koposov, S. E., et al. 2014, MNRAS, 441, 2124

Belokurov, V., Walker, M. G., Evans, N. W., et al. 2010, ApJ, 712, L103

Belokurov, V., Zucker, D. B., Evans, N. W., et al. 2007, ApJ, 654, 897

Belokurov, V., Zucker, D. B., Evans, N. W., et al. 2006, ApJ, 647, L111

Bennet, P., Sand, D. J., Crnojević, D., et al. 2017, ApJ, 850, 109

Bertin, E. & Arnouts, S. 1996, A&AS, 117, 393

Bertin, E., Mellier, Y., Radovich, M., et al. 2002, in Astronomical Society of the Pacific Conference Series, Vol. 281, Astronomical Data Analysis Software and Systems XI, ed. D. A. Bohlender, D. Durand, & T. H. Handley, 228

Bessell, M. S. 2005, ARA&A, 43, 293

Bílek, M., Thies, I., Kroupa, P., & Famaey, B. 2017, ArXiv e-prints

Binggeli, B. 1989, in Astrophysics and Space Science Library, Vol. 151, Large Scale Structure and Motions in the Universe, ed. M. Mezzetti, G. Giuricin, F. Mardirossian, & M. Ramella, 47–61

Binggeli, B. 1994, in European Southern Observatory Conference and Workshop Proceedings, Vol. 49, European Southern Observatory Conference and Workshop Proceedings, ed. G. Meylan & P. Prugniel, 13

Binggeli, B. & Cameron, L. M. 1993, A&AS, 98, 297

Binggeli, B. & Jerjen, H. 1998, A&A, 333, 17

Binggeli, B., Sandage, A., & Tammann, G. A. 1985, AJ, 90, 1681

Binggeli, B., Sandage, A., & Tarenghi, M. 1984, AJ, 89, 64

Binggeli, B., Tammann, G. A., & Sandage, A. 1987, AJ, 94, 251

Bond, N. A., Strauss, M. A., & Cen, R. 2010, MNRAS, 409, 156
Bosma, A. 1981, AJ, 86, 1791
Bournaud, F. & Duc, P.-A. 2006, A&A, 456, 481
Bournaud, F., Duc, P.-A., Brinks, E., et al. 2007, Science, 316, 1166
Boyarsky, A., Ruchayskiy, O., & Shaposhnikov, M. 2009, Annual Review of Nuclear and Particle Science, 59, 191
Boylan-Kolchin, M., Bullock, J. S., & Kaplinghat, M. 2011, MNRAS, 415, L40
Boylan-Kolchin, M., Springel, V., White, S. D. M., Jenkins, A., & Lemson, G. 2009, MNRAS, 398, 1150
Bremnes, T., Binggeli, B., & Prugniel, P. 1999, A&AS, 137, 337
Brooks, A. & Christensen, C. 2016, Galactic Bulges, 418, 317
Buck, T., Dutton, A. A., & Macciò, A. V. 2016, MNRAS, 460, 4348
Bullock, J. S. & Boylan-Kolchin, M. 2017, ARA&A, 55, 343
Candlish, G. N., Smith, R., & Fellhauer, M. 2015, MNRAS, 446, 1060
Carlin, J. L., Sand, D. J., Price, P., et al. 2016, ApJ, 828, L5
Carrillo, A., Bell, E. F., Bailin, J., et al. 2017, MNRAS, 465, 5026
Carrillo, A. J., Bell, E. F., Bailin, J., & Monachesi, A. 2016, in American Astronomical Society Meeting Abstracts, Vol. 227, American Astronomical Society Meeting Abstracts, 136.25
Cautun, M., Bose, S., Frenk, C. S., et al. 2015a, MNRAS, 452, 3838
Cautun, M. & Frenk, C. S. 2017, MNRAS, 468, L41
Cautun, M., Wang, W., Frenk, C. S., & Sawala, T. 2015b, MNRAS, 449, 2576
Chiboucas, K., Jacobs, B. A., Tully, R. B., & Karachentsev, I. D. 2013, AJ, 146, 126
Chiboucas, K., Karachentsev, I. D., & Tully, R. B. 2009, AJ, 137, 3009
Combes, F. 1991, A&A, 243, 109
Cooke, R. J., Pettini, M., Jorgenson, R. A., Murphy, M. T., & Steidel, C. C. 2014, ApJ, 781, 31
Cote, S., Freeman, K. C., Carignan, C., & Quinn, P. J. 1997, AJ, 114, 1313
Courtois, H. M., Pomarède, D., Tully, R. B., Hoffman, Y., & Courtois, D. 2013, AJ, 146, 69
Crnojević, D., Ferguson, A. M. N., Irwin, M. J., et al. 2013, MNRAS, 432, 832
Crnojević, D., Grebel, E. K., & Cole, A. A. 2011a, A&A, 530, A59
Crnojević, D., Grebel, E. K., & Cole, A. A. 2012, A&A, 541, A131
Crnojević, D., Grebel, E. K., & Koch, A. 2010, A&A, 516, A85
Crnojević, D., Rejkuba, M., Grebel, E. K., da Costa, G., & Jerjen, H. 2011b, A&A, 530, A58
Crnojević, D., Sand, D. J., Caldwell, N., et al. 2014, ApJ, 795, L35
Crnojević, D., Sand, D. J., Spekkens, K., et al. 2016, ApJ, 823, 19
Da Costa, G. S. & Armandroff, T. E. 1990, AJ, 100, 162
D'Agostino, R. B. & Stephens, M. A. 1986, Goodness-of-fit techniques
Danieli, S., van Dokkum, P., Merritt, A., et al. 2017, ApJ, 837, 136
de Blok, W. J. G. 2010, Advances in Astronomy, 2010, 789293
de Vaucouleurs, G., de Vaucouleurs, A., Corwin, Jr., H. G., et al. 1991, Third Reference Catalogue of Bright Galaxies. Volume I: Explanations and references. Volume II: Data for galaxies between 0^h and 12^h. Volume III: Data for galaxies between 12^h and 24^h.
Di Cintio, A., Brook, C. B., Dutton, A. A., et al. 2017, MNRAS, 466, L1
Diemand, J., Kuhlen, M., & Madau, P. 2006, ApJ, 649, 1
Diemand, J., Kuhlen, M., Madau, P., et al. 2008, Nature, 454, 735
Dobbs, C. L., Theis, C., Pringle, J. E., & Bate, M. R. 2010, in Astronomical Society of the Pacific Conference Series, Vol. 423, Galaxy Wars: Stellar Populations and Star Formation in Interacting Galaxies, ed. B. Smith, J. Higdon, S. Higdon, & N. Bastian, 240

Dolphin, A. 2016, DOLPHOT: Stellar photometry, Astrophysics Source Code Library
Doyle, M. T., Drinkwater, M. J., Rohde, D. J., et al. 2005, MNRAS, 361, 34
Dubois, Y., Pichon, C., Welker, C., et al. 2014, MNRAS, 444, 1453
Dunn, L. P. & Jerjen, H. 2006, AJ, 132, 1384
Eisenstein, D. J., Zehavi, I., Hogg, D. W., et al. 2005, ApJ, 633, 560
Elbert, O. D., Bullock, J. S., Kaplinghat, M., et al. 2016, arxiv:1609.08626
Famaey, B., McGaugh, S., & Milgrom, M. 2018, arxiv:1804.04167
Famaey, B. & McGaugh, S. S. 2012, Living Reviews in Relativity, 15, 10
Ferguson, H. C. 1990, PhD thesis, Johns Hopkins Univ., Baltimore, MD.
Ferguson, H. C. & Sandage, A. 1988, AJ, 96, 1520
Ferguson, H. C. & Sandage, A. 1990, AJ, 100, 1
Ferrarese, L., Ford, H. C., Huchra, J., et al. 2000, ApJS, 128, 431
Forero-Romero, J. E. & Arias, V. 2018, arxiv:1805.03188
Fouquet, S., Hammer, F., Yang, Y., Puech, M., & Flores, H. 2012, MNRAS, 427, 1769
Frei, Z. & Gunn, J. E. 1994, AJ, 108, 1476
Frenk, C. S. & White, S. D. M. 2012, Annalen der Physik, 524, 507
Fritz, T. K., Battaglia, G., Pawlowski, M. S., et al. 2018, arxiv:1805.00908
Gaia Collaboration, Helmi, A., van Leeuwen, F., et al. 2018, arxiv:1804.09381
Garaldi, E., Romano-Díaz, E., Borzyszkowski, M., & Porciani, C. 2018, MNRAS, 473, 2234
Garrison-Kimmel, S., Wetzel, A., Bullock, J. S., et al. 2017, MNRAS, 471, 1709
Genel, S., Vogelsberger, M., Springel, V., et al. 2014, MNRAS, 445, 175
Gillet, N., Ocvirk, P., Aubert, D., et al. 2015, ApJ, 800, 34
Golub, G. & Kahan, W. 1965, SIAM Journal on Numerical Analysis, 2, 205
González, R. E. & Padilla, N. D. 2010, MNRAS, 407, 1449
Graham, A. W. & Driver, S. P. 2005, PASA, 22, 118
Gunn, J. E., Siegmund, W. A., Mannery, E. J., et al. 2006, AJ, 131, 2332
Guo, Q., White, S., Angulo, R. E., et al. 2013, MNRAS, 428, 1351
Hammer, F., Yang, Y., Arenou, F., et al. 2018a, arxiv:1805.01469
Hammer, F., Yang, Y., Fouquet, S., et al. 2013, MNRAS, 431, 3543
Hammer, F., Yang, Y. B., Wang, J. L., et al. 2018b, MNRAS, 475, 2754
Hartigan, P. M. 1985, Journal of the Royal Statistical Society. Series C (Applied Statistics), 34, 320
Haynes, M. P., Giovanelli, R., Martin, A. M., et al. 2011, AJ, 142, 170
Henden, A. & Munari, U. 2014, Contributions of the Astronomical Observatory Skalnate Pleso, 43, 518
Henkel, C., Javanmardi, B., Martínez-Delgado, D., Kroupa, P., & Teuwen, K. 2017, A&A, 603, A18
Hibbard, J. E., van der Hulst, J. M., Barnes, J. E., & Rich, R. M. 2001, AJ, 122, 2969
Hubble, E. P. 1936, Realm of the Nebulae
Huchtmeier, W. K., Karachentsev, I. D., & Karachentseva, V. E. 2001, A&A, 377, 801
Huchtmeier, W. K., Karachentsev, I. D., & Karachentseva, V. E. 2003, A&A, 401, 483
Hui, X., Ford, H. C., Freeman, K. C., & Dopita, M. A. 1995, ApJ, 449, 592
Ibata, N. G., Ibata, R. A., Famaey, B., & Lewis, G. F. 2014a, Nature, 511, 563
Ibata, R. A., Famaey, B., Lewis, G. F., Ibata, N. G., & Martin, N. 2015, ApJ, 805, 67
Ibata, R. A., Gilmore, G., & Irwin, M. J. 1994, Nature, 370, 194
Ibata, R. A., Ibata, N. G., Lewis, G. F., et al. 2014b, ApJ, 784, L6
Ibata, R. A., Lewis, G. F., Conn, A. R., et al. 2013, NAT, 493, 62

Jacobs, B. A., Rizzi, L., Tully, R. B., et al. 2009, AJ, 138, 332
Jang, I. S., Hatt, D., Beaton, R. L., et al. 2018, ApJ, 852, 60
Javanmardi, B., Martinez-Delgado, D., Kroupa, P., et al. 2016, A&A, 588, A89
Jennings, Z. G., Romanowsky, A. J., Brodie, J. P., et al. 2015, ApJ, 812, L10
Jerjen, H., Binggeli, B., & Freeman, K. C. 2000a, AJ, 119, 593
Jerjen, H., Freeman, K. C., & Binggeli, B. 2000b, AJ, 119, 166
Jerjen, H. & Rejkuba, M. 2001, A&A, 371, 487
Jerjen, H., Rekola, R., Takalo, L., Coleman, M., & Valtonen, M. 2001, A&A, 380, 90
Kallivayalil, N., Sales, L., Zivick, P., et al. 2018, arxiv:1805.01448
Karachentsev, I. D. 2005, AJ, 129, 178
Karachentsev, I. D., Kaisina, E. I., & Makarov, D. I. 2014, AJ, 147, 13
Karachentsev, I. D. & Karachentseva, V. E. 2004, Astronomy Reports, 48, 267
Karachentsev, I. D., Karachentseva, V. E., & Huchtmeier, W. K. 2001, A&A, 366, 428
Karachentsev, I. D., Karachentseva, V. E., Huchtmeier, W. K., & Makarov, D. I. 2004, AJ, 127, 2031
Karachentsev, I. D., Karachentseva, V. E., & Sharina, M. E. 2005, in IAU Colloq. 198: Near-fields cosmology with dwarf elliptical galaxies, ed. H. Jerjen & B. Binggeli, 295–302
Karachentsev, I. D., Kopylov, A. I., & Kopylova, F. G. 1994, Bulletin of the Special Astrophysics Observatory, 38, 5
Karachentsev, I. D., Makarov, D. I., & Kaisina, E. I. 2013, AJ, 145, 101
Karachentsev, I. D., Riepe, P., Zilch, T., et al. 2015, Astrophysical Bulletin, 70, 379
Karachentsev, I. D., Sharina, M. E., Dolphin, A. E., et al. 2002, A&A, 385, 21
Karachentsev, I. D., Sharina, M. E., Dolphin, A. E., et al. 2003, A&A, 398, 467
Karachentsev, I. D., Tully, R. B., Dolphin, A., et al. 2007, AJ, 133, 504
Karachentseva, V. E. & Karachentsev, I. D. 1998, A&AS, 127, 409
Kauffmann, G., White, S. D. M., & Guiderdoni, B. 1993, MNRAS, 264, 201
Keller, S. C., Schmidt, B. P., Bessell, M. S., et al. 2007, PASA, 24, 1
Kim, D. & Jerjen, H. 2015, ApJ, 799, 73
Kim, D., Jerjen, H., Mackey, D., Da Costa, G. S., & Milone, A. P. 2015, ApJ, 804, L44
Kim, D., Jerjen, H., Mackey, D., Da Costa, G. S., & Milone, A. P. 2016, ApJ, 820, 119
Kirby, E. M., Koribalski, B., Jerjen, H., & López-Sánchez, Á. 2012, MNRAS, 420, 2924
Klypin, A., Kravtsov, A. V., Valenzuela, O., & Prada, F. 1999, APJ, 522, 82
Kniazev, A. Y., Grebel, E. K., Pustilnik, S. A., et al. 2004, AJ, 127, 704
Koch, A. & Grebel, E. K. 2006, AJ, 131, 1405
Koda, J., Milosavljević, M., & Shapiro, P. R. 2009, ApJ, 696, 254
Koda, J., Yagi, M., Yamanoi, H., & Komiyama, Y. 2015, ApJ, 807, L2
Koposov, S. E., Belokurov, V., Torrealba, G., & Evans, N. W. 2015, ApJ, 805, 130
Koribalski, B. S., Staveley-Smith, L., Kilborn, V. A., et al. 2004, AJ, 128, 16
Kormendy, J., Drory, N., Bender, R., & Cornell, M. E. 2010, ApJ, 723, 54
Kraan-Korteweg, R. C. & Tammann, G. A. 1979, Astronomische Nachrichten, 300, 181
Kroupa, P. 2012, PASA, 29, 395
Kroupa, P., Famaey, B., de Boer, K. S., et al. 2010, A&A, 523, A32
Kroupa, P., Theis, C., & Boily, C. M. 2005, A&A, 431, 517
Kunkel, W. E. & Demers, S. 1976, in Royal Greenwich Observatory Bulletins, Vol. 182, The Galaxy and the Local Group, ed. R. J. Dickens, J. E. Perry, F. G. Smith, & I. R. King, 241
Kunth, D., Maurogordato, S., & Vigroux, L. 1988, A&A, 204, 10
Laporte, C. F. P., Agnello, A., & Navarro, J. F. 2018, arxiv:1804.04139

Lauberts, A. & Valentijn, E. A. 1989, The surface photometry catalogue of the ESO-Uppsala galaxies
Lee, M. G., Freedman, W. L., & Madore, B. F. 1993, ApJ, 417, 553
Lelli, F., Duc, P.-A., Brinks, E., et al. 2015, A&A, 584, A113
Lelli, F., McGaugh, S. S., Schombert, J. M., & Pawlowski, M. S. 2017, ApJ, 836, 152
Libeskind, N. I., Hoffman, Y., Tully, R. B., et al. 2015, MNRAS, 452, 1052
Libeskind, N. I., Knebe, A., Hoffman, Y., & Gottlöber, S. 2014, MNRAS, 443, 1274
Lipnicky, A. & Chakrabarti, S. 2017, MNRAS, 468, 1671
Lisker, T., Grebel, E. K., & Binggeli, B. 2008, AJ, 135, 380
López-Corredoira, M. & Kroupa, P. 2016, ApJ, 817, 75
Lovell, M. R., Eke, V., Frenk, C. S., et al. 2012, MNRAS, 420, 2318
Lupton, R. 2005, Transformations between SDSS magnitudes and other systems https://www.sdss3.org/dr10/algorithms/sdssUBVRITransform.php/
Lynden-Bell, D. 1976, MNRAS, 174, 695
Maji, M., Zhu, Q., Marinacci, F., & Li, Y. 2017a, arxiv:1702.00485
Maji, M., Zhu, Q., Marinacci, F., & Li, Y. 2017b, arxiv:1702.00497
Makarov, D. & Karachentsev, I. 2011, MNRAS, 412, 2498
Makarov, D. I., Makarova, L. N., & Uklein, R. I. 2013, Astrophysical Bulletin, 68, 125
Makarova, L., Karachentsev, I., Rizzi, L., Tully, R. B., & Korotkova, G. 2009, MNRAS, 397, 1672
Makarova, L. N., Makarov, D. I., Antipova, A. V., Karachentsev, I. D., & Tully, R. B. 2018, MNRAS, 474, 3221
Martin, N. F., Collins, M. L. M., Longeard, N., & Tollerud, E. 2018, arxiv:1804.04136
Martin, N. F., Ibata, R. A., McConnachie, A. W., et al. 2013, ApJ, 776, 80
McConnachie, A. W. 2012, AJ, 144, 4
McConnachie, A. W. & Irwin, M. J. 2006, MNRAS, 365, 902
McConnachie, A. W., Irwin, M. J., Ibata, R. A., et al. 2009, Nature, 461, 66
McQuinn, K. B. W., Skillman, E. D., Dolphin, A. E., Berg, D., & Kennicutt, R. 2016, ApJ, 826, 21
Merritt, A., van Dokkum, P., & Abraham, R. 2014, ApJ, 787, L37
Merritt, A., van Dokkum, P., Danieli, S., et al. 2016, ApJ, 833, 168
Metcalfe, N., Godwin, J. G., & Peach, J. V. 1994, MNRAS, 267, 431
Metz, M., Kroupa, P., & Jerjen, H. 2007, MNRAS, 374, 1125
Metz, M., Kroupa, P., & Libeskind, N. I. 2008, ApJ, 680, 287
Michel-Dansac, L., Duc, P.-A., Bournaud, F., et al. 2010, ApJ, 717, L143
Mihos, J. C., Harding, P., Spengler, C. E., Rudick, C. S., & Feldmeier, J. J. 2013, ApJ, 762, 82
Milgrom, M. 1983, ApJ, 270, 365
Monachesi, A., Bell, E. F., Radburn-Smith, D. J., et al. 2014, ApJ, 780, 179
Moore, B., Ghigna, S., Governato, F., et al. 1999, ApJ, 524, L19
Mould, J. & Sakai, S. 2009, ApJ, 697, 996
Müller, O., Jerjen, H., & Binggeli, B. 2015, A&A, 583, A79
Müller, O., Jerjen, H., & Binggeli, B. 2017a, A&A, 597, A7
Müller, O., Jerjen, H., & Binggeli, B. 2018a, arxiv:1802.08657
Müller, O., Jerjen, H., Pawlowski, M. S., & Binggeli, B. 2016, A&A, 595, A119
Müller, O., Pawlowski, M. S., Jerjen, H., & Lelli, F. 2018b, Science, 359, 534
Müller, O., Rejkuba, M., & Jerjen, H. 2018c, arxiv:1803.02406
Müller, O., Scalera, R., Binggeli, B., & Jerjen, H. 2017b, A&A, 602, A119

Nataf, D. M. 2015, MNRAS, 449, 1171
Navarro, J. F., Frenk, C. S., & White, S. D. M. 1997, ApJ, 490, 493
Nelson, D., Pillepich, A., Genel, S., et al. 2015, Astronomy and Computing, 13, 12
Newton, I. 1687, The Principia: Mathematical Principles of Natural Philosophy
Nikiel-Wroczyński, B., Soida, M., Bomans, D. J., & Urbanik, M. 2014, ApJ, 786, 144
Oñorbe, J., Boylan-Kolchin, M., Bullock, J. S., et al. 2015, MNRAS, 454, 2092
Ordenes-Briceño, Y., Taylor, M. A., Puzia, T. H., et al. 2016, MNRAS, 463, 1284
Ostriker, J. P. & Steinhardt, P. J. 1995, Nature, 377, 600
Otsu, N. 1979, IEEE Trans. Syst. Man Cybern, 9, 62
Papaderos, P., Loose, H.-H., Fricke, K. J., & Thuan, T. X. 1996a, A&A, 314, 59
Papaderos, P., Loose, H.-H., Thuan, T. X., & Fricke, K. J. 1996b, A&AS, 120, 207
Park, H. S., Moon, D.-S., Zaritsky, D., et al. 2017, ApJ, 848, 19
Paturel, G., Petit, C., Prugniel, P., et al. 2003, A&A, 412, 45
Pawlowski, M. S. 2016, MNRAS, 456, 448
Pawlowski, M. S. 2018, Modern Physics Letters A, 33, 1830004
Pawlowski, M. S., Dabringhausen, J., Famaey, B., et al. 2017, Astronomische Nachrichten, 338, 854
Pawlowski, M. S., Famaey, B., Jerjen, H., et al. 2014, MNRAS, 442, 2362
Pawlowski, M. S., Famaey, B., Merritt, D., & Kroupa, P. 2015a, ApJ, 815, 19
Pawlowski, M. S. & Kroupa, P. 2013, MNRAS, 435, 2116
Pawlowski, M. S., Kroupa, P., Angus, G., et al. 2012a, MNRAS, 424, 80
Pawlowski, M. S., Kroupa, P., & de Boer, K. S. 2011, A&A, 532, A118
Pawlowski, M. S., Kroupa, P., & Jerjen, H. 2013, MNRAS, 435, 1928
Pawlowski, M. S., McGaugh, S. S., & Jerjen, H. 2015b, MNRAS, 453, 1047
Pawlowski, M. S., Pflamm-Altenburg, J., & Kroupa, P. 2012b, MNRAS, 423, 1109
Peng, E. W., Ford, H. C., & Freeman, K. C. 2004, ApJ, 602, 685
Peterson, R. C. & Caldwell, N. 1993, AJ, 105, 1411
Phillips, J. I., Cooper, M. C., Bullock, J. S., & Boylan-Kolchin, M. 2015, MNRAS, 453, 3839
Pietrinferni, A., Cassisi, S., Salaris, M., & Castelli, F. 2004, ApJ, 612, 168
Planck Collaboration, Ade, P. A. R., Aghanim, N., et al. 2014, A&A, 571, A16
Planck Collaboration, Ade, P. A. R., Aghanim, N., et al. 2016, A&A, 594, A13
Ploeckinger, S., Recchi, S., Hensler, G., & Kroupa, P. 2015, MNRAS, 447, 2512
Puzia, T. H. & Sharina, M. E. 2008, ApJ, 674, 909
Radburn-Smith, D. J., de Jong, R. S., Seth, A. C., et al. 2011, ApJS, 195, 18
Rejkuba, M., da Costa, G. S., Jerjen, H., Zoccali, M., & Binggeli, B. 2006, A&A, 448, 983
Rejkuba, M., Greggio, L., Harris, W. E., Harris, G. L. H., & Peng, E. W. 2005, ApJ, 631, 262
Rejkuba, M., Minniti, D., Silva, D. R., & Bedding, T. R. 2001, A&A, 379, 781
Rekola, R., Jerjen, H., & Flynn, C. 2005, A&A, 437, 823
Richardson, J. C., Irwin, M. J., McConnachie, A. W., et al. 2011, ApJ, 732, 76
Riess, A. G., Casertano, S., Yuan, W., et al. 2018, ApJ, 855, 136
Rizzi, L., Held, E. V., Saviane, I., Tully, R. B., & Gullieuszik, M. 2007a, MNRAS, 380, 1255
Rizzi, L., Tully, R. B., Makarov, D., et al. 2007b, ApJ, 661, 815
Robles, V. H., Bullock, J. S., Elbert, O. D., et al. 2017, MNRAS, 472, 2945
Rubin, V. C., Burstein, D., Ford, Jr., W. K., & Thonnard, N. 1985, ApJ, 289, 81
Salomon, J.-B., Ibata, R. A., Famaey, B., Martin, N. F., & Lewis, G. F. 2016, MNRAS, 456, 4432
Sand, D. J., Crnojević, D., Strader, J., et al. 2014, ApJ, 793, L7

Sandage, A. & Binggeli, B. 1984, AJ, 89, 919
Saviane, I. & Jerjen, H. 2007, AJ, 133, 1756
Sawala, T., Frenk, C. S., Fattahi, A., et al. 2016, MNRAS, 457, 1931
Schechter, P. 1976, ApJ, 203, 297
Schechter, P. L., Mateo, M., & Saha, A. 1993, PASP, 105, 1342
Schlafly, E. F. & Finkbeiner, D. P. 2011, ApJ, 737, 103
Schlegel, D. J., Finkbeiner, D. P., & Davis, M. 1998, ApJ, 500, 525
Schneider, S. 1985, ApJ, 288, L33
Schombert, J. M., Pildis, R. A., & Eder, J. A. 1997, ApJS, 111, 233
Secker, J. 1995, Publications of the Astronomical Society of the Pacific, 107, 496
Sersic, J. L. 1968, Atlas de galaxias australes
Shaya, E. J. & Tully, R. B. 2013, MNRAS, 436, 2096
Simon, J. D. 2018, arxiv:1804.10230
Simon, J. D. & Geha, M. 2007, ApJ, 670, 313
Smercina, A., Bell, E. F., Slater, C. T., et al. 2017, ApJ, 843, L6
Smith Castelli, A. V., Faifer, F. R., & Escudero, C. G. 2016, A&A, 596, A23
Speller, R. & Taylor, J. E. 2014, ApJ, 788, 188
Spergel, D. N., Bean, R., Doré, O., et al. 2007, ApJS, 170, 377
Staveley-Smith, L., Davies, R. D., & Kinman, T. D. 1992, MNRAS, 258, 334
Stetson, P. B. 1987, PASP, 99, 191
Stetson, P. B. 2000, PASP, 112, 925
Stierwalt, S., Haynes, M. P., Giovanelli, R., et al. 2009, AJ, 138, 338
Taylor, M. A., Muñoz, R. P., Puzia, T. H., et al. 2016, arxiv:1608.07285
Taylor, M. A., Puzia, T. H., Muñoz, R. P., et al. 2017, MNRAS, 469, 3444
Thilker, D. A., Bianchi, L., Boissier, S., et al. 2005, ApJ, 619, L79
Tikhonov, N. A., Lebedev, V. S., & Galazutdinova, O. A. 2015, Astronomy Letters, 41, 239
Tody, D. 1993, in Astronomical Society of the Pacific Conference Series, Vol. 52, Astronomical Data Analysis Software and Systems II, ed. R. J. Hanisch, R. J. V. Brissenden, & J. Barnes, 173
Tolstoy, E., Hill, V., & Tosi, M. 2009, ARA&A, 47, 371
Tonry, J. & Schneider, D. P. 1988, AJ, 96, 807
Tonry, J. L., Dressler, A., Blakeslee, J. P., et al. 2001, ApJ, 546, 681
Toomre, A. & Toomre, J. 1972, in BAAS, Vol. 4, Bulletin of the American Astronomical Society, 214
Trentham, N. & Tully, R. B. 2002, MNRAS, 335, 712
Tully, R. B. 1988a, Nearby galaxies catalog
Tully, R. B. 1988b, AJ, 96, 73
Tully, R. B. 2015a, AJ, 149, 54
Tully, R. B. 2015b, AJ, 149, 171
Tully, R. B., Courtois, H. M., Dolphin, A. E., et al. 2013, AJ, 146, 86
Tully, R. B. & Fisher, J. R. 1987, Atlas of Nearby Galaxies
Tully, R. B. & Fisher, J. R. 1988, Catalog of Nearby Galaxies
Tully, R. B., Libeskind, N. I., Karachentsev, I. D., et al. 2015, ApJ, 802, L25
Tully, R. B., Shaya, E. J., Karachentsev, I. D., et al. 2008, ApJ, 676, 184
Valdes, F., Gruendl, R., & DES Project. 2014, in Astronomical Society of the Pacific Conference Series, Vol. 485, Astronomical Data Analysis Software and Systems XXIII, ed. N. Manset & P. Forshay, 379

van den Bergh, S. 1972, ApJ, 171, L31
van der Burg, R. F. J., Muzzin, A., & Hoekstra, H. 2016, A&A, 590, A20
van der Marel, R. P. & Guhathakurta, P. 2008, ApJ, 678, 187
van Dokkum, P., Abraham, R., Brodie, J., et al. 2016, ApJ, 828, L6
van Dokkum, P., Danieli, S., Cohen, Y., et al. 2018, Nature, 555, 629
van Dokkum, P. G., Abraham, R., & Merritt, A. 2014, ApJ, 782, L24
van Dokkum, P. G., Abraham, R., Merritt, A., et al. 2015a, ApJ, 798, L45
van Dokkum, P. G., Romanowsky, A. J., Abraham, R., et al. 2015b, ApJ, 804, L26
Venhola, A., Peletier, R., Laurikainen, E., et al. 2017, A&A, 608, A142
Vogelsberger, M., Genel, S., Springel, V., et al. 2014, Nature, 509, 177
Walker, M. 2013, Dark Matter in the Galactic Dwarf Spheroidal Satellites, ed. T. D. Oswalt & G. Gilmore, 1039
Walsh, J. R., Rejkuba, M., & Walton, N. A. 2015, A&A, 574, A109
Walsh, S. M., Willman, B., Sand, D., et al. 2008, ApJ, 688, 245
Watkins, A. E., Mihos, J. C., Harding, P., & Feldmeier, J. J. 2014, ApJ, 791, 38
Watkins, L. L., Evans, N. W., & An, J. H. 2010, MNRAS, 406, 264
Welker, C., Devriendt, J., Dubois, Y., Pichon, C., & Peirani, S. 2014, MNRAS, 445, L46
Wetzel, A. R., Hopkins, P. F., Kim, J.-h., et al. 2016, ApJ, 827, L23
Wetzels, R. & Wagenmakers, E.-J. 2012, Psychonomic Bulletin & Review, 19, 1057
White, S. D. M., Navarro, J. F., Evrard, A. E., & Frenk, C. S. 1993, Nature, 366, 429
Willman, B., Dalcanton, J. J., Martinez-Delgado, D., et al. 2005, ApJ, 626, L85
Wittmann, C., Lisker, T., Ambachew Tilahun, L., et al. 2017, MNRAS, 470, 1512
Wong, O. I., Ryan-Weber, E. V., Garcia-Appadoo, D. A., et al. 2006, MNRAS, 371, 1855
Woodley, K. A. 2006, AJ, 132, 2424
Woodley, K. A., Gómez, M., Harris, W. E., Geisler, D., & Harris, G. L. H. 2010, AJ, 139, 1871
Woodley, K. A., Harris, W. E., Beasley, M. A., et al. 2007, AJ, 134, 494
York, D. G., Adelman, J., Anderson, Jr., J. E., et al. 2000, AJ, 120, 1579
Zentner, A. R., Kravtsov, A. V., Gnedin, O. Y., & Klypin, A. A. 2005, ApJ, 629, 219
Zwicky, F. 1956, Ergebnisse der exakten Naturwissenschaften, 29, 344